CHALMERS
UNIVERSITY OF TECHNOLOGY

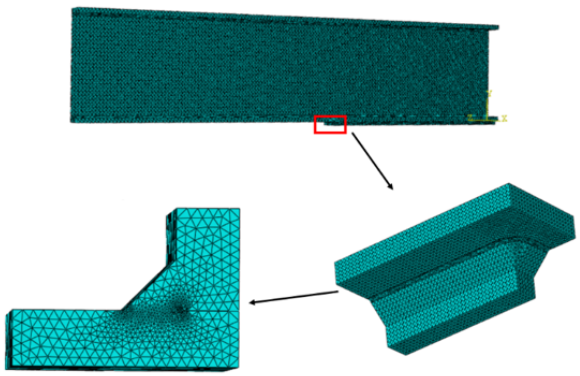

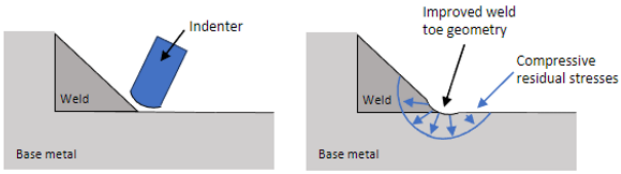

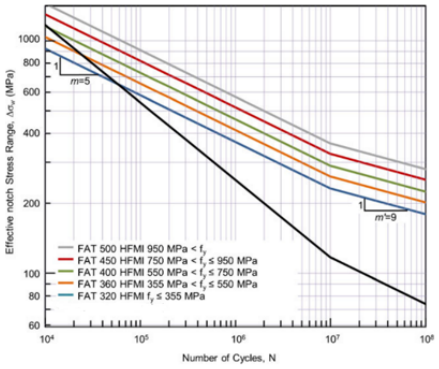

Evaluation of HFMI in welded cover-plates for strengthening of steel bridges

Master's thesis in Master Program Structural engineering and building technology

AMILIA ENGDAHL
NOORA KHOULANI

Department of Architecture and Civil Engineering
CHALMERS UNIVERSITY OF TECHNOLOGY
Master's thesis ACEX30
Gothenburg, Sweden 2023

Master's thesis ACEX30

Evaluation of HFMI in welded cover-plates for strengthening of steel bridges

A review of previous research and Finite Element Analysis based on Effective Notch Stress method to evaluate HFMI's applicability on steel bridges

Amilia Engdahl
Noora Khoulani

CHALMERS
UNIVERSITY OF TECHNOLOGY

Department of Architecture and Civil Engineering
Division of Structural engineering
Lightweight Structures group
Chalmers University of Technology
Gothenburg, Sweden 2023

Evaluation of HFMI in welded cover-plates for strengthening of steel bridges
A review of previous research and Finite Element Analysis based on Effective Notch Stress method to evaluate HFMI's applicability on steel bridges
AMILIA ENGDAHL
NOORA KHOULANI

Supervisor: Victor Andersson, Ramboll Sweden
Examiner: Professor Mohammad Al-Emrani, Department of Architecture and Civil Engineering

Master's Thesis 2023
Department of Architecture and Civil Engineering
Division of Structural engineering
Lightweight Structures group
Chalmers University of Technology
SE-412 96 Gothenburg
Telephone +46 31 772 1000

Cover: An illustration shows the applied mesh in FE model of a beam with welded cover-plate. An illustration of HFMI application technique and the IIW recommended S-N curves for HFMI-treated details.

Department of Architecture and Civil Engineering
Gothenburg, Sweden 2023

Evaluation of HFMI in welded cover-plates for strengthening of steel bridges
A review of previous research and Finite Element Analysis based on Effective Notch Stress method to evaluate HFMI's applicability on steel bridges.
AMILIA ENGDAHL
NOORA KHOULANI
Department of Architecture and civil engineering
Chalmers University of Technology

Abstract

Europe had an expansion in infrastructure during the 20th century, which led to the construction of a large number of bridges. The majority of bridges in service today are over 50 years old, meaning that they have either surpassed or are approaching their expected service life span. Additionally, due to increased traffic and traffic loads, old bridges are burdened significantly more than what they were originally designed for. A common way to reinforce steel beam bridges is by adding cover-plates to the bottom flange. Currently, these cover plates are connected using bolts. This is because the more attractive welding method contributes to poor fatigue performance, resulting in shorter bridge service lives. Hence, post-weld treatment techniques are being studied as a possible solution to fatigue-related issues in welded details. High-frequency mechanical impact (HFMI) is one of today's most promising methods. However, there is a lack of research on HFMI-treated cover-plates fatigue performance. But this is currently an area of interest. Therefore, this master's thesis assesses whether HFMI-treated cover plates are a viable solution for strengthening steel bridges.

The research was conducted by reviewing and re-analysing previous studies on HFMI-treated cover-plated structures. This was done by performing Finite Element analyses in Abaqus. Maximum principal stresses were obtained at weld toe and root to perform fatigue assessment according to the Effective Notch Stress method. Additionally, the stress behaviour of different cover-plated structures was examined and compared. Finally, the cover-plates have been modified to expand the study. The study concluded that HFMI-treatment is an effective solution to increase fatigue performance of welded cover-plated structures subjected to bending. Furthermore, it was found that treated cover-plates have the potential to provide fatigue strength comparable to, or even exceeding, bolted ones. It was also concluded that, unlike as-welded and axially loaded cover-plates, the most likely failure location for HFMI-treated cover-plates subjected to bending is at the weld root. A solution to increase the fatigue strength of the weld root was investigated in this study. It was shown that changing the root position results in additional improvement in the fatigue strength of treated cover-plates.

Keywords: Cover-plates, HFMI, UIT, Effective Notch Stress method, Weld, S-N curve, Fatigue, Cover-plates in bending, bridges, Finite Element analysis, Abaqus.

Acknowledgements

This master's thesis was conducted through a collaboration between the Department of Architecture and Civil Engineering at Chalmers University of Technology and Bridge Department at Ramboll Sweden (Gothenburg office), between January and July 2023.

We would like to express our deepest gratitude to our examiner Professor Mohammad Al-Emrani from Chalmers For his guidance, encouragement and patience throughout this journey. Also for having provided us with the necessary and appropriate materials which has help us to understand and complete the study.

We would also like to thank our supervisor Victor Andersson from ramboll, who through his experience as a bridge engineer gave us support, feedback and guidance throughout the project. This also extend to the Bridge Department at Ramboll for welcoming us and providing a comfortable working environment.

Finally, we would like to extend our heartfelt thanks to our families for their unwavering encouragement and support, which has been a constant source of strength and motivation.

Amilia Engdahl and Noora Khoulani, Gothenburg, July 2023

Notations

Dictionary

As-welded	Non post treated welds
Fillet weld	A weld that connects two metals positioned at right angles to each other
Leg-length	Idealistic length between weld toe and root
Throat thickness	The shortest distance between the weld root and the weld surface.
Residual stresses	Stresses caused by welding process as a result of gradually cooling
Detail category	A classification to define the fatigue strength of a detail.
S-N curve	Fatigue design curve
FAT-class	Detail category/Characteristic fatigue strength
Characteristic load cycles	Load cycles calculated using fatigue S-N curve
Knee-point	The point where the S-N curve changes slope (occurring at $N = 10^7$)
Cut-of-limit	The minimum nominal stress range where fatigue failure occurs/Maximum stress where no fatigue failure occurs
Run-out	Specimens that did not experience any cracks until the test was completed
Stress ratio (R-ratio)	The relation between the maximum and minimum applied stress
Crack propagation	The process by which a fatigue crack in the detail grows
Failure mode	The location where fatigue cracks initiate and propagate causing failure

Acronyms

AASHTO	American Association of State Highway and Transportation
HFMI	High Frequency Mechanical Impact post welding treatment
SMAW	Shielded Metal Arc Weld
IIW	International Institute of Welding
SCF	Stress Concentration Factor
CAFL	Constant Amplitude Fatigue Limit
ENS	Effective Notch Stress
NS	Nominal Stress
FE	Finite Element
FEM	Finite Element Method
BEM	Boundary Element Method
ISR	Intermidiate stress range
HDR	High stress range

Greek symbols

σ	Stress
$\Delta\sigma/S_r$	Stress range
$\Delta\sigma_C$	Stress range at $N = 2 \times 10^6$ (Detail category)
$\Delta\sigma_D$	Stress range at knee-point $N = 1 \times 10^7$ (CAFL)
$\Delta\sigma_L$	Stress range at $N = 1 \times 10^8$ (Cut-of-limit)
σ_n	Normal Nominal stress
σ_m	Normal nominal stress calculated with normal load, N
σ_b	Normal nominal stress calculated with bending moment, M
$\sigma_{n.w}$	Nominal stress transverse through weld
$\sigma_\perp$	Perpendicular normal nominal stress
$\tau_\perp$	Perpendicular shear nominal stress
σ_{max}/S_{max}	Maximum (amplitude) stress
σ_{min}/S_{min}	Minimum (amplitude) stress
ϕ	Diameter
α	Angle degree
δ	Deflection
ν	Poisson's ratio

Roman symbols

a	Weld throat thickness
t	Plate thickness
t_c	Cover-plate thickness
t_b	Base-plate thickness
b	Width
L	Length
c	Distance to neutral axis
M	Bending moment
V	Shear force
I	Moment of inertia
W	Section modulus
E	Elastic modulus
P	Applied load
P_{min}	Minimum load
f_y	Yeild stress
N	Number of load cycles
m	Slope of fatigue design curve at $\Delta\sigma_i > \Delta\sigma_C$
m'	Slope of fatigue design curve at $\Delta\sigma_C > \Delta\sigma_i > \Delta\sigma_D$
r_{ref}	Reference radius

r	Ratio between calculated design load cycles at weld toe and root
k_f/K_f	Stress concentration factor (SCF)
K_w	Effective notch stress concentration factor
R	Stress ratio (R-ratio)
$f(t)$	Thickness reduction factor
t_{eff}	Effective thickness
n	Correction factor
P_s	Survival probability
U	Transnational degree of freedom
UR	Rotational degree of freedom

Contents

List of Figures

List of Tables

1
Introduction

1.1 Background

Europe witnessed significant growth in infrastructure (Haghani et al., 2012) including bridges during industrial development in the 20th century and many of today's bridges date from that period. A survey conducted in 2004 (6th Framework Programme of EU, 2007) found that 67 % of railway bridges across the continent are older than 50 years with more than 35 % over 100 years old. This means that several current bridges have already surpassed their designed lifespan. In addition, because of the increase in traffic, today's bridges experience more load. It has therefore became necessary to either build new bridges that meet the current traffic demands, or repair and strengthen the old ones in order to remain steadfast and serve their purpose. Because constructing new bridges (6th Framework Programme of EU, 2007) is a very expensive and non-environmental solution, efforts have been made to find effective ways to strengthen and upgrade old steel beam bridges. One efficient method for enhancing steel beam bridges is by increasing the cross-section of structural members by adding additional material.

For this purpose, cover-plates are commonly fastened in highly loaded areas to reinforce, upgrade, and extend the life of existing steel beam bridges. The methods (Hu, 2011) by which the cover-plates are fixed to the attached elements have varied over the years between bolted and welded connections and each method offers its own advantages and challenges. Bolted connections are commonly used today but because one cover-plate can have hundreds of bolts and a bridge thousands, the installation is very time-consuming compared to welded cover-plates. Thus, welded cover-plates are still desirable as an alternative to bolted ones.

In the past and before there was sufficient knowledge about fatigue performance and fatigue failure, many old steel beam bridges (Vilhauer et al., 2012) were strengthened using welded cover-plates. But the use of welded cover-plates has dramatically decreased after many cases of bridges failing with welded cover-plates. The Yellow Mill Pond Bridge in Connecticut and the King's Bridge in Melbourne are two examples of such bridges (Haghani et al., 2012). Whose failures were caused by fatigue cracks developed at the end of the welded cover-plates. So it was discovered that these welded cover-plates offered poor fatigue performance, particularly at their ends. The reason for this (Haghani et al., 2012) is explained by stress behaviour at the end, where the stress is concentrated due to the change in the cross section.

Accordingly, it has been observed (Marquis & Barsoum, 2016) that the fatigue strength of cover-plates can be enhanced, if the stress concentration at the end region is reduced. Therefore, many research studies have been conducted to come up with efficient methods

for reducing stress concentrations, thus trying to extend the fatigue life of welded cover-plates.

High-frequency Mechanical Impact (HFMI) treatment has drawn researchers' attention as one of the most promising methods to increase fatigue strength for welded details. The term HFMI has been used for about a decade. It was first introduced (Marquis & Barsoum, 2016) by 2010 Commission XIII (Fatigue of welded components and structures) of IIW (the International Institute of Welding) to refer to a number of applications. The main principle of those applications (Shams-Hakimi, 2017) is to apply a high-frequency impact of more than 90 Hz at the toe of the welds. A primary benefit of this method is the reduction of tensile residual stresses at the weld toe, as well as smoothing the surface near the weld toe that reduces geometric stress concentration. Moreover, treated details have better cracking resistance than untreated details because the treatment improves the local hardness of the material.

1.2 Aim

The aim of this thesis is to evaluate if welded cover-plates treated with HFMI is a possible solution for strengthening steel bridges, and examine if the current bolted solution can be replaced.

1.3 Objective

To achieve the project's aim, the work is divided into the following steps:

1. Fundamental knowledge relevant to the field of study will be established through a literature review.

2. Some previous tests conducted on HFMI-treated welded cover-plates under different load conditions (axially and in bending) will be studied and then modelled and analysed using Abaqus software according to the Effective Notch Stress method (ENS).

3. The analysis results will be evaluated and compared to the existing design S-N curves. Moreover, the interrelationship between cover-plates loaded axially and those loaded in bending will be detected.

4. Factors that may affect fatigue performance of welded cover-plates will be investigated in exploratory studies.

5. According to the evaluated results, suggestions will be made to adjust the existing design method for HFMI-treated details to be applicable for HFMI-treated cover-plates in beams loaded in bending.

1.4 Method

To fulfill the aim and objective of this master thesis, the thesis was divided into two phases, containing a total of four parts. Which were as follows:

1. The first phase involves the collection of a variety of investigated and critically reviewed scientific reports, arti cles, journals, etc, from authorised publications. Where the objective was to gather knowledge about the main subject of study. This was executed in two parts:

    - A literature study where the investigation focused on three main subjects. The first subject being about welded cover-plates, the second being about post welding treatments used to improve fatigue performance of welded details and the third and last subject being about fatigue life assessment methods.

    - A collection and review of previous research on varied welded cover-plated structures, which is to be studied and analysed for the second phase of the masters thesis.

2. The second phase consists of performing numerical Finite Element analysis of different welded cover-plated structures. Thereafter, evaluate the potential of reinforcing steel beam bridges with HFMI-treated cover-plates, from the perspective of fatigue performance. This phase was also executed in two parts:

    - Firstly, FE analyses were performed by modeling the test specimens used in the previous research in the computer software Abaqus. The obtained results were evaluated to verify the potential of HFMI-treated details compared to as-welded details for different structures. Furthermore, the characteristic load cycles were calculated to investigate if the generic designing method correlates with the previous research test results.

    - Secondly, by utilizing a cover-plated beam model specimen from the previous research. Exploratory studies were conducted to investigate the effects when various changes are made to the cover-plate design. This includes changing the location, thickness and length of the cover plate, as well as altering the end weld. Theses studies were performed to further evaluate potential variables that might need to be considered for designing HFMI-treated cover-plates.

1.5 Limitation

This project focuses on the fatigue performance of as-welded and HFMI-treated cover-plated steel structures, whose purpose is to strengthen load-carrying steel girders. In order to conduct fatigue life assessment, load cycle data needs to be collected, which can only be obtained by conducting practical tests. Hence, the first part of the project is limited to the use of previous tests. To simplify the procedure, four previous research projects were selected. For which three test specimens were modeled in Abaqus. The specimens of the previous research is limited to one axially loaded cover-plated structures and three cover-plated structures loaded in bending, where one is a flange-girder and the other two are beam girders.

Furthermore, because fatigue design is included in Serviceability limit state (SLS), elastic material properties are assumed. For the purpose of this project it is necessary to compute the weld toe and root stresses. Therefore, the Effective Notch Stress (ENS) method was implemented for the FE analyses. Henceforth, the ENS method was also used for fatigue life assessment and this means that a stress ratio (R-ratio) of < 0.15 is assumed for all models.

The purpose of the exploratory studies is to further evaluate different potential variables that can affect the fatigue performance of treated cover-plated beams. In order to limit the scope of the study, the exploratory studies were limited to four fields. Which is then limited to a set number of analyses, due to the time restriction of creating new models in Abaqus. Moreover, because the exploratory studies do not have pre-existing practical test results, the analyses are limited to evaluating stress changes at the weld notches and calculating the theoretical cracking mode through load cycles.

2

Literature review

In this chapter three subjects are studied for the literature review. Where the purpose is to gather general and specific knowledge to reinforce and clarify the aim of this master thesis. The three subjects relates to cover-plates (mainly as-welded), post welding treatments (mainly HFMI) and fatigue life assessment methods (mainly Nominal Stress method and Effective Notch Stress method).

2.1 Cover-plates

Cover-plates are often used (Wang et al., 2015) for strengthening existing bridges which have been damaged by structural aging, defected due to incorrect design or require additional capacity due to an increased in live-load. Thereby, the main purpose of cover-plates (Mohammadzadeh & Bhowmick, 2022) is to increase the buckling and bending capacity of steel beams constructing a bridge, by enhancing the stiffness and durability, or changing the structural behaviour. Mohammadzadeh and Bhowmick (2022) further explains that reinforcements are typically assembled while the structure is in service, implying that cover-plates are applied under preloading conditions, which influences the capacity of cover-plated beams.

An experiment conducted by Wang et al. (2015) on strengthening steel I-beams with welded cover-plates on both the top and bottom flanges, determined that preloading has little effect on the beam's lateral capacity as long as there are enough lateral supports. If not, the beam's capacity decreases. Nevertheless, when reinforcing a preloaded I-beam, the most economical choice is to weld the cover-plate to the bottom flange, since it is the easiest flange to access. And the study performed by Mohammadzadeh and Bhowmick (2022) showed that I-beams strengthened with welded cover-plates at the bottom flange under preloading conditions, experience a reduction in ultimate capacity. Despite that, the ultimate capacity will be greater than for non-strengthened beams, regardless of the preloading level.

Because of the inexpensiveness of increasing a steel beam bridge's life and capacity by adding cover-plates to the beams flanges, they became popular (Wang et al., 2015), and especially welded ones, due to being easy and fast to assemble. For this reason, after WWII in the 1950s the construction of highway and railway bridges expanded all around the world and cover-plated steel beam bridges were included. In the USA steel beam bridges were designed using guidelines from before the 1940s (Fisher, 1997), which had been developed from test data of small-scale specimens and with limited knowledge. In these guidelines it was stated that 2 million cycles was the fatigue life limit for welded cover-plates.

But in the late 1960s, Fisher (1997) states that fatigue cracking was frequently observed on these steel beam bridges built before and in the 50s. An example is the Yellow Mill Pond bridge constructed in 1929 seen in Figure 2.1. Fisher also mentions that during the 1960 AASHO Road Test, fatigue cracks were observed in welded cover-plated steel beams. Because of these findings, experimental studies with full-scale specimens started in 1967 to evaluate the cause of fatigue cracking. The test results concluded that the provisioned fatigue resistance design codes of 2 million cycles used in the 1940s and 50s were insufficient and optimistic. This changed the understanding and concept of fatigue design and new alterations to the design code were made, where more construction details were changed to details with lower fatigue strength.

Henceforth, there are two common ways (Hu, 2011) to fasten cover-plates to the bottom flange of a beam, either by welding or by bolted joints, but both techniques introduce their own challenges. For welded cover-plates the challenge is their fatigue strength (Haghani et al., 2012) and it is known that the cover-plate transverse end weld has very low fatigue strength. This concludes that bolted joints are used to fasten cover-plates, due to them being less prone to fatigue cracking, which is further demonstrated in Eurocode 3. Where the detail category of cover-plated beams connected with high-strength bolts has a detail category of 80-90 MPa (European standard, 2008, *Table 8.1*). While the highest fatigue detail category of welded cover-plates can reach a detail category of 56 MPa, which is shown in Figure 2.7.

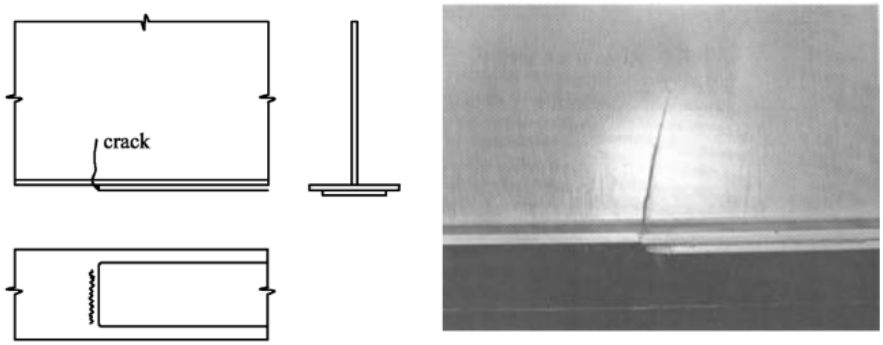

Figure 2.1: Cracks at as-welded cover-plate end from Yellow Mill Pond bridge. [Source: Table 5-3 from Kühn et al. (2008), *p.68*]

2.1.1 Fatigue strength of welded cover-plates

Among all other welded details of a bridge (Haghani et al., 2012), the end of cover-plates has the lowest fatigue strength and can be described as a lower bound on the fatigue strength of welded elements. Figure 2.2 illustrates a typical example of a welded beam with a partial cover-plate attached to the upper flange. As can be seen in the figure, the cover-plate ends have a detail category of fatigue strength E (FAT 56, see Table 2.1) while a higher fatigue strength can be found away from the edges in the longitudinal welds (Fisher, 1977).

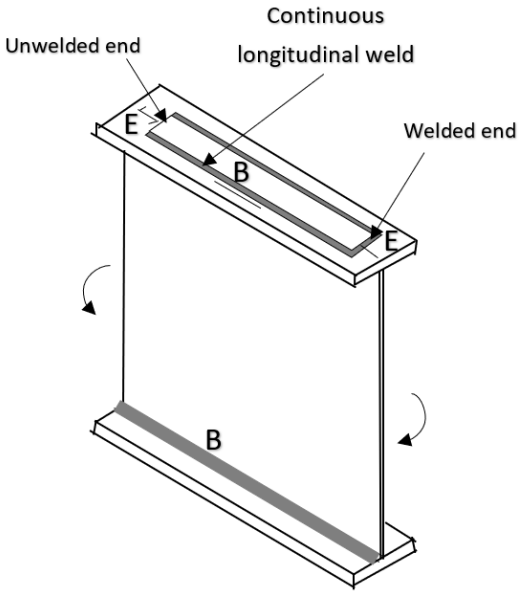

Figure 2.2: Fatigue detail categories in the AASHTO for different construction details in welded beam with a cover-plate. Category E and category B, FAT 56 and FAT 125 in Eurocode 3, see Table 2.1. [Writers own figure]

The reason for this low performance of welded cover-plates is explained (Al-Emrani & Åkesson, 2020) by the stress behaviour in the vicinity of the end of the cover-plate. In general, it is well known that the nominal stress is evenly distributed across the flange unless the cross-section changes. It is therefore inevitable that at the end of the cover-plate the stress distribution will change, as a result of the change in cross-sectional area. As a part of the structure, the cover-plate is integrated as a load-carrying element. Thus, a part of the load carried by the flange is transferred to the cover-plate through the weld. This causes the stress to be concentrated along a certain distance from the edge of the plate, called "anchorage length", and the material in this area is subjected to a higher stress level, as indicated in Figure 2.3. Due to the low section modulus of the weld, it is the most stressed area within this anchorage length. It is also the region where fatigue cracks are more likely to appear due to the existence of stress raisers at the toe of the weld.

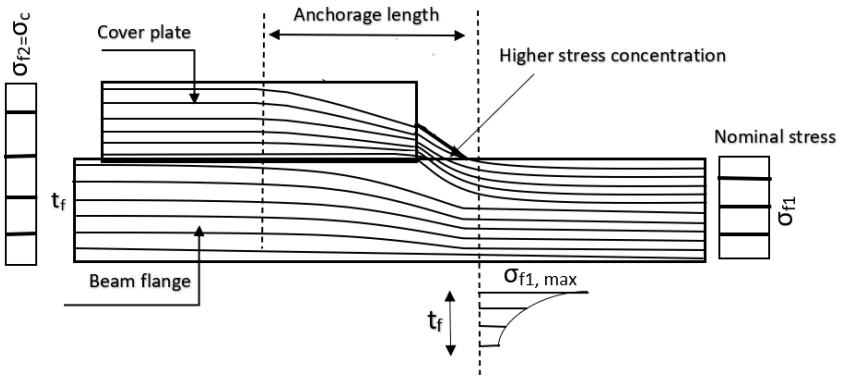

Figure 2.3: Stress distribution at the end of welded cover-plate, illustrates stress concentration at weld toe and anchorage length. [Writers own figure]

Because the sections with the lowest fatigue strength in welded cover-plates are the transverse ends, numerous investigations have been carried out to determine whether altering the end details could improve their fatigue strength. Fisher et al. (1967) published a review of related studies that have been conducted up until 1967 in order to provide appropriate recommendations for the design of welded cover-plates. The aforementioned review involved a number of fatigue tests on beams with both rolled and welded sections of various steel quality connected to cover-plates with different end details.

Examples of end details that have been studied can be found in Figure 2.4. Some of the results in terms of S-N curves can be seen in Figure 2.5 for details (c), (b) and (d) and Figure 2.6 for squared cover-plates, details (a) and (g). As can be seen in the figures, cover-plates with non-squared ends reported higher fatigue strength than traditional cover-plates with squared ends. However, the differences are not significant, and the structures will not experience much longer fatigue life. In light of this, square-ended cover-plates were strongly recommended in Fisher et al. (1967) report, as their fatigue life does not differ significantly from other shapes. Thus, avoiding an unnecessary increase in the cost of manufacturing other shaped cover-plates. The report also noted that cover-plates could be fastened to beams with both rolled and welded sections without decreasing their fatigue strength.

Furthermore, in the study program conducted by Fisher et al. (1969), 374 rolled and welded beams with different welded details were examined. A total of 240 beams with cover-plates of various thicknesses, geometries and steel qualities were tested to evaluate their fatigue performance. All cover-plates were fastened to the beams by two longitudinal welds and one transverse weld at one edge while the other edge was unwelded. It has been observed from the test results that, as long as the cover-plate is narrower than the attached flange, the presence of transverse welds does not affect the fatigue strength of welded cover-plates. In contrast, the test results showed that when the cover-plate is wider than the flanges, beams without transverse end welds (Figure 2.4, detail(h)) exhibited lower fatigue strength than beams with transverse end welds.

A further conclusion from Fisher et al. (1969) test was that the quality of steel has no significant effect on fatigue strength of welded cover-plates. So using steel with a higher yield strength will not increase their fatigue life. In addition, results showed that specimens with multiple cover-plates had the same fatigue strength as those with only one cover-plate.

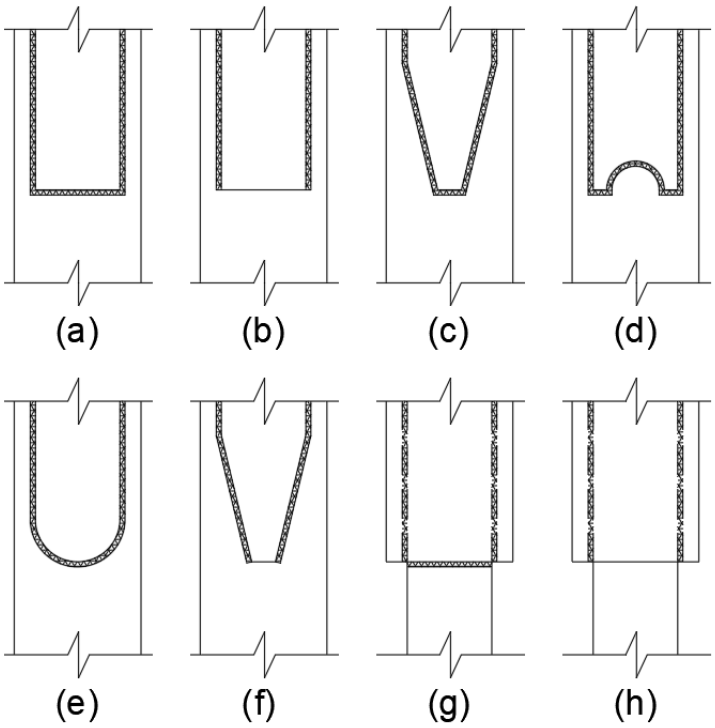

Figure 2.4: Examples of welded cover-plates with different geometries and end details. Detail (h) has lower fatigue strength than other details. [Writers own figure based from Fisher et al.(1967), *p.101*]

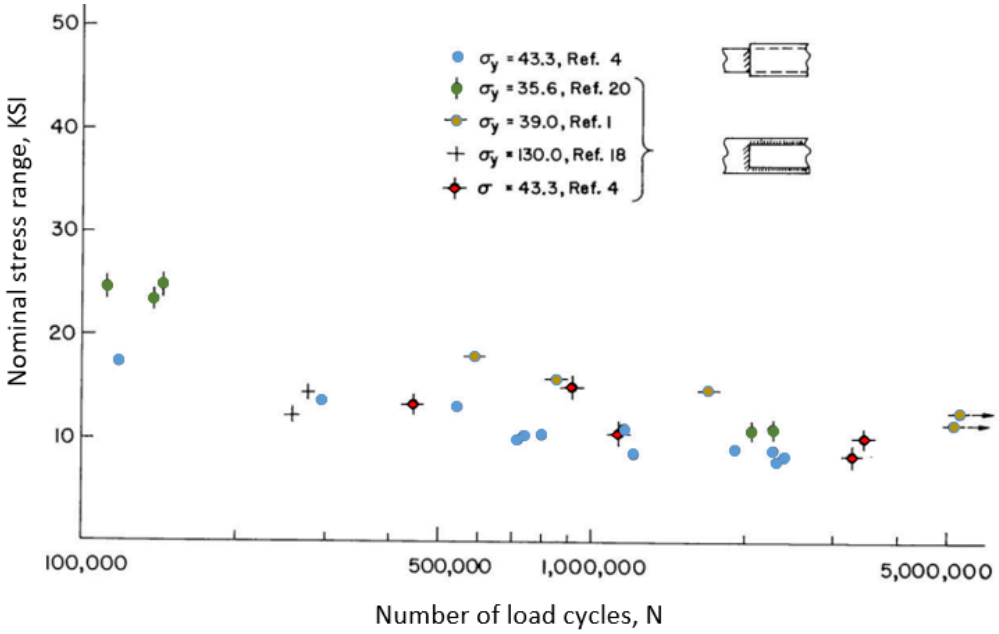

Figure 2.5: S-N relationship for beams with partial length squared cover-plates with different end details (g) and (a). [Writers own figure based on data from Figure 7 from Fisher et al.(1967), *p.103*]

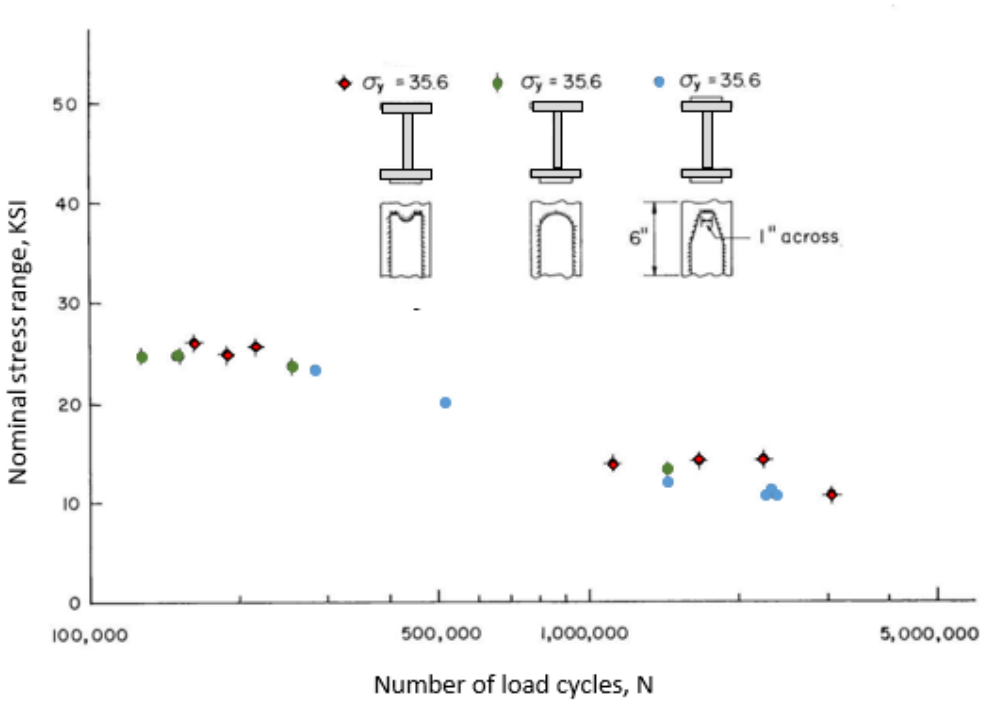

Figure 2.6: S-N relationship for beams with partial length cover-plates with different end details (d), (e) and (c). [Writers own figure based on data from Figure 6 from Fisher et al. (1967), *p.103*]

Although in some cases the end weld does not affect the fatigue strength of welded cover-plates, it is still imperative to have an end weld (Haghani et al., 2012) to provide a continuous seal around the cover-plate. This is necessary to prevent water and moisture from getting between the cover-plate and the attached flange and causing corrosion damage to the beam. In such cases, if water gets between the cover-plate and the attached flange, corrosion damage is likely to occur as it takes a long time for such details to dry out, as noted by Department of Transportation (2017).

Depending on the reinforcement requirements for different structures, cover-plates can be of various lengths. The effect of the cover-plate length on fatigue strength was investigated, and research has shown (Fisher et al., 1974) that the length of the cover-plate does not affect the stress concentration at the edge. In other words, fatigue strength remains the same no matter the length of the cover-plate. There is, however, a tendency (Hui et al., 2018) for fatigue resistance of cover-plates to decrease in large structures. This conclusion was reached after several instances of fatigue damage were discovered in large structures with cover-plates. In this case, the Yellow Mill Pond bridge is an excellent example as many cracks were found at the edges of the cover-plates even though the bridge was only 13 years old. The fatigue damages that have been discovered in this bridge inspired Fisher et al. (1979) to conduct a test to investigate the fatigue performance of cover-plates attached to large girders. In this test, rolled beams of 20 feet in length were studied under constant cyclic fatigue loading. Based on the test results, these specimens exhibited lower fatigue strength compared to the smaller beams tested by Fisher et al. in 1969. Accordingly, Fisher et al. (1979) proposed a fatigue category E' to account for the decrease in fatigue strength of cover-plates in large structures.

As a result of all studies and research, Eurocode 3 (European Standard, 2022) specified one fatigue strength class for all cover-plates regardless of their geometries, lengths and shapes. The only factors to consider are the thickness of the cover-plate and the attached flange. However, it was mentioned by Albrecht et al. (2007) that the thickness of the element where the cracks are propagated (typically the flange in the case of bridge-strengthening cover-plates) has the greatest influence on the fatigue strength of welded cover-plates. Figure 2.7 shows the Eurocode 3 fatigue detail category for cover-plates with various flange thicknesses.

Eurocode 3 (European standard, 2008) defines a minimum length of 300 mm for welded cover-plates that are assigned according to the fatigue detail categories shown in Figure 2.7. Shorter attachments have higher fatigue strength and the fatigue detail category for such details can be found in Table 8.1 (detail 10-12) in Eurocode 3 (2008). It is also worth mentioning again that an end weld is required for cover-plates wider than the flanges to achieve the same fatigue strength shown in Figure 2.7.

	$t_c<t$	$t_c \geq t$
56*	$t \leq 20$	-
50	$20<t \leq 30$	$t \leq 20$
45	$30<t \leq 50$	$20<t \leq 30$
40	$t>50$	$30<t \leq 50$
36	-	$t>50$

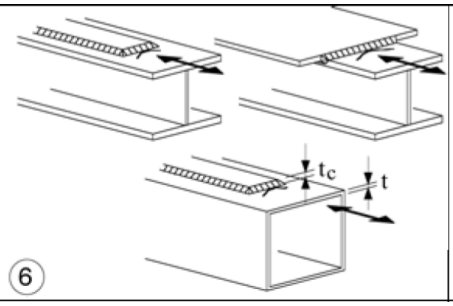

Cover plates in beams and plate girders:

6) End zones of single or multiple welded cover plates, with or without transverse end weld.

Figure 2.7: Fatigue detail category for cover-plates with a plate thickness t_c in relation to the flange thicknesses t. [Source: Table 10.6 from European standard (2008)]

Table 2.1: AASHTO detail categories converted to the characteristic nominal stress ranges. [Source: Table 5 from Bowman et al. (2012)]

Detail category	Nominal stress range	
	ksi	MPa
A	23.2	160
B	18.1	125
B'	14.5	100
C	13	90
D	10.3	71
E	8.1	56
E'	5.8	40

2.2 Welding treatments to improve fatigue life of welded structures

Welded details are highly susceptible to fatigue cracking accumulated from cyclic live-loads, also known as load-induced fatigue, consequently (Hui et al., 2018) because of defects and tensile residual stresses that's introduced during welding. This wasn't well understood before the 1960s, explain Fisher (1997), where he specify that the tests completed in the 60s were the first tests to confirm what initiates fatigue cracking. Which is the results of the materials' initial discontinuities, such as defects, stress concentration regions and tensile residual stresses.

It has been observed (Fisher, 1997) that defects caused by internal discontinuities, such as porosity and trapped slag from incomplete fusion between base metal and weld metal, can cause fatigue cracking. Other type of defects (Marquis & Barsoum, 2016), such as imperfections in weld toe geometry, disturbs the stress field and introduce local stress concentrations at the toe between weld and plate, causing micro-cracks that may grow larger under tensile induced-loading. Furthermore, Hui et al. (2018) and Fisher (1997) specify that tensile residual stresses are the result of the weldment gradually cooling. The surface cools and hardens faster than the interior, which restrains the still contracting interior, creating tensile stresses that are locked at the weld toe. These tensile residual stresses can be as high as the weld metals yield strength. Hence, when cyclic tensile stresses are introduced at the weld toe, fatigue cracking and low fatigue life can be anticipated.

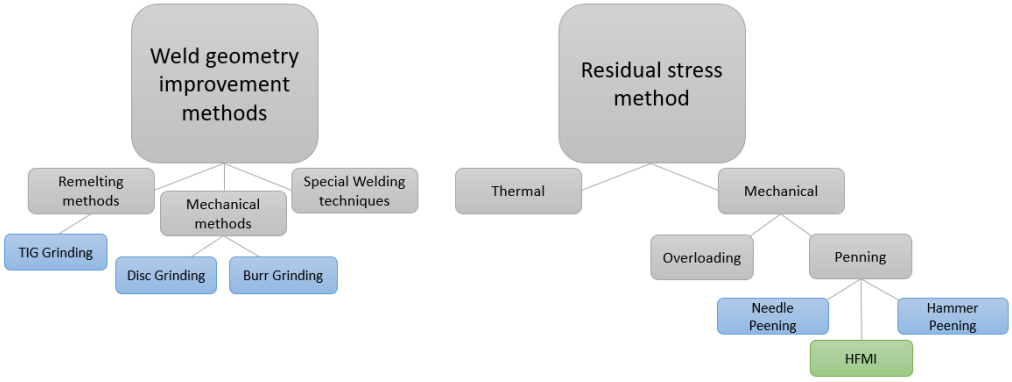

Figure 2.8: Overview of different weld improvement methods. The *blue* techniques are covered by IIW and the *green* is the method covered in this master thesis. [Writers own figure based on Figure 1 from Marquis and Barsoum (2016), *p.4*]

There are two main post welding treatments (Marquis & Barsoum, 2016) to improve welded connections, as seen in Figure 2.8. The first one is Weld Geometry Improvement Methods, like Burr Grinding. Their intention is to reduce stress concentration and improve surface transition from base-plate to weld toe by locally modify the weld toe geometry.

The second post treatment is the Residual Stress Method, which includes mechanical techniques like Needle Peening and HFMI. Whose purpose is to reduce the tensile residual stresses sealed at the weld toe by introducing compressive residual stresses. Thereby, the tensile strength of the welded connection is improved and can withstand larger tensile cyclic-loading, hence increasing its fatigue life.

Furthermore, excluding post welding treatments, the first optimisation to improve a steel structure's fatigue performance (Marquis & Barsoum, 2016) is by applying good design practice during design process. Some practices include selecting joints with a low stress concentration factor, or locating high stress regions so welded connections can be placed in areas with low stresses.

2.2.1 HFMI-treatment of welded joints

The term HFMI was commissioned in 2010 to be the generic term for similar post welding treatment technologies (Marquis & Barsoum, 2016), such as Ultrasonic impact treatment (UIT), Ultrasonic penning (UP), High frequency impact treatment (HiFiT) and Pneumatic impact treatment (PIT). See Figure 2.10(a-c). HFMI is mainly used to induce compressive residual stresses at the weld toe to increase the fatigue strength of welded connections. However, HFMI also has weld geometry improvement qualities, which improve local geometry by changing the micro-structure, eliminating defects and smoothing the transition between plate and weld. Thus, HFMI has a double effect on improving fatigue strength, as seen in Figure 2.9.

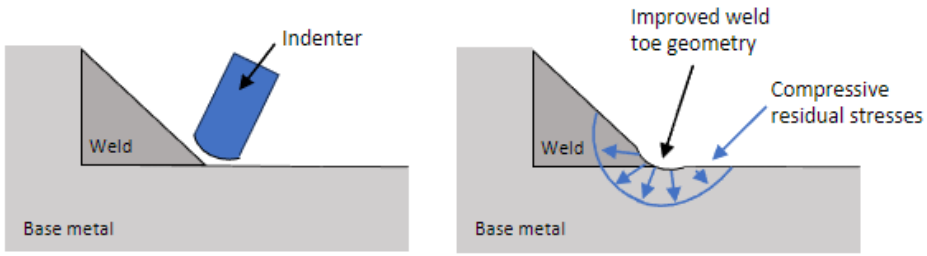

Figure 2.9: Example on HFMI application technique. [Writers own figure based on Figure 6 from Fuštar et al. (2020), *p.424*]

For how HFMI works and how to apply the treatment, it can be read in the guide line "*IIW Collection IIW Recommendations for the HFMI Treatment For Improving the Fatigue Strength of Welded Joints*". Where IIW (Marquis & Barsoum, 2016) specify that the main working principle of HFMI is to apply compressive stresses utilizing an accelerated indenter with a high frequency over >90 Hz at the toe of the welded joints. There exists many devices worldwide with similar operating principles, as seen in Figure 2.10(a-c), which provide the same quality of fatigue improvement when accurately used. All ultrasonic devices contains a power unit and tools. The tools, called indenters, whose tip can be customized by the manufacturer with different diameters, configurations and geometries, as seen in Figure 2.10(d).

To utilize the full effect of the treatment, IIW (Marquis & Barsoum, 2016) highlights that HFMI-treatment is to be applied during construction. So that the tensile stresses from the structures dead weight are taken into account when compressive residual stresses are implemented, otherwise, the effect will be neglected. Additionally, IIW highlights that when the weld toe is treated with HFMI, the possibility of fatigue failure shifting to another location must always be taken into consideration during design. For an example, shifting from toe failure to root failure. Because there is a possibility that the intended improvement in fatigue performance may be insufficient and the treatment will be rendered

meaningless for some details. This is due to fatigue root failure being governed by a different design S-N curve than fatigue toe failure.

(a) High frequency impact treatment tool (HiFiT)

(b) Pneumatic impact treatment tool (PIT)

(c) Ultrasonic impact treatment tool (UIT)

(d) Different indernters modifications

Figure 2.10: Different examples of HFMI-treatment devices in (a), (b) and (c). Figure (d) shows different indenter modifications that can be manufactured. [Source: Figure 3 and 4 from Marquis and Barsoum (2016), *pp.6-7*]

IIW 2016 does also gives guidelines on how to post treat welds with HFMI. It is explained that some weld preparations and conditions are to be considered for treatment. This includes identifying fatigue-prone details of the structure, which is crucial for a cost-efficient procedure. Furthermore, if some defects prior to treatment are observed, some light grinding can be necessary. However, IIW 2016 explain that crack-like defects due to insufficient contact between weld and base metal are unavoidable, but these dose not necessarily decrease the improved fatigue performance.

After the treatment is completed, additional recommendations are provided. IIW (Marquis & Barsoum, 2016) 2016 establish that other post-weld treatments should not be applied to HFMI-treated welds. What could occur is that the benefits of introducing compressive residual stresses with HFMI may be reduced or eliminated by the benefits of other treatments. It is therefore to be assumed that the fatigue strength acquired from HFMI can not be accounted for, instead, only the fatigue strength acquired from the other post-treatment can be considered. But for proper identification, the weld's fatigue strength should be determined by fatigue testing.

2.3 Fatigue life assessment methods

Fatigue strength analysis (Kaffenberger et al., 2012) is often performed using S-N curves, and a variety of assessment approaches can be used to estimate the fatigue life of welded structures. Generally, the approaches are categorized into two main groups: Global approaches and Local approaches, see Figure 2.11. In addition to those two groups, the Structural Stress approach (Heshmati et al., 2012) lies between the global and the local approaches. This method considers stress concentrations caused only by overall geometry and ignores the influence of weld geometry.

For global approaches, each component is evaluated using its own S-N curve based on the assumption of a uniform or linear stress distribution as a result of external loads (Kaffenberger et al., 2012). One example of a global approach (Heshmati et al., 2012) is the Nominal Stress method which is the most dominant approach since it has been used for a long time as the basis of most codes. This is a simplified method since it considers only the overall stress distribution and ignores stress concentration caused by many reasons, such as a change in the cross-section or the presence of a weld. Thus, the results obtained by this method might not be accurate. In addition, the method is not applicable to complicated details that normally exist in large structures.

In comparison to global approaches, local approaches (Heshmati et al., 2012) offer a more realistic estimation of fatigue life, especially for complicated details. This is due to the consideration of local stress concentrations caused by changes in geometries and loading conditions. Thus, such approaches are more appropriate for fatigue life estimation of large structures such as bridges where different loads are applied and complex details exists. However, analytical estimation of local stresses for some details can be very difficult, so a computer-based analysis method such as FEM is needed to determine the stresses at critical points. Thus, different computer-based local approaches have been developed to estimate the fatigue life of various components with high accuracy and efficiency.

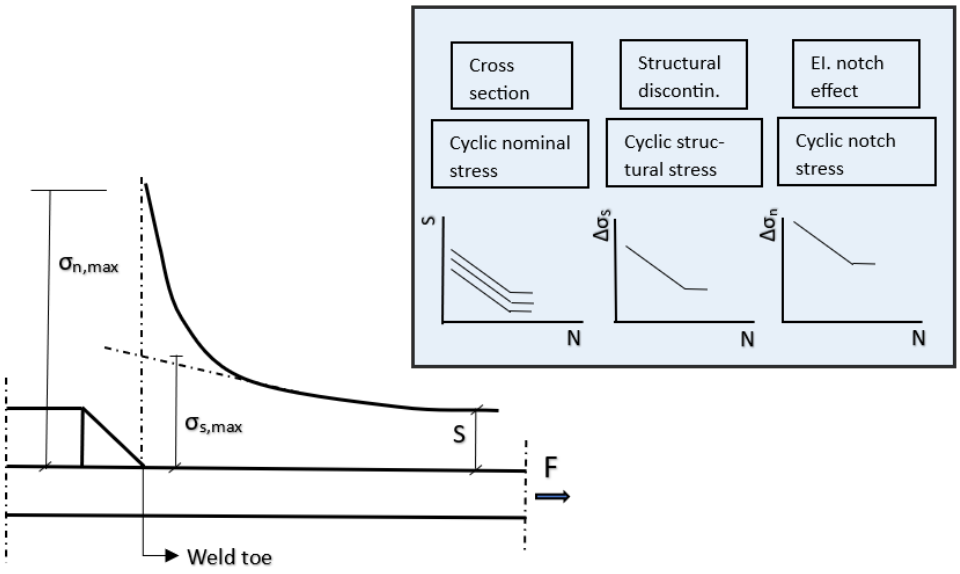

Figure 2.11: Global and Local fatigue life assessment approaches. [Writers own figure based on Figure 2 from Kaffenberger et al.(2012), *p.288*]

Overall there are three popular assessment methods (Hobbacher, 2016) to determine the fatigue strength of as-welded joints. The three methods are: the Nominal Stress method, the Structural Hot-Spot Stress method or the Effective Notch Stress method. The same assessment methods can be used for HFMI-treated welded joints (Marquis & Barsoum, 2016). The difference being that design resistance curves (S-N curves) and detail categories of treated welded joints are significantly higher than non-treated welded joints. This master thesis will focus on the Nominal Stress method and Effective Notch Stress method when discussing the theory of designing HFMI-treated joints in this section, and the Effective Notch Stress method is used for the structural analyses performed in chapter 4.

2.3.1 Nominal Stress method

Nominal Stress method (Radaj et al., 2006) is a common global assessment method for fatigue design, as stated in section 2.3, and is universally used within fields of mechanical and structural engineering. It can therefore be found in design guidelines such as IIW and Eurocode 3. The fields of engineering that do not use the Nominal Stress method are for example, aircraft engineering (Radaj et al., 2006). Where, due to the high demands for lightweight structures and exceptional tolerance against damage, the preferred assessment method to apply being that of local approaches.

For non-welded construction details and construction details that are predetermined to fail at the weld toe, the nominal stress (European Standard, 2022) is calculated as the normal or shear stress at a sectional area of the base-metal that's influenced by a load. Thereby, the nominal normal stress (Fricke, 2011) can be calculated with Equation 2.1 for details loaded in axial force and Equation 2.2 for details loaded in bending.

$$\sigma_{n.m} = \frac{F}{A} \tag{2.1}$$

$$\sigma_{n.b} = \frac{M}{W} \tag{2.2}$$

When calculating nominal stress the increasing stress effects of the welded joint are not taken into consideration (Hobbacher, 2016). However, it is important to consider the effect of the micro-geometric shape of a member. Depending on the sectional shape of a construction detail, the nominal stress may vary over different sections and redistribution of stresses may occur. In addition to micro-geometric shapes, this is also the case for components influenced by concentrated loads. Redistribution is considered by calculating the local modified nominal stress of each section. Which according to European Standard (2022) is accomplished by multiplying the nominal stress σ_n with a stress concentration factor k_f, as illustrated in Figure 2.12.

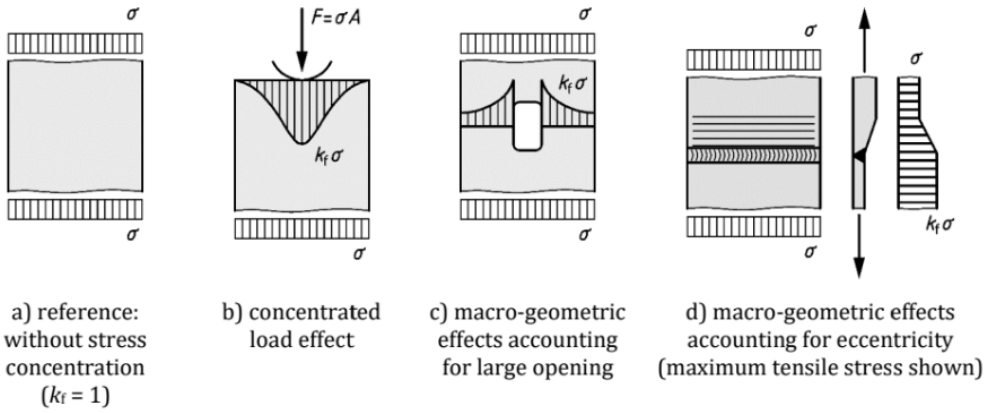

Figure 2.12: Illustration of concentration factor k_f for four different load and geometric effects, where σ is the nominal stress, k_f is the concentration factor,A is the cross-sectional area and F is the concentrated load. [Source: European Standard (2022), *p.11*]

For construction details with predetermined weld root failure, the failure mode (Fricke, 2011) depends on the stress located in the weld rather than the parent steel plate. This is shown in Figure 2.3, where the stresses from the parent plate are transferred through the weld to the welded plate, which only occurs for load-carrying welds. The relevant nominal stresses to consider for root failure are at the weld throat, which (European Standard, 2022) are the nominal stresses σ_{wf} transverse to the weld axis and the shear stresses τ_{wf} longitudinal to the weld axis. By dividing these with the throat size a the stresses in the weld can be calculated with Equation 2.3.

$$\sigma_{n.w} = \sqrt{\sigma_{\perp}^2 + \tau_{\perp}^2} \tag{2.3}$$

2.3.1.1 Nominal Stress method for as-welded joints

For welded structures (Radaj et al., 2006), S-N curves are determined based on the joints detailing, loading conditions and quality of manufacture, and can be found in IIW and Eurocode 3. The data needed to determine the S-N curves (Hobbacher, 2016) are derived from extensive experimental testing of small and large specimens subjected to constant or variable amplitude loading. Each S-N curve is assigned a fatigue class in MPa, known as FAT-class or as detail category in Eurocode 3. And the class is established by the detail's characteristic fatigue strength at 2 million load cycles.

The S-N curves for normal stresses (Hobbacher, 2016) are linearised with a slope of $m = 3$ up to the constant amplitude knee point of $N = 10^7$ load cycles. Thereafter, the common assumption is that the slope changes to a horizontal line. In theory this corresponds to no fatigue limit below the line where no failure will occur and is known as the constant amplitude fatigue limit (CAFL). Henceforth, the S-N curves for each construction detail with a corresponding FAT-class (Radaj et al., 2006) are genially parallelised and equidistantly positioned within a logarithmic scale graph, which can be seen in Figure 2.13.

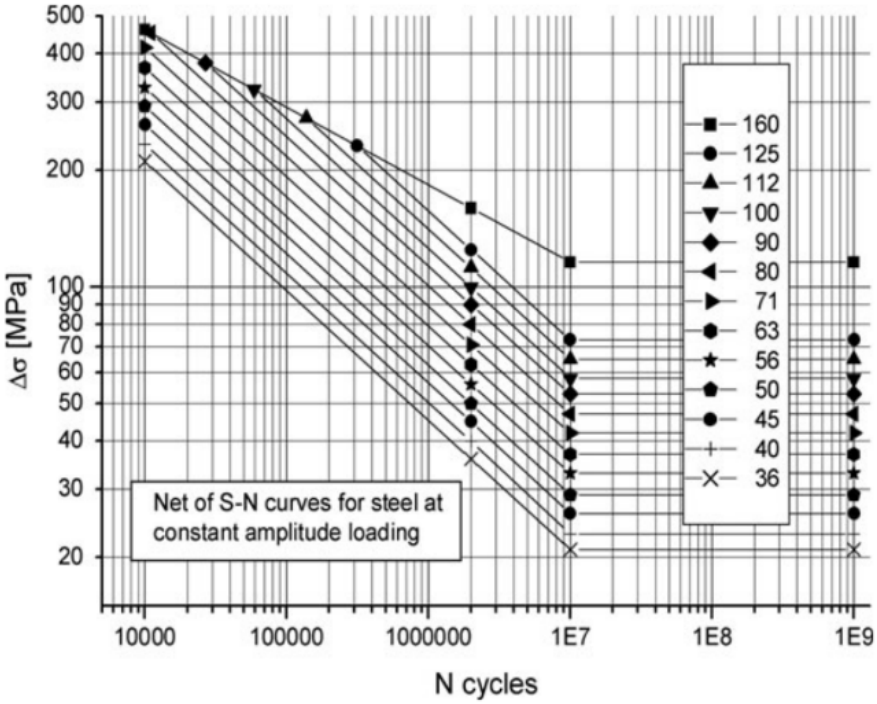

Figure 2.13: IIW fatigue resistance S-N curve for normal stresses in steel, with standard application. [Source: Figure 3.1 from Hobbacher (2016), *p.38*]

The S-N curves for shear stresses differ from the S-N curves for normal stresses. This is due to the existence of only two FAT-classes for all construction details, FAT 80 and FAT 100. The slope of the curves is also different. The slope is that of $m = 5$ up to the knee point of $N = 10^8$ load cycles (Hobbacher, 2016) and then continues as a horizontal line. But the S-N curves for shear stresses are arranged the same within a logarithmic graph as for normal stresses.

However, Hobbacher (2016) writes that the latest experimental data reveal that the common assumption of CAFL after the first knee point does not reflect reality and technically does not exist. Instead the S-N curves should have a decline of about 10% per load cycle decade, which gives a slope of $m = 22$, for both normal and shear S-N curves. Hobbacher further highlights that these S-N curves are used for structures needed to withstand constant amplitude loading, while for variable amplitude load the slope is that of $m = 9$. On the other hand, Eurocode 3 (2008 and 2022) includes a declining CAFL with a slope of $m = 5$ up to the knee point of $N = 10^8$ in the normal stress S-N curve graph, as seen in Figure 2.14. Thereafter, there should be a horizontal line known as the fatigue failure cut-off limit, where no fatigue failure occurs. However, European standard (2008 and 2022) does not include this in the S-N curves for shear stress.

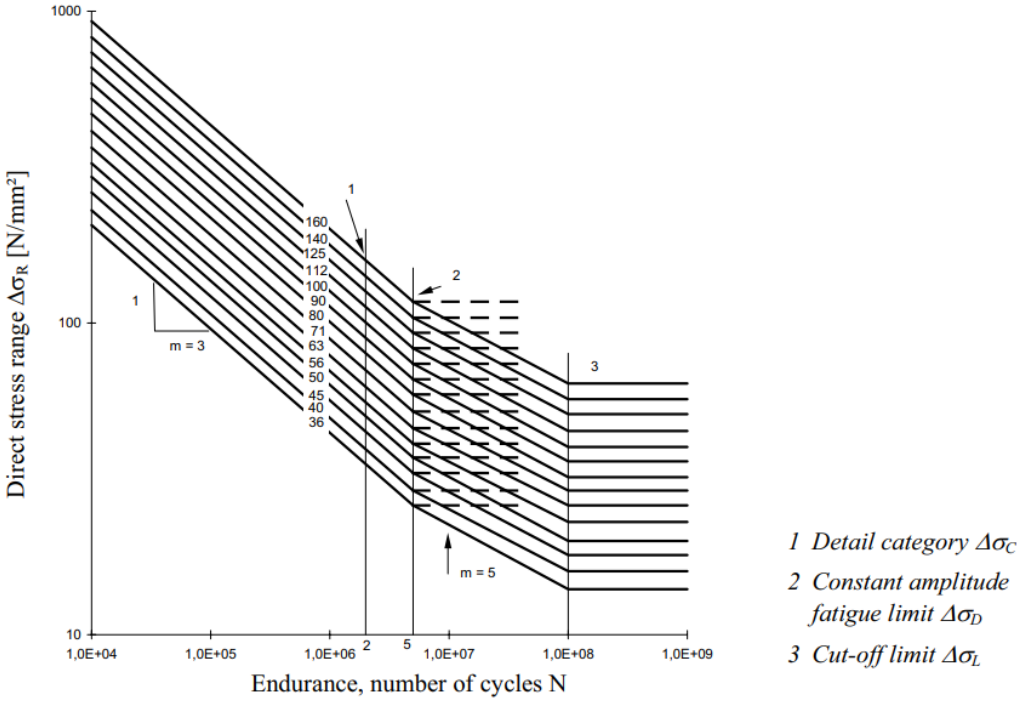

Figure 2.14: Eurocode 3 fatigue resistance S-N curve for normal stresses in direct stress range. [Source: Figure 7.1 from European standard (2008), *p.15*]

2.3.1.2 Nominal Stress method for HFMI-treated joints

When applying HFMI-treatment to the toe of as-welded construction details the fatigue strength will improve and the FAT-class increases. The FAT-classes for three construction details improved by HFMI have been determined in the updated Eurocode 3 (European Standard, 2022). However, Marquis and Barsoum (2016) writes that IIW has published S-N curves for normal stress ranges of welds treated with HFMI, that has an as-welded detail category of FAT 50 to FAT 90. Higher detail categories are not included because they contain non-welded details, as well as details not governed by toe failure.

The slope of these S-N curves is that of $m = 5$ up to the knee point of $N = 10^7$ load cycles. For cases with constant amplitude loading, IIW recommend (Marquis & Barsoum, 2016) a slope change of $m' = 22$ at load cycles $> N = 10^7$, which is the same for as-welded construction details. While for more common cases of variable amplitude loading, IIW recommends a slope change of $m' = (2m-1)$, which is equivalent to a slope of $m' = 9$ after the knee point of $N = 10^7$ load cycles. This change in slope from $m = 5$ to $m' = 9$, does the updated Eurocode 3 (2022) also recommend for construction details improved with HFMI.

When designating a S-N curve for HFMI-treated welded construction details, the steel strength of the joint needs to be considered, which is not needed for as-welded joints. This (Marquis & Barsoum, 2016) is because, for every 200 MPa increase in static yield strength the fatigue strength will increase of about 12.5% in strength. Hence, the characteristic nominal stress S-N curves for as-welded details of FAT 50 to FAT 90 have different curves for each interval of steel strength. S-N curves for joints of steel strength of $f_y < 355$ MPa, 355 MPa $\leq f_y \leq$ 550 MPa, 550 MPa $\leq f_y \leq$ 750 MPa, 750 MPa $\leq f_y \leq$ 950 MPa and $f_y \geq 950$ MPa can be seen in Figure 2.15.

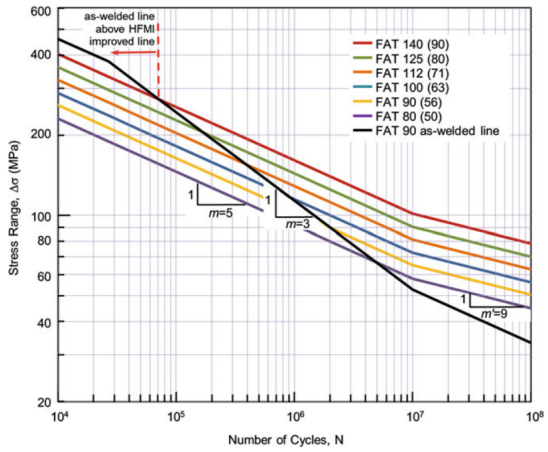

(a) S-N curve for joints in steel strength $f_y <$ 355 MPa (includes as-welded curve of FAT 90 as reference to curve FAT 140)

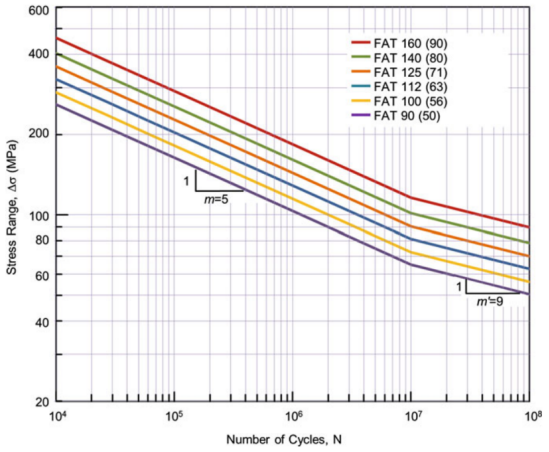

(b) S-N curve for joints in steel strength 355 MPa $\leq f_y \leq$ 550 MPa

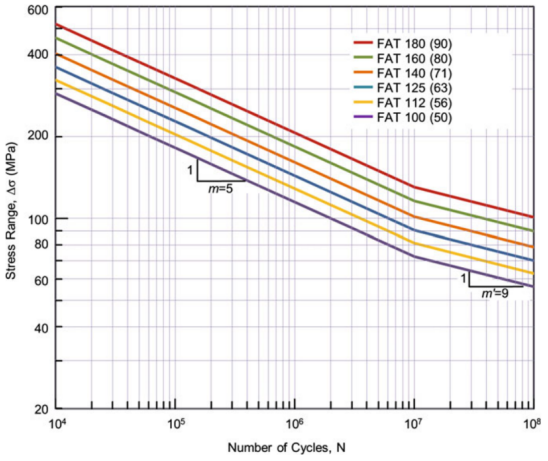

(c) S-N curve for joints in steel strength 550 MPa $\leq f_y \leq$ 750 MPa

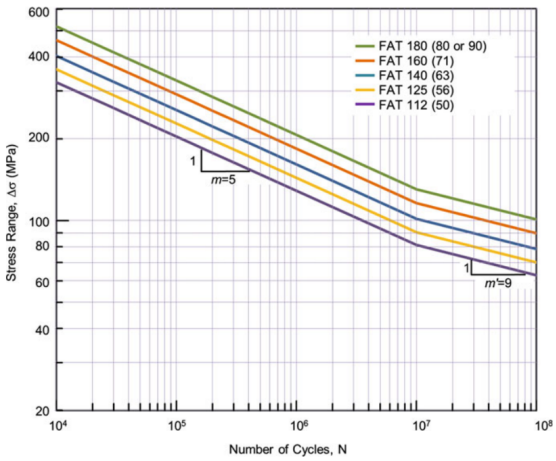

(d) S-N curve for joints in steel strength 750 MPa $\leq f_y \leq$ 950 MPa

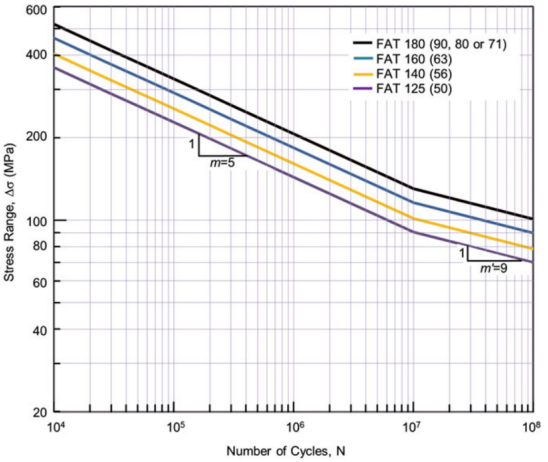

(e) S-N curve for joints in steel strength $f_y \geq$ 950 MPa

Figure 2.15: In Figure (a), (b), (c), (d) and (e) shows the complete characteristic nominal stress S-N curve for HFMI-treated welded joints of different steel strengths based on stress ratio $R \leq 0.15$. The value within the "()" represents the FAT-class of the corresponding joint in as-welded state. [Source: Figure 14, 17, 18, 19 and 20 from Marquis and Barsoum (2016), *pp.18-23*]

2.3.1.3 Modifications to fatigue strength when designing with Nominal Stress method

When designing the fatigue resistance of welded joints using the nominal stress approach some design requirements must be considered for both as-welded and HFMI-treated welds.

The first factor is the effect of plate thickness. Which (Hobbacher, 2016) needs to be considered in cases where fatigue failure is possible at the weld toe. The fatigue strength of the S-N curves given by IIW are for members with a maximum plate thickness of 25 mm. Hereby, the FAT-class of thicker members is to be multiplied with a thickness reduction factor $f(t)$, which is stated in Equation 2.4. Where the correction exponent n equals to 0.3 for as-welded joints (Hobbacher, 2016) and 0.2 for HFMI-treated joints (Marquis & Barsoum, 2016). The effective thickness is the thickness of the member $t_{eff} = t$ for when $\frac{L}{t} \geq 2$ and $t_{eff} = \frac{L}{2}$ for when $\frac{L}{t} < 2$. For members thinner than 25 mm, or have a t_{eff} value smaller than 25 mm, no reduction of the FAT-class is needed. But for very thin members, the FAT-class can be increase with the same Equation.

$$f(t) = \left(\frac{25}{t_{eff}}\right)^n \tag{2.4}$$

Another aspect to consider that influences the FAT-class of both as-welded and HFMI-treated welded joints (Radaj et al., 2006) is the stress ratio (R-ratio), which is a factor for the mean stress effect applied to welded joints (Fricke, 2011). For constant stress ranges, the stress ratio can be calculated as the ratio between the minimum stress σ_{min} and the maximum stress σ_{max}, and is calculated with Equation 2.5.

$$R = \frac{\sigma_{min}}{\sigma_{max}} \tag{2.5}$$

It is known (Fricke, 2013) that high tensile residual stresses have a negative effect and reduce fatigue performance. In contrast, compressive residual stresses have a positive effect and increase fatigue performance. Therefore, when considering the effect of stress ratio and residual stresses (compressive or tensile), Hobbacher (2016) writes that for non-welded and thin plated as-welded steel members, there is a fatigue enhancement factors $f(R)$ which increases the FAT-class for different stress ratios smaller than $R < 0.5$. In contrast, for complex as-welded members the FAT-class is unchanged, and only reduces under special circumstances. Although, according to Marquis and Barsoum (2016) there is a reduction in FAT-classes for HFMI-treated complicated welded members with a stress ratio larger than $R > 0.15$, which can be seen in Table 2.2.

Table 2.2: IIW minimum FAT-class reduction for HFMI-treated welded joints based on stress ratio (R-ratio). [Source: Table 4 from Marquis and Barsoum (2016), *p.23*]

R ratio	Minimum FAT class reduction
R $\leq$ 0.15	No reduction due to stress ratio
0.15 < R $\leq$ 0.28	One FAT class reduction
0.28 < R $\leq$ 0.4	Two FAT classes reduction
0.4 < R $\leq$ 0.52	Three FAT classes reduction
0.52 < R	No data available. The degree of improvement must be confirmed by testing

2.3.2 Effective Notch Stress method (ENS)

The Effective Notch Stress method (Heshmati et al., 2012) is a computer-based local fatigue assessment approach where the largest elastic stress (notch stress) at the weld toe and root is determined by numerical methods such as the Boundary Element Method (BEM) and Finite Element Method (FEM). Hence, experimentally estimating (Al-Emrani & Aygül, 2014) the effective notch stresses at the toe and root is impossible because the effective notch strain cannot be measured in the test.

It was further explained by Heshmati et al. (2012), that when using the Effective Notch Stress method, all parameters affecting the stress concentration at the notch are considered. This is because the effective notch stress is computed as a combination of the geometrical stress and the highest non-linear stress. The level of stress at the notch (Al-Emrani & Aygül, 2014) is highly dependent on the degree of sharpness, also known as notch radius. Thus, when the radius of a notch is close to zero and becomes very sharp, the theoretical elastic stress at the notch rises to an infinite value. To deal with this problem, the effective notch stress is calculated as a mean of the stresses within a specified length or volume.

However, the actual notch stress (Hobbacher, n.d.) is difficult to estimate due to the irregularity of the critical section profile (toe and root). Thus, an effective notch is used instead of the actual uneven notch. A reference radius of the effective notch is suggested in the IIW (Fricke, 2010) to be $r_{ref} = 1$ mm for steel and aluminium plates thicker than 5 mm. This reference radius (Al-Emrani & Aygül, 2014) is estimated based on the most severe conditions. For plates thinner than 5 mm, a smaller notch radius is considered (Fricke, 2010) since the effective notch radius of 1 mm is relatively large. This can reduce the plate cross-section which influences the analysis outcomes. Therefore, IIW recommends a reference effective notch radius of $r_{ref} = 0.05$ mm for thin plates.

It is important to note that, when using the Effective Notch Stress method for evaluating the fatigue life of a construction detail, the effect of plate thickness (Al-Emrani & Aygül, 2014) is already considered when computing the notch stress. Therefore, it is not needed to reduce the construction detail's fatigue strength, which is the case for the Nominal Stress method, as explained in section 2.3.1.3, and also for the Hot-Spot stress method.

2.3.2.1 Finite element modeling based on the Effective Notch Stress method

The effective notch stress (Al-Emrani & Aygül, 2014) can be analysed using 3D solid elements as well as 2D planar elements. 3D elements are widely used for complicated details, while 2D planer elements can be utilized for simple geometries and specific load cases. To use a 2D model, the International Institute Of Welding (Fricke, 2010) requires two conditions to be satisfied. Firstly, the shape and dimensions of the weld should remain consistent within the analysed region to ensure that an accurate model of its geometry can be chosen. The second condition is that the external forces acting on the weld should mainly act perpendicular to its line.

A suitable element density should be ensured in the model to obtain more accurate results. Moreover, it is also crucial (Heshmati et al., 2012) to use the correct weld geometries as well as to model the region in the vicinity of the weld toe and root with a very small mesh

size. To achieve this, two different methods can be used. The first one is to partition the region in the vicinity of the weld toe and progressively decrease the mesh size so that the area at the toe and root has the smallest mesh size. Another method is to create sub-models to generate a finer mesh in the critical sections. Besides the sub-model, a global model is also required for the definition of boundary conditions for the sub-model. Both methods are applied in this report, in which the geometry of the specimens in chapter 4.1 and 4.2 was partitioned in order to define appropriate meshes. While the sub-models were utilized in chapter 4.3 where larger specimens were analysed. The IIW (Fricke, 2010) provided practical recommendations for meshing according to ENS. The suggested element size at the notch region at weld toe and root is listed in Table 2.3.

Table 2.3: IIW recommendation for element size for different reference radius r_{ref} and element type (r in table indicates r_{ref}). [Writers own table based on Table 3.1 from Fricke (2010), *p.12*]

Element type	Relative size	size for $r_{ref} = 1$ mm	Size for $r_{ref} = 0.05$ mm
quadratic	$\leq \frac{r}{4}$	≤ 0.25 mm	≤ 0.012 mm
linear	$\leq \frac{r}{6}$	≤ 0.15 mm	≤ 0.008 mm

It is further explained by Al-Emrani and Aygül (2014) that the weld toe and root are rounded in different ways in the model depending on the weld type (fillet or butt) or the load-carrying conditions. Thus, the fillet weld can either be modeled using a realistic weld shape or by assuming an idealized shape with a 45° inclination. While the butt weld can be idealized with an inclination of 30°. Moreover, the weld root can be modelled as a Keyhole or a U-shape, see Figure 2.16. As can be seen in the figure, the base plate and the attached plate should utilize separate nodes. Therefore, a certain gap should exist between these connected plates.

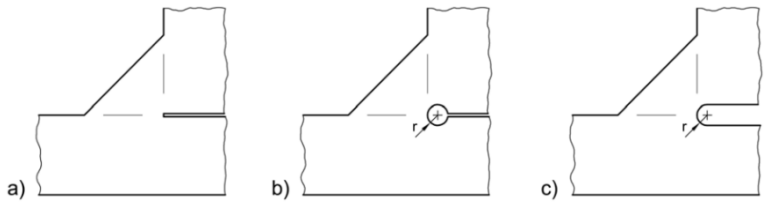

Figure 2.16: Rounding of fillet weld root based on the Effective Notch Stress method. a) Not rounded, b) Keyhole shape and c) U-shape. [Source: Figure 3.2 from Fricke (2010), *p.9*]

Furthermore, Kaffenberger et al. (2012), carried out an experimental test and the corresponding numerical analysis to determine an appropriate modelling approach for modelling the weld end and evaluating the fatigue performance of thin components using the Effective Notch Stress method. As a result of Kaffenberger et al. study, a standardized approach is proposed for plates with a thickness of $t = 2.24$ mm and an effective notch with a reference radius of $r_{ref} = 0.2$ mm. This model can be proportionally adapted for other plates with other thicknesses, as depicted in Figure 2.17 where the effective notch radius is given as a function of the plate thickness. The figure also includes recommendations provided by Kaffenberger et al. (2012) regarding element size for different regions within the welded detail.

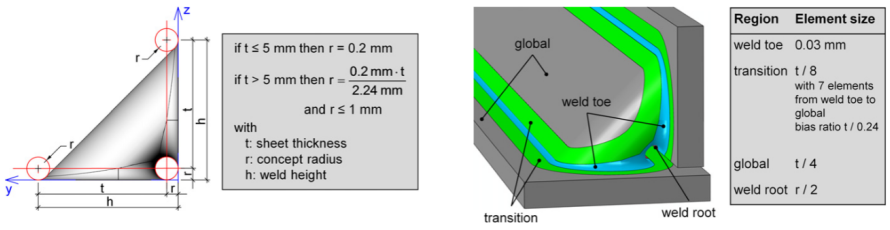

Figure 2.17: Recommendations for effective notch radius and meshing using the finite element method according to ENS method. [Source: Figures 6 and 7 from Kaffenberger et al. (2012), *p.289*]

2.3.2.2 Effective Notch Stress method for as-welded joints

The fatigue life of all as-welded details,(Hobbacher, n.d.) can be evaluated based on the computed effective notch stress using one universal S-N curve regardless of the geometry and the loading condition. Based on a series of experiments, it has been determined that the S-N curve for welded steel details with an effective notch of 1 mm radius is FAT 225 for all steel types, as shown in Figures 2.18 and 2.4. This curve (Al-Emrani & Aygül, 2014) assumes the maximum principal stress. If Von Mises stress is used for fatigue life assessment, a S-N curve with FAT 200 is applied. See Figure 2.18. For plates thinner than 5 mm, S-N curves with FAT 630 and FAT 560 are applied based on the maximum principal stress or the von Mises stress respectively. The S-N curves for as-welded details continue with the same slope of $m = 3$ until the number of cycles reaches $N = 10^7$. After that, a cut-off limit is defined and a slope of $m = 22$ is applied as can be seen in Figure 2.18.

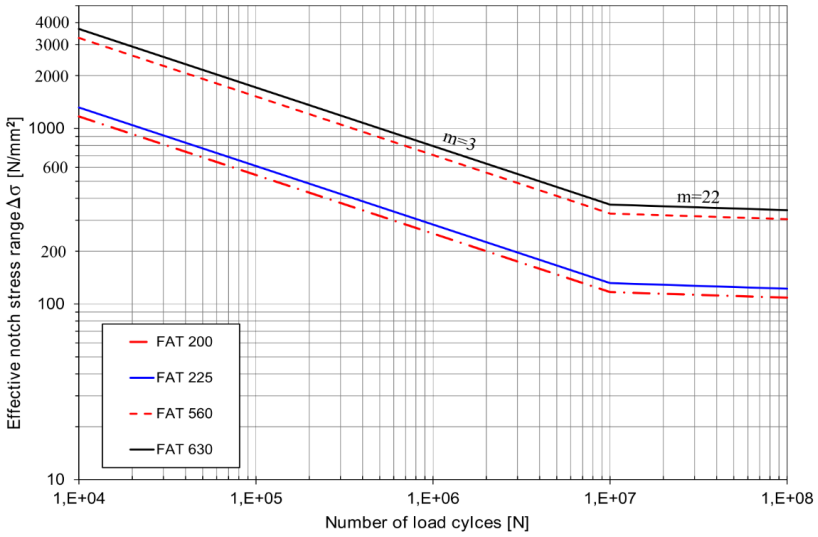

Figure 2.18: S-N curves for all as-welded steel details based on the Effective Notch Stress method. [Source: Figure 6.5 from Al-Emrani and Aygül (2014), *p.135*]

2.3.2.3 Effective Notch Stress method for HFMI-treated joints

For HFMI-treated welds, different S-N fatigue curves (Marquis & Barsoum, 2016) have been proposed for different steel types, as can be seen in Table 2.4. It should be noted that each S-N curve has two slopes depending on the number of loading cycles N, where $m = 5$ when $N \leq 10^7$ and $m' = 9$ when the number of cycles is more than $> 10^7$, see

Figure 2.19. The S-N curves shown in the figure are applied when maximum principal stress is used in analysis. If Von Mises stress is considered in analysis, one FAT-class must be decreased. In a similar manner to the nominal stress method, discussed in section 2.3.1.1, the characteristic S-N curves are estimated after a number of load cycles equal to 2×10^6. It was further explained by Marquis and Barsoum that the effective notch stress curves should remain below the largest approved S-N curve for the nominal stress method, which is FAT 180 for a slope of $m = 5$. This is to avoid any calculation issues that may occur in the case of welded components with low levels of structural stress concentration. Hence, when dealing with such details, it is also recommended that the effective notch stress concentration K_w "defined as the ratio between the effective notch stress and the structural stress" should not fall below 1.6. In case the calculated value of K_w is less than 1.6, the value of 1.6 should be employed in the analysis.

Table 2.4: Existing IIW S-N curves for as-welded and HFMI-treated details for plates thicker than 5 mm according to ENS method. [Source: Table 6 from Marquis and Barsoum (2016), *p.27*]

f_y (MPa)	Effective notch stress characteristic curve modelled using $\rho_f = 1$ mm
	As-welded, $m = 3$
All f_y	225
	Improved by HFMI, $m = 5$
$235 < f_y \leq 355$	320
$355 < f_y \leq 550$	360
$550 < f_y \leq 750$	400
$750 < f_y \leq 950$	450
$950 \leq f_y$	500

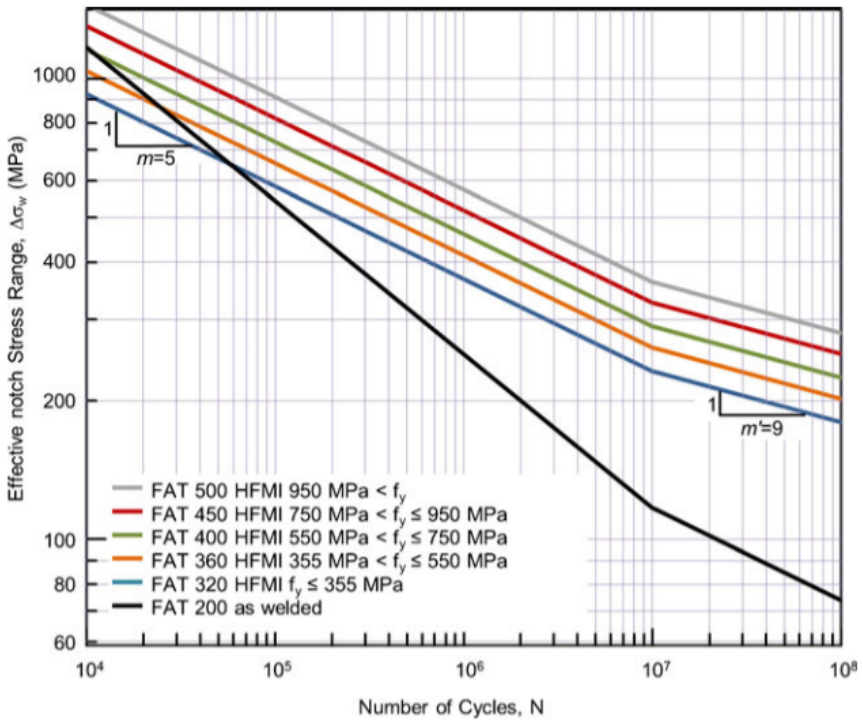

Figure 2.19: Existing IIW Characteristic S–N curves for HFMI-treated welded details for R≤0.15 according to ENS method. For comparison, the as-welded FAT 200 S–N curve is also shown. [Source: Figure 12 from Marquis et al. (2013), *p.814*]

3

Previous tests on cover-plates treated with HFMI

As previously stated in chapter 2.1.1, cover-plated details are very prone to fatigue cracking due to the low fatigue strength at the end toe. Therefore, the end toes of cover-plates are construction details suitable for HFMI improvement, but there are not a lot of previous studies of the fatigue strength of cover-plated beams treated with HFMI. In this thesis, four published tests that includes some form of cover-plate details are examined. That will later in chapter 4 be used for structural analysis, to further develop the field of research about cover-plated beams loaded in bending.

- **The first test** is by Leitner and Stoschka (2020) named *"Effect of load stress ratio on nominal and effective notch fatigue strength assessment of HFMI-treated high-strength steel cover plates"*, where thin cover-plated girder-plates are subjected to axial loading for both as-welded and HFMI-treated welds.

- **The second test** is by Vilhauer et al. (2012) named *"Fatigue behavior of welded coverplates treated with Ultrasonic Impact Treatment and bolting"*, where one-sided cover-plated flange-girders are subjected to bending moment for as-welded, UIT-treated end welds and bolted cover-plated ends.

- **The third test** is by Roy and Fisher (2006) named *"Modified AASHTO design S-N curves for post-weld treated welded details"*, where rolled I-beams with different cover-plated weld configurations, e.g. non-welded, as-welded and UIT-treated ends, are tested in bending.

- **The fourth test** is by Hui et al. (2018) named "*Fatigue life improvement of welded girders with ultrasonic impact treatment*", where the tested rolled I-beams are similar to one test series from Roy and Fisher (2006) test, the difference being that the UIT-treated cover-plates are treated with 20 kHz instead of 27 kHz.

3.1 Leitner and Stoschka, 2020

The aim of the test performed by Leitner and Stoschka (2020) was to determine the effect on fatigue strength, when a higher stress ratio (R-ratio) is applied to HFMI-treated cover-plated plate-girders of thermo-mechanically rolled high strength steel S700. Two experiments were performed: practical testing utilizing the Nominal Stress approach and a Finite Element study utilising the Effective Notch Stress approach. In this specimen, 50 mm long welded cover-plates are symmetrically placed on each side of a 280 mm long and 50 mm wide plate-girder. All plates have a thickness of 3.25 mm, as seen in Figure 3.1. There were three series of welded specimens tested in the study. The first test series is of as-welded cover-plates with a stress ratio of $R = 0.1$, the second series is of HFMI-treated welded cover-plates with a stress ratio of $R = 0.1$, and lastly, HFMI-treated welded cover-plates with a stress ratio of $R = 0.5$. All specimens was subjected to a cyclic uni-axial tensile load.

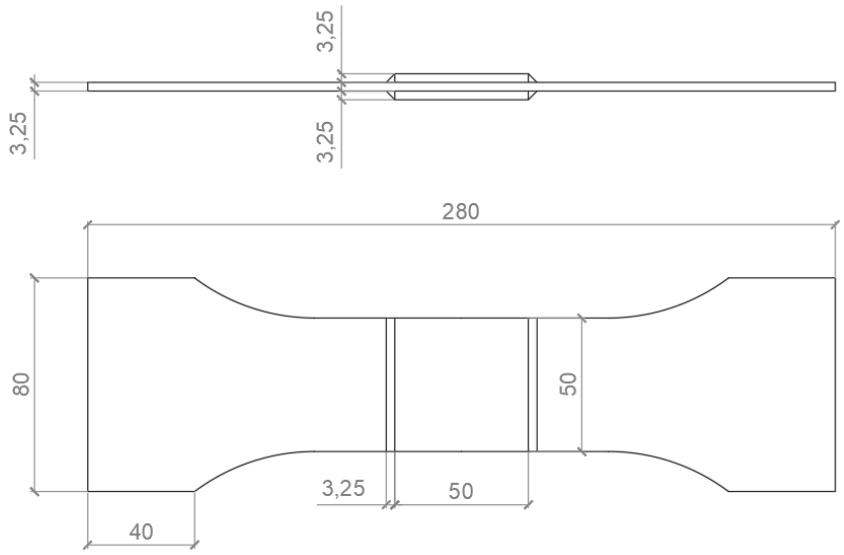

Figure 3.1: Dimension's of test specimen with a cover-plated plate-girder (all units are in mm). [Writers own figure based on Figure 1 from Leitner and Stoschka (2020)]

The FAT-class for the as-welded specimen, using the Nominal Stress approach, writes Leitner and Stoschka is 80 MPa for the corresponding construction detail, which can be read in IIW (Hobbacher, 2016) and Eurocode 3 (European standard, 2008 and 2022). The FAT-class for the HFMI-treated specimen is 180 MPa with a stress ratio of $R = 0.1$ and 125 MPa with a stress ratio of $R = 0.5$. Which was accumulated from IIW S-N curve graph in Figure 2.15(c) and IIW recommendation for plate thickness effect in Section 2.3.1.3. Thus, the fatigue strength of the HFMI-treated specimen has an increase of 1.5 due to the effect of having excessive thin plates. In other words, when FAT 160 was multiplied by Equation 2.4, a detail category of 240 MPa was obtained. But, since the S-N curve graph for welded high-strength steel joints of S700 has a maximum increase up to FAT 180, this value was instead used for the assessment. Lastly, the FAT-class for the HFMI-treated specimen with a stress ratio of $R = 0.5$ was reduced because of the larger stress ratio. Which according to IIW recommendation should be reduced by three FAT-classes, as seen in Table 2.2. A summary of the three test series can be seen in Table 3.1.

Table 3.1: Each test series plate thickness, weld properties and fatigue strength from Nominal Stress method for high strength steel $f_y \geq 700MPa$. [Writers own table combined from data provided from Leitner and Stoschka (2020)]

Joint detail	$t_b[mm]$	$t_c[mm]$	Weld type	Leg length	FAT class
As-welded	3.25	3.25	Fillet	3.25 mm	80 MPa
HFMI-treated (R=0.1)	3.25	3.25	Fillet	3.25 mm	180 MPa
HFMI-treated (R=0.5)	3.25	3.25	Fillet	3.25 mm	125 MPa

It was determined during the practical test that the HFMI-treated specimen was strengthened with a compressive residual stress of -400 to -450 MPa at the end weld toe. Furthermore, fatigue cracks were observed to initiate from the end weld toe in all three test series. Every specimen was loaded until failure was reached or to $N = 2 \times 10^7$ load cycles if no failure had been reached. The results of the fatigue test can be seen as dots in Figure 3.2 together with the statically evaluated S-N curves for a survival probability of $P_s = 97.7\%$. It is then observed in Figure 3.2 that HFMI-treated specimen possesses higher fatigue strength. But a reduction in fatigue strength is evident for specimens with a higher stress ratio. This can be seen, where the HFMI-treated specimen with a stress ratio of $R = 0.5$ exhibit lower fatigue strength compered to the HFMI-treated specimen with a stress ratio of $R = 0.1$. Although, the fatigue strength of both HFMI-treated test series is higher than that of the as-welded test series.

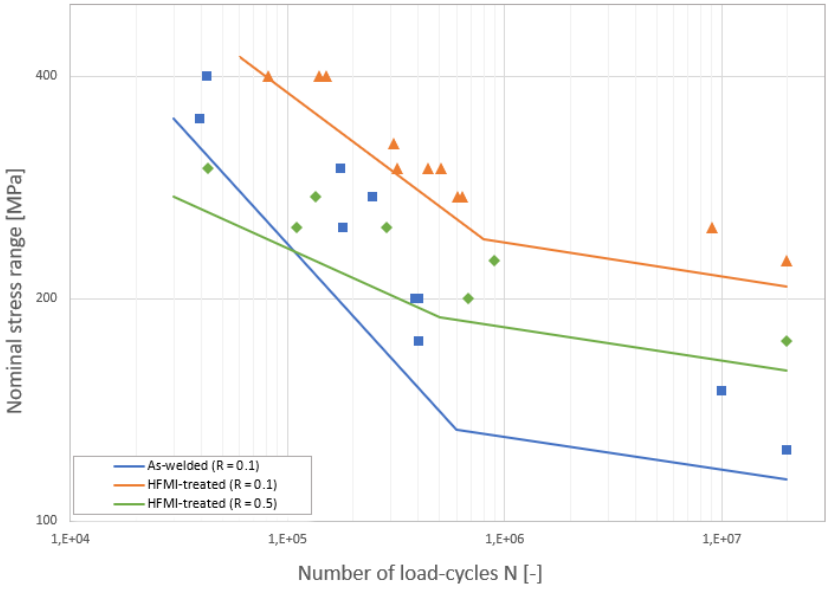

Figure 3.2: Fatigue test results shown as dots and the statically evaluated fatigue S-N curves for the three test series. [Writers own figure based on Figure 5 and Table 5 from Leitner and Stoschka (2020), *p.4*]

With the results from the practical fatigue test, the statically evaluated S-N curves for the HFMI-treated specimen were then compared with the corresponding S-N curves from IIW (Marquis & Barsoum, 2016). Where Leitner and Stoschka concludes that for the nominal stress approach the recommended S-N curves given by IIW are applicable, but slightly conservative. This was further highlighted when Leitner and Stoschka concluded to that the knee point can be changed from $N = 10^7$ load cycles to $N = 10^6$ load cycles, and the fatigue assessment will still be conservative.

For the finite element study, Leitner and Stoschka used Finite Element Analysis based on the Effective Notch Stress method to determine the S-N curves for the HFMI-treated test series. Using a reference radius of $r_{ref} = 1$ mm and a unit load of 1 N to determine the stress concentration factor K_t from the maximum principle stress. With the stress concentration factor, the effective notch stress was calculated by multiplying the nominal stress with K_t. Thus, the fatigue strength of the HFMI-treated specimen was calculated and their respective statically evaluated fatigue S-N curve was plotted.

The statically evaluated S-N curves was then compared to the recommended S-N curves for HFMI-treated joints from IIW (Marquis & Barsoum, 2016). The FAT-classes according to the Effective Notch Stress method are provided by IIW recommendations and can be read in section 2.3.2.3. Hence, for HFMI-treated series with a stress ratio of $R = 0.1$, the recommended FAT-class is FAT 400. While there are no recommendations for the FAT-class of HFMI-treated joints with a stress ratio of $R = 0.5$, Leitner and Stoschka decided to reduce the FAT-class according to nominal stress requirements. Which is a reduction of three steps as mentioned previously. But the lowest FAT-class for the Effective Notch Stress method is that of FAT 320, which is a reduction of two steps. Hence, to solve this problem Leitner and Stoschka decided to reduce the FAT-class by another 40 MPa, and thereby, used a FAT-class of 280 MPa for the HFMI-treated series with a stress ratio of $R = 0.5$.

With the assembled S-N graphs Leitner and Stoschka concludes that the recommended S-N curve for HFMI-treated specimen with a stress ratio of $R = 0.1$ are applicable, and relatively conservative. Due to that, the same knee point change from $N = 10^7$ load cycles to $N = 10^6$ load cycles conclude Leitner and Stoschka will produce similar results as for nominal stress. Although for HFMI-treated specimens, a stress ratio of $R = 0.5$ gives a non-conservative assessment below $N = 3 \cdot 10^5$ load cycles. But the same conclusion as the previous tests can be applied to higher load cycles. However, Leitner and Stoschka finalises by writing that only the test series with a stress ratio of $R = 0.1$ gives a reasonable applicability than for the test series with a stress ratio of $R = 0.5$, and thereby, Leitner and Stoschka concludes that a further reduction of the FAT-class may be needed for joints with a stress ratio of $R = 0.5$ to ensure a conservative assessment.

3.2 Vilhauer et al, 2011

The aim of the test performed by Vilhauer et al. (2012) was to study the interaction of different repairing methods when applied to fatigue-prone details. In this study, the focus is on the welded connection between a flange-girder and a cover-plate, which were loaded by a point load causing the specimen to be subjected to three-point bending. There were a total of two tests: a practical experiment and a Finite Element study using Abaqus.

A total of 15 specimen were tested in four test series; these are shown in Table 3.2, where a total of 6 as-welded specimen were tested to verify if the studied repairing methods contributes to improve fatigue strength. The repairing methods include: applying UIT-treatment at the end weld toe, installing bolts at the cover-plates ends, and lastly, combining the two methods by applying UIT-treatment to the welds and installing bolts.

Table 3.2: Summary of Vilhauer et al. four test series with treatment specification and number of tested specimens. [Writers own table]

Test series	Treatment specification	Number of specimen
CONTROL	No treatment (As-welded)	6
UIT	UIT-treatment along the weld toe	3
BOLT	Installed tension bolts at the cover-plate ends	3
UIT/BOLT	UIT-treatment along weld toe and tension bolts at the cover-plate ends	3

All 15 test specimen was fabricated using S235J2 (A36) grade steel. The components geometry can be seen in Table 3.3 and Figure 3.3, where the test set-up can also be seen. The welds are made of shilded metal arc (SMAW) fillet welds with a throat-thickness a of 7.94 mm, which gives a leg-length of 11.23 mm. The UIT-treatment was applied at the transverse end weld toe and 152 mm of the longitudinal weld toe. The bolts were installed 31.8 mm from the edge of the cover-plate and tensioned with a force of 227 kN.

Table 3.3: Material data and geometry of the three components composing the steel specimen. [Writers own table based on data provided from Vilhauer et al. (2012), *pp.164-165*]

	Steel grade	$f_y[MPa]$	l $[mm]$	b $[mm]$	t $[mm]$	$\phi[mm]$
Plate-flange	S235J2 (A36)	235	1270	114	25.4	-
Cover-plate	S235J2 (A36)	235	600	76.2	25.4	-
Bolt	ASTM A325	660	-	-	-	25.4

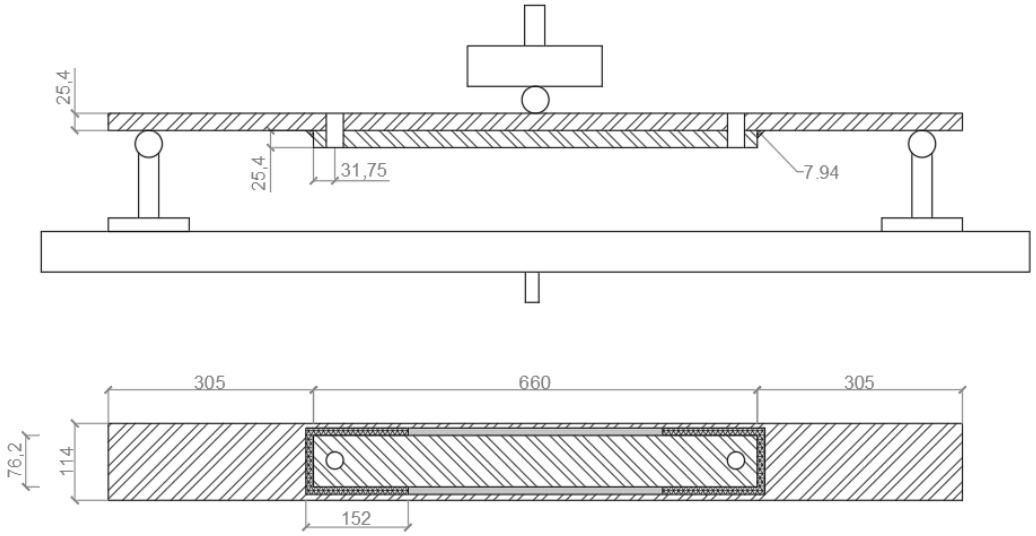

Figure 3.3: The above Figure shows the set-up of the fatigue test and the bottom Figure visualises the geometry of the specimen (all units are in mm). [Writers own figure based on Figure 1 and 3 from Vilhauer et al. (2012), *pp.165-166*]

The experiment was performed by applying a force, P, at the specimens mid-point as seen in Figure 3.3 and with this set-up arrangement, Vilhauer et al. writes that the specimens can be considered statically determinate. By computing the linear moment diagram, the moment at the end weld toe was determined and Vilhauer et al. used the moment to calculate the theoretical nominal stress at the end weld toe by using Equation 3.1 from beam theory. Where the inertia, I, is that of the flange-girder. From the neutral axis to the end weld toe, the distance c was estimated to be 12.7 mm. With this, the nominal stress range was calculated for each specimen, which ranges from intermediate stress range (ISR) with 59 MP, 96.5 MPa and 138 MPa to high stress range (HSR) with 193 MPa.

$$\sigma = \frac{Mc}{I} \tag{3.1}$$

For the ISR specimens (CONTROL 1, 2, 3, 4 and UIT 1), two CONTROL specimens (2 and 1) were determined to have no observable fatigue cracks, with nominal weld toe stresses of 59 MPa and 96.5 MPa respectively. And each specimen achieved run-out at 3.85 million load cycles and 2.16 million load cycles respectively. The other two CONTROL specimen (3 and 4) was subjected to a nominal weld toe stress of 138 MPa. CONTROL 3 had after 930,000 load cycles a 6.4 mm long crack in the centre of the weld toe. It was estimated that the crack first developed after 500,000 load cycles. As for CONTROL 4, a fatigue crack first developed after 350,000 load cycles. The reason why the load cycles for CONTROL 4 were 25% lower than for CONTROL 3, was due to the fabrication of this specimen being of lower quality. Regarding the UIT specimen which was subjected to a nominal stress of 138 MPa, it reached run-out after 5 million load cycles without the initiation of a fatigue crack. After these tests, Vilhauer et al. decided that the remaining specimen would be performed under a nominal weld toe stress of 193 MPa. This is because the specimens has a higher chance of developing fatigue cracks instead of reaching run-out.

For the HSR specimen composed of 2 CONTROL specimen, 2 UIT specimen, 3 BOLT specimen and 3 UIT/BOLT specimen, it was concluded that fatigue cracking of the CONTROL specimen initiated after an average of 65,000 load cycles and for the BOLT specimens the initiation began after an average of 70,000 load cycles. This assigns both the CONTROL and BOLT specimens as Category E details according to AASHTO. With this result, Vilhauer et al. concludes that post-installing tension bolts at cover-plate ends has a negligible effect on fatigue life performance. Vilhauer et al. also highlights that this result was not unexpected. This is because the load transfer would continue primary through the weld and not through the bolt if the weld was not removed.

As for the UIT specimen, fatigue crack initiation developed after an average of 1,7 million load cycles. This is approximately 25 times longer than for the CONTROL specimen, which designates the specimens as Category A details according to AASHTO. Lastly, regarding the combined UIT/BOLT-treated specimen, fatigue crack initiation developed after an average of 1 million load cycles which is approximately 41% lower than the average for the UIT-treated specimen. Of all the tests, the UIT/BOLT specimen had the most scattered results and Vilhauer et al. suggest that it is due to the additional stresses the post-installed bolt introduces. Accompanying the large scatter of data, two of the UIT/BOLT specimen are reduced to Category B details while the third is a Category A detail.

Thus, Vilhauer et al. establishes that the most effusive method to increase fatigue performance is to only apply UIT-treatment to the weld and that post-installing a tension bolt close to the treated weld will negate some of the effect of UIT-treatment. But if tension bolts are to be used, Vilhauer et al. recommend that they should be placed so that the tensile stresses from the post-installed bolt do not interact with the compressive residual stresses from the UIT-treatment and reduce the effectiveness of the UIT-treated weld. This study confirms the recommendations from Marquis and Barsoum (2016) written in chapter 2.2.1, where post-treating after HFMI are not recommended due to negating the enhancement.

For each test series, full crack propagation up to failure was conducted to estimate the fatigue performance of the treatments and to visualise the final crack propagation. Figure 3.4 illustrate the crack propagation for UIT-treated (a), BOLTED (b) and UIT/BOLT (c) specimens. Similarly to the as-welded CONTROL specimen, the BOLTED specimen in Figure 3.4(b) cracked at the end weld toe. However, for the UIT-treated specimen in Figure 3.4(a) the crack propagated through the transverse end weld, and the same occurred for the UIT/BOLT specimen seen in Figure (c). The crack propagation in the UIT-treated specimen indicates that a change in stress concentration has occurred from the weld toe to the weld root, which was a risk discussed in chapter 2.2.1.

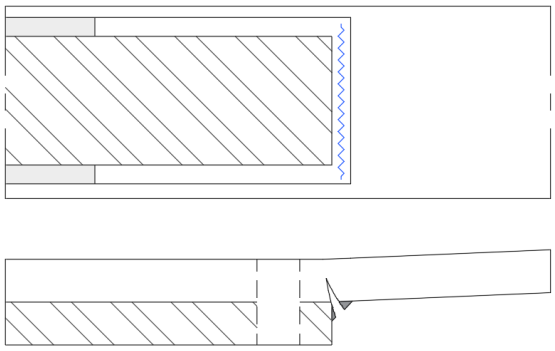

(a) Complete propagation of transverse end crack at a UIT-treated specimen

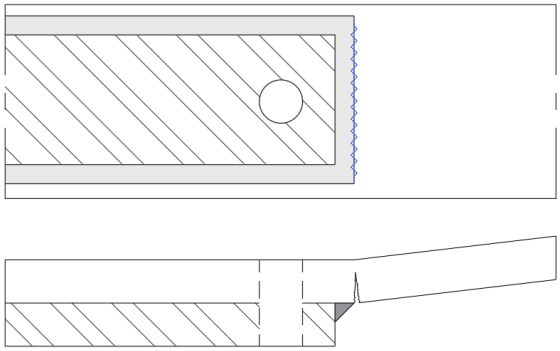

(b) Complete propagation of toe crack at a bolted specimen

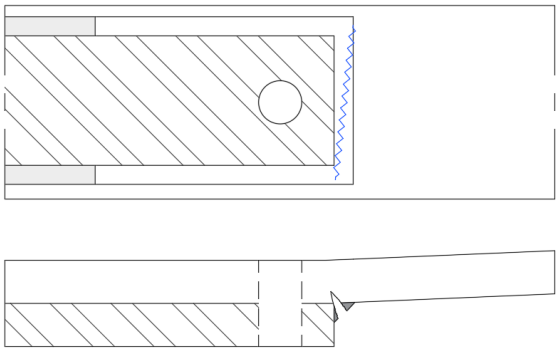

(c) Complete crack propagation of a UIT-treated and bolted specimen

Figure 3.4: In Figure (a), (b) and (c) illustrates and visualises the complete crack propagation of the three studied repair methods of Vilhauer et al. test specimens. [Writers own figures based on Figure 10, 11 and 12 from Vilhauer et al. (2012), *pp.170-171*]

3.3 Roy and Fisher, 2006

The test was conducted at Lehigh University by Roy and Fisher (2006), and the aim was to evaluate the fatigue performance of UIT-treated cover-plates and transverse stiffeners attached to full-size beams. The test was divided into two segments. The first being an experiment on rolled-beams W690X192 made of ASTM A588 Grade 345W steel with a minimum yield strength of 366-435 MPa. The primary objective of this segment was to provide recommendations for fatigue evaluation of UIT-treated welded cover-plates. While the second segment focuses on the fatigue performance of UIT-treated transverse stiffeners in built-up girders manufactured in HPS grade 690W steel at Lehigh University.

Considering the focus of this master's thesis is solely on cover-plates, only the first segment of the test is discussed here. The first segment of tests involves 18 rolled-beams constructed with 36pcs 25 mm thick cover-plates made of ASTM A709 grade 345W steel with a minimum yield strength of 407 MPa. Moreover, the beams were also constructed with welded transverse stiffeners, as seen in Figure 3.5. In addition to the tests performed by Roy and Fisher, the results from a pilot study carried out prior to the analysis of the same rolled-beam with a yield strength of $f_y = 485$ MPa were included in the analysis.

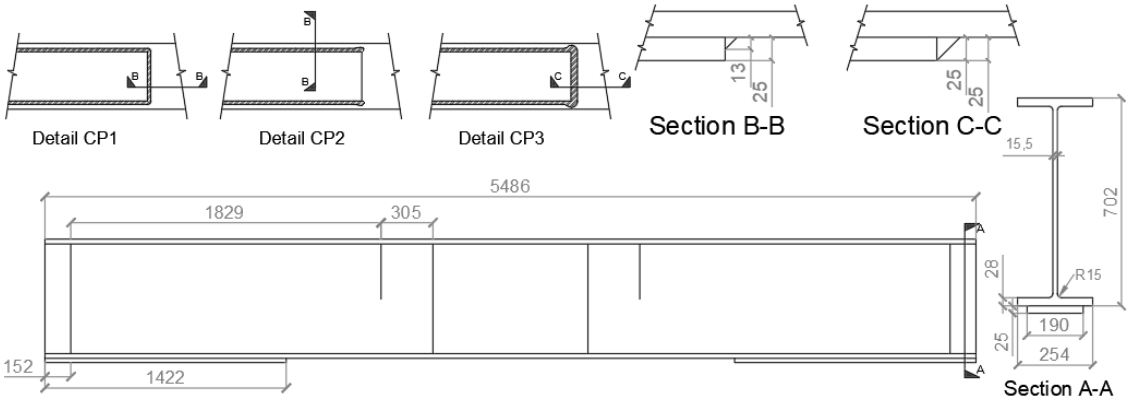

Figure 3.5: Details of Roy and Fisher test specimens (grade 345W beams) (all units are in mm). [Writers own figure based on Figure 2 from Roy and Fisher (2006), *p.244*]

Three different types of cover-plate end details were tested. The first type CP1 is for cover-plates with an end fillet weld of 13 mm leg-length, CP2 is for cover-plates without any end welds and the third type CP3 is for cover-plates having an end weld of 25 mm leg-length (weld size is equal to the cover-plate thickness). This can be seen in Figure 3.5 and Table 3.4. The purpose of testing different end details was to empirically confirm the previous findings by (Gurney, 1979 and Takamori, 1999). That the larger the weld size, the lower the stress concentration will be at the weld root. Thus cover-plates with larger end welds have higher fatigue strength.

Following that, the specimens were categorised into three groups depending on their end detail combinations. The first group contains detail types of CP1 and CP3 and is referred to as Group I. Group II includes cover-plates with details for CP1 and CP2. While specimens having cover-plates with CP3 details at both edges belong to Group III. The test matrix can be seen in Table 3.5. Which results into 7 CP1 specimen, 2 CP2 specimen and 27 CP3 specimen.

Table 3.4: Details of Grade 345W specimens, weld properties and treatments type. [Writers own table assembled form data provided from Roy and Fisher (2006)]

End detail	$t_b[mm]$	$t_c[mm]$	weld type	end weld size	treatment type
CP1	28	25	Fillet	13 mm	UIT 27000 Hz
CP2	28	25	Fillet	no weld	UIT 27000 Hz
CP3	28	25	Fillet	25 mm	UIT 27000 Hz

The specimens were subjected to a constant cyclic load placed at the top flange. This causes the beams to be loaded in four-pint bending, which has the same test setup as seen in Figure 3.8. The 18 beams were divided into two test series, where each series was imposed to a minimum stress S_{min} of 10 MPa and 62 MPa respectively. Each test series consists of various groups of beams imposed by different maximum stresses S_{max}, which produce different stress ranges S_r and stress ratios R. This can be seen in Table 3.5. All cover-plates were treated with UIT at a frequency of 27,000 Hz. This generated a groove of about 3 mm width and 0.5 mm depth.

Table 3.5: Test matrix for Grade 345W beams (only cover-plates). G refers to girder, Arabic numbers refer to beam serial number, Roman numbers refer to specimens group. [Writers own table based on data in Table 1 from Roy and Fisher (2005), *p.244*]

Smin (MPa)	Sr (MPa)						
	52	62	67	72	97	124	152
10	-	-	-	-	G1(I)	-	G7(I)
	-	-	-	-	G2(I)	-	G8(I)
	-	-	-	-	G3(I)	-	G9(III)
	-	-	-	-	G1-2(III)	-	G18(III)
	-	-	-	-	(R=0.09)	-	(R=0.06)
62	-	-	-	-	G4(III)	-	-
	-	-	-	-	G13(II)	-	-
	-	-	-	G6(III)	G14(II)	G16(III)	-
	G11(III)	G5(III)	G10(III)	G12(III)	G15(III)	G17(III)	-
	(R=0.55)	(R=0.5)	(R=0.48)	(R=0.46)	(R=0.39)	(R=0.33)	-

The fatigue strength of as-welded cover-plates is assigned the lowest detail category of E' according to AASHTO specifications, as mentioned in section 2.1.1. This will determine the maximum enhancement in fatigue performance which can be anticipated when applying UIT-treatment to as-welded details.

The testing was discontinued when fatigue cracks appeared at the end weld of the cover-plate and propagated through the flange to the web. For the most specimens, fatigue failure was reached when the test finished. If no cracking occurred, the tests were carried out until they surpassed the 95% confidence limit and reached 95% failure limit of the least critical untreated detail of the tested beam specimen.

All beams with Grade 345W steel failed due to cracking at one of the cover-plate ends, except for five specimens. All of these non-failed specimens had end welds equal to the cover-plate thickness (detail CP3). That even though they had been subjected to $N = 15 \times 10^6$ load cycles no fatigue cracks were discovered on those specimens. In addition, all five Group I specimens that had both details CP1 and CP3 failed due to cracks at the end weld of detail CP1. This confirms that weld size has a considerable effect on fatigue performance. All Group I specimens were reported to have cracks that started at the end weld toe and continued through the flange to the web, with the exception of one cover-plate where the crack appeared because of a flaw at the root. Moreover, all the failed CP3 specimens showed cracks at the toe. For CP2 specimens, the cracks started at the end of the longitudinal weld. The test results can be found in Figure 3.6 and 3.7 in terms of S-N curves.

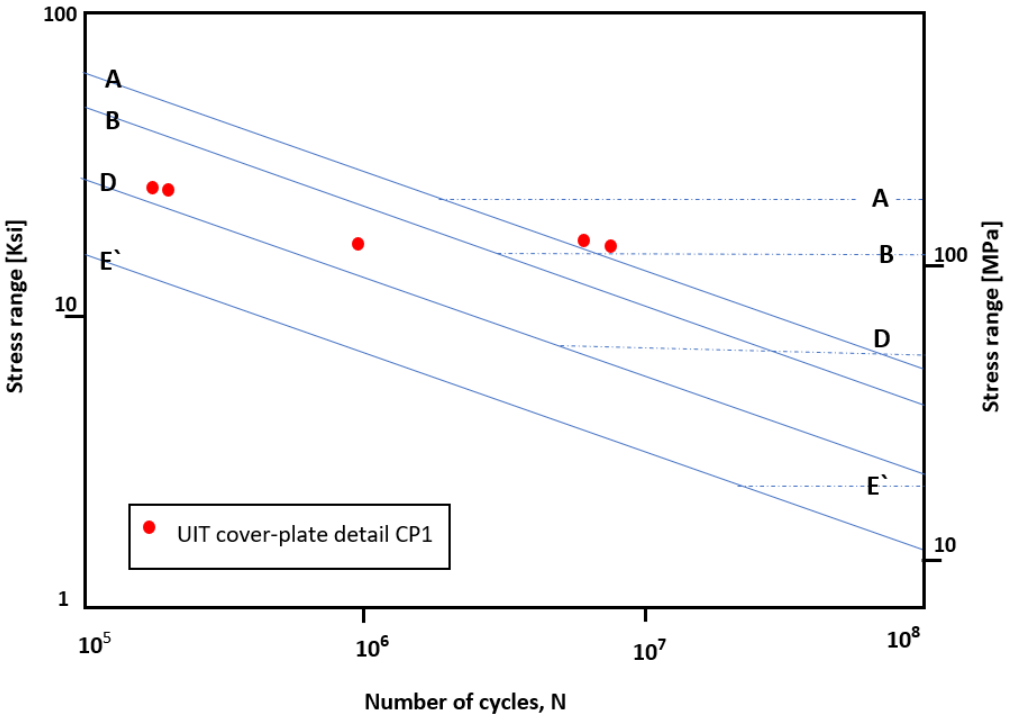

Figure 3.6: Fatigue test results for cover-plates detail CP1. [Writers own figure based on provided test data from Figure 6 from Roy and Fisher (2006), *p.214*]

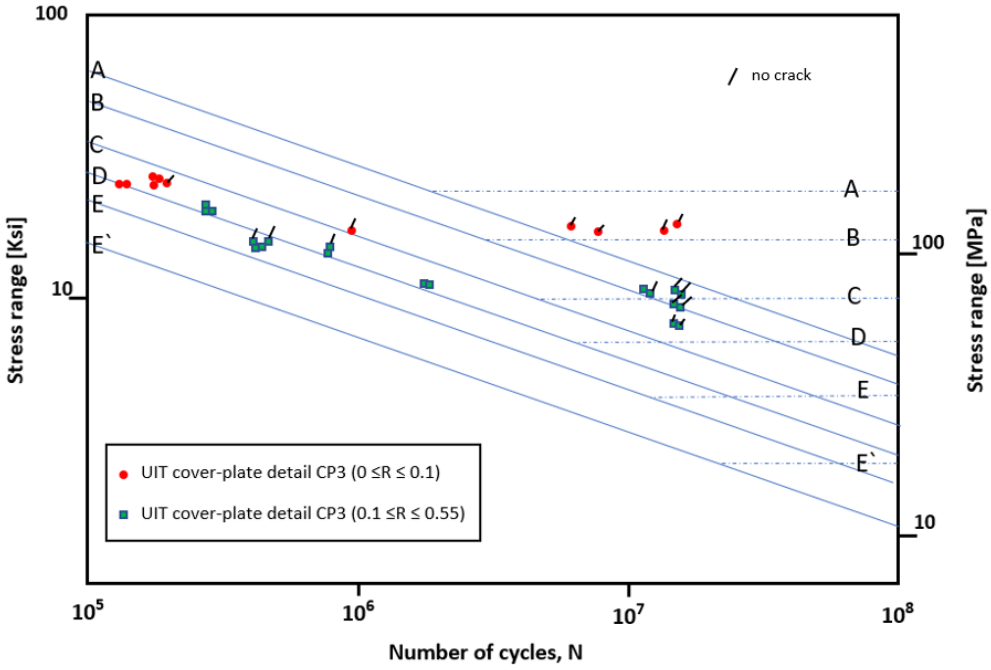

Figure 3.7: Fatigue test results for cover-plates detail CP3. [Writers own figure based on provided test data from Figure 7 from Roy and Fisher (2006), *p.214*]

It can be seen from Figure 3.6 and 3.7 that all the tested specimens have a higher detail category compared to as-welded cover-plates. Accordingly, all specimens with CP1 details exceeded detail category D at a stress ratio $R < 0.1$. While CP3 details reported higher fatigue performance, no specimens had cracked at a stress ratio of $R \leq 0.1$ when the test was discontinued. In addition, two CP3 specimens exceeded fatigue category A without developing fatigue cracks until the test was terminated. Hence, UIT treatment improves the fatigue performance of cover-plates, but the treatment effect depends on the detail of the end weld.

In addition, the minimum stress and stress range also have a significant influence on the improvement gained from the treatment. Where the treatment effect decreases dramatically at larger minimum stress that results in a larger stress ratio of $0.1 < R \leq 0.55$, as seen figure 3.7. The results also showed that UIT-treatment on cover-plates without end welds didn't yield much benefit, since the fatigue strength of detail CP2 only increased by one fatigue category. Based on the test results, design curves for UIT-treated cover-plates under different stress ratios were recommended, which can be found in figures 10 and 11 in Roy and Fisher (2006).

3.4 Hui et al, 2018

The test was carried out at Purdue University by Hui et al. (2018) in order to investigate the efficacy of applying Ultrasonic impact treatment of 20,000 Hz to enhance the fatigue performance of welded cover-plate details. The test results were then compared with the results obtained from a previous test conducted by Roy et al. (2003) where the specimens were treated by UIT of 27,000 Hz. Thus, the specimens and beams in this test were similar to the ones used in Roy and Fisher's test presented in section 3.3, which can be seen in Figure 3.5. The only difference being that the test was limited to only one cover-plate detail (CP), which was represented by detail CP1 in the previous test. Moreover, it was planned to use a similar test matrix, with the same stress ranges and minimum stresses as test variables. However, some changes were made to the variables for the test, and the applied test matrix can be seen in Appendix C.1.

The test involved 14 full-scale 6.4 m long $W690 \times 250 \times 192$ (W27$\cdot$129) rolled-beams. The beams were made of ASTM A709 Grade 345W steel. The beams had two types of welded details, cover-plates and transverse stiffeners. The cover-plates were $190.5mm \times 25,4mm$ in width and thickness and were fastened to the flange using fillet welds of 12.7 mm leg-length. The cover-plates on the first 6 beams were approximately 1.36 m long while the rest had slightly longer cover-plates of approximately 1.4 m. The cover-plates were positioned at the beams edges, as seen in Figure 3.8, which gives a total of 28 cover-plate specimens. The beams were simply supported and imposed by a constant cyclic load that for the majority of the beams started at approximately $P_{min} = 4.45$ kN. The load was distributed at the upper flange of the beam using a $406.4mm \times 609.6mm \times 50.8mm$ plates fastened to the underside of the actuators, seen Figures 3.8 and 3.9.

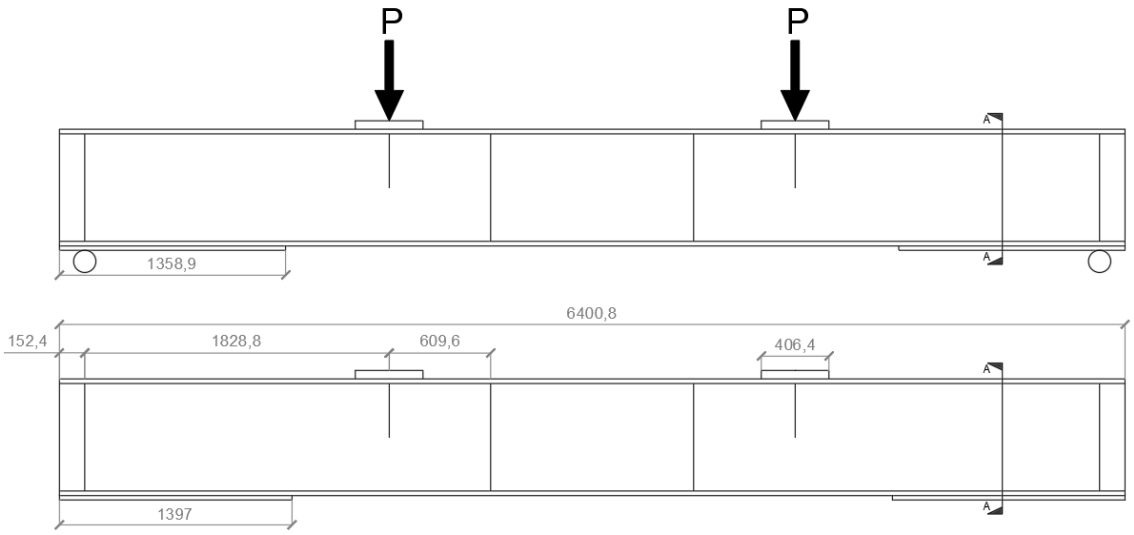

Figure 3.8: At the top figure: Illustrates the first 6 beams (S1-S6) and shows the test set up. Figure at the bottom: Illustrates the 8 remaining beams (S7-S14) and shows the beams dimensions (all units are in mm). [Writers own figure based on Figure 3:3-4 and 3:11-12 from Hui et al. (2018), *pp.40-45*]

The test consisted of two test series. The first test series is called UIT and involves 10 beams where 20 cover-plate specimens were treated with UIT at 20,000 Hz while subjected to the beams' self-weight. The UIT-treatment was applied at the transverse end weld toe

of the cover-plates, and similarly to Vilhauer et al., treatment was also applied along 152 mm to 203 mm of the longitudinal welds. The second test series is called CONTROL and consists of the remaining 4 beams (S1, S2, S7 and S8), which includes 8 as-welded cover-plate specimens. The purpose of those untreated specimens is to give reference data to evaluate the performance of the treated specimens.

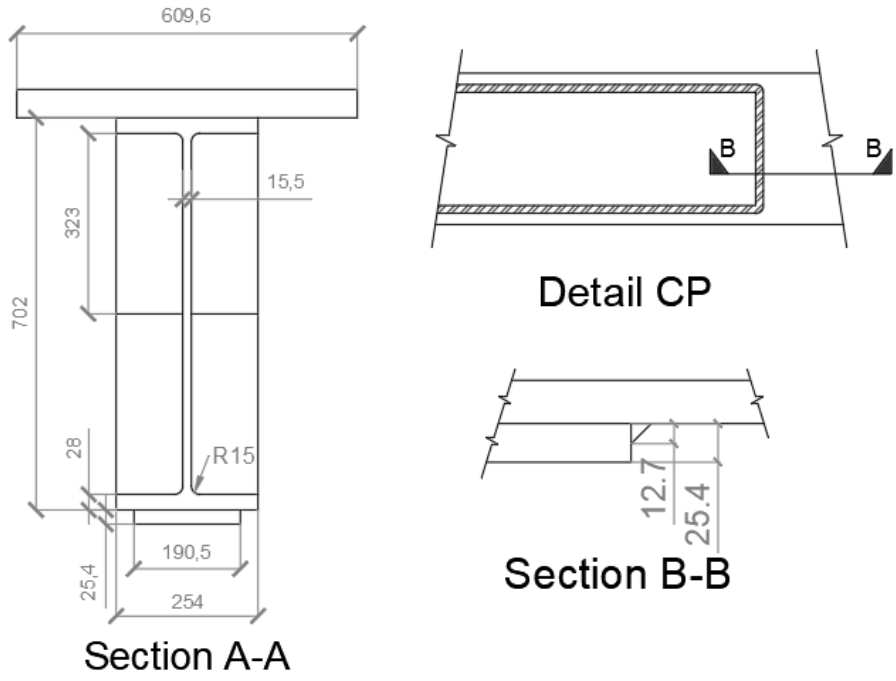

Figure 3.9: Illustrates section A-A from Figure 3.8 and the cover-plate end detailing (all units are in mm). [Writers own figure based on Figure 3:3-4 and 3:11-12 from Hui et al. (2018), *pp.40-45*]

Roy et al. (2003) proposed that UIT-treated stiffeners and cover-plates are to be assigned detail categories B and C respectively. Therefore, the fatigue tests were run until failure or until the tested specimen exceeded the aforementioned detail categories. At a minimum, the tested cover-plate specimens for the UIT test series exceeded detail category C design life and the majority reached failure at detail category C mean life.

After the test was completed, 12 of the 20 UIT-treated specimens were found to have cracks initiated at the root of the end weld. While only 3 specimens cracked at the treated end weld toe. 5 specimens did not report any cracks and remained uncracked until the test was terminated. For the CONTROL test series it showed that all as-welded cover-plate specimens cracked at the end weld toe and achieved detail category E'. While the UIT-treated cover-plates exceeded detail category C. The fatigue test results for both CONTROL and UIT can be seen in Appendix C.3.

The study concluded that applying UIT-treatment of 20,000 Hz to a cover-plate's end weld toe improve their fatigue performance. Hui et al. also highlights that the fatigue test results obtained from the study are identical to the results from Roy and Fisher's test. This finding confirms that a UIT-treatment of 20,000 Hz offers comparable benefits to a treatment of 27,000 Hz, since the fatigue strength of the specimens in both tests increased from detail category E' to category C or more.

However, compared to Roy and Fisher's test, the majority of the specimens had crack propagation at the weld root instead of at the weld toe. Which indicates that the failure mode has shifted from toe failure to root failure for cover-plated beams, which was discussed as a risk for treated welds in section, 2.2.1. Therefore, Hui et al. concludes that for cover-plated beams, toe failure is the predominant failure mode for as-welded cover-plates, whereas root failure is the predominant failure mode for treated cover-plates.

4
Finite element modeling

In this Chapter, three of the tests discussed in Chapter 3 are performed for numerical analysis using the Effective Notch Stress method. The purpose of this analysis is to evaluate and verify the results of the tests. As well as to collect additional data based on root stresses at the cover-plate's transverse end weld to evaluate the location of fatigue crack initiation. Thus, identifying the dominant failure mode (root or toe) for both treated and untreated cover-plates under different load situations (tension and bending). The analysis includes two test series for each analysed test; as-welded and HFMI-treated cover-plates.

The three tests that will be modelled are Leitner and Stoschka (2020) that was presented in section 3.1, Vilhauer et al. (2012) presented in section 3.2 and Hui et al. (2018) presented in section 3.4. The remaining test conducted by Roy and Fisher (2006) in section 3.3 will not be modelled, because the tested specimens are similar to those used in Hui et al. test. Moreover, the results from Hui et al. test have been written and summarized in a more comprehensive manner than Roy and Fisher test. As the number of load cycles obtained under each stress range was presented in a table.

Furthermore, the FE analysis for all represented tests was performed using the finite element model software Abaqus/CAE. The specimens are represented using 3D solid element models. In those models, elastic material parameters were considered, since the Effective Notch Stress method requires only elastic analysis. In addition, all model components (including the weld) were defined with the same material properties. As such, the elastic modulus E and the Poisson's ratio v were defined as 210 GPa and 0.3 respectively. Moreover, all models were appointed tetrahedral mesh elements. By utilizing this element type, the time needed for analysis is greatly reduced (Heshmati et al., 2012).

4.1 Leitner and Stoschka, 2020

As stated before in section 3.1, Leitner and Stoschka utilised both the Nominal Stress method and the Effective Notch Stress method for the fatigue life analyses. However, the root analysis was not covered in the study as only the effective notch stress at the weld toe was reported. Leitner and Stoschka also made some simplifications during the modelling and analysis, for example, the effective notch at the toe was represented by a reference radius of $r_{ref} = 1$ mm, as shown in Figure 4.1 Detail A-A (2). Which is the recommended value for plates thicker than 5 mm, as explained in section 2.3.2. Thereby, the model was constructed in accordance with the provided recommendations for plates thicker than 5 mm and as a result of this assumption the suggested S-N curves for thicker plates were used when comparing the fatigue tests results.

In this study, an updated FE model is created according to the IIW recommendations for plates thinner than 5 mm, as explained in section 2.3.2.1. This recreation of the FE model aims to construct a suitable model according to the provided recommendations, and to investigate if it exhibits reasonable and similar results as Leitner and Stoschka obtained from their experiment. Additionally, the aim of including Leitner and Stoschka experiment is to establish the results from non-treated and UIT-treated welded cover-plated plate-girder loaded in tension by an axial force. The dimensions of the modelled specimen can be seen in Figure 3.1, Detail A-A (1).

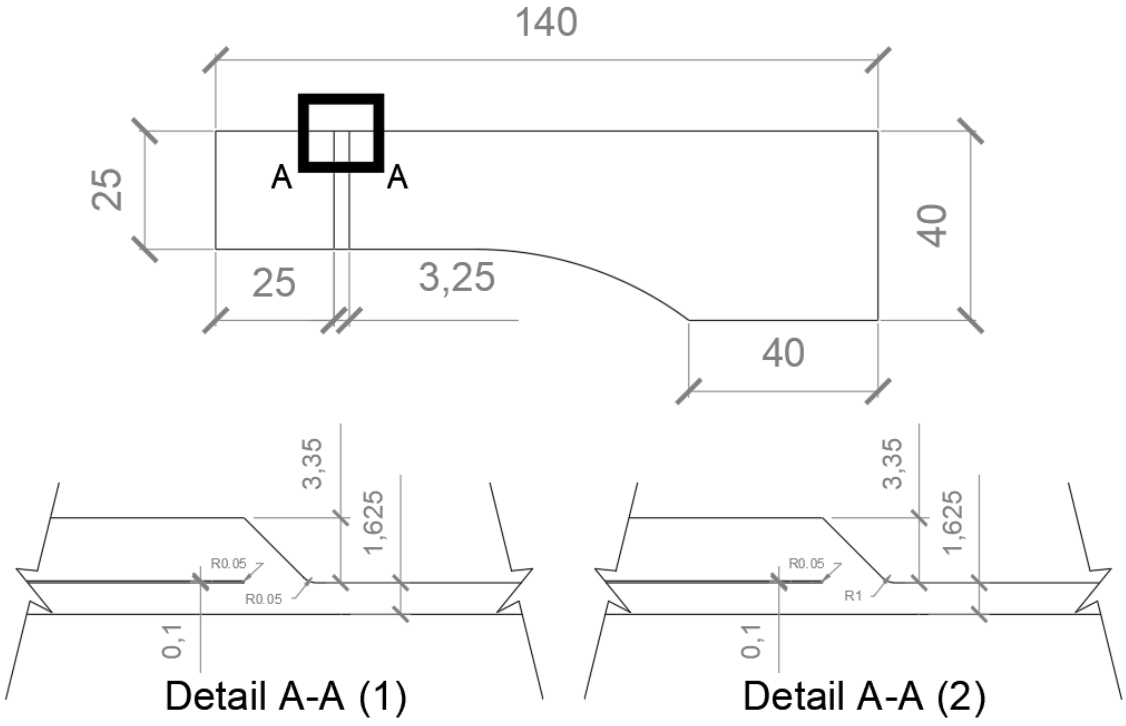

Figure 4.1: The dimensions of the axially loaded Abaqus model, with the recreated details illustrated in Detail A-A (1), and the details used by Leitner and Stoschka in Detail A-A (2) (all units are in mm). [Writers own figure]

The specimen fulfils the IIW Fricke (2010) requirements for 2D modelling described in section 2.3.2.1 and therefore the geometry can be represented using a 2D planer or 3D

solid Finite Element model. However, because the location of the highest effective notch stress is in the transverse direction, the location of fatigue crack initiation cannot be seen in a 2D model. Therefore, a 3D solid Finite Element model was created for analysis.

4.1.1 Geometry

As the specimen exhibits symmetric geometry and was loaded uniformly, only a portion of the specimen needed to be modelled instead of the entire geometry. This simplified the model and reduced the amount of work involved in analysis. Accordingly, only one-eighth of the specimen was modelled, as shown in Figure 4.2. It can also be seen in the figure that a gap of 0.1 mm was modelled between the plate-girder and the cover-plate.

The weld geometry was also included in the model assuming an idealised shape with a 45° inclination. The weld volume was created using the "solid extrude" in Abaqus software where the weld geometry was sketched as an triangle with a leg-length of 3.25 mm and with an ideal angle of 45°, thereafter extruded along the cover-plate width. The effective notches at the weld toe and root were modelled according to the recommendation provided in Fricke (2010). Thus the notch at the weld root was represented by a U-shape with a 0.05 mm radius. While the effective notch at the weld toe was rounded to a radius of 0.05 mm.

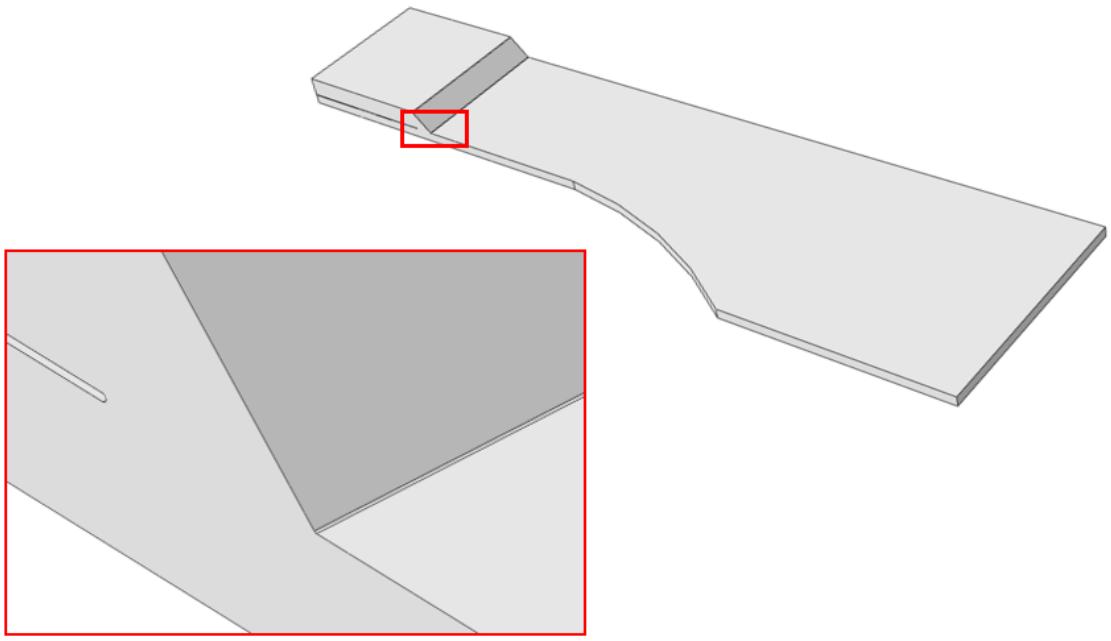

Figure 4.2: Visualization of FE model in Abaqus of the test specimen shown in Figure 4.1, with root and toe notch details.

4.1.2 Loading and boundary conditions

As mentioned previously, only elastic analysis is assumed for computing effective notch stresses. This means that the computed stresses increase linearly with the increase in applied nominal stresses. That makes it possible to use a unit load (nominal stress) instead of the real stress. Thus a unit nominal stress of 1 MPa is applied to the model as a uniform pressure with a negative sign as seen in Figure 4.3. As a result of applying a unit load, a factor called Stress Concentration Factor K_f (SCF) is calculated, which is defined as the ratio between effective notch stress and nominal stress. The resulting effective notch stresses at the toe and root can then be obtained by multiplying the SCF with the actual nominal stress.

Furthermore, because the Abaqus model was partitioned due to symmetric conditions, symmetry boundary conditions were assumed on three sides of the model. This can be seen in Figure 4.3.

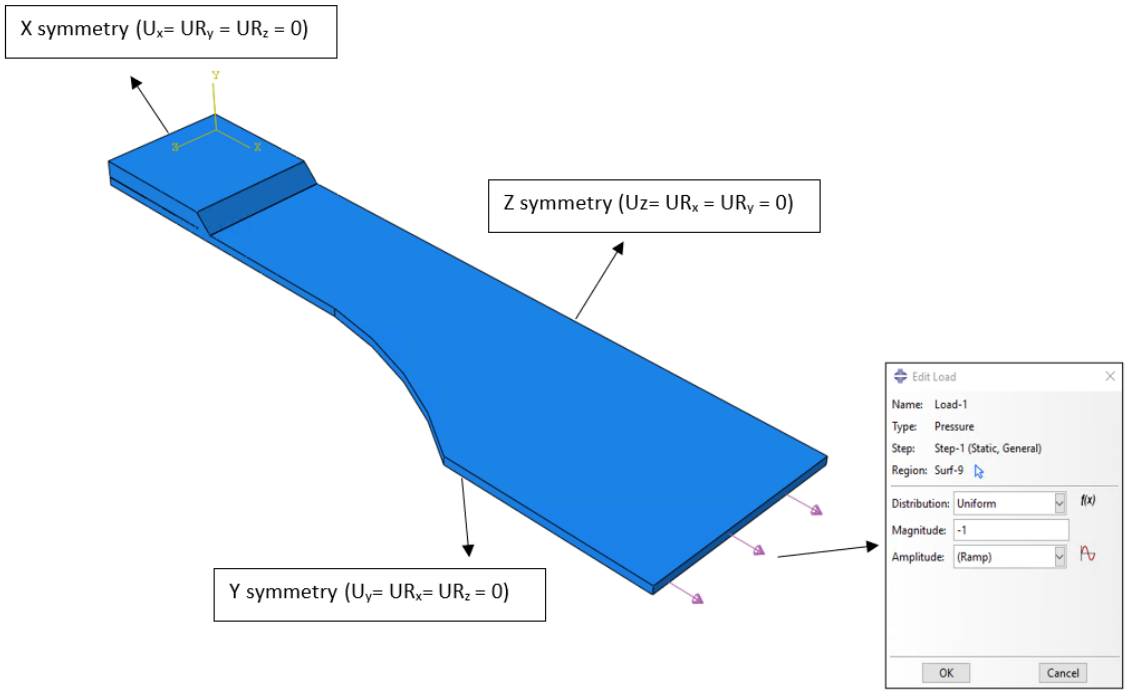

Figure 4.3: The applied load and boundary conditions for the axially loaded FE model (Leitner and Stoschka).

4.1.3 Meshing

As discussed previously in section 2.3.2.1, a fine mesh in the region near the effective notches can be obtained by creating a sub-model or dividing the model into partitions. Since the modelled specimen is small and has a simple shape without complicated details, the best approach would be to create partitions instead of a sub-model. Thus the geometry was divided into partitions and cells, as shown in Figure 4.4, where each part was meshed locally so that the mesh size gradually increased from the inside to the outside. In contrast, the remaining un-partitioned geometry was assigned a global mesh.

The notch regions were meshed with an element size of 0.008 mm. This is in agreement with IIW Fricke (2010) recommendations, see Table 2.3. In addition, the global element size was set to 1.625 mm (equal to half of the plate thickness) and the element type was linear with tetrahedral elements.

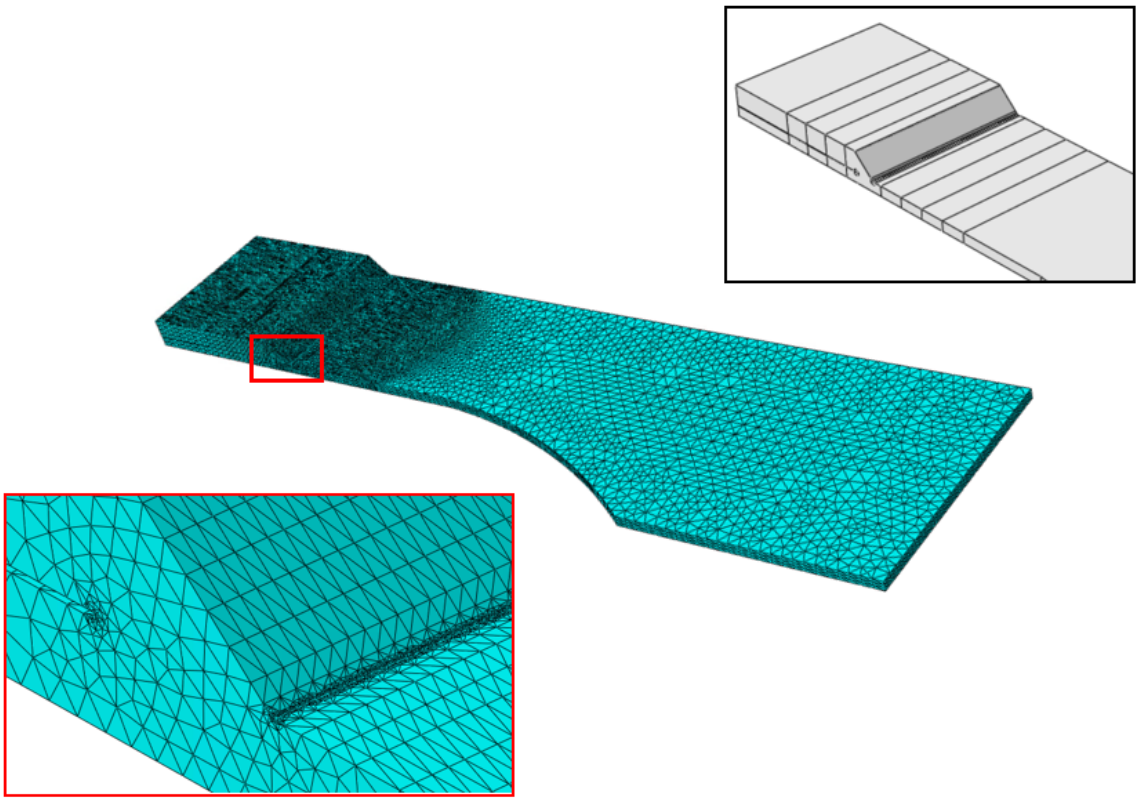

Figure 4.4: The created partitions and applied mesh for the axially loaded FE model (Leitner and Stoschka).

4.2 Vilhauer et al, 2011

The second recreated fatigue test is from Vilhauer et al. (2012) experiment on cover-plated flange-girder loaded in three-point bending. Because the test performed by Vilhauer et al. does not utilise ENS for the Finite Element analysis, the only comparison between the analyses can be of fatigue failure (cracking). The fatigue strength is instead compared to the IIW fatigue S-N curves for as-welded and HFMI-treated joints. In short, the aim of including Vilhauer et al. experiment is to evaluate if the specimen modeled according to the Effective Notch Stress method gives reasonable results according to IIWs ENS fatigue S-N curve guidelines. The notch stresses are attained by performing a convergence study of five different notch element sizes.

The joint of the analysed specimen is a complicated detail with asymmetric geometry and intricate stress distribution due to three point bending. Therefore, the specimen does not meet the requirements for 2D modeling according to the IIW (Fricke, 2010) guidelines. Hence, the specimen will be modeled using a 3D solid finite element model in Abaqus.

4.2.1 Geometry

The dimensions of the specimen used for the analysis can be seen in Figure 3.3 in section 3.2. In the figure it can be observed that the specimen has a symmetric geometry. It can therefore be partitioned into a quarter of its original size to simplify the procedure of the 3D modelling in Abaqus. The dimensions used to model the specimen in Abaqus can be seen in Figure 4.5.

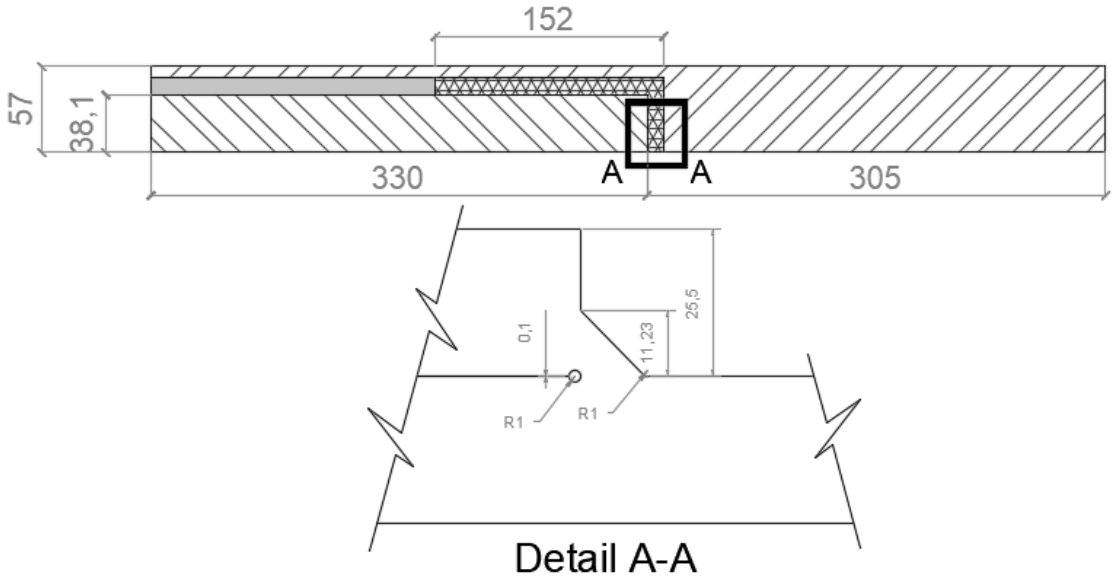

Figure 4.5: Dimension's of the quarter test specimen modeled in Abaqus with a flange-girder and one sided cover-plate i bending (all units are in mm). [Writers own figure based on Figure 1 in Vilhauer et al. (2012)]

When creating the model in Abaqus the volumes for the cover-plate and flange-girder were created separately and then assembled together with the 0.1 mm gap between the plates. The weld volume was then added using Abaqus built-in features. Firstly, the command "solid extrude" was used, where the weld geometry was sketched according to Figure 4.5 with an idealised shape of 45° inclination and extended to the cover-plate corner. Then, the extruded weld volume was rotated around the cover-plate corner via the command "solid revolve" and lastly, the weld volume was stretched along the remaining cover-plate with the command "solid sweep".

To perform the FE analysis based on the Effective Notch Stress method, the effective notches at the weld toe and root were modeled according to the recommendations mentioned in section 2.3.2.1. The plates have a thickness of 25.4 mm, which corresponds to a reference radius of $r_{ref} = 1$ mm. The toe notch was rounded using the command "fillet". Lastly, the root notch was modeled with a keyhole shape using the command "cut extrude". The arrangement of the effective notches can be seen in detail in Figure 4.5 Detail A-A, and the finalised Abaqus model is seen in Figure 4.6.

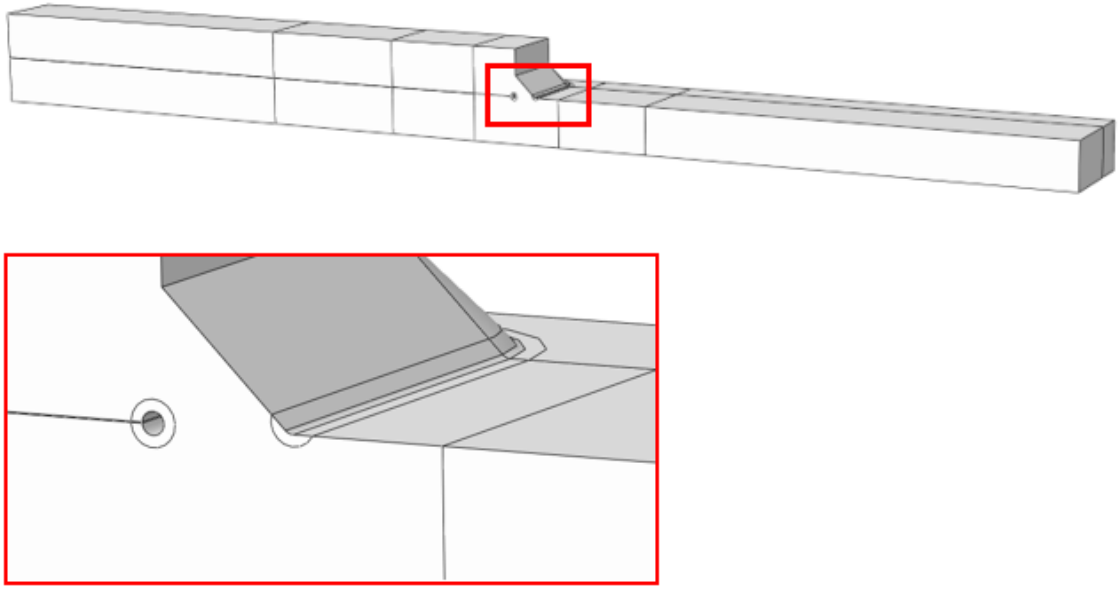

Figure 4.6: Visualization of FE model in Abaqus of the test specimen shown in Figure 4.5.

4.2.2 Loading and boundary conditions

The load applied to Vilhauer et al. specimen is a point load placed at the centre of the full-size flange-girder, and to perform the analysis the load $P_{V,u}$ was calculated assuming a unit nominal stress of 1 MPa. This was accomplished by the help of Equation 3.1 that Vilhauer et al. used to estimate the stress at the end weld toe. The moment at the end weld toe could then be determined from the unit nominal stress of 1 MPa at the weld toe. With the assumption that the supports are placed at the transverse edges of the flange-girder, because the exact test set up was not specified, the load $P_{V,u}$ was determined by the moment equation derived from basic mechanics. Which was determined to be 83.5 N. Although, for the Abaqus model a quarter of the calculated load ($P_{V,u.a} = 21$ N) was applied. This load was verified by calculating the load $P_{V,a}$ of each nominal stress that Vilhauer et al. used in the test and multiplying the load $P_{V,u.a}$ by the nominal stresses to see if the same load $P_{V,a}$ was derived. The detailed calculation of the loads for each nominal stress can be viewed in Appendix B.1. Henceforth, the load is placed on the flange-girder as a pressure equivalent to the total force, as shown in Figure 4.7.

Furthermore, symmetric boundary conditions are applied at the partitioned edges and a support is placed at the free plate-girder edge, which can also be seen in Figure 4.7.

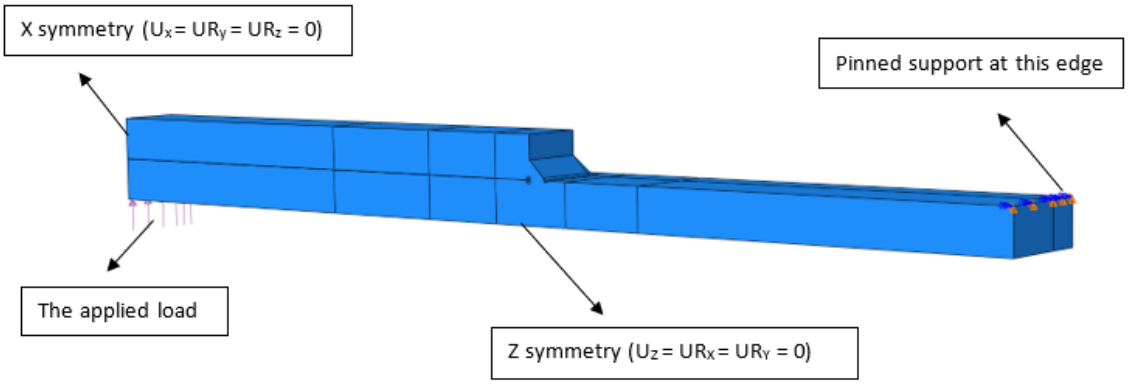

Figure 4.7: The applied load and boundary conditions for the first FE model subjected to bending (Vilhauer et al.).

4.2.3 Meshing

The prime focus of Vilhauer et al. specimen is the notches of the transverse end weld, and the focal point is the approximate maximum principal stresses at the weld toe and root. Therefore, cells were created at the notches and a finer element size was applied. As previously explained in section 4.1.3 this can be achieved either by dividing the model into partitions or creating a sub-model of the primary part to be analysed. For the same reason as stated for Leitner and Stoschka model in section 4.1.3, the alternative chosen was to divide Vilhauer et al. specimen model into partitions.

The model has six main partitions (regions), which can be seen in Figure 4.8. The finest element size was applied at the transverse end weld, which gets gradually larger for each partition. In region 1 the element size used was 2.5 mm, in region 2 it was 5 mm, in region 3 it was 7.5 mm, and in region 4 it was 12.7 mm. Considering that a convergence study was performed for this test, the element size of the main six partitions was not altered for each convergence, instead the element size at the notches was altered.

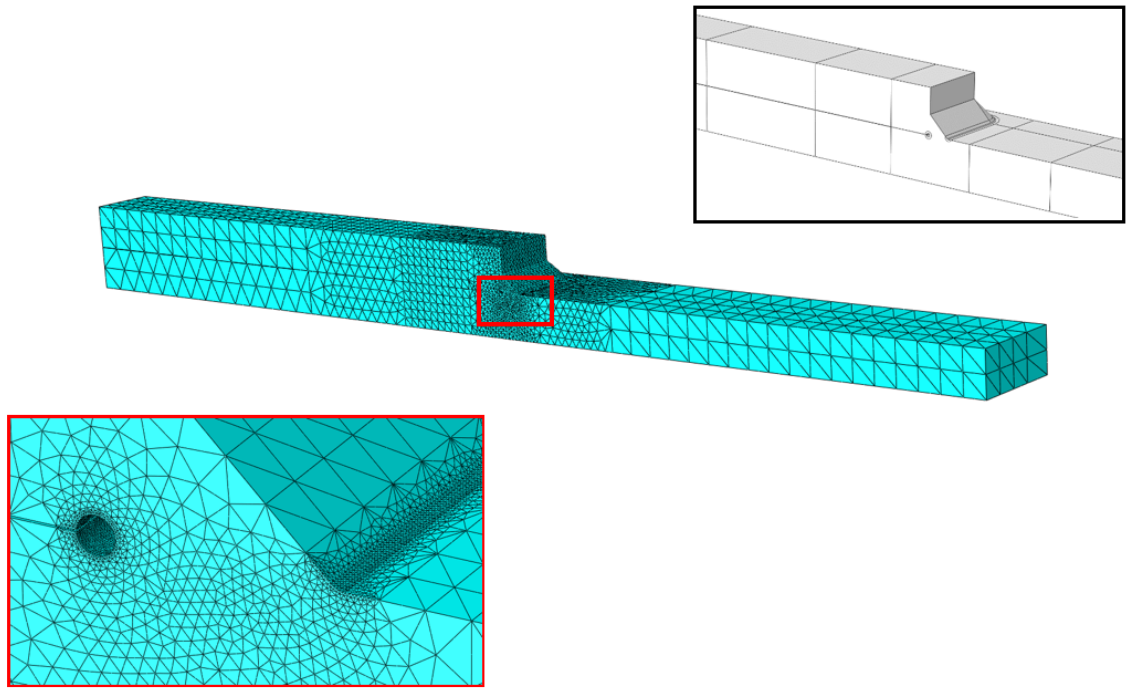

Figure 4.8: The created partitions and applied mesh for the first FE model subjected to bending (Vilhauer et al.).

The recommended notch element size according to IIW (Fricke, 2010) for models with a reference radius of $r_{ref} = 1$ mm is that of ≤ 0.15 mm for a linear finite element study, as seen in Table 2.3. This element size is used as a starting point for the convergence study. A total of five analyses were performed with element sizes of 0.3 mm, 0.25 mm, 0.2 mm, 0.15 mm and 0.1 mm as the notch element size. The method used to designate the element size was to use the Abaqus command to appoint the mesh size at the model's edges. Therefore, an intricate fine mesh could be applied to the notch cells and a coarse mesh to the partitions. The full detail of the appointed element size of each assessment can be seen in Appendix B.2 and the resulted mesh size used for the finalised analysis is presented in section 5.2.

4.3 Hui et al, 2018

As stated previously in section 3.4 the test was conducted on full-scale I-beams provided with transverse stiffeners and cover-plates of two different lengths, see figure 3.8. Thus two different finite element models were constructed for the analysis and in order to simplify the modelling process, transverse stiffeners were not modelled. Because the tested specimens are relatively large and have more details than the specimens presented in sections 4.1 and 4.2, the sub-modelling approach was implemented, and the model was developed in two stages. Firstly, a global model was created where the entire geometry shown in Figure 4.9 was modelled. The second stage involved to construct a local model (sub-model) of small region surrounding the effective notches.

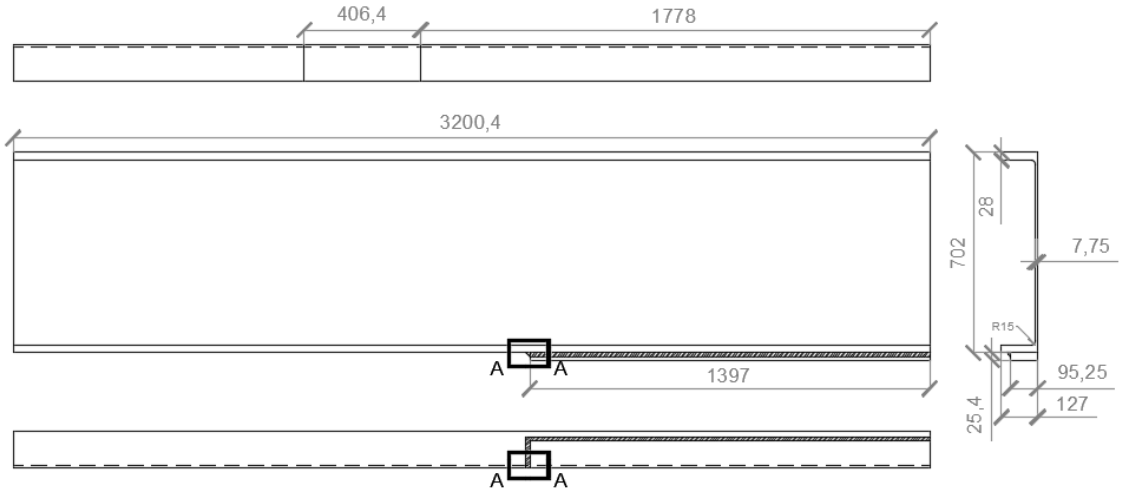

Figure 4.9: The dimensions of the modeled specimen in Abaqus, illustrates a quarter of the S7-S14 beams with the longer cover-plate (all units are in mm). [Writers own figure]

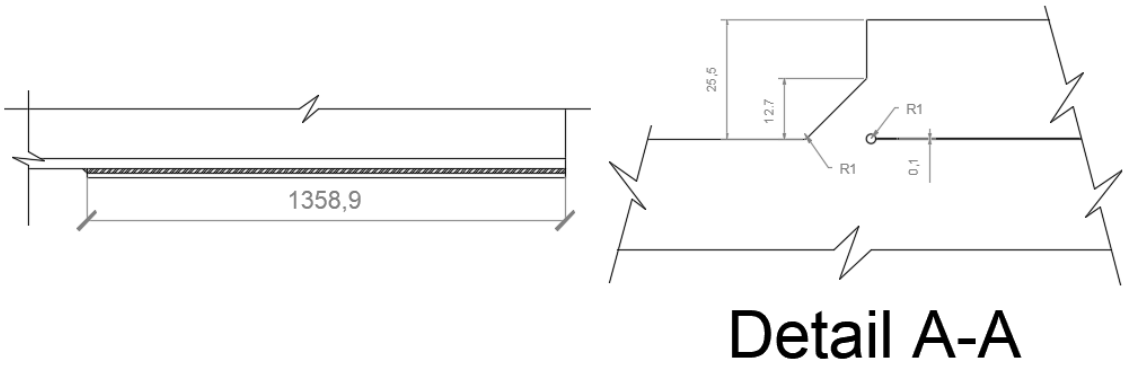

Figure 4.10: Figure on the left illustrates the section of the S1-S6 beams with the shorter cover-plate. Figure on the right illustrates the notch detailing of the weld presented as Detail A-A in figure 4.9 (all units are in mm). [Writers own figure]

4.3.1 Geometry

Since the specimens exhibit symmetric geometry in two directions, the global model included only a quarter of the specimen, see Figure 4.9. When creating the model, the volumes of the structure were constructed in the same way as the previous model, seen in section 4.2.1. Moreover, the effective notches at the weld toe and root were constructed according to IIW recommendations (Fricke, 2010). Due to the fact that the cover-plate thickness is more than 5 mm, the notch at the toe was rounded by a reference radius of $r_{ref} = 1$ mm and the notch in the root was modeled as a keyhole shape with the same radius. In addition, partitions measuring 25 mm from the cover-plate end were created to define the sub-model. The global model and sub-model are shown in Figure 4.11.

The aim of creating a global model is to compute the displacement at the boundary of the sub-model. That is why it is imperative (Heshmati et al., 2012) that the nodal coordinates of the sub-model region are the same in both the global and the local models. That can be obtained by creating the sub-model separately and then transferring it to the correct position, or by cutting the sub-model from the global model. To ensure that the sub-model is in the right position, the latter method was used for constructing the sub-model. Thus, the entire global model was created first, and then copied and renamed. After that, the geometry of this new module was modified by removing all faces and cells not relevant to the sub-model.

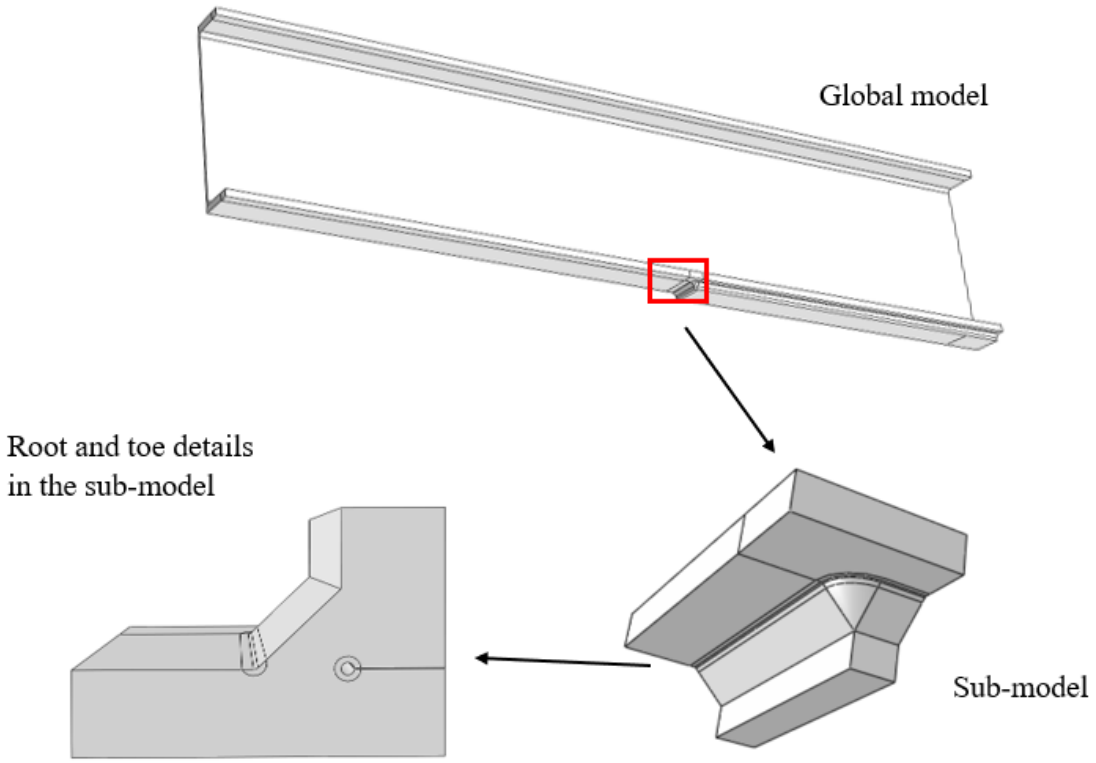

Figure 4.11: Visualization of FE model in Abaqus of the test specimen shown in Figures 4.9 and 4.10.

4.3.2 Loading and boundary conditions

The applied load was calculated in an identical way to that used in section 4.2.2. The only difference is that in this case, the support position is known and there is no need to make an assumption. The calculated load $P_{H,u}$ for a unit nominal stress range of 1 MPa is 4.624 kN for beams S1-S6 and 4.484 kN for S7-S14 and the detailed calculations are shown in Appendix C.2. The calculated loads were then divided by two ($P_{H,u.a1} = 2.312$ kN and $P_{H,u.a2} = 2.242$ kN) since the model have symmetric boundaries. The load was applied onto about a third of the beam, in the same location as seen in Figure 3.8. Furthermore, the load was represented in the model as a pressure equivalent to the total force. For the load to be included in the sub-models, the global models must firstly be analysed and then the results are transferred to the sub-models in the form of boundary conditions.

Furthermore, two types of boundary conditions were applied to the global models, symmetric boundary conditions at the partitioned faces and a displacement boundary at the rolled support, see Figure 4.12. For the sub-models, symmetry boundary condition were applied in the x-direction, similarly to the global models. Additionally, the joint boundaries between the sub-models and global models were restrained for all three translational degrees of freedom (U1, U2, U3), as seen in Figure 4.12. The displacements are determined from the results obtained from the global analysis.

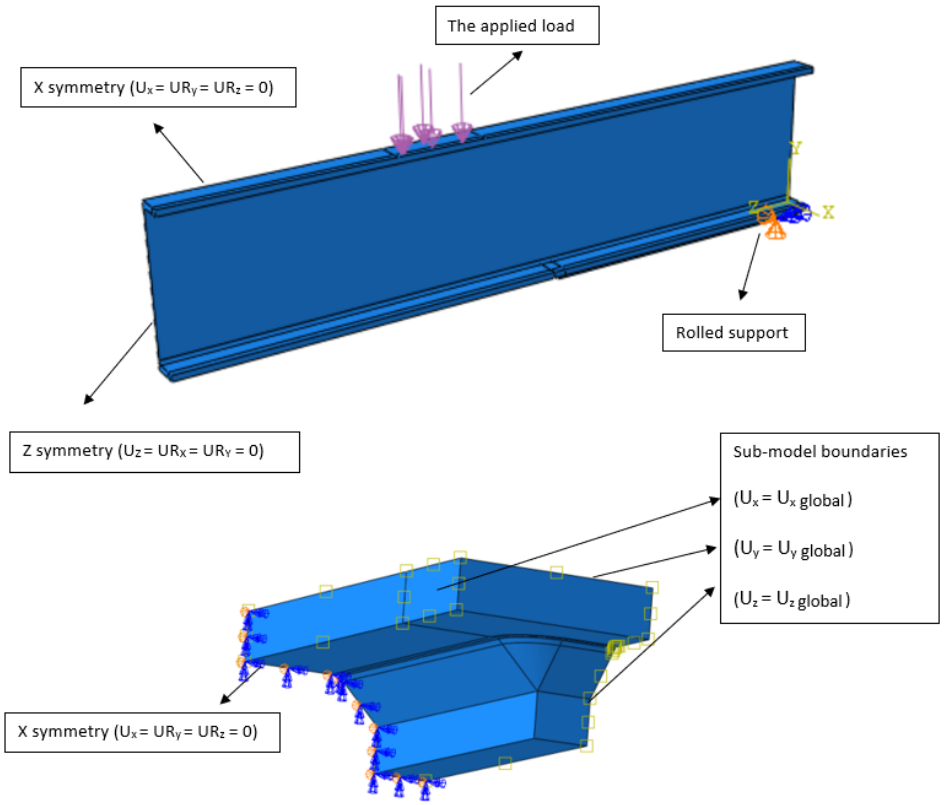

Figure 4.12: The applied load and boundary conditions to the global-model and sub-model for the second FE model subjected to bending (Hui et al.).

4.3.3 Meshing

As explained previously, the aim of using the sub-modelling technique is to reduce the required time and work for analyses. Accordingly, the global model was meshed with a coarse mesh with an element size of 25 mm, see Figure 4.13. Whereas the sub-model was meshed with the same refined mesh obtained from the convergence study performed on the model in the previous test. This can be read in section 4.2.3 and section 5.4.

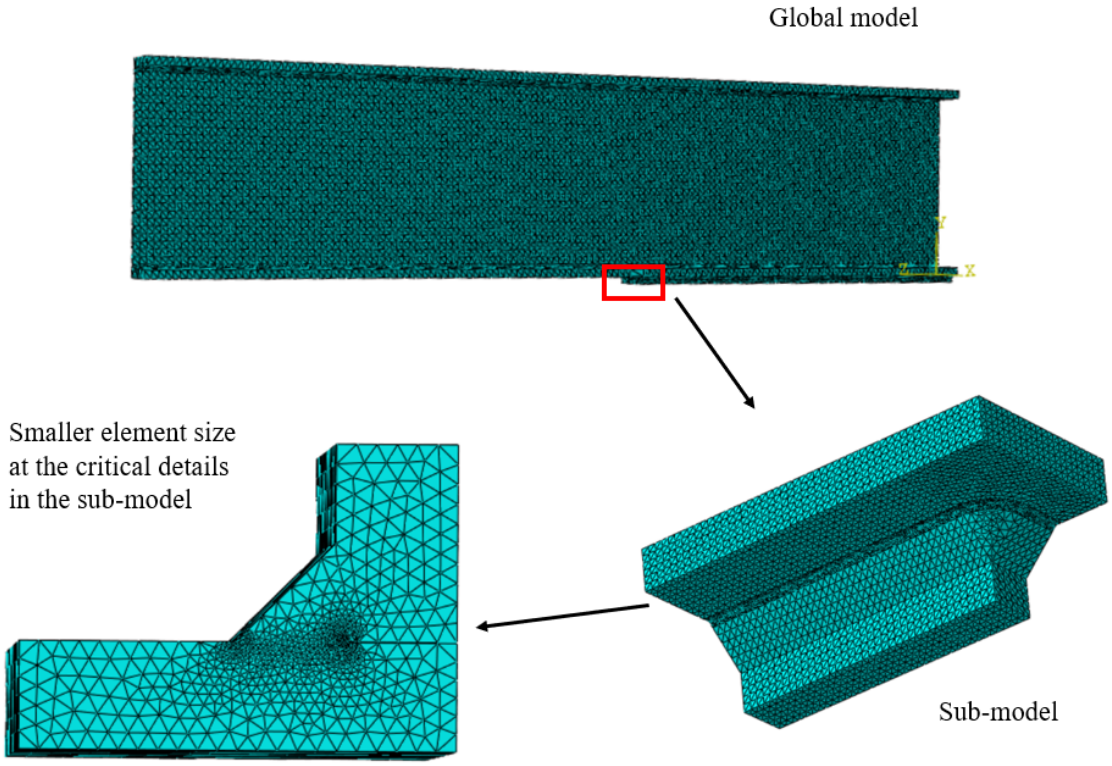

Figure 4.13: The applied mesh to the global-model and sub-model of the second FE model subjected to bending (Hui et al.).

5
Results

In this chapter the results from the Finite Element analyses performed in chapter 4 are assembled for the purpose of compiling S-N graphs. The objective is to evaluate and compare the test results with the design fatigue S-N curves from IIW for both as-welded and treated cover-plates. Since Eurocode (European Standard, 2022) has not yet finalized S-N curves for HFMI-treated details with ENS method. Due to the FE analyses being conducted using the Effective Notch Stress method, the fatigue life assessment of the cover-plates was also conducted using the Effective Notch Stress method by utilizing the corresponding S-N curves presented in section 2.3.2.2 and 2.3.2.3.

The issue is further investigated by conducting a theoretical evaluation to determine what cracking mode is most prevalent to occur. Thus, it can be determined if the design methods used today are in accordance with the practical test results and hence relevant when designing cover-plated structures.

To further contribute to the aim of this master thesis, it is necessary to understand how stress distribution flows through cover-plated details and how stress concentration varies for different structures. Hence, stress fields were extracted from Abaqus for each test model. Thus, a thorough examination of the results can be discussed and compared to understand the structural behaviour of different cover-plated steel components and perhaps predetermine the failure mode.

Lastly, the stress distribution from the weld root to the weld toe is extracted from Abaqus from each model. Which is then used to define the difference in cracking mode between cover-plates loaded axially and those loaded in bending.

5.1 Leitner and Stoschka, 2020

As mentioned in section 4.1, the analysis for Leitner and Stoschka test was performed for a unit nominal stress equal to 1 Mpa. The obtained results from the FE analysis are the maximum principal stresses at the toe and root notches. Figure 5.1 shows the resulting stress distribution of the model.

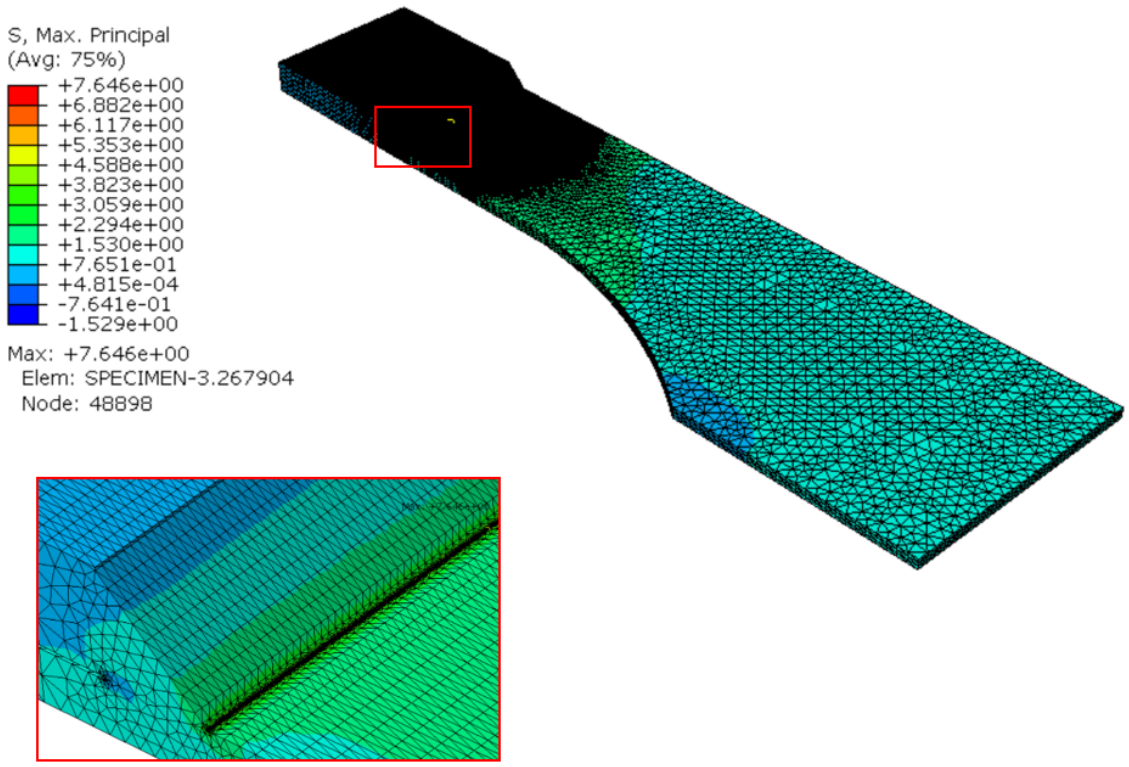

Figure 5.1: Maximum principal stress results of the FE analysis for the axially loaded model (Leitner and Stoschka) under a unit nominal stress of 1 Mpa applied at weld toe.

The maximum principal stress at the toe equals to 7.646 Mpa, as shown in the figure. Furthermore, the maximum principal stress at the root is found to be a compressive stress equal to -0.6 MPa. The effective notch stresses are calculated by multiplying the results from the FE analysis with the respective nominal stress ranges Leitner and Stoschka used for the practical tests seen in Figure 3.2. The nominal stresses that are derived from the figure are for as-welded specimens and HFMI-treated specimens with a stress ratio of $R = 0.1$. Because for this master thesis treated cover-plates with a stress ratio of $R > 0.15$ will not be considered. It should be mentioning that the nominal stresses are approximated from the figure, since no exact values were provided in Leitner and Stoschka report. The calculated effective notch stress for each nominal stress is presented in Table 5.1.

Table 5.1: Effective notch stress ranges at toe and root for each nominal stress range from Leitner and Stoschka test.

$\Delta\sigma_{NS}$	$\Delta\sigma_{Toe_{ENS}}$	$\Delta\sigma_{Root_{ENS}}$	$\Delta\sigma_{NS}$	$\Delta\sigma_{Toe_{ENS}}$	$\Delta\sigma_{Root_{ENS}}$
1	7.646	-0.6	250	1,912	-150
125	955	-75	275	2,103	-165
150	1,147	-90	300	2,294	-180
175	1,338	-105	325	2,485	-195
200	1,529	-120	350	2,676	-210
225	1,720	-135	400	3,058	-240

5.1.1 Fatigue study

With the effective notch stresses obtained from the FE analysis seen in Table 5.1 and the load cycle data Leitner and Stoschka obtained from the practical test presented in Figure 3.2, two S-N graphs were assembled. One for the as-welded specimens and another for HFMI-treated specimens. Similarly to the nominal stress, the number of load cycles for each specimen were approximated from the figure. Hence, the S-N graphs were assembled using the effective notch stresses from Table 5.1 and load cycles from Table 5.2.

Table 5.2: Number of load cycles the specimens reach during Leitner and Stoschka practical test, based on provided data in Figure 3.2. [Writer own table]

$\Delta\sigma_{NS}$ [MPa]	As-welded specimen Load cycles	HFMI-treated specimen Load cycles
125	20,000,000	-
150	10,000,000	-
175	400,00	-
200	425,000	-
	375,000	-
225	-	20,000,000
250	175,000	9,000,000
275	230,000	640,000
	-	600,000
300	160,000	500,000
	-	435,000
	-	325,000
325	-	310,000
350	40,000	-
400	42,500	150,000
	-	130,000
	-	80,000

The S-N graph for untreated specimens is shown in Figure 5.2, where the dots represent the specimen and the black curve corresponds to the IIW recommended fatigue curve for as-welded joints with plates thinner than 5 mm. As mentioned in Section 2.3.2.2, this corresponds to a fatigue curve of FAT 630, as seen in Figure 2.18. Accordingly, the same recommended curve can be applied to both toe and root stresses. Leitner and Stoschka (2020) writes that all untreated specimens cracked at the weld toe. This means that the effective notch stresses applied to the graph are the toe stresses seen in Table 5.1 and the root stresses are excluded. It can be seen in Figure 5.2 that the FE analysis results correlate well with the recommended fatigue curve.

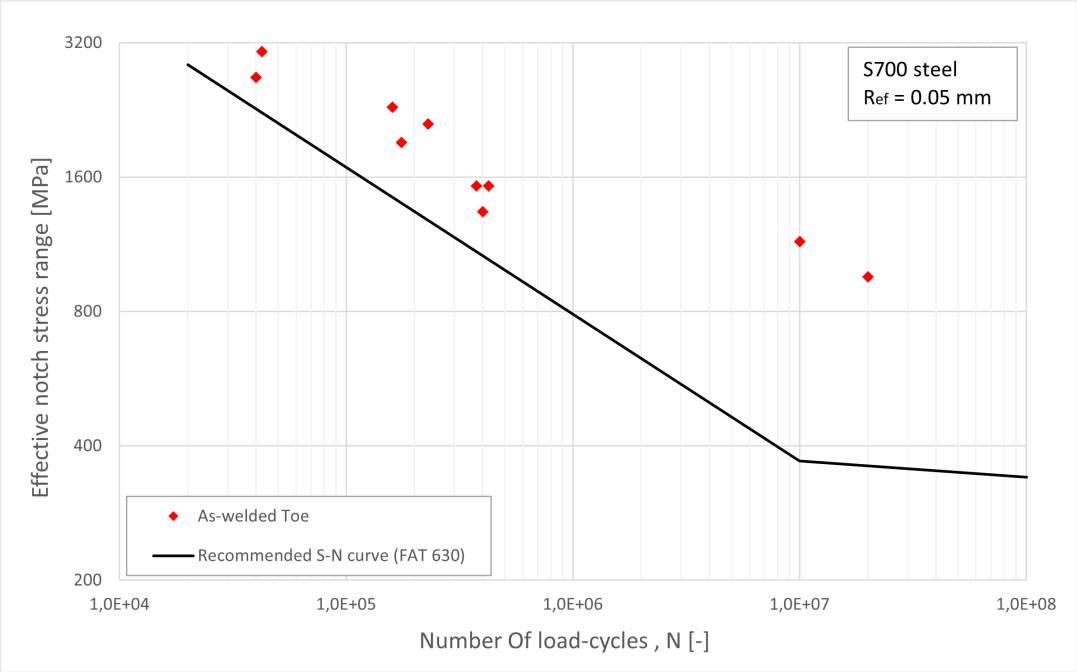

Figure 5.2: Effective notch stress ranges at weld toe from FE analysis applied to a S-N graph for Leitner and Stoschka as-welded specimens loaded axially. With the recommended S-N curve FAT 630.

Figure 5.3 shows the S-N graph for the HFMI-treated specimens. Similarly to Figure 5.2, the dots in the graph represent the specimens treated with HFMI. Equally to the untreated specimens, Leitner and Stoschka mentions that cracking initiated at the weld toe for all HFMI-treated specimens. Which means that the effective notch stresses assigned to the graph are of the weld toe stresses seen in Table 5.1.

Furthermore, the ENS recommended S-N curve for HFMI-treated details with plates thinner than 5 mm could not be found in any publications. As the curves suggested by the IIW Marquis and Barsoum are only applicable to joints with plates between $5 \leq t \leq 50$ mm thick. A fatigue design curve for thinner plates with steel strength S700 is calculated. The curve is shown by the blue curve in Figure 5.3. This S-N curve was developed by using similarity theorem with the IIW recommended fatigue curves FAT 225 and FAT 400 for thicker plates and FAT 630 for thinner plates. This can be seen in Equations 5.1 and 5.2, which result in the fatigue curve FAT 1,120.

$$\frac{\Delta\sigma_{C_{HFMI,plates<5mm}}}{\Delta\sigma_{C_{plates<5mm}}} = \frac{\Delta\sigma_{C_{HFMI,plates\geq5mm}}}{\Delta\sigma_{C_{plates\geq5mm}}} \tag{5.1}$$

$$\Delta\sigma_{C_{HFMI,plates<5mm}} = 630 \times (\frac{400}{225}) = 1,120MPa \tag{5.2}$$

By comparing the relation between the calculated S-N curve FAT 1,120 and the FE analysis results, it can be seen in Figure 5.3 that the suggested design curve is very conservative in comparison to the results. However, this indicates that the calculated S-N curve correlates well with the specimens' fatigue behaviour in various stress ranges.

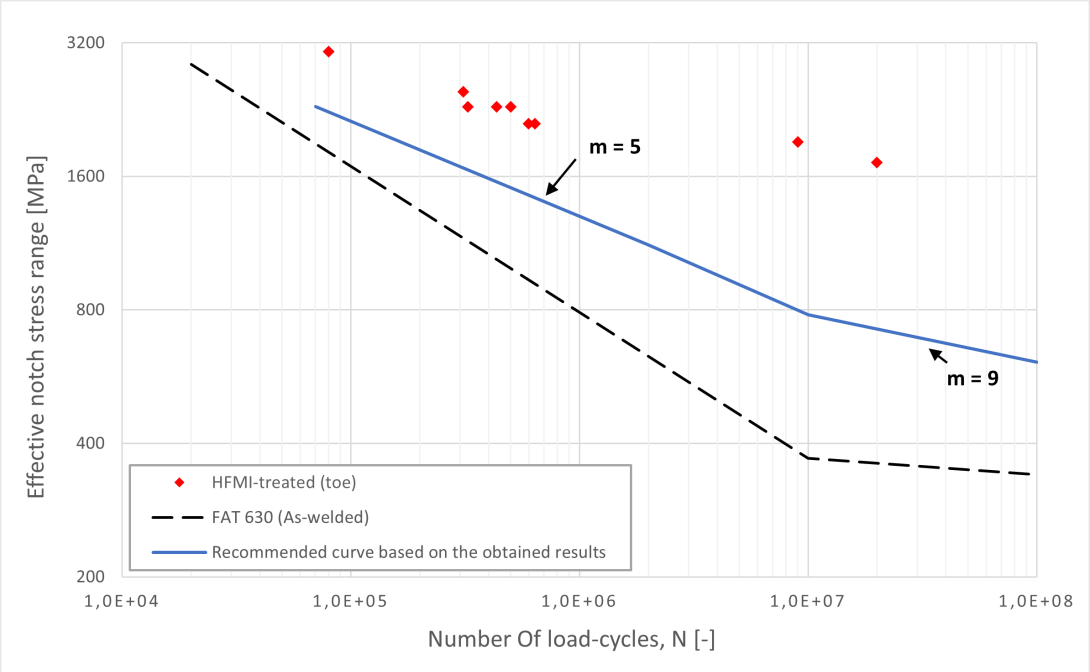

Figure 5.3: Effective nocth stress ranges at weld toe from FE analysis applied to a S-N graph for Leitner and Stoschka HFMI-treated specimens loaded axially. With the recommended S-N curve FAT 630 and calculated S-N curve FAT 1,120.

Moreover, from the results of Figure 5.2, 5.3 and Table 5.2, it is evident that HFMI-treated cover-plated plate-girders subjected to uni-axial loading exhibit improved fatigue performance. Which Leitner and Stoschka also states in section 3.1.

Aside from this, the cracking mode for both as-welded and HFMI-treated cover-plated structures loaded uni-axially occurs at the weld toe according to Leitner and Stoschka results. This is proven in Table 5.1, where the maximum principal stresses at the weld toe are in tension, while the stresses at the weld toe are in compression.

5.1.2 Stress fields

Maximum principal stress fields of Leitner and Stoschka specimen were obtained from Abaqus and can be seen in Figure 5.4, where various stress ranges are visible in each sub-figure, which can also be seen in Appendix A.1. In Figure 5.4(a) it is observed that the maximum compressive principal stresses are located at the root notch of the weld. From Figures (b) and (c) it is apparent that the higher stresses in the plate-girder are divided between the cover-plate and plate-girder by flowing through the weld, hence the lower stresses in Figure (b).

Furthermore, the largest tensile stresses are concentrated at the weld toe, as shown in Figure (d). This concentration difference between the weld root and toe is consistent with the results in Table 5.1, as well as Leitner and Stoschka result and the premise that fatigue failure occurs at the weld toe for cover-plated structures loaded uniaxially. Due to the accumulation of compressive stresses at the weld root no cracks will be developed. While the concentration of tensile stresses accumulating at the weld toe will develop cracks at the midpoint of the stress vectors in Figure (d).

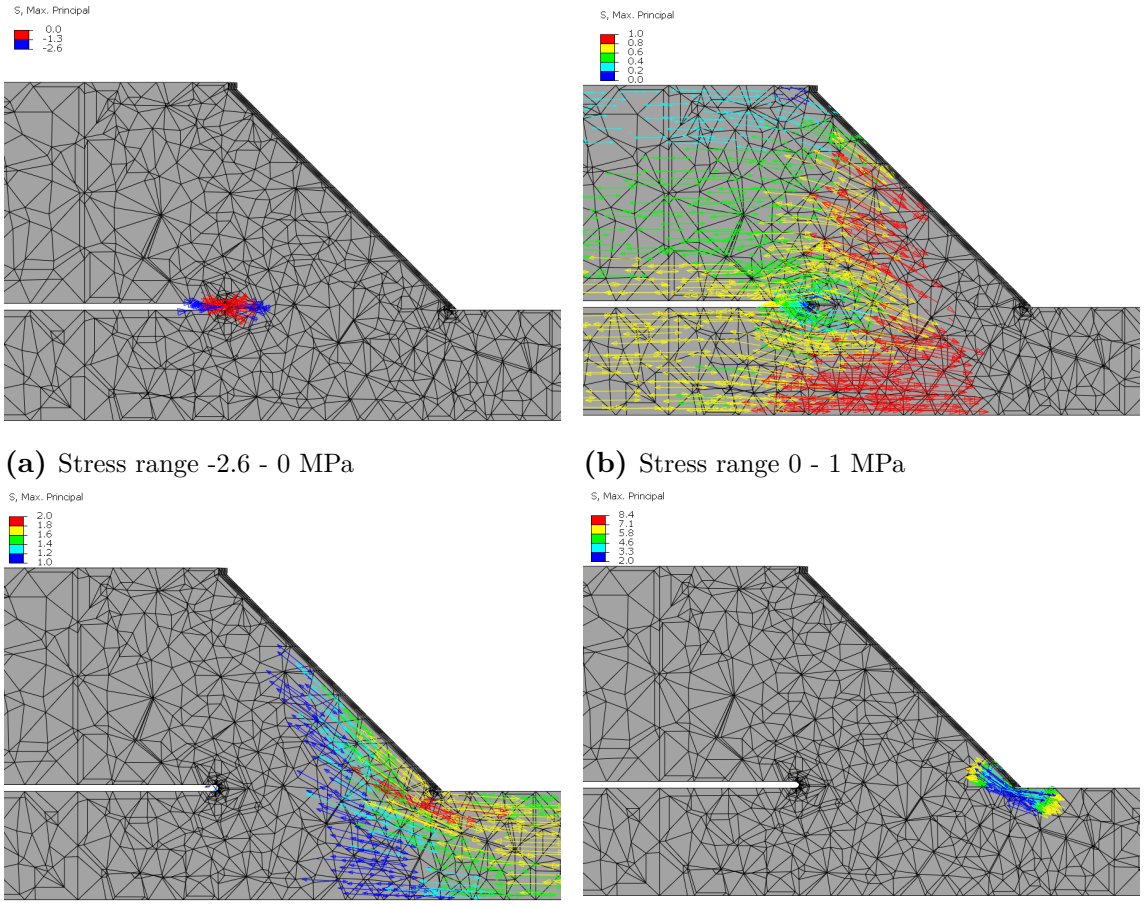

(a) Stress range -2.6 - 0 MPa

(b) Stress range 0 - 1 MPa

(c) Stress range 1 - 2 MPa

(d) Stress range 2 - 8.4 MPa

Figure 5.4: Maximum principal stress field distribution in 4 different stress ranges for Leitner and Stoschka test model loaded axially, under a unit nominal stress of 1 MPa.

5.2 Convergence study of element size for cover-plated structures loaded in bending

A convergence study was performed on Vilhauer et al. test model described in section 4.2, for the purpose of determining the most appropriate element size to mesh weld root and toe notches of structural elements with cover-plates thicker than 5 mm. Vilhauer et al. model was used for the convergence study because it is the most relevant and simple model to perform the convergence study on. This is because Leitner and Stoschka model has cover-plates that's thinner than 5 mm and Hui et al. model is more complex compared to Vilhauer et al. model. Hence, the intention of performing the convergence study on Vilhauer et al. model was to determine element sizes that could be used for the following analyses. This includes Hui et al. model in section 4.3 and the models analysed for the exploratory studies in chapter 7.

The recommended element size for linear analyses of cover-plates thicker than 5 mm is a size of ≤ 0.15 mm as shown in Table 2.3. Therefore, a total of five element sizes were selected as specified in section 4.2.3, namely 0.3 mm, 0.25 mm, 0.2 mm, 0.15 mm, and 0.1 mm. The exact meshing layout for all element sizes and partitions is displayed in Appendix B.2. The selected mesh can be seen in Figure 4.8.

To perform the convergence study, a total of 10 maximum principal stresses were extracted from each analysis. 5 stresses at weld toe and 5 stresses at weld root. These stresses can be seen in Appendix B.3 Table B.1. Subsequently, the average stress was calculated from the 5 stresses and a convergence study was conducted, as seen in Table 5.3.

Table 5.3: Average maximum principal stress at toe and root of each convergence study performed for Vilhauer et al. model subjected to bending under a unit nominal stresses of 1 MPa at weld toe.

Model loaded with 1 MPa at weld toe				
Mesh size [mm]	Average stress at Toe [MPa]	Difference [%]	Average stress at Root [MPa]	Difference [%]
0.3	3.613		1.894	
0.25	3.693	2.21	1.892	0.08
0.2	3.707	0.37	1.914	1.15
0.15	3.705	0.05	1.914	0
0.1	3.728	0.62	1.903	0.59

It was decided that convergence is acceptable at a difference of $\leq 0.5\%$. The results in Table 5.3 demonstrate that root stresses converge at a notch element size of 0.15 mm. In contrast, toe stresses converge at a notch element size of 0.2 mm, but are refined at 0.15 mm. Hence, it is concluded that for both toe and root notches the most applicable element size is 0.15 mm, which is in accordance to the recommended size by IIW (Fricke, 2010).

5.3 Villhauer et al, 2011

After the convergence study was performed, described in section 5.2, the maximum principal stresses from the appropriate element size were used to proceed with the study. Which is the element size of 0.15 mm at the notches. Hence, the maximum principal stresses obtained from the FE analysis were 3.705 MPa at the toe and 1.914 MPa at the root. In Figure 5.5 the results from the Abaqus model of Vilhauer et al. specimen can be seen. Where it is possible to see the deflection and the maximum principal stress distribution. The deflection indicates that the model is subjected to bending. The stress distribution indicates that the greatest accumulation of tensile stresses occurs at the toe, but they also develop at the root.

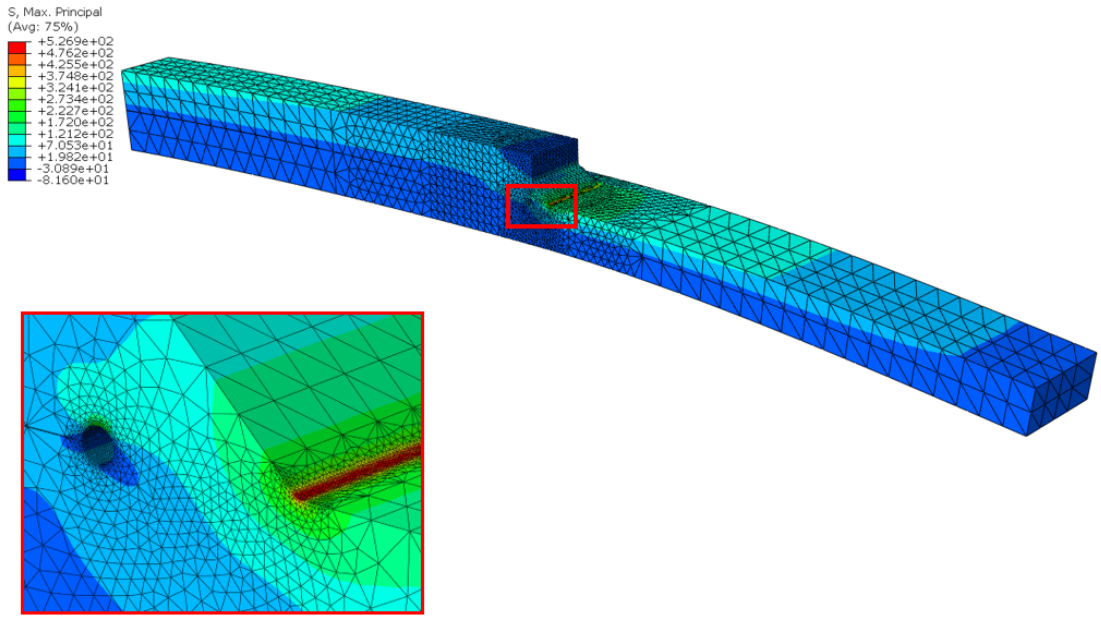

Figure 5.5: Maximum principal stress results of the FE analysis for the first model subjected to bending (Vilhauer et al.) under a unit nominal stress of 1 MPa applied at weld toe.

With the stresses acquired from the FE analysis, the effective notch stresses could be calculated for the nominal stresses Vilhauer et al. used in the practical tests (58.6, 96.5, 138 and 193 MPa), for both the ISR and HSR specimens as noted in section 3.2. The resulting effective notch stresses were calculated with the same procedure utilised in Leitner and Stoschka study described in section 5.1 and the results can be seen in Table 5.4.

Table 5.4: Effective notch stress at toe and root for each nominal stress for Vilhauer et al. test.

$\Delta\sigma_{NS}$ [MPa]	$\Delta\sigma_{Toe_{ENS}}$ [MPa]	$\Delta\sigma_{Root_{ENS}}$ [MPa]
1	3.705	1.915
58.6	210	109
96.8	358	185
138	511	264
193	715	369

5.3.1 Fatigue study

With the effective notch stresses determined from the FE analysis, the stresses were assembled into two fatigue S-N graphs, one for as-welded cover-plates and the other for HFMI-treated cover-plates. To assemble the S-N graphs, the effective notch stresses from Table 5.4 was used, together with the load cycles obtained from the practical tests performed by Vilhauer et al. The load cycles for each specimen and nominal stress can be seen in Table 5.5. In addition, it is important to emphasize that the load cycles used to assemble the S-N graphs are for crack initiation. This is because not all of Vilhauer et al. specimen reach failure.

Table 5.5: Stress range and load cycles of each specimen conducted by Vilhauer et al. test. The coloured rows indicate the specimens utilized for this study. [Writers own table based on values from Table 1 and 2 in Vilhauer et al. (2012), *pp.166.167*]

Specimen	$\Delta\sigma_{NS}$ [MPa]	Cycles to crack initiation	Cycles to failure
CONTROL 1	96.5	$2,160,000^a$	Not achieved
CONTROL 2	58.6	$3,850,000^a$	Not achieved
CONTROL 3	138	500,000	Not achieved
CONTROL 4	138	350,000	Not achieved
CONTROL 5	193	80,000	290,000
CONTROL 6	193	50,000	Not achieved
BOLT 1	193	80,000	530,000
BOLT 2	193	50,000	300,000
BOLT 3	193	70,000	400,000
UIT 1	138	$5,000,000^a$	Not achieved
UIT 2	193	1,300,000	Not achieved
UIT 3	193	2,100,000	Not achieved
UIT/BOLT 1	193	550,000	2,400,000
UIT/BOLT 2	193	1,070,000	Not achieved
UIT/BOLT 3	193	1,370,000	Not achieved

[a] Achieved run-out and no crack was detected

The test series relevant to this master thesis are the as-welded specimens (CONTROL) and the UIT-treated specimens (UIT and UIT/BOLT) from Table 5.5. Bolted specimens (BOLT) are therefore not studied, except for specimens treated with both UIT and applied bolts (UIT/BOLTS). Because, as Vilhauer et al. stated, the bolts do not contribute to fatigue improvement. As a result, both the CONTROL and BOLT HSR specimens have the same load cycles at crack initiation. Although for the UIT/BOLT specimens, the bolts may negate the effect of UIT-treatment. Considering that the reduction is marginal, and that there are few tests conducted with UIT-treatment, the UIT/BOLT specimens can be considered UIT-treated. Hence, 12 specimens were included in the study.

The S-N graph for the as-welded specimen (CONTROL) is seen in Figure 5.6. Where the black curve corresponds to IIWs recommended fatigue curve for as-welded joints with a FAT-class of 225 MPa and the red dots represent the specimens. The stress range on the y-axis displays the corresponding specimens effective notch stresses at the toe from Table 5.4 and the load cycles on the x-axis refer to the number of cycles to crack initiation seen in Table 5.5.

Furthermore, the effective notch stresses applied to the graph are the toe stresses. This is because according to Vilhauer et al. results, all cracked CONTROL specimens cracked at the end weld toe. Therefore, root stresses are not included. It can be observed in Figure 5.6 that the FE analysis results correspond well to the recommended IIW S-N curve.

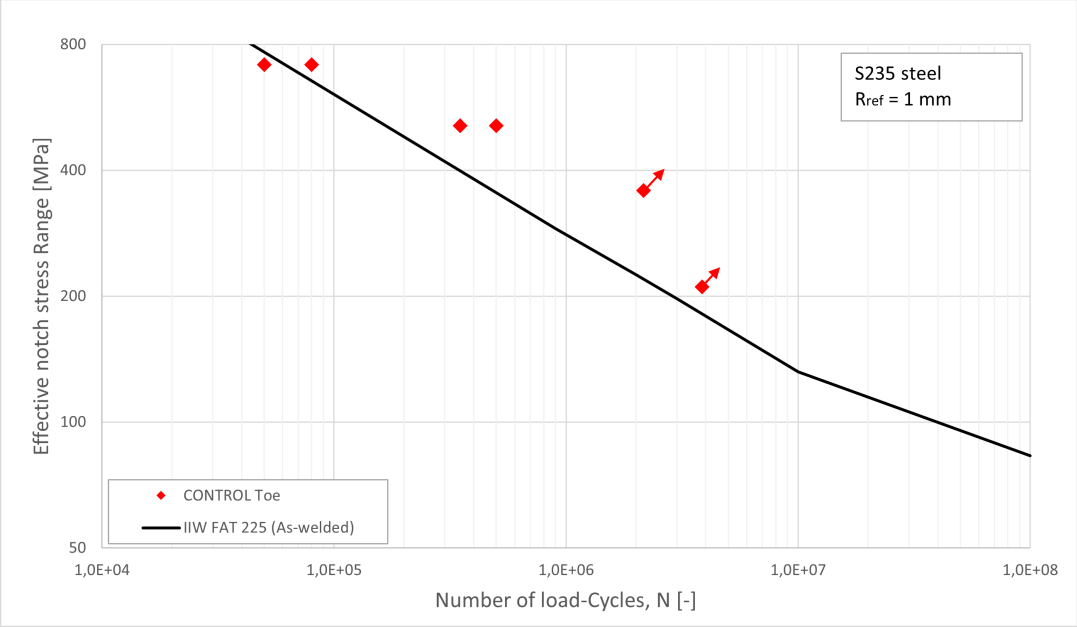

Figure 5.6: Effective notch stress ranges at weld toe from FE analysis applied to a S-N graph for Vilhauer et al. as-welded specimens loaded in bending.

In addition, the S-N graph for UIT-treated specimens (UIT and UIT/BOLT) can be seen in Figure 5.7. Similar to the previous figures, the dots represent the corresponding specimens that were treated with UIT in Vilhauer et al. test. Differently to the as-welded specimens, the UIT-treated specimens cracked along the transverse weld throat (Vilhauer et al., 2012), which is interpreted as root cracking. Hence, the effective notch stresses assigned to the graph are the root stresses calculated from the FE analysis seen in Table

5.4. Because the weld root have not undertaken UIT-treatment the recommended fatigue curve for as-welded joint is used, which can be seen as the black curve in Figure 5.7. However, IIW recommended fatigue curve for HFMI-treated welded joints is also shown as the blue curve in the figure. For this particular specimen with steel strength 235 MPa is the S-N curve FAT 320.

It can be observed in Figure 5.7 that the FE analysis results correspond well to the recommended IIW S-N curve for as-welded joints, but interestingly also to the S-N curve for HFMI-treated joints. Except for one specimen, the outlawed UIT/BOLT 1. This can be dismissed since, as the Vilhauer et al. stated, this scattering is most likely caused by the interaction between the tensile bolt and UIT-treatment.

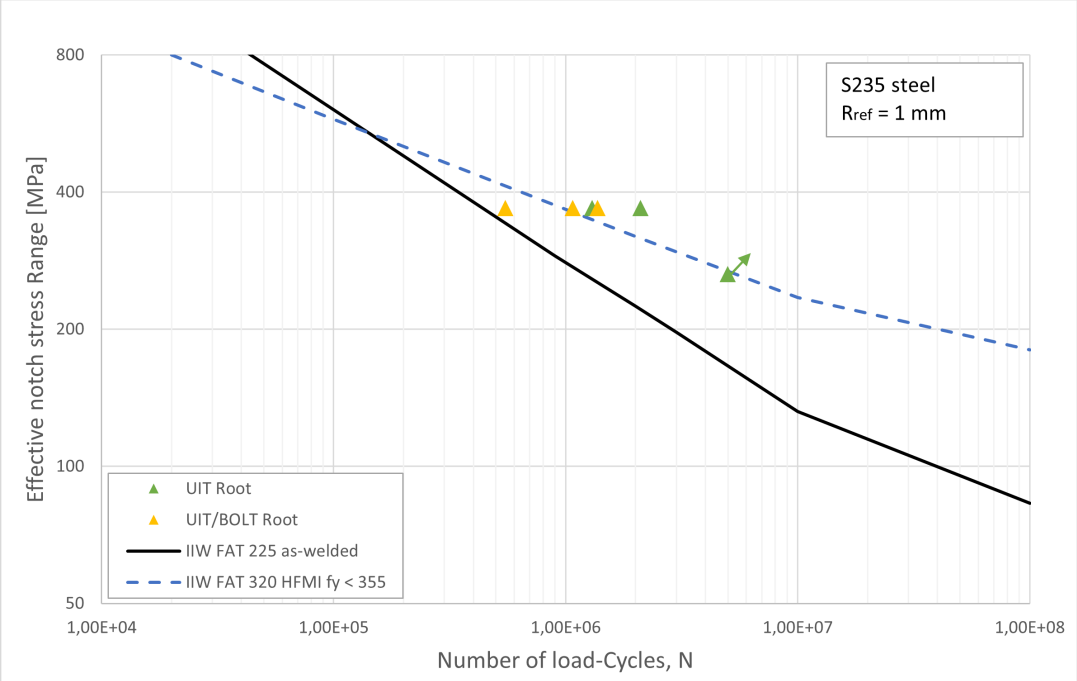

Figure 5.7: Effective notch stress ranges at weld root form FE analysis applied to a S-N graph for Vilhauer et al. UIT-treated specimens loaded in bending.

For the theoretical evaluation, design load cycles are calculated for each effective notch stress range obtained from the FE analysis seen in Table 5.4. The design load cycles are determined using Equation 5.3 and 5.4 in according to the procedure described in Appendix B.4. The calculated design load cycles are shown in Table 5.6 for as-welded specimens and in Table 5.7 for treated specimens.

$$N = 2 \cdot 10^6 (\frac{\Delta\sigma_C}{\Delta\sigma_{i,Ed}})^{m_1} \rightarrow \text{for } \Delta\sigma_{i,Ed} \geq \Delta\sigma_D \tag{5.3}$$

$$N = N_D (\frac{\Delta\sigma_D}{\Delta\sigma_{i,Ed}})^{m_2} \rightarrow \text{for } \Delta\sigma_L \leq \Delta\sigma_{i,Ed} \leq \Delta\sigma_D \text{ and } N_D = 10^7 \tag{5.4}$$

What can be noted from Table 5.6 is that according to the design method, the cracking mode occurs at the end weld toe for as-welded cover-plates. Since the ratio is >1 it implies that the design load cycles for the toe are significantly lower than the root's. For the majority of cases the weld root can sustain 7 times the number of cycles compared to the weld toe. Which agrees with the results from Vilhauer et al. test, since all specimens that developed cracks occurred at the weld toe.

Table 5.6: Calculated design load cycles for Vilhauer et al. as-welded specimens (CONTROL) at weld toe and root, as well as the ratio (r) between load cycles of root and toe.

CONTROL					
$\Delta\sigma_{NS}$ [MPa]	ENS [MPa]		Load cycles [-]		Ratio [-]
	$\Delta\sigma_{Toe_{ENS}}$	$\Delta\sigma_{Root_{ENS}}$	N_{Toe}	N_{Root}	$\frac{N_{Root}}{N_{Toe}}$
193	715	369	62,325	453,420	7.28
138	511	264	170,730	1,238,130	7.25
96.5	358	185	496,510	3,598,010	7.25
56.8	210	109	2,459,910	25,677,900	10.44

The red color indicates that the as-welded design curve of FAT 225 was used to calculate the design load cycles for the HFMI-treated toe.

For the UIT-treated specimen the cracking mode according to the design method is at the weld toe for all cases except for the specimen with a nominal stress of 58.6 MPa. However, according to the test results of Vilhauer et al. treated specimens, the cracking mode for specimens subjected to a nominal stress of 193 MPa and 138 MPa occurred at the weld root. Which contradicts the design results in Table 5.7. Furthermore, according to the design method it can be observed that for UIT-treated cover-plated flanges-girder, the expected failure mode is at the weld toe for stresses larger than approximately 57 MPa, whereas for lower stresses it shifts from toe failure to root failure.

Table 5.7: Calculated design load cycles for Vilhauer et al. UIT-treated specimens (UIT) at weld toe and root, as well as the ratio (r) between load cycles of root and toe.

UIT and UIT/BOLT					
$\Delta\sigma_{NS}$ [MPa]	ENS [MPa]		Load cycles [-]		Ratio [-]
	$\Delta\sigma_{Toe_{ENS}}$	$\Delta\sigma_{Root_{ENS}}$	$N_{Toe_{HFMI}}$	N_{Root}	$\frac{N_{Root}}{N_{Toe_{HFMI}}}$
193	715	369	62,325	453,420	7.28
138	511	264	192,610	1,238,130	6.43
96.5	358	185	1,141,210	3,598,010	3.15
56.8	210	109	27,519,280	25,677,900	0.93

The red color indicates that the as-welded design curve of FAT 225 was used to calculate the design load cycles for the HFMI-treated toe.

5.3.2 Stress fields

Maximum principal stress fields of Vilhauer et al. specimen were obtained from Abaqus and can be seen in Figure 5.8, where various stress ranges are visible in each sub-figure, which can also be seen in Appendix B.5. In Figure 5.8(a) the maximum compressive stresses are observed at one point of the weld root and at the top of the flange-girder. The compressive stresses at the top of the flange-girder relate to how the specimen is subjected to bending, which are to be expected. This is also illustrated in Figure 5.9(a) where the absolute compressive principal stresses can be seen. Hence, in Abaqus the compressive stresses are distributed throughout the flange-girder but cluster above the weld as seen in Figure 5.8(a).

In Figure 5.8(b) the stress vectors between 0-1 MPa are shown. It can be observed that it is in this stress range that the majority of stresses are distributed throughout the specimen. As seen in both Figure (b) and Figure 5.9(b), the tensile stresses are concentrated at the weld and along the cover-plate. The stresses in the cover-plate are the result of bending and the cluster of stresses at the weld are the result of tensile stresses being transferred to the cover-plate from the flange-girder. Aside from that, in Figures (c) and (d) it is apparent that the highest stresses are concentrated at the weld toe and at the lowest point of the weld root. But as is evident in Figure (d) the highest stresses are at the weld toe. Which explains that weld toe failure occurs for as-welded specimens, as demonstrated by Vilhauer et al. result. However, for UIT-treated specimens the failure mode is not entirely obvious by the stress fields, since higher stresses are both presented at the weld root and weld toe, the assumption that root failure would occur is possible but not concrete. But because the test performed by Vilhauer et al. resulted in weld root failure for most UIT-treated specimens, the stresses at the weld root in Figure (c) are evident that Vilhauer et al. results are feasible.

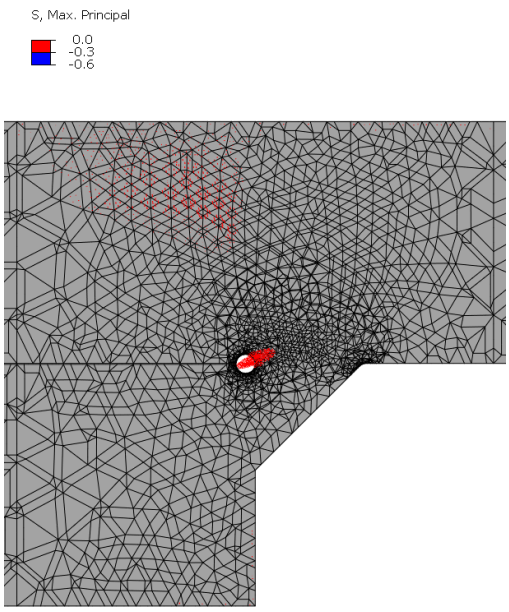

(a) Stress range -0.6 - 0 MPa

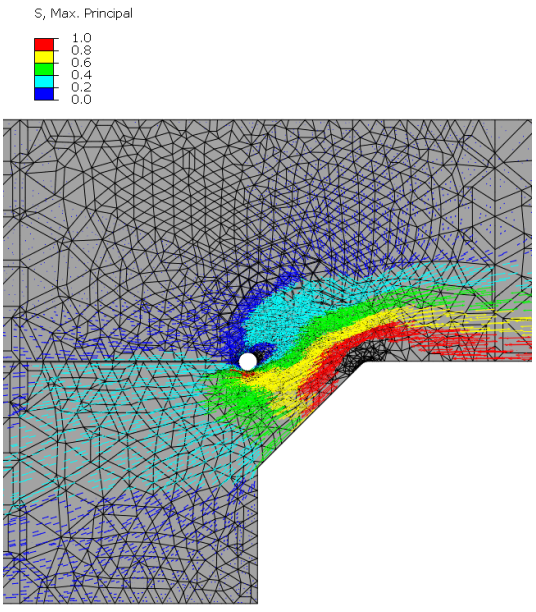

(b) Stress range 0 - 1 MPa

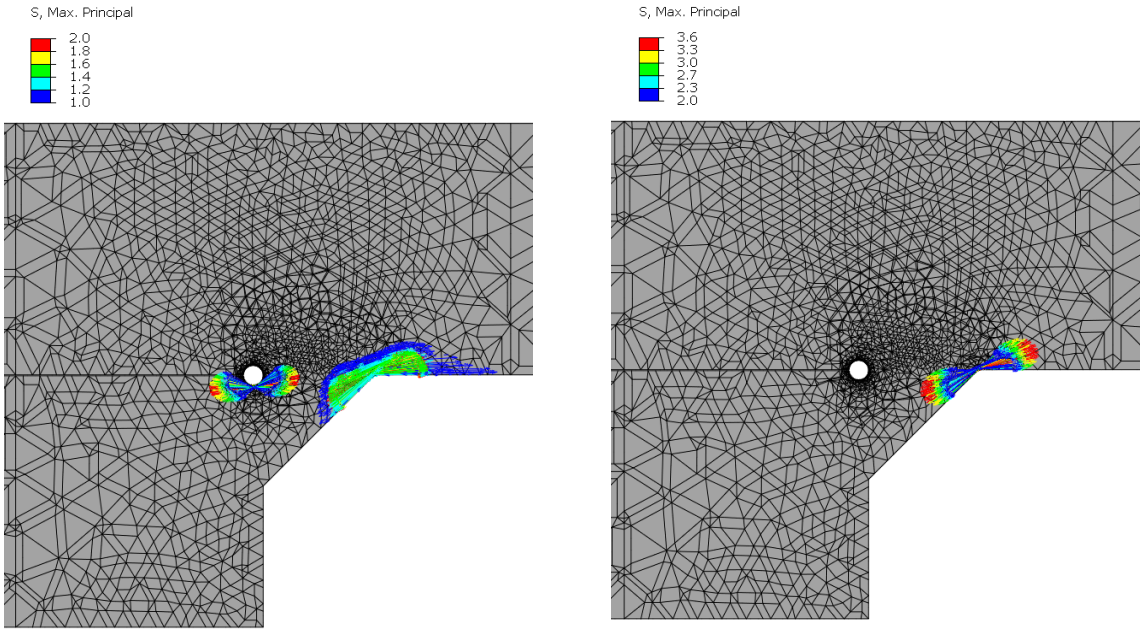

(c) Stress range 1 - 2 MPa

(d) Stress range 2 - 3.6 MPa

Figure 5.8: Maximum principal stress field distribution in 4 different stress ranges for Vilhauer et al. test model loaded in bending, under a unit nominal stress of 1 MPa.

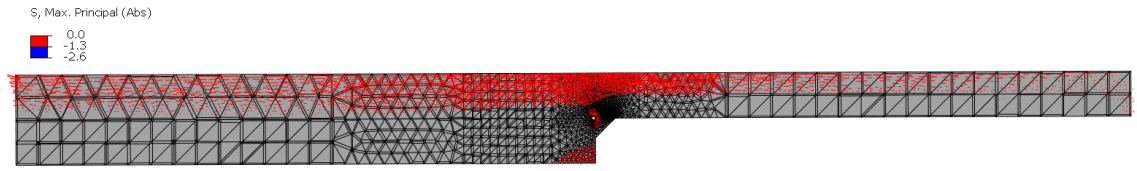

(a) Stress range -2.6 - 0 MPa

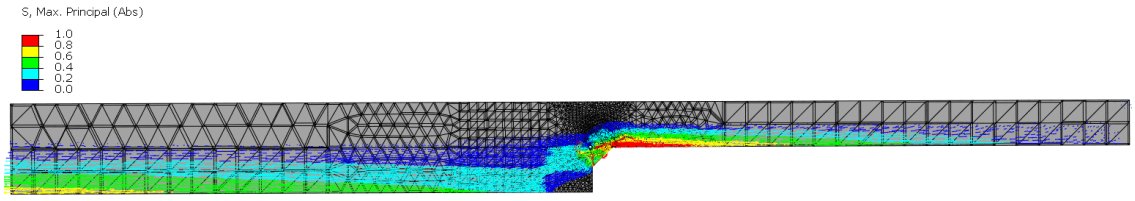

(b) Stress range 0 - 1 MPa

Figure 5.9: Absolute maximum principal stress field distribution in stress ranges -2.6 - 0 MPa and 0 - 1 MPa for Vilhauer et al. whole test model loaded in bending, under a unit nominal stress of 1 MPa.

5.4 Hui et al, 2018

Similarly to the previous two analyses, the maximum principal stresses obtained from the FE analysis section 4.3 were derived from a unit nominal stress of 1 MPa at the weld toe. Which were determined to be 4.32 MPa at the weld toe and 3.64 MPa at the weld root for the beams with shorter cover-plates (beams S1-S6). For the beams with longer cover-plates (beams S7-S14), the stresses were estimated to be 4.37 MPa at the weld toe and 3.75 MPa at the weld root. In Figures 5.10 and 5.11 the results from Abaqus model of Hui et al. S1-S6 and S7-S14 beams can be seen. It is possible to see the maximum principal stress distributions of the sub-models. The stress distributions of the sub-models shows that the highest accumulation of maximum principal stresses occurs at the weld toe and root.

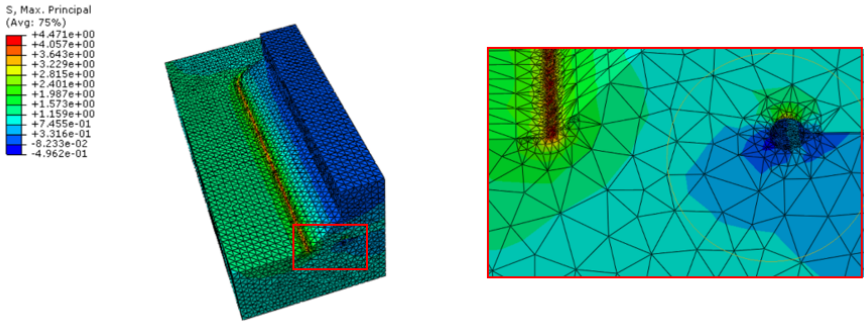

Figure 5.10: Maximum principal stress results of the FE analysis for the second model subjected to bending (Hui et al.) under a unit nominal stress of 1 Mpa for beams S1-S6.

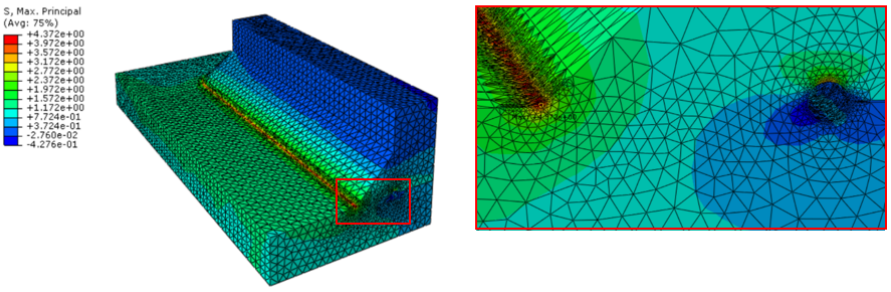

Figure 5.11: Maximum principal stress results of the FE analysis for the second model subjected to bending (Hui et al.) under a unit nominal stress of 1 Mpa for beams S7-S14.

The effective notch stresses are determined with the same procedure used for Vilhauer et al. and Leitner and Stoschka study in section 5.3 and 5.1. Hence, the nominal stress ranges for each specimen Hui et al. used in their practical tests are multiplied with the maximum principal stresses obtained from the FE analysis. For these two beams, the resulting effective notch stresses can be seen in Table C.4 in Appendix C.4.

5.4.1 Fatigue study

With effective notch stresses generated from the FE analysis in Abaqus, the stresses were assembled into three S-N graphs, one for as-welded cover-plate specimens (CONTROL) and the two for UIT-treated cover-plate specimens (UIT) with either weld toe failure or weld root failure. To assemble the S-N graph, the effective notch stresses from Table C.4 was used with the corresponding load cycle Hui et al. determined for each specimen, which is seen in Table C.3 in Appendix C.3.

The S-N graph for as-welded specimens (CONTROL) can be seen in Figure 5.12. The black cuve correspond to IIWs recommended fatigue curve for as-wedled joint with a FAT-class of 225 MPa, and the red dots represent the specimens. Where the diamond dots are for beams with shorter cover-plated specimens and the triangular dots are for beams with longer cover-plated specimens. The stress range on the y-axis presents the corresponding specimens' effective notch stresses at the weld toe from Table C.4 in Appendix C.4.

Furthermore, only toe stresses were applied to the S-N graph, because according to Hui et al. test results, all CONTROL specimens cracked at the end weld toe except for beam S1 which reached run-out. Hence, root stresses were not included in the graph. It can be seen in the graph that the shorter specimens have better fatigue performance than the longer specimens. This is despite the relatively close stress ranges. Overall, the FE analysis results correspond relatively well to the recommended IIW S-N curve.

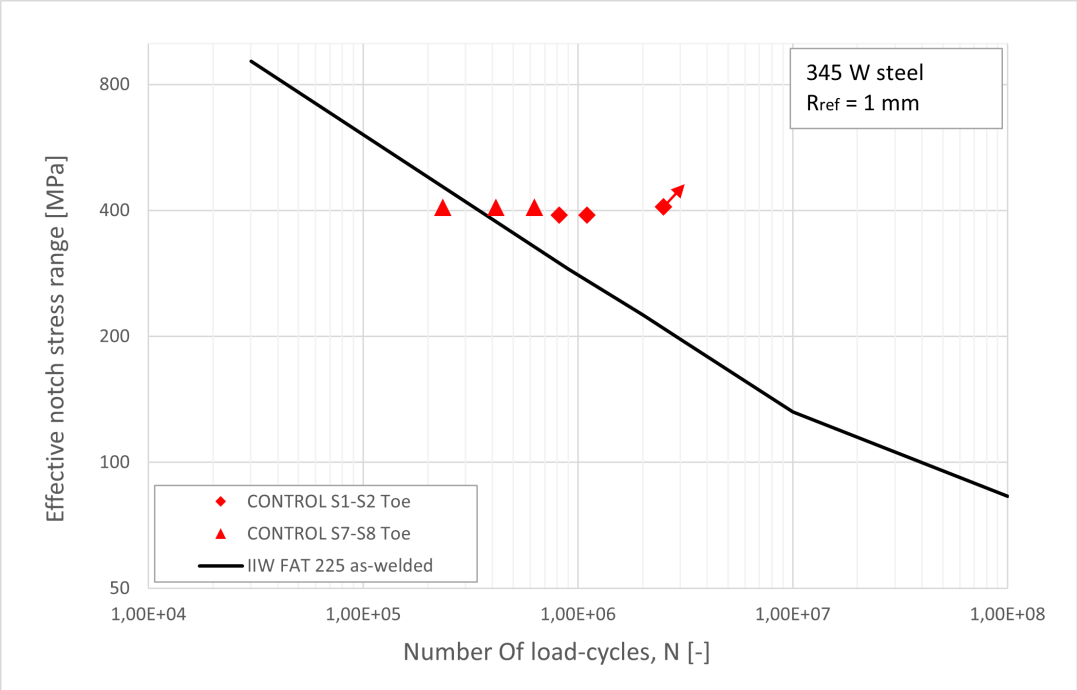

Figure 5.12: Effective notch stress ranges at weld toe from FE analysis applied to a S-N graph for Hui et al. as-welded specimens laded in bending. (Diamonds represent the beams with shorter cover-plate specimens and the triangles the beams with longer cover-plate specimens)

In addition, the S-N graph for UIT-treated specimens (UIT) can be seen in Figure 5.13 for specimens that developed weld toe failure and in Figure 5.14 for specimens that developed weld root failure according to Hui et al. test results. Furthermore, the dots in the figures refer to the results acquired from the FE analysis seen in Table C.4 for each specimen with the respective load cycles Hui et al. obtained seen in Table C.3. Similarly as in Figure 5.12, the diamond dots are for the beams with shorter cover-plate specimens and the triangular dots are for the beams with longer cover-plate specimens.

It can be observed in Figure 5.13, that for specimens who failed at the weld toe, that the recommended HFMI S-N curve of FAT 320 for steel strengths of $f_y \leq 355$ MPa correlates well to the test results. Furthermore, it is apparent in the figure that all of the shorter specimens achieved run-out, and no cracks were detected by Hui et al., hence generally exhibiting longer fatigue life. Henceforth, when the FE analysis results are compared with the S-N curve FAT 360 for steel strength $355 < f_y \leq 550$ MPa it is also observed that this fatigue curve also correlates well to the test results.

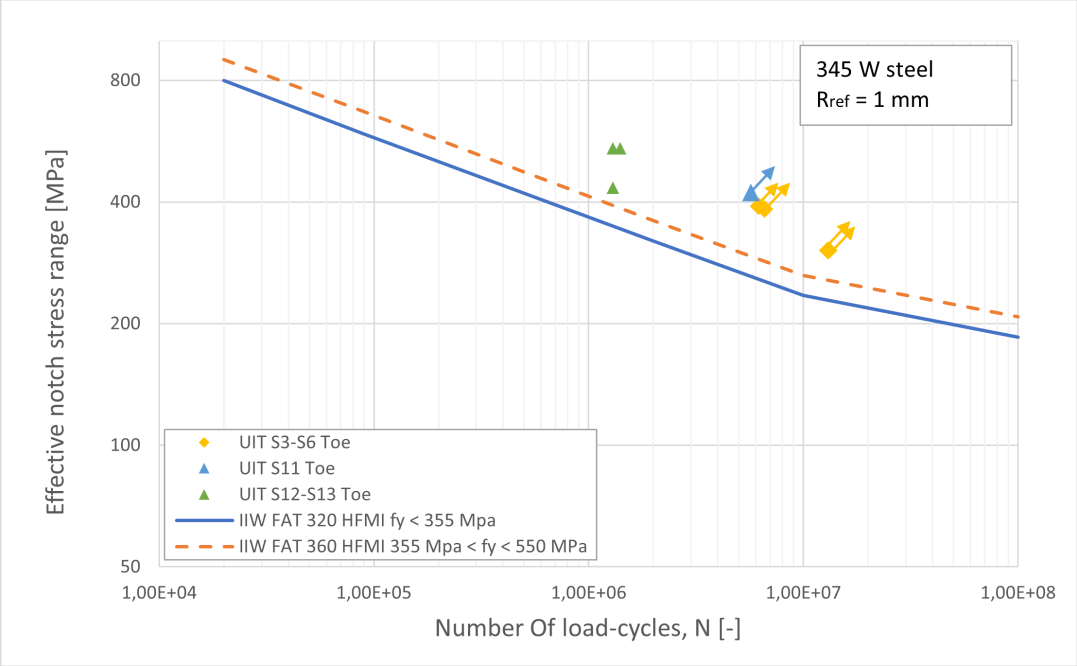

Figure 5.13: Effective notch stress ranges at weld toe from FE analysis applied to a S-N graph for Hui et al. UIT-treated specimens laded in bending that failed at weld toe. (Diamonds represent the beams with shorter cover-plate specimens and the triangles the beams with longer cover-plate specimens)

In contrast, most UIT-treated specimens suffered root failure, as seen in Table C.3. Hence, the fatigue design curve FAT 225 for as-welded joints is to be used for fatigue assessment. However, what can be observed in Figure 5.14 is that all specimens are above the recommended S-N curve FAT 320 for HFMI-treated joints. Hence, even if root failure occurs, fatigue performance is still improved. However, for the S-N curve FAT 360, which correlated well to the specimens that failed at the weld toe, does not fully correlate with the specimens that failed at the weld root. As a result, it is still possible to debate what S-N curve should be used for design.

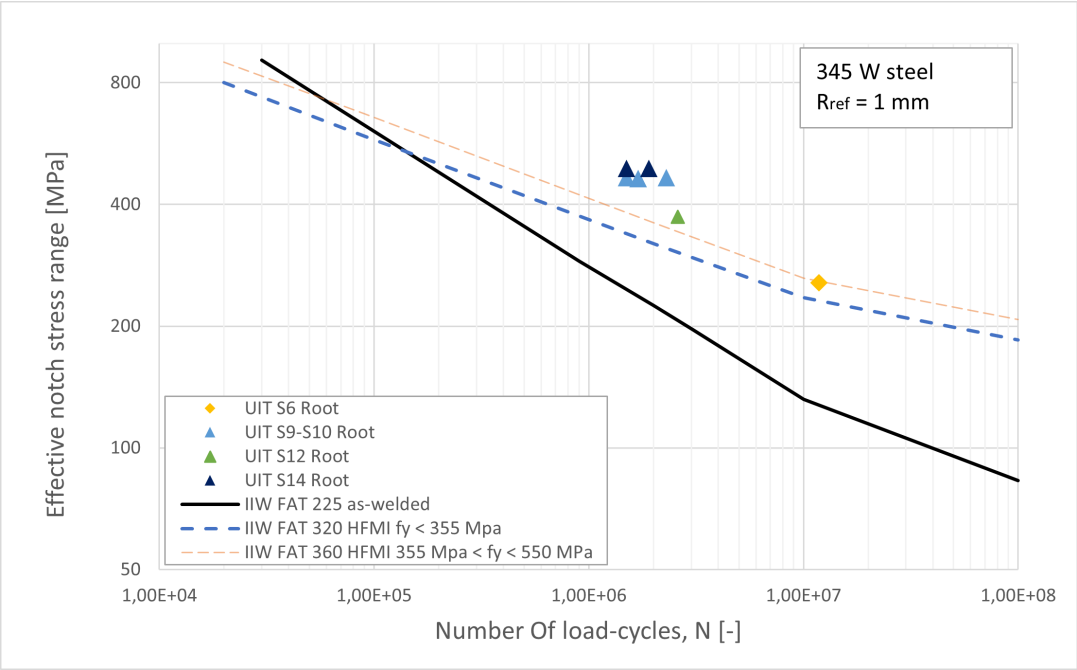

Figure 5.14: Effective notch stress ranges at weld toe from FE analysis applied to a S-N graph for Hui et al. UIT-treated specimens laded in bending that failed at weld root. (Diamonds represent the beams with shorter cover-plate specimens and the triangles the beams with longer cover-plate specimens)

In the theoretical evaluation process, the same procedure was employed for Hui et al. specimens as for Vilhauer et al. specimens. Hence, design load cycles were calculated for each effective notch stress range obtained from the FE analysis, shown in Table C.4 in Appendix C.4. The load cycles are determined using Equations 5.3 and 5.4, and calculated in accordance with the steps described in Appendix C.2. The design load cycles for each specimen's effective notch stresses are presented in Table 5.8 for as-welded specimens (CONTROL) and in Table 5.9 for treated specimens (UIT).

It can be seen in Table 5.8 that according to the design method, the cracking mode for as-welded cover-plated beams occurs at the end weld toe. Since the ratio between design load cycles at the weld root and toe is >1 it is implied that the weld toes' fatigue life is lower than the weld root. Therefore, theoretically cracking for as-welded cover-plated beams will take place at the weld toe, but because the ratio is <2 the possibility of root failure are not impossible. But with the higher possibility that failure will occur at the weld toe, the design method is in accordance with the test results obtained by Hui et al.

Table 5.8: Calculated design load cycles for Hui et al. as-welded specimens (CONTROL), the ratio (r) between load cycles of root and toe and cracking modes from Hui et al. test results are also included.

CONTROL						
Specimen (S_r [MPa])	ENS [MPa]		Load cycles [-]		Ratio [-]	Hui et al. Cracking mode
	$\Delta\sigma_{Toe}$	$\Delta\sigma_{Root}$	N_{Toe}	N_{Root}	$\frac{N_{Root}}{N_{Toe}}$	
S1 (94.458)	408	344	335,282	560,476	1.67	Not achieved[a]
S2 (90.32)	390	329	383,508	641,094	1.67	Toe
S7 (93)	407	349	338,913	537,075	1.58	Toe
S8 (93)	407	349	338,913	537,075	1.58	Toe

[a] Achieved run-out and no crack was detected

Referring to Table 5.9, according to the theoretical design method, UIT-treated specimens subjected to a nominal stress $>$ 99 MPa will crack at the weld toe, while for nominal stresses $<$ 99 MPa will crack at the weld root. This agrees with the possibility that weld root cracking is possible for UIT-treated welds. However, this occurs only at a certain loading threshold. When compared with Hui et al. test results, it shows that the theoretical cracking mode does not always correlate with the practical test. For example, specimen S10 and S13 which are identical in both specimen and loading. According to the design method, failure will occur at weld toe for both S10 and S13. However, according to Hui et al. test results, the two S10 specimens cracked at the weld root, while the two S13 specimens cracked at the weld toe. Due to this, an undetermined cracking mode is determined within the range of a load cycle ratio of $0.5 < r \leq 2$. Which all treated specimens reside within.

Table 5.9: Calculated design load cycles for Hui et al. UIT-treated specimens (UIT), the ratio (r) between load cycles of toe and root and cracking modes from Hui et al. test results are also included.

UIT						
Specimen (S_r [MPa])	ENS [MPa]		Load cycles [-]		Ratio [-]	Hui et al. Cracking mode
	$\Delta\sigma_{Toe}$	$\Delta\sigma_{Root}$	$N_{Toe_{HFMI}}$	N_{Root}	$\frac{N_{Root}}{N_{Toe_{HFMI}}}$	
S3 (88.94)	384	324	801,448	671,401	0.84	Not achieved[a]
S4 (90.32)	390	329	742,064	641,094	0.86	Not achieved[a]
S5 (70.326)	304	256	2,592,875	1,358,081	0.52	Not achieved[a]
S6 (70.326)	304	256	2,592,875	1,358,081	0.52	Not achieved[a]/Root
S9 (123.4)	540	463	146,826	229,900	1.57	Root
S10 (124.1)	543	465	142,732	226,031	1.58	Root
S11 (96.5)	422	362	502,045	480,731	0.96	Not achieved[a]
S12 (99.28)	434	372	435,582	441,467	1.01	Toe/Root
S13 (124.1)	543	465	142,732	226,031	1.58	Toe
S14 (131)	573	491	121,261	192,163	1.58	Root

[a] Achieved run-out and no crack was detected

The red color indicates that the as-welded design curve of FAT 225 was used to calculate the design load cycles for the HFMI-treated toe.

5.4.2 Stress fields

Maximum principal stress fields of Hui et al. specimens were obtained from Abaqus. They can be seen in Figure 5.15 for beams S1-S6 with slightly shorter cover-plate specimens, and in Figure 5.16 for beams S7-S14 with slightly longer cover-plate specimens. Each Figure has sub-figures illustrating maximal principal stresses of different stress ranges, which can also be seen in Appendices C.6. It is observed in both Figures that the stress distribution for the different stress ranges is strikingly similar for each beam. Hence, when discussing the stress field of each sub-figure, the referenced figure will be both sub-figures in Figure 5.15 and 5.16.

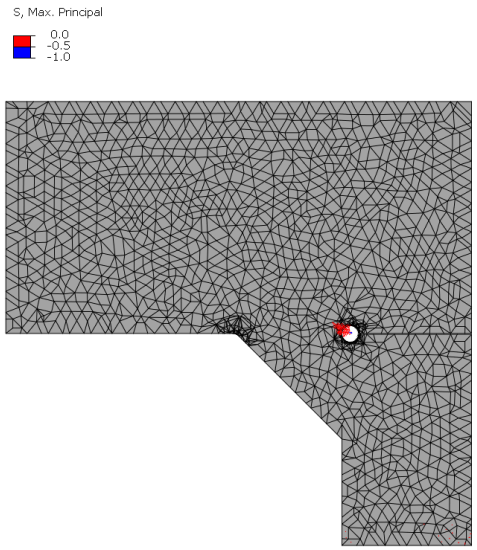

(a) Stress range -1 - 0 MPa

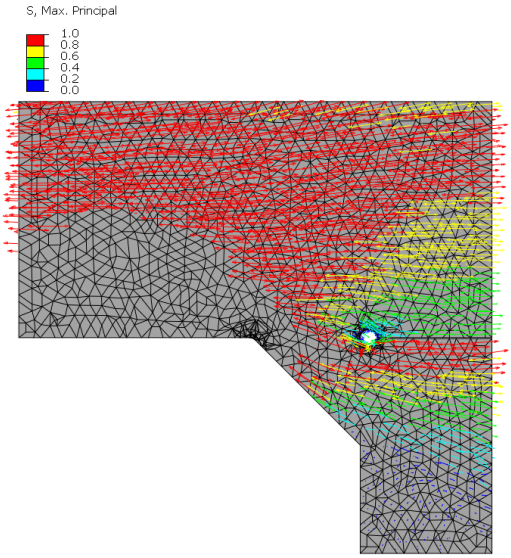

(b) Stress range 0 - 1 MPa

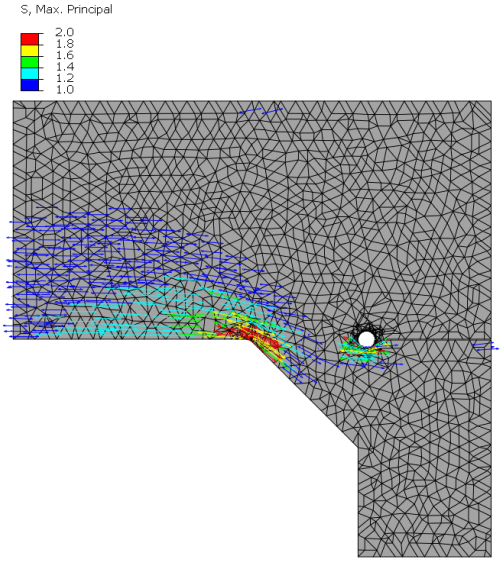

(c) Stress range 1 - 2 MPa

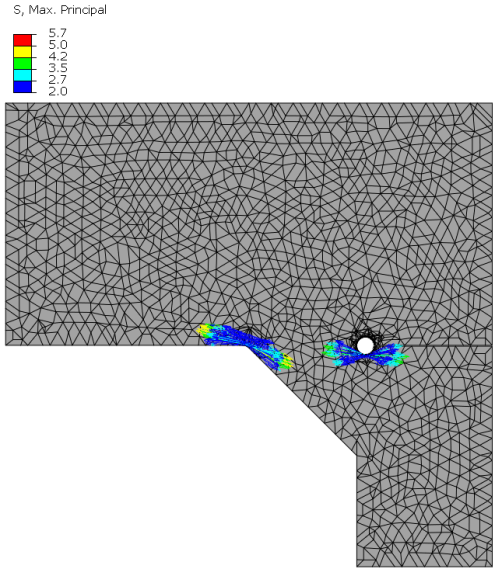

(d) Stress range 2 - 5.7 MPa

Figure 5.15: Maximum principal stress field distribution in 4 different stress ranges for Hui et al. test model with shorter cover-plates loaded in bending, under a unit nominal stress of 1 MPa.

It is observed that the maximum compressive stresses shown in Figures (a) are concentrated in one region of the weld root. For the sub-figures illustrating the stress range of 0 - 1 MPa, Figures (b), it is apparent that the majority of all stresses distributed throughout the whole two beams are within this stress range. Correlating with Figures (c), the largest stress range distributed throughout the beams is at the bottom flanges, and this is related to the fact that the beams are loaded in bending. Furthermore, it can be observed that the tensile stresses from Figures (c) are then divided between the cover-plate and flange. Hence, the tensile stresses at the bottom flange in Figures (c) are reduced after distribution, as indicated in Figures (b).

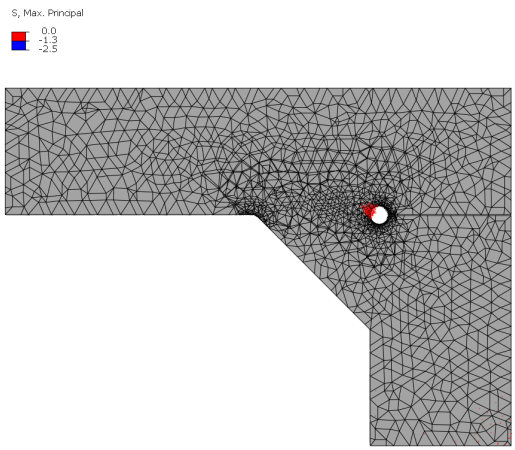

(a) Stress range -2.5 - 0 MPa

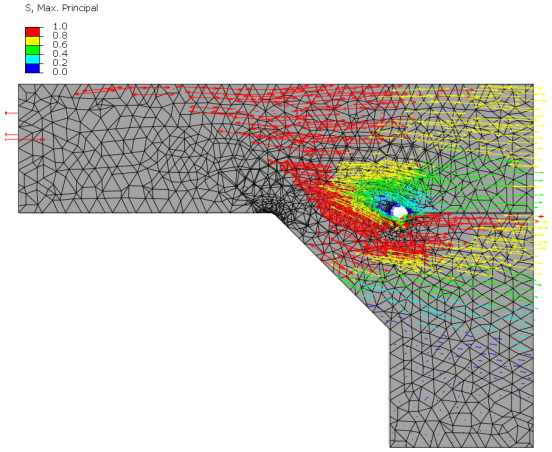

(b) Stress range 0 - 1 MPa

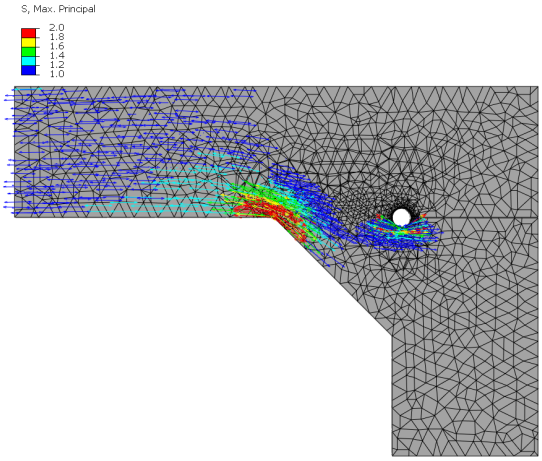

(c) Stress range 1 - 2 MPa

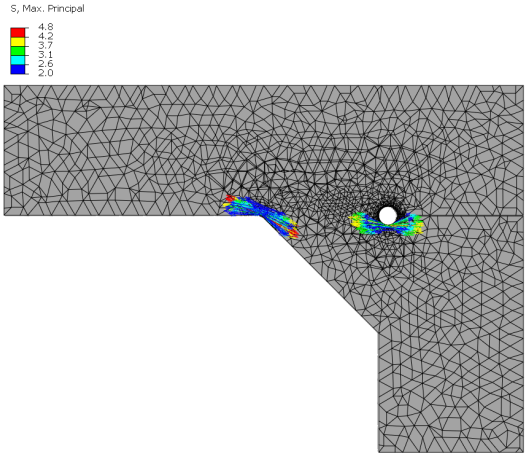

(d) Stress range 2 - 4.8 MPa

Figure 5.16: Maximum principal stress field distribution in 4 different stress ranges for Hui et al. test model loaded in bending with longer cover-plate, under a unit nominal stress of 1 MPa.

Lastly in Figure (d) it is evident in both Figure 5.15 and 5.16 that the highest maximum principal stresses are located at the weld root and weld toe. This confirms that for cover-plated beams the failure mode can either be at the weld toe or at the weld root. Therefore, since weld toe failure was observed in Hui et al. as-welded specimens, it is safe to assume that the minimal stress difference does not affect a change in failure mode. But for UIT-treated specimens, there is a higher possibility the failure mode will occur at the weld root, because of the minimal difference between the maximum stresses at the weld

root and toe. Hui et al. reported that the majority of the treated specimens achieved weld root failure, thus confirming that the large stresses at the weld root contributed to a shift in failure mode. Which was a risk discussed in section 2.2.1.

Apart from showing the direction of stress distribution through the weld, the stress fields also visualises the direction fatigue cracks would develop if they are formed. Hence, Figure (d) shows that toe cracking starts at the midpoint of the stress vectors and moves towards the beam flange. While root cracking starts at the midpoint of the stress vectors inside of the weld and moves outwards towards the welds surface.

5.5 Comparison of stress distribution in welds subjected to bending and axial loading

From the FE analysis in Abaqus the stress distribution throughout the weld of each model was gathered and assembled into graphs. This was conducted in order to visualise the stress distribution throughout the welds leg-length and throat to compare between the different models. The stresses were obtained by using the Abaqus command "path", then the stresses were extracted from the nodes along the path. After the true distance and maximum principal stresses were gathered from each node, the true distance of each node was divided by the longest distance, and the principal stresses were divided by the maximum stress. Thereafter, graphs could be assembled. This was done for each model presented in chapter 5.

The paths and resulting graph of each model can be seen in Appendix A.2 for Leitner and Stoschka test model, Appendix B.6 for Vilhauer et al. test model and Appendix C.7 for Hui et al. test model. Each curve starts at the maximum principal stress at the root and extends to the weld end. Within each graph in appendix it is observed that each curve maintains a relation to each other. This indicates that the stress distribution is constant throughout the same weld section. It can also be seen that the stresses at the weld surface decrease further away from the toe. This agrees with the results attained from the stress fields.

Furthermore, each model can be compared based on the leg-length stresses between weld root and weld toe, to identify the differences between the structural models, as depicted in Figure 5.17.

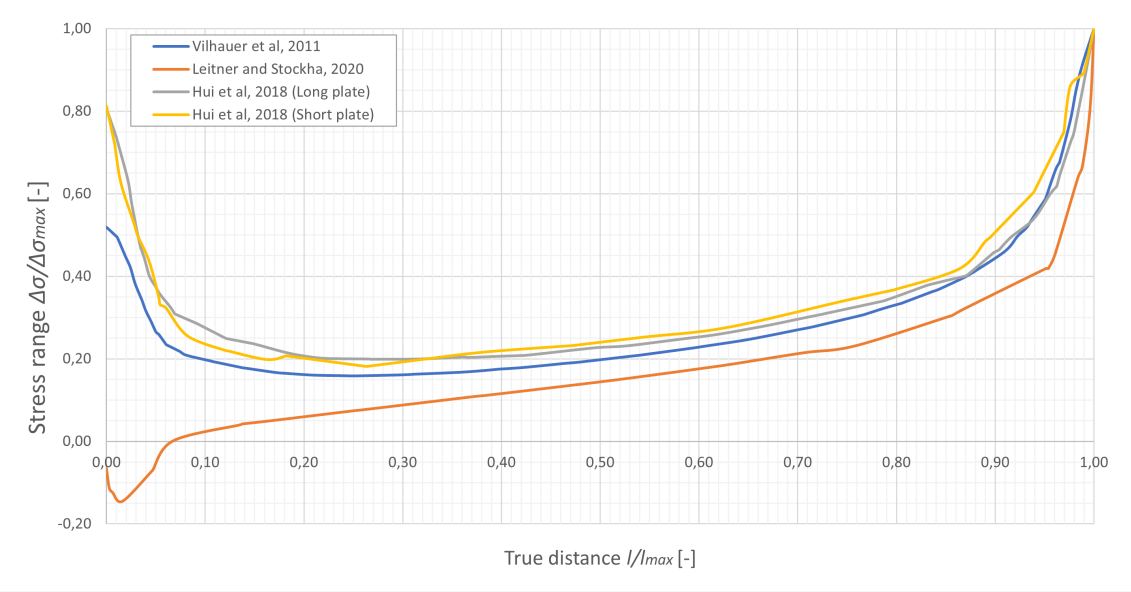

Figure 5.17: Comparison of stress distribution through weld leg-length between root (x=0) and toe (x=1) for all examined models.

The most distinctive stress curve in Figure 5.17 is for Leitner and Stoschka test model, where it is evident that compressive stresses are located at the weld toe. Which is addressed in section 5.1. While the other stress curves have tensile stresses at the weld root, they also have the same curve shape despite the different cover-plate placement. It is seen that both Hui et al. beams are almost identical. The difference with Vilhauer et al. test model is that it has lower stresses at the weld root. Otherwise, it can be determined that no matter the structural model, from the middle of the weld (0.5) to the toe (1), the stress curve has comparable shapes and gradients, but different magnitudes. This indicates that the distribution of stresses through the leg-length are coinciding although the cover-plate positioning and loading are different from each test model.

6
Discussion

The reviewed tests in chapter 3 demonstrated that HFMI-treatment improves fatigue performance of welded cover-plate details subjected to bending or axial loads. All four reviewed tests indicate that the expected crackling mode for as-welded cover-plates is at the weld toe. However, this is not the case for HFMI-treated cover-plates, since the cracking mode can vary depending on loading conditions.

6.1 Cracking mode for treated and untreated cover-plates loaded axially and in bending

It was anticipated that cover-plated structures loaded axially would crack at the weld toe for both as-welded and HFMI-treated joints. This was confirmed by the results from Leitner and Stoschka test in section 3.1, where all tested specimens suffered weld toe failure, and the same results were verified by FE analysis in this study read in section 5.1. Where the highest tensile effective notch stresses were observed at the weld toe and only compressive effective notch stresses were observed at the weld root. As seen from the stresses in Table 6.1 and stress fields in Figure 5.4. Therefore, failure will only occur at weld toe for both untreated and treated welds. In other words, applying HFMI-treatment to cover-plated structures loaded axially, will increase their fatigue strength and the cracking mode will remain at the weld toe.

Table 6.1: Summering of the FE analysis results (maximum principal stresses) for the modeled tests under a unit nominal stress of 1 MPa at weld toe. Results extracted from Tables 5.1, 5.4 and C.4, (all units in MPa).

Test	**Loading**	**Girder**	**FE analysis results**	
			$\Delta\sigma_{Toe}$	$\Delta\sigma_{Root}$
Leitner and Stoschka	Axially	Plate-girder	7.646	-0.600
Vilhauer et al.	Bending	Flange-girder	3.705	1.915
Hui et al. (S1-S6)	Bending	Beam-girder	4.320	3.640
Hui et al. (S7-S14)			4.372	3.750

For HFMI-treated cover-plated structures loaded in bending, there is a risk of the cracking mode shifting from weld toe to weld root. Hence, the improved toe cannot reach its full capacity before cracking develops at the root. This was confirmed by the tests performed by Vilhauer et al. and Hui et al., since most of the treated cover-plates failed due to cracks initiated at the weld root.

From the FE analysis results, it was determined that, compared to cover-plates loaded axially, tensile effective notch stresses were developed at weld root for cover-plates loaded in bending. However, the highest stresses remain at weld toe, as seen in Table 6.1 for Vilhauer et al. and Hui et al. test models. This explains why Vilhauer et al. and Hui et al. achieved toe failures for as-welded specimens. But this is not as straightforward for HFMI-treated cover-plates, because the treated weld toe has better fatigue performance compared to the weld root. It is therefore necessary to determine the theoretical cracking mode, by calculating the load cycles for both weld root and toe using their corresponding fatigue design curves. As a general rule, the location with the fewest load cycles has the greatest possibility of cracking first.

6.2 Comparing test results with design S-N curves

When comparing the FE analysis results that were assembled into S-N graphs with IIW recommended fatigue curves, it was observed that all tests' results overall correspond well to the recommended fatigue curves.

6.2.1 Axially loaded cover-plates (Leitner and Stoschka, 2020)

The S-N graphs assembled from the test results of Leitner and Stoschka FE model can be seen in Figure 6.1. As seen in the graph shown in Figure 6.1(a) for as-welded specimens, the S-N curve after the transition knee point of $N = 10^7$ gives very conservative results. To design for more accurate fatigue life, the transition knee point of the design S-N curve can be reduced to $N = 10^6$. The proposed change to the curve is indicated by the blue dashed line. However, this suggestion is based on these test results, and due to the fact that the S-N curve FAT 630 is recommended for all as-welded details with plats $<$ 5mm, the change of knee point can not be suggested to other structural details and/or loading conditions without further testing.

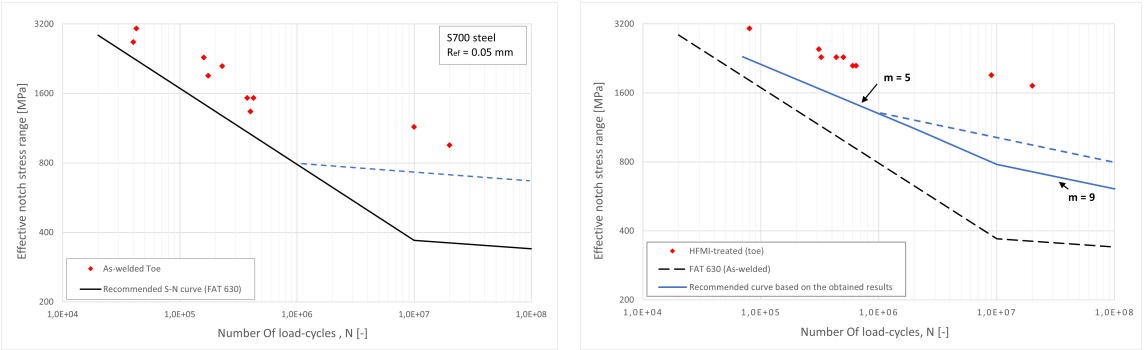

(a) As welded specimens **(b)** HFMI-treated specimens

Figure 6.1: Modification of design S-N curves for axially loaded cover-plates based on FE analysis results of Leitner and Stoschka test model presented in Figures 5.2 and 5.3.

Moreover, due to a recommended S-N curve for HFMI-treated welded details with plates $<$ 5 mm could not be found in any literature or guidelines, a design S-N curve was calculated based on similarity theorems using recommended design curves for thicker plates. The calculated curve is illustrated by the continuous blue line in Figure 6.1(b) and has a

characteristic fatigue strength of 1,120 MPa. The slope of the curve is the same as other IIW S-N curves for HFMI-treated details. Due to fatigue curve FAT 400 was used in the calculation, it is presumed that the calculated curve is only applicable to structures with a steel strength of $550 < f_y \leq 750$ MPa. Lastly, the same reduction in the transition knee point can also be applied to the determined S-N curve, which is illustrated by the dashed blue line in Figure 6.1(b). But additional testing is needed to verify the applicability of FAT 1,120 and the shift in knee-point.

6.2.1.1 Comparison between the FE modeling procedure used in this thesis with that used by Leitner and Stoschka

ENS method was used in Leitner and Stoschka's study, as previously mentioned in section 4.1. The study, however, did not report root stresses, as only effective notch stresses at weld toe were reported. This may be because in all specimens, the cracks appeared at the weld toe due to the specimens being loaded axially. Thus, root stresses are not needed to be computed since the S-N graphs will only display toe stresses. The maximum principal stresses at the root were however computed in this project. The purpose was to investigate the stress conditions at the root when the specimens are loaded axially and compare them with those loaded in bending.

It is obvious in the figure from the FE model in Leitner and Stoschka (2020) study that the roots and toes were rounded differently. The root was rounded to 0.05 mm while the toe was rounded to 1 mm (which is the recommended reference radius for plates ≥ 5 mm). The purpose may have been to simplify the assessment process so that the S-N curve FAT 400 could be used, since there is no recommended curve for HFMI treated welds in plates thinner than 5 mm. The root and toe notch details can be found in Figure 9 in Leitner and Stoschka (2020).

In contrast, in this study, both root and toe were rounded by $r_{ref} = 0.05$ mm and the design curve for HFMI-treated details was calculated as mentioned earlier, see Figure 6.1. When the correlation between the test results and the design curve in this study is compared with the correlation between them in Leitner and Stoschka's study, it has been shown that both FAT 1,120 and FAT 400 curves can be used for the design and they both provide more conservative results after the knee point. The comparison of test results and recommended S-N curve FAT 400 can be seen in Figure 10 in Leitner and Stoschka (2020). Consequently, the HFMI recommended curve FAT 400 is also applicable to thinner plates, if the toe is rounded by 1 mm. However, the root needs to be rounded by 0.05 mm as a 1 mm notch will greatly reduce the detail's area.

6.2.2 Cover-plates loaded in bending (Vilhauer et al, 2012 and Hui et al, 2018)

The S-N graphs assembled from both Vilhauer et al. and Hui et al. test models were compared to IIW recommended design S-N curves FAT 225 for as-welded and FAT 230 for HFMI-treated specimens. This is because all as-welded details thicker than 5 mm are assigned the S-N curve FAT 225. Moreover, due to both specimens having a steel strength $f_y \leq 355$ MPa, the same S-N curve FAT 320 is assigned for HFMI-treated specimens. However, because most of the treated specimens failed at weld root, the test results for those specimens were compared to S-N curve FAT 225 for as-welded details.

6.2.2.1 As-welded cover-plates

Comparing the tests' results of as-welded specimens with the recommended fatigue curve, it was observed that the design curve FAT 225 corresponds well to both tests' results. However, it is important to note that for Vilhauer et al. S-N graphs, the reported load cycles for crack initiation were used instead of those for failure. Which is not the case for Hui et al. It can therefore be assumed that a large number of load cycles can be achieved for Vilhauer et al. specimens before failure is reached. This is proven in Table 5.5 where most of the tested CONTROL specimens did not achieve failure when the test was terminated. Henceforth, the dots in Figure 6.2(a) will be shifted to the right and the recommended S-N curve will give more conservative results. In contrast, Hui et al. test for as-welded specimens continued until failure was reached and as seen in Figure 6.2(b), the FE results are relatively close to the S-N curve.

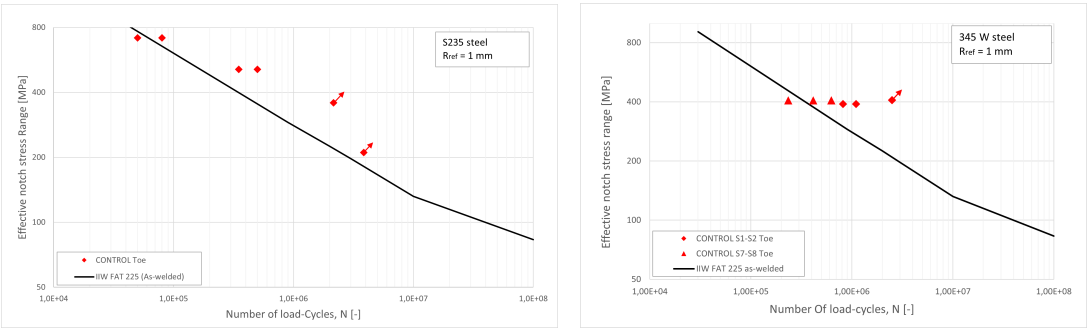

(a) As-welded S-N graph of Vilhauer et al. FE analysis test results

(b) As-welded S-N graph of Hui et al. FE analysis test results

Figure 6.2: Assembled S-N graph from FE analysis results of Vilhauer et al. and Hui et al. test models presented in Figures 5.6 and 5.12.

This variation between the two graphs could be due to the type and size difference between specimens. Since Vilhauer et al. specimens are of a 1,270 mm long cover-plated flange-girder and Hui et al. specimens are of a 6,400 mm long cover-plated beams. In addition, the cover-plates are attached differently. In Vilhauer et al., the cover-plate is attached in the middle of the flange, while in Hui et al., the cover-plates are attached at the edges of the beam.

Additionally, when calculating the design load cycles to determine the theoretical cracking modes using the recommended design S-N curve FAT 225 for both tests. The theoretical

cracking modes were determined to be the same as the practical test results for both tests, which were at weld toe.

6.2.2.2 HFMI-treated cover-plates

When comparing the tests' results of HFMI-treated specimens with the recommended fatigue curve for HFMI, it was observed that the design curves correspond well to both tests' results. Similarly to the as-welded S-N graph, Vilhauer et al. S-N graph for HFMI-treated specimen contains load cycles at crack initiation and therefore the same observation can be made. For Hui et al. test, there were some specimens that achieved failure at weld toe and others at weld root, therefore the test results were divided into two S-N graphs, as seen in Figure 6.3, (a) and (b).

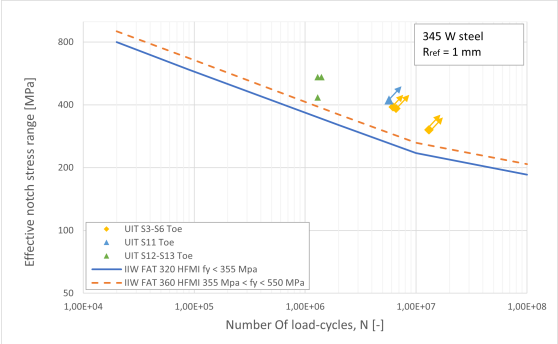

(a) Specimens that failed at weld toe in Hui et al.

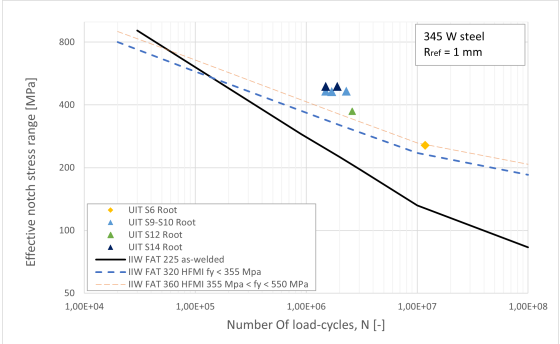

(b) Specimens that failed at weld root in Hui et al.

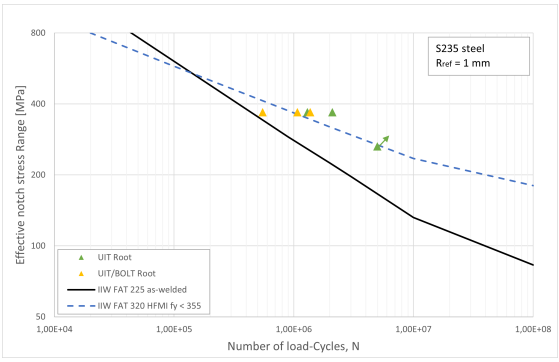

(c) Results for Vilhauer et al. test model (all specimens failed at root)

Figure 6.3: Assembled S-N graphs from FE analysis results of Vilhauer et al. and Hui et al. test models for UIT treated specimens presented in Figures 5.14, 5.13 and 5.7.

It is shown in Figure 6.3(b) for root failure that the results are placed above both S-N curves FAT 225 and FAT 320. This is also assumed for the results from Vilhauer et al. S-N graph, because the only specimen to be under the fatigue curve FAT 320 will be above the curve when assuming failure, see Figure 6.3(c). It can therefore be discussed if it is possible to only use HFMI S-N curves for designing treated cover-plated structures loaded in bending. However, further studies are needed to determine which stress needs to be considered (toe stress or root stress) and what S-N curve that could be used.

Moreover, when calculating the design load cycles to determine the theoretical cracking modes, the calculated results did not correspond well to the cracking modes Vilhauer et al. and Hui et al. obtained from their tests. According to Vilhauer et al. test results, specimens under a nominal stress range of 193 MPa and 138 MPa failed at weld root. On the other hand, the theoretical cracking mode was determined to be at weld toe for these stress ranges, as seen in Table 5.7. The same is true for Hui et al. overall test results shown in Table 5.9. But because the majority of theoretical cracking modes are considered to be undetermined, as mentioned in section 5.4.1, both cracking modes are possible to occur. Which corresponds to the observed results from the practical tests.

Consequently, the existing design S-N curves for HFMI-treated details do not reflect reality when determining the theoretical cracking mode for HFMI-treated cover-plated structures loaded in bending. However, the S-N curves can be used for fatigue life design, but it should be kept in mind that if the effective notch stresses at the weld toe are used for design, there is a possibility to underestimate fatigue life of the structure and over dimension.

6.3 Stress fields of different cover-plates

The maximum principal stress fields of the different test models show the stress distribution through the weld and illustrate the structures behaviour. As stated previously, Leitner and Stoschka test specimens will always have fatigue failure at the weld toe, because as long as the cover-plates are loaded with an axial force, the weld root will be in compression. This can also be proven by the stress fields, as no other stresses are located at the weld root. In addition, because tensile stresses from the load are first redistributed at the weld toe and then transferred to the cover-plate, the weld toe becomes a critical point for tensile stresses.

In contrast, this is not the case for Vilhauer et al. and Hui et al. test specimens loaded in bending, because tensile stresses accumulate at weld root. However, as proven in all models, the largest stresses are located at the weld toes. This implies that for as-welded cover-plates, failure will occur at the weld toe for specimens loaded in bending, like those loaded axially. But when including HFMI-treatment the cracking mode becomes uncertain when analysing the stress field.

Excluding cracking modes, the stress field illustrates the flow of stresses through the weld and the structural behaviour of each test model can be examined. Leitner and Stoschka test specimen in Figure 5.4 shows that the tensile stresses are divided between the cover-plate and plate-girder through the weld and the stresses in the plate-girder are reduced. This stress distribution is different for Vilhauer et al. and Hui et al. test specimens, due to them being subjected to bending moments.

The stress fields of half Vilhauer et al. test specimens are shown in Figure 6.4. It is observed that, excluding the tensile stresses at the notches, the largest tensile stresses are distributed throughout the cover-plate and the bottom side of the flange-girder (that is not reinforced). This shows that bending creates large tensile stresses at the bottom and mostly compressive stresses at the top of the girder. Henceforth, these tensile stresses are the primary stresses distributed throughout the weld.

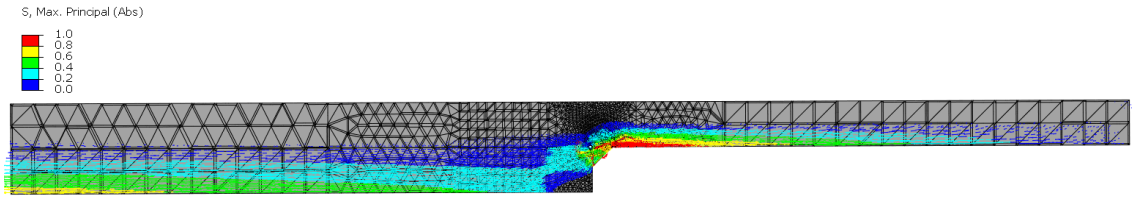

Figure 6.4: Overview of absolute maximum principal stress field of Vilhauer et al. whole test model within the stress range of 0-1 MPa presented in Figure 5.9(b).

However this is slightly different for Hui et al. tested specimens, because of the the model being that of full size beams and not a flange-girder. Additionally, because the cover-plates are attached at the beams edges and not in the middle. Instead of a fully translation of tensile stresses, a redistribution of tensile stresses occurs between the cover-plate and beam flange, similarly to Leitner and Stoschka specimen.

6.4 HFMI-treated cover-plates as a promising alternative to bolted ones

The reviewed tests in chapter 3 demonstrated that HFMI-treatment significantly enhances fatigue performance of welded cover-plate details. The tests conducted on full-scale beams loaded in bending showed that the treatment improved fatigue strength from detail category E' to at least category C (From detail category 40 to 90 in Eurocode). As previously mentioned in section 2.1, the detail category of cover-plated beams connected with high-strength bolts is between 80-90 MPa. Consequently, HFMI-treated welded cover plates can offer fatigue strength that is at least comparable to bolted cover plates.

Furthermore, because the fatigue failure mode may change from toe to root in HFMI-treated cover plates, the fatigue strength of HFMI-treated cover plates is limited by the fatigue strength of the weld root. This means that in most cases, failure will occur at the root before the treated toe's resistance is fully utilized. Therefore, when the fatigue strength of the root is improved, the fatigue resistance of treated cover-plates will increase even more. Additionally, the maximum benefit from treatment can be reached if the failure mode is shifted back to the treated toe instead of the root. A way to achieve that is by increasing the weld size in order to decrease the stress concentration at the root. That was indicated in Roy and Fisher (2006) test, as all CP3 specimens (having weld leg length equals the cover- plate thickness) achieved higher fatigue strength than CP1 specimens (having weld leg length equals half of the cover- plate thickness). Additionally, all failed CP3 specimens showed cracks at the treated toe. Hence, to increase the performance of HFMI-treated welded cover-plates, it is imperative to ensure enough weld size in the design.

To achieve better fatigue performance of welded cover-plates, it can be established that with today's technologies and solutions, the most optimum way is by post treating the weldments with HFMI. Because of the reduction in tensile residual stresses and defects at weld toe. But as established by IIW in section 2.2.1, other post treatments should not be applied after HFMI-treatment. This was also concluded by Vilhauer et al. (2012) in Section 3.2. Where the application of a high tension bolt at HFMI-treated cover-plate edges were proven to reduce the specimens fatigue strength. This can be explained by

that an interaction had occurred between the bolt and HFMI-treatment, which causes the improvement of the HFMI-treatment to decrease.

In addition, with Vilhauer et al. results it could be established that post treating welded cover-plates by applying high tension bolts at the cover-plates ends do not improve the fatigue performance. This is for both as-welded and HFMI-treated cover-plates, since the resulted load cycles for BOLTED and UIT/BOLTED specimens did not particularly differ from the resulted load cycles from the corresponding CONTROL and UIT specimens. Which can be seen in Table 5.5. This can be explained by that tensile stresses will primarily be distributed throughout the transverse end weld and not the bolt, until failure has occurred at the weld.

7
Exploratory studies

The aim of the exploratory study is to further investigate the stress situation at the end weld toe and root of cover-plates having different geometries and positions. In this way, it is possible to gain a better understanding of the fatigue performance of cover-plated beams and find factors that can influence the fatigue strength of those beams. Hence, find out if the same design method can be applied to all cover-plated beams no matter the geometry or position of cover-plates.

For this purpose, 14 new models were created in Abaqus based on the specimen used in Hui et al. (2018) test (S7-S14 beams) shown in section 3.4. Hence, the same beam was used for all exploratory models, and the weld size (12.7 mm) was kept constant during all parts of this study except for one model, where the weld size was increased in the last analyzed model. The same loading set-up was implemented for all models except for one where the load was moved to the middle of the beam. In addition, similar loading principles were followed, where the load applied to the models was calculated so that the applied nominal stress on weld toe equal to 1 MPa.

Overall, the finite element models for this study were constructed in Abaqus exactly the same way as for Hui et al. test in section 4.3. Thus, sub-modelling was used and the same boundary conditions were applied to both the global models and sub-models, as well as the same element size for meshing.

Furthermore, the study has been conducted in five parts where one parameter was assessed for each part as follows:

1. **The effect of cover-plate position:** The cover-plate from Hui et al. (2018) test was changed so the model included one cover-plate in the middle of the beam instead of two cover-plates at the flange ends. This model is named modified model and was used as a base model for all other exploratory models. The results will be presented in section 7.1.

2. **The effect of cover-plate thickness:** The analysis includes 6 new models having cover-plates of different thicknesses starting from 15 mm to 50 mm. The results will be presented in section 7.2.

3. **The effect of cover-plate length:** The analysis includes 4 new models with different cover-plate lengths, starting from 889 mm up to 5334 mm. The results will be presented in section 7.3.

4. **The effect of optimizing the end weld:** This study includes two weld modifications to be analysed. The first analysis includes 2 new models where the weld root position was changed by creating an inclination to the cover-plate edge. The results will be presented in section 7.4.1. The second analysis included one model where the weld size was increased to be equal to cover-plate thickness. The results will be presented in section 7.4.2.

For all exploratory studies, the characteristic load cycles were calculated to determine the theoretical cracking mode. The nominal stress ranges used to calculate the effective notch stress ranges are not the same ranges used for the original test model in section 5.4.1. Because those stress ranges are too large to derive comprehensive results, more realistic nominal stress ranges are used, which are 5 stresses ranging from 40 MPa to 80 MPa.

7.1 Effect of cover-plate position

In this section, a modified model was created based on the specimens used in Hui et al. (2018) test, where the cover-plate position was changed. As previously shown in section 3.4, Hui et al. conducted the experiment on beams each containing two cover-plates attached to the underside at both ends of the beam. But the majority of strengthening cover-plates are applied across the middle of the bottom flange and not at the flange ends, due to the moment being at its largest across the middle of the beams. Therefore, the modified model was created to compare the results to the original beam model. To find out if the same principles can be applied to cover-plated beams no matter where the cover-plates are attached.

The changes made to the specimen can be seen in Figure 7.1. As can be seen in the figure, the cover-plate was attached to the bottom flange so that the toe is placed at the same location as the toe of Hui et al. beam, which is highlighted in Figure 7.1.

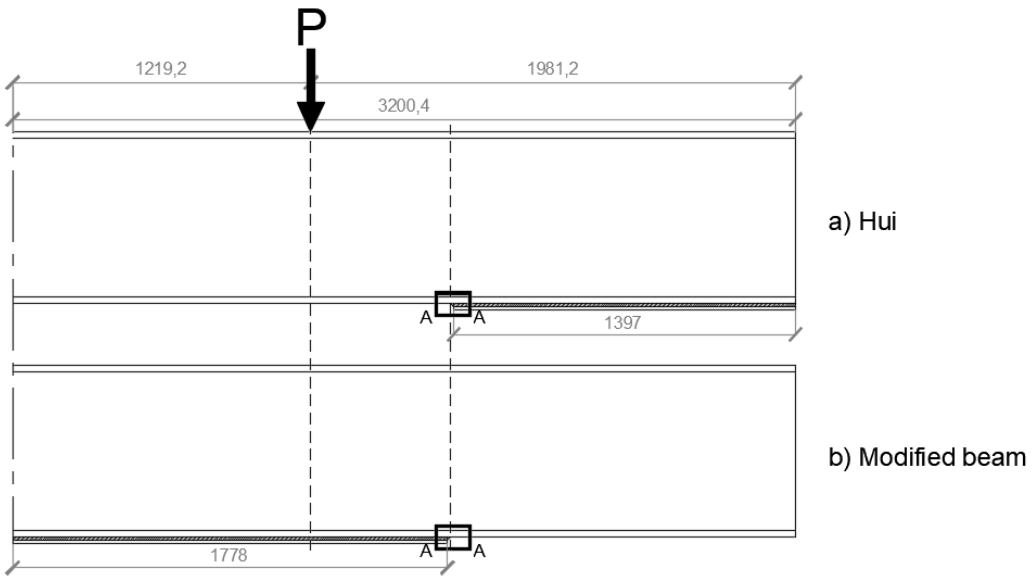

Figure 7.1: Illustration of the modified beam partitioned in half used in Abaqus. Figure a) shows the original Hui beam for S7-S14 and b) shows the modified beam. All beams has the same weld detail (Detail A-A) as shown in Figure 4.10 (all units are in mm). [Writers own figure]

7.1.1 FE results and fatigue study

As previously stated, the analysis was conducted for a unit nominal stress equal to 1 MPa applied at weld toe and, therefore, the same load written in section 4.3.2 was used for this model. The analysis showed that the largest tensile effective notch stresses occur at weld toe, where the maximum principal stress is 6.154 MPa, while the maximum principal stress the weld root is 5.9 MPa. The results from both the modified and original (Hui et al) models are presented in table 7.1. It is evident from the table that the model with the cover-plate positioned in the middle of the beam has higher stresses at both weld toe and root than the model with the cover plate at the end. But the highest increase occurs at weld root, with 57.3% while the weld toe has an increase of 40.8%.

Table 7.1: Maximum principal stress results obtained from Abaqus for both the original and modified models assuming 1 MPa nominal stress at the weld toe.

Cover plate position	$\Delta\sigma_{ENS_{Toe}}$ [MPa]	$\Delta\sigma_{ENS_{Root}}$ [MPa]	Difference
a) Hui et al (at the end of the beam)	4.370	3.750	15.3 %
b) Modified (in the middle of the beam)	6.154	5.900	4.2 %
Increase	40.8%	57.3%	

From the maximum principal stresses presented in Table 7.1 the effective notch stresses at both the toe and root were calculated for nominal stress ranges (40, 50, 60, 70 and 80 MPa) and the results can be seen in Table 7.2. With the effective notch stresses, the characteristic load cycles at weld toe and root were calculated for HFMI-treated cover-plates to perform the theoretical evaluation process. Applying the same procedure used in section 5.4.1. The calculated load cycles can be seen in Table 7.2. The same calculations were performed for the respective stress ranges Hui et al. used for the practical tests, and the results can be seen in Appendix D.1.1.

Table 7.2: Calculated characteristic load cycles at weld toe and root for modified HFMI-treated beam within the nominal stress ranges of 40-80 MPa, as well as the ratio (r) between load cycles of the toe and root.

S_r [MPa]	ENS [MPa]		Load cycles [-]		Ratio [-]
	$\Delta\sigma_{Toe}$	$\Delta\sigma_{Root}$	$N_{Toe_{HFMI}}$	N_{Root}	$\frac{N_{Root}}{N_{Toe}}$
One cover-plate in the middle of the beam					
40	246	236	7,424,932	1,733,172	0.23*
50	308	295	2,433,002	887,384	0.36*
60	369	354	977,769	513,532	0.53
70	431	413	452,379	323,391	0.71
80	492	472	232,029	216,646	0.93

* Cover-plates whose cracking mode occurs at the weld root.

The calculated characteristic load cycle ratio shown in Table 7.2 for each nominal stress is assembled into a graph shown in Figure 7.2. As seen in the figure, the theoretical cracking modes for lower nominal stresses (40 and 50 MPa) are determined to be at weld root, because the ratio is $r \leq 0.5$. In contrast, for higher nominal stresses (60, 70 and 80 MPa) the theoretical cracking mode is undetermined since the ratio is $0.5 < r \leq 2$. The determination of load cycle ratio (r) can be read in section 5.4.1.

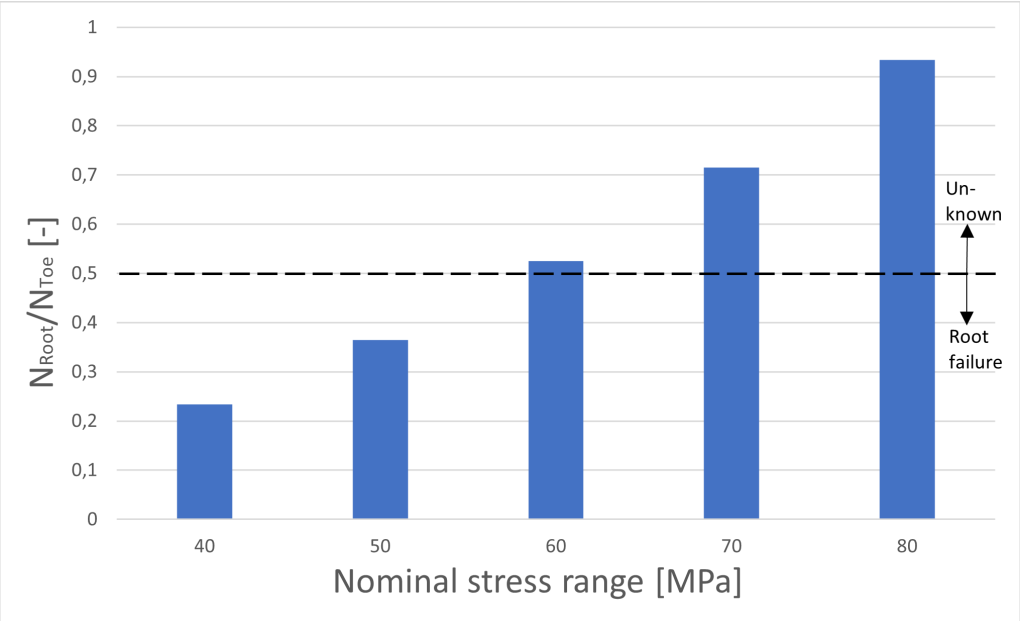

Figure 7.2: The ratio (r) between the calculated design load cycles at weld toe and root for HFMI-treated beam within the nominal stress ranges of 40-80 MPa. A ratio $r \leq 0.5$ indicates cracking mode at weld root and for $0.5 < r \leq 2$ indicating undetermined cracking mode.

7.1.2 Stress fields

The maximum principal stress fields of the modified beam were extracted from Abaqus and can be seen in Figure 7.3. Each sub-figure illustrates the maximum principal stresses of different stress ranges, which can also be seen in Appendix D.1.2. It is observed that the maximum compressive principal stresses shown in Figure 7.3(a) are concentrated at one region of the weld root.

For what is seen in Figure (b) it is apparent that the majority of all tensile stresses distributed throughout the beam is within the stress range 0-1 MPa. When compared with Figure (c), it is observed that the maximum tensile stresses in the beam are within the stress range of 1-2 MPa and are located at the bottom flange following the end of the cover-plate. Moreover, it can be seen in Figure (c) that the tensile stresses are distributed along the top side of the cover-plate and through the weld. The tensile stresses at the cover-plate and the bottom flange are the result of bending and the cluster of stresses through the weld are the result of tensile stresses being transferred to the cover-plate from the flange.

Lastly, Figure (d) shows that the highest maximum principal stresses are located at the toe and root of the weld. Due to similarities between stress fields of the modified beam and Hui

et al. modeled beam it is likely that the cover-plate of the modified beam could fail at either the weld toe or weld root. Therefore, with treated cover-plates having enhanced fatigue performance at weld toe, the high root stresses and the minimal difference in maximum principal stresses between the two notches indicate that there is a high probability that the cover-plate will crack at weld root. The direction of stress field distribution in Figure (d) also visualizes the location and direction of fatigue cracks if formed. Hence, toe cracks will form at the weld's surface at the midpoint of the stress vectors and develop through the beam's flange. While root cracks will form inside the weld at the midpoint of the stress vectors and move outwards through the weld.

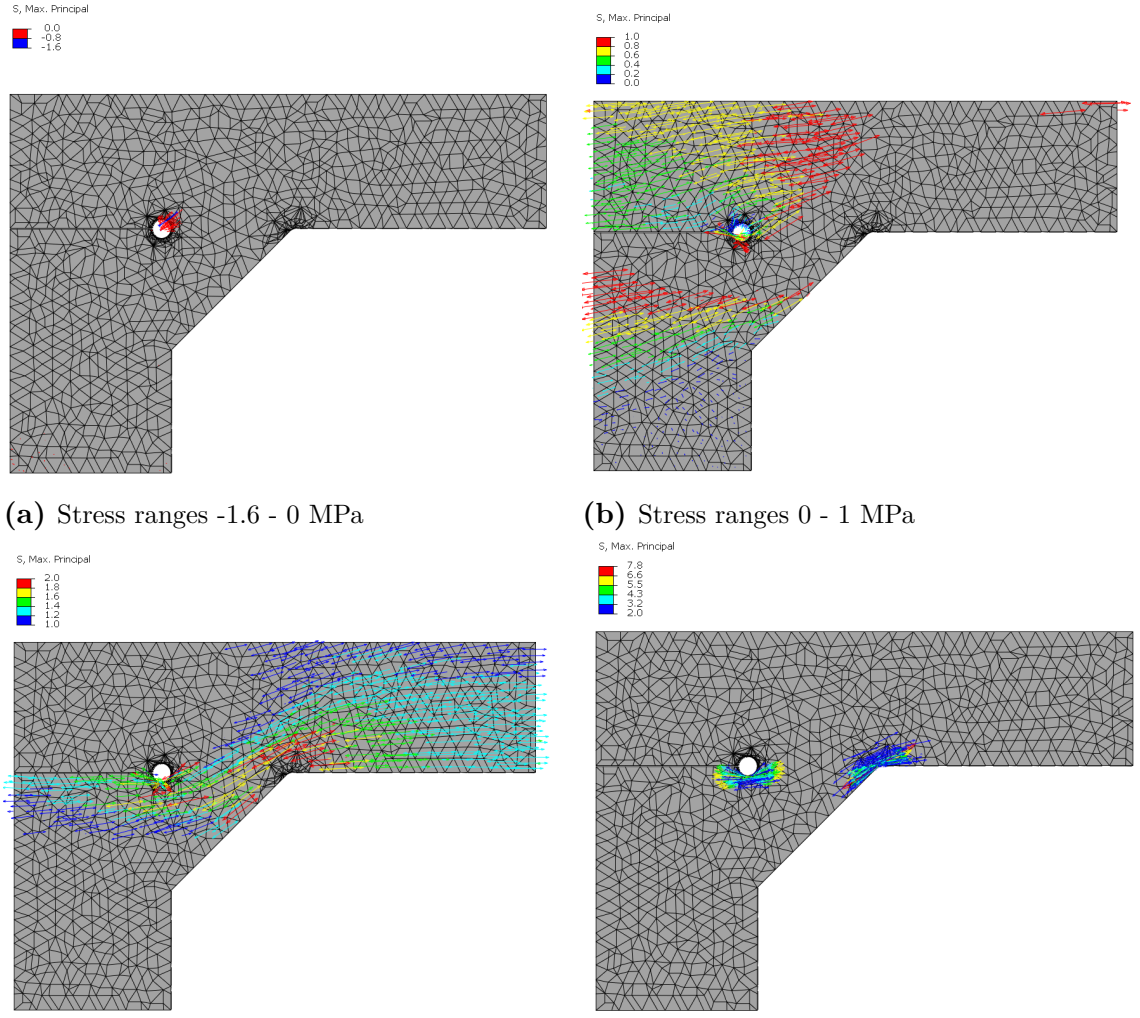

(a) Stress ranges -1.6 - 0 MPa

(b) Stress ranges 0 - 1 MPa

(c) Stress ranges 1 - 2 MPa

(d) Stress ranges 2 - 7.8 MPa

Figure 7.3: Maximum principal stress field distribution in 4 different stress ranges for modified beam model loaded in bending, under a unit nominal stress of 1 MPa at weld toe.

7.2 Thickness effect

This section investigates the effect cover-plate thickness has on fatigue performance of welded cover-plated beams. This is to gain a better understanding of how the stress situation at both weld root and toe differs when the thickness is altered. In this regard, 7 thicknesses was studied, which includes 6 additional models constructed in Abaqus based on the modified cover-plated beam described in section 7.1. For each model, the cover-plate thickness has been altered while all other dimensions were kept constant. Accordingly, the weld size was not adjusted to fit the recommended dimensions for each plate thickness, see Figure 7.4 and figures in Appendix D.2.1 for detailed dimensions.

As can be seen in the figure, the thicknesses range from 15 mm up to 50 mm. These cover-plate thicknesses were chosen based on a number of criteria. The first being that, because the weld leg-length equals to 12.7 mm, cover-plates thinner than 12,7 mm cannot be included in this study. Secondly, since this thesis focuses on welded cover plates for strengthening steel bridges, the thicknesses have been selected to be between 15 mm and 40 mm, which are the thicknesses most commonly used by structural engineers. Lastly, since Eurocode 3 (European standard, 2008) assigns cover-plates thicker than 50 mm to the lowest fatigue category among all cover-plates, see Figure 2.7, the last studied thickness (50 mm) was chosen.

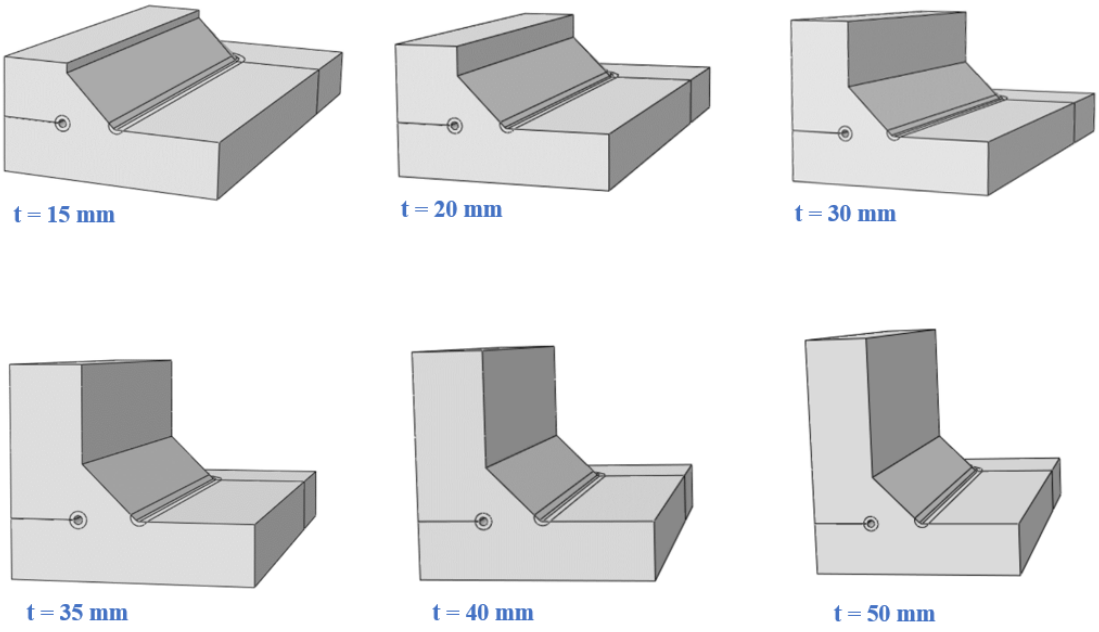

Figure 7.4: Sub-models in Abaqus for the studied cover-plate thicknesses. only half of the flange thickness is included.

7.2.1 FE results and fatigue study

The results obtained from Abaqus are the maximum principal stresses at weld toe and root. These results can be seen in Table 7.3. As shown in the table, altering cover-plate thickness affects the stresses at both weld toe and root. In this case, there is an observation that the thicker the cover-plate becomes the higher the stresses.

Table 7.3: Maximum principal stress results obtained from Abaqus for different cover-plate thicknesses (t_c), assuming 1 MPa nominal stress at weld toe. The difference between the toe and root stresses are shown for each plate thickness.

t_c [mm]	$\Delta\sigma_{ENS_{Toe}}$ [MPa]	$\Delta\sigma_{ENS_{Root}}$ [MPa]	Difference
15	5.8	4.7	21%
20	5.94	5.55	6.8%
25.4	6.15	5.9	4.2%
30	6.7	6.5	3.0%
35	6.99	6.7	4.2%
40	7.44	7.28	2.2%
50	8.69	8.03	7.9%

In order to better visualize how root and toe stresses differ when cover-plate thickness changes, the data acquired for the thicker cover-plate (50 mm) was used as a reference. Therefore, the stresses obtained for each thickness were divided by the stresses obtained for thickness 50 mm. The calculated data can be seen in Table 7.4, while the relationship between stress change and thickness change is visualized in Figure 7.5. It is observed from the table and the figure that by reducing the cover-plate thickness to almost half (from 50 to 25.4 mm), the weld toe and root stresses decreased by 29% and 27%, respectively. Furthermore, when the cover-plate thickness is more than 20 mm, the reduction in toe stresses was slightly greater than the reduction in root stresses when the thickness was decreased. In contrast, when the cover plate thickness was reduced to less than 20 mm, the root stress was remarkably decreased. Thus, reducing the cover-plate thickness from 50 to 15 mm reduced the weld toe and root stresses by 33% and 41%, respectively.

Table 7.4: The ratio between maximum principal stresses (at weld toe and root) for cover-plates of different thicknesses and the maximum principal stresses for the cover-plate of the maximum thickness ($t_c = 50$ mm). The stresses can be found in Table 7.3.

t_c [mm]	$\frac{t_c}{t_{max}}$	$\frac{\Delta\sigma_{ENS_{Toe}}}{\Delta\sigma_{ENS_{Toe,max}}}$	$\frac{\Delta\sigma_{ENS_{Root}}}{\Delta\sigma_{ENS_{Root,max}}}$
15	0.3	0.67	0.59
20	0.4	0.68	0.69
25.4	0.508	0.71	0.73
30	0.6	0.77	0.81
35	0.7	0.80	0.83
40	0.8	0.86	0.91
50	1	1	1

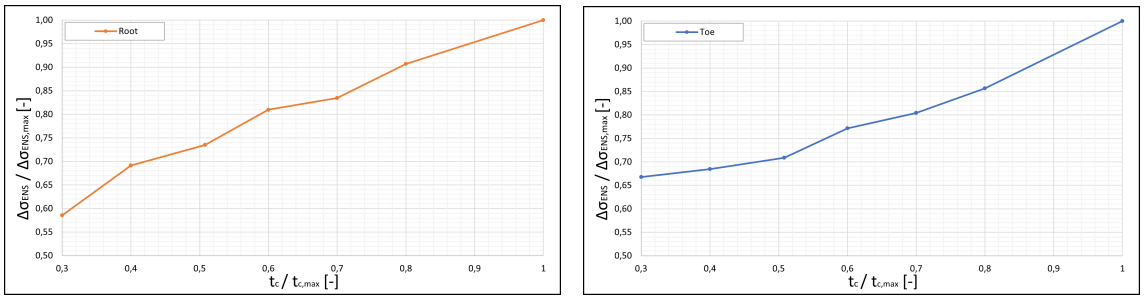

(a) Root **(b)** Toe

Figure 7.5: Graphs show the effect of cover-plate thickness has on the effective notch stresses at weld root and toe.

With the results obtained from FE analysis shown in Table 7.3, the effective notch stresses at the root and toe for nominal stress ranges (40, 50, 60, 70 and 80 MPa) were derived for each cover-plate thickness. With the effective notch stresses, the characteristic load cycles at weld toe and root were calculated for HFMI-treated cover-plates to perform the theoretical evaluation process. This was done by applying the same procedure used in section 5.4.1. The results for the effective notch stresses at the toe and the root, as well as the determined load cycles, are shown in Table 7.5. The same calculations were performed for the respective stress ranges Hui et al. used for the practical tests, and the results can be seen in Appendix D.2.2.

Table 7.5: Calculated characteristic load cycles at weld toe and root for HFMI-treated beams with different cover-plate thicknesses within nominal stress ranges of 40-80 MPa, as well as the ratio (r) between load cycles of the toe and root.

S_r [MPa]	ENS [MPa]		Load cycles [-]		Ratio [-]
	$\Delta\sigma_{Toe}$	$\Delta\sigma_{Root}$	$N_{Toe_{HFMI}}$	N_{Root}	$\frac{N_{Root}}{N_{Toe_{HFMI}}}$
Cover-plate thickness: 15 mm					
40	232	188	11,225,841	3,428,499	0.31*
50	290	235	3,271,824	1,755,391	0.54
60	348	282	1,314,873	1,015,851	0.77
70	406	329	608,345	639,720	1.05
80	464	376	312,025	418,562	1.37
Cover-plate thickness: 20 mm					
40	238	222	8,832,546	2,082,182	0.24*
50	297	278	2,894,249	1,066,077	0.37*
60	357	333	1,163,134	616,943	0.53
70	416	389	538,141	388,512	0.72
80	476	444	276,017	260,273	0.94

Cover-plate thickness: 25.4 mm					
40	246	236	7,424,932	1,733,172	0.23*
50	308	295	2,433,002	887,384	0.36*
60	369	354	977,769	513,532	0.53
70	431	413	452,379	323,391	0.71
80	492	472	232,029	216,646	0.93
Cover-plate thickness: 30 mm					
40	273	265	4,425,544	1,226,941	0.28*
50	341	331	1,450,162	628,194	0.43*
60	410	397	582,788	363,538	0.62
70	478	463	269,635	228,934	0.85
80	546	530	139,959	153,368	1.10
Cover-plate thickness: 35 mm					
40	279	268	3,938,556	1,183,513	0.3*
50	349	335	1,290,586	605,959	0.47*
60	419	402	518,658	350.671	0.68
70	489	469	239,964	220,830	0.92
80	559	536	130,503	147,939	1.13
Cover-plate thickness: 40 mm					
40	298	291	2.874,850	922,579	0.32*
50	372	364	942,031	472,360	0.50*
60	446	437	378,581	273,357	0.72
70	521	510	175,156	172,143	0.98
80	595	582	108,041	115,322	1.07
Cover-plate thickness: 50 mm					
40	347	321	1,326,267	687,979	0.52
50	434	401	434,591	352,245	0.81
60	521	481	174,652	203,846	1.17
70	608	562	101,385	128,369	1.27
80	695	642	67,920	85,997	1.27

* Cover-plates whose cracking mode occurs at the weld root.

The red color indicates that the as-welded design curve of FAT 225 was used to calculate the load cycles for the HFMI-treated toe.

7.2.2 Stress fields

The maximum principal stress fields of two cover-plate thicknesses were extracted from Abaqus. These stress fields can be seen in Figure 7.6 for $t_c = 15$ mm and Figure 7.7 for $t_c = 50$ mm, all can be seen in Appendix D.2.3. The sub-figures illustrate the maximum principal stress distributions for different stress ranges and it can be observed in both figures that the stress fields for each stress range are relatively similar. Therefore, when referencing a sub-figure, both the sub-figures in Figures 7.6 and 7.7 are discussed.

As previously mentioned, the thickness effect studies were performed with the same FE model used for the modified model in section 7.1. The difference being that the cover-plate thickness was changed for each analysis. Therefore, it is to be expected that the extracted stress fields are distributed in a similar manner to the modified model's stress fields with a plate thickness of $t_c = 25.4$ mm. This assumption is verified, when comparing the sub-figures in Figures 7.6 and 7.7 with sub-figures in Figure 7.3. Hence the general description of the stress field distribution of the modified beam is also accurate for different cover-plate thicknesses. However, it is observed that the minimum compressive stresses in Figures (a) and the maximum tensile stresses in Figures (d) increase with thicker cover-plates. This correlates with the results discussed previously.

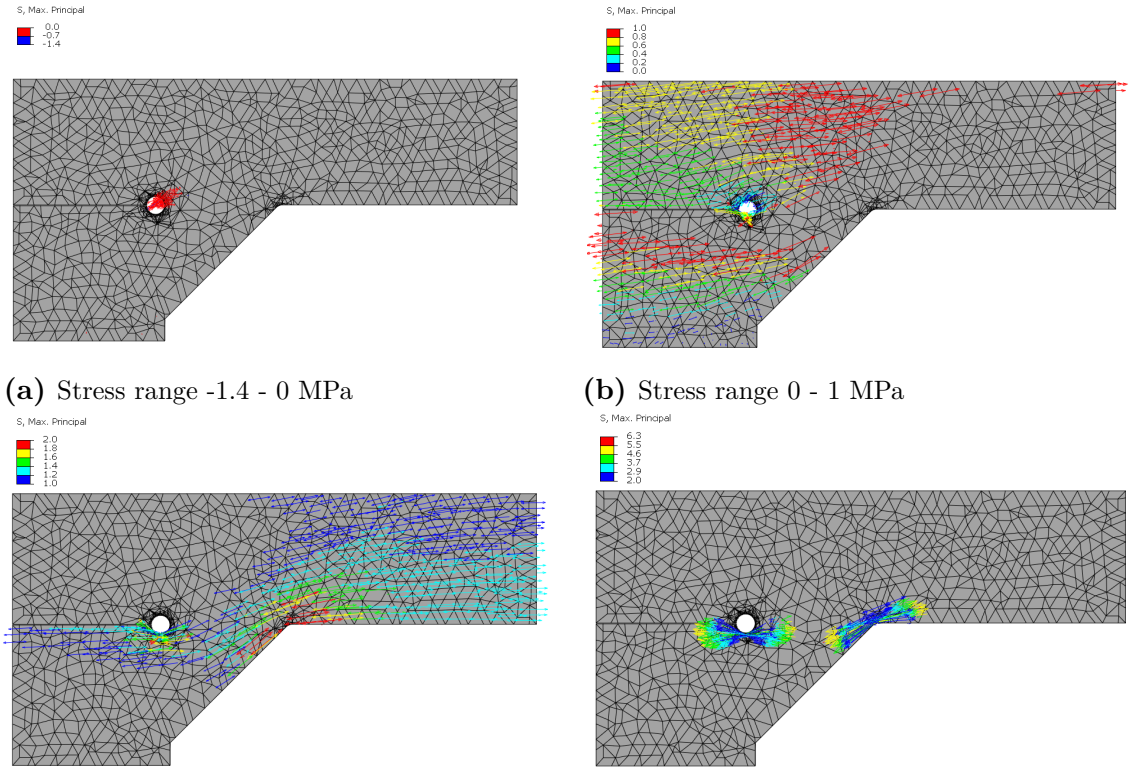

(a) Stress range -1.4 - 0 MPa

(b) Stress range 0 - 1 MPa

(c) Stress range 1 - 2 MPa

(d) Stress range 2 - 6.3 MPa

Figure 7.6: Maximum principal stress field distribution in 4 different stress ranges for the modified beam with a cover-plate thickness of 15 mm, under a unit nominal stress of 1 MPa at weld toe.

Excluding the similar stress field distributions of the different cover-plate thicknesses, there are some noticeable differences. For the stress range of 0-1 MPa, see Figures (b), it is observed that for the thinnest cover-plate ($t_c = 15$ mm) the distribution of stresses is closer to the top of the cover-plate and the weld. But for the thickest cover-plate ($t_c = 50$ mm) the distribution has lessened. Meaning that, the maximum principal stresses within the stress range of 1-2 MPa, shown in Figures (c), have a broader distribution throughout the cover-plate and weld for thicker cover-plates. The same can be seen for stresses >2 MPa. When comparing Figures (d) it is observed that stresses are developed outside of the weld toe and root. In the case of the thickest cover-plate seen in Figure 7.7(d), a concentration of stresses is distributed throughout the weld in-between the weld toe and root.

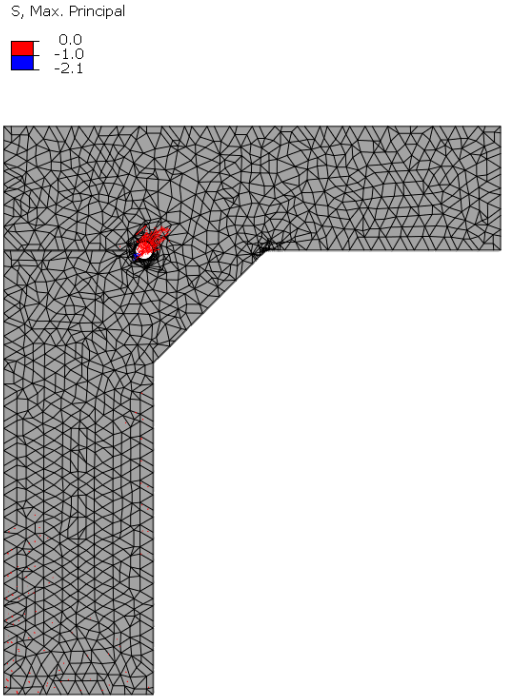

(a) Stress range -2.1 - 0 MPa

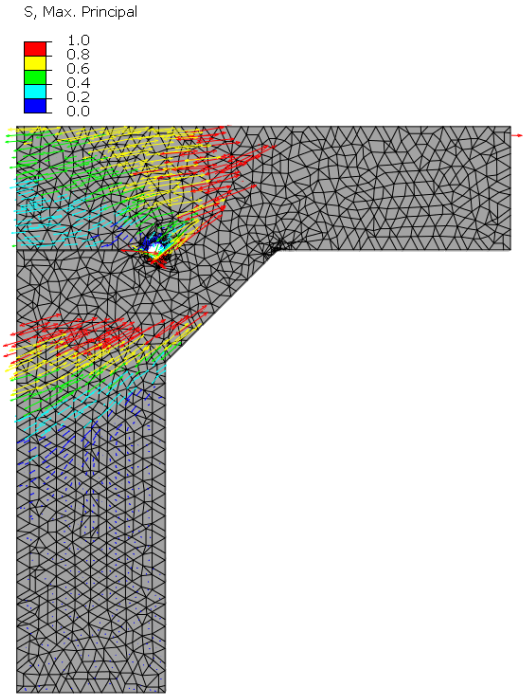

(b) Stress range 0 - 1 MPa

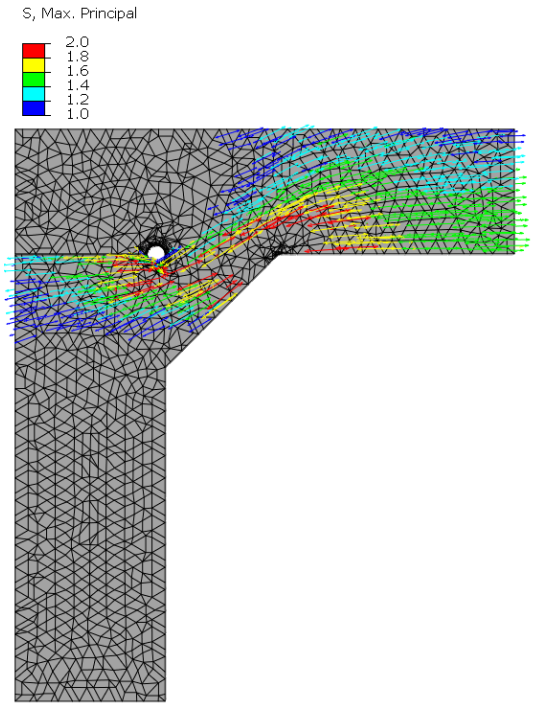

(c) Stress range 1 - 2 MPa

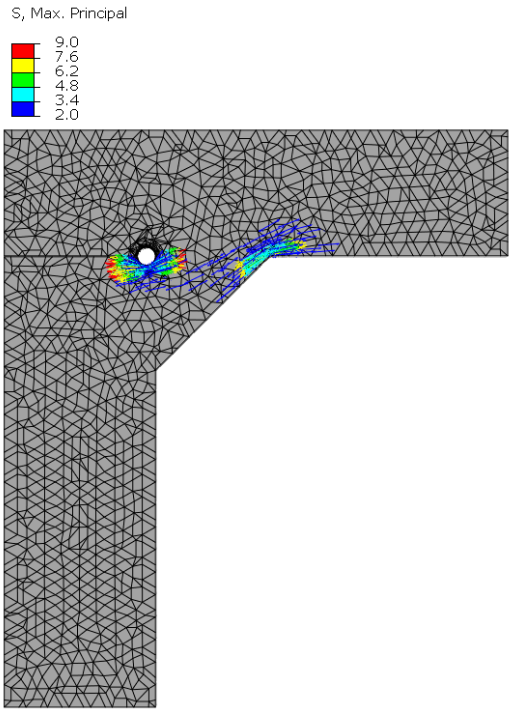

(d) Stress range 2 - 9.0 MPa

Figure 7.7: Maximum principal stress field distribution in 4 different stress ranges for the modified beam with a cover-plate thickness of 50 mm, under a unit nominal stress of 1 MPa at weld toe.

7.3 Length effect

The following section examines the effect cover-plate length has on fatigue performance of welded cover-plated beams. This is to get a better understanding of how the cover-plate length influences the stress distribution at the weld toe and root when the length is altered. In order to do so, 5 lengths were studied as illustrated in Figure 7.8, which includes 4 additional models constructed in Abaqus based on the modified beam model in section 7.1. To perform the analysis the cover-plate length was altered for each model, but other dimensions were kept constant. This means that the original cover-plate thickness and weld size were retained for each model, and the original dimensions are depicted in Detail A-A of Figure 4.10.

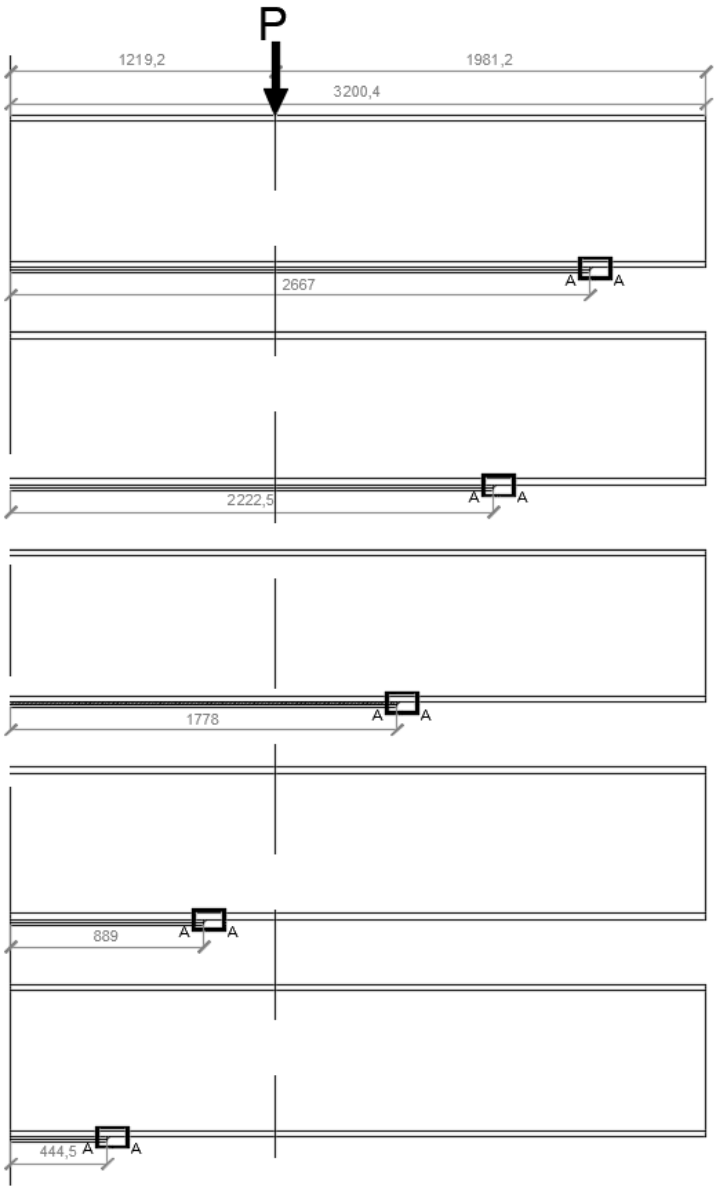

Figure 7.8: Illustration of the studied lengths of cover-plated beams partitioned in half used for Abaqus. The third beam is the modified beam shown in Figure 7.1 and the remaining four are the additional models. All cover-plated beams have the same weld detail (Detail A-A) shown in Figure 4.10 (all units are in mm).

The studied lengths are depicted in Figure 7.8 and it can be seen that the shortest cover-plate has a total length of 889 mm (44.5 mm in Abaqus) and the others follow with a total length of 1,778 mm (889 mm in Abaqus), 3,556 mm (1,778 mm in Abaqus), 4,445 mm (2,222.5 mm in Abaqus) and lastly the longest has a total length of 5,334 mm (2,667 mm in Abaqus).

The initial assumption was to have the load placed at the same location as in Hui et al. test, which was also used for all other exploratory studies. But because the load is located about a third of the beam, the two shortest studied cover-plates are subjected to a constant moment and zero shear force. It was therefore decided to include a second analysis where the load was moved to the middle of the beam. The load was calculated using the same method used for Hui et al. model described in section 4.3.2, where the weld toe of all cover-plates is subjected to a unit nominal stress of 1 MPa. The calculation and load for each cover-plate length can be seen in Appendix D.3.1.

7.3.1 FE results and fatigue study

The results obtained from the FE analysis in Abaqus are the maximum principal stresses at weld toe and root of each cover-plate length model. The results for the two load situations can be seen in Table 7.6. As can be seen in the table, changing cover-plate length affects the stresses at both weld toe and root. In this case, it is observed that the longer the cover-plate becomes, the higher the stresses. This applies to both load positions. Excluding the increase in stresses, it is also observed that for longer cover-plates weld root stresses are larger than weld toe stresses.

Table 7.6: Maximum principal stress results obtained from Abaqus for different cover-plates lengths (L_c) and the ratio between root and toe stresses for two load situation, under a unit nominal stress of 1 MPa at weld toe.

L_c [mm] (L_c/L_B [-])	**Load position: Third of beam**			**Load position: Middle of beam**		
	ENS [MPa]		Ratio [-]	ENS [MPa]		Ratio [-]
	$\Delta\sigma_{Toe}$	$\Delta\sigma_{Root}$	$\frac{\Delta\sigma_{Root}}{\Delta\sigma_{Toe}}$	$\Delta\sigma_{Toe}$	$\Delta\sigma_{Root}$	$\frac{\Delta\sigma_{Root}}{\Delta\sigma_{Toe}}$
889 (0.14)	5.19	4.80	0.92	5.71	5.56	0.97
1,778 (0.28)	5.40	5.16	0.95	5.74	5.93	1.03
3,556 (0.56)	6.15	5.90	0.96	5.89	6.54	1.11
4,445 (0.69)	6.65	8.00	1.20	6.54	7.90	1.21
5,334 (0.83)	8.53	10.34	1.21	7.70	10.12	1.31

To better illustrate the change in weld toe and root stresses of each cover-plate length, the ratio acquired from Table 7.6 is assembled into the bar graph seen in Figure 7.9. Where it is further highlighted that for a curtain cover-plate length the highest stress concentration point shifts from the weld toe to the weld root. It is also evident that the shift occurs differently in the two loading situations. When the load is positioned at a third of the beam, the shift appears at a cover-plate to beam length ratio of about $L_C/L_B = 0.6$. On the other hand, when the load is positioned at the middle of the beam, the shift occurs at a ratio of about $L_C/L_B = 0.2$. Hence, indicating that the loading situation influences the ratio between weld toe stresses and weld root stresses. When the load is placed in

the middle the stress ratio increases almost linearly for each cover-plate length. However, when the load is placed at a third of the beam, the ratio remains stagnant for the first three and last two lengths.

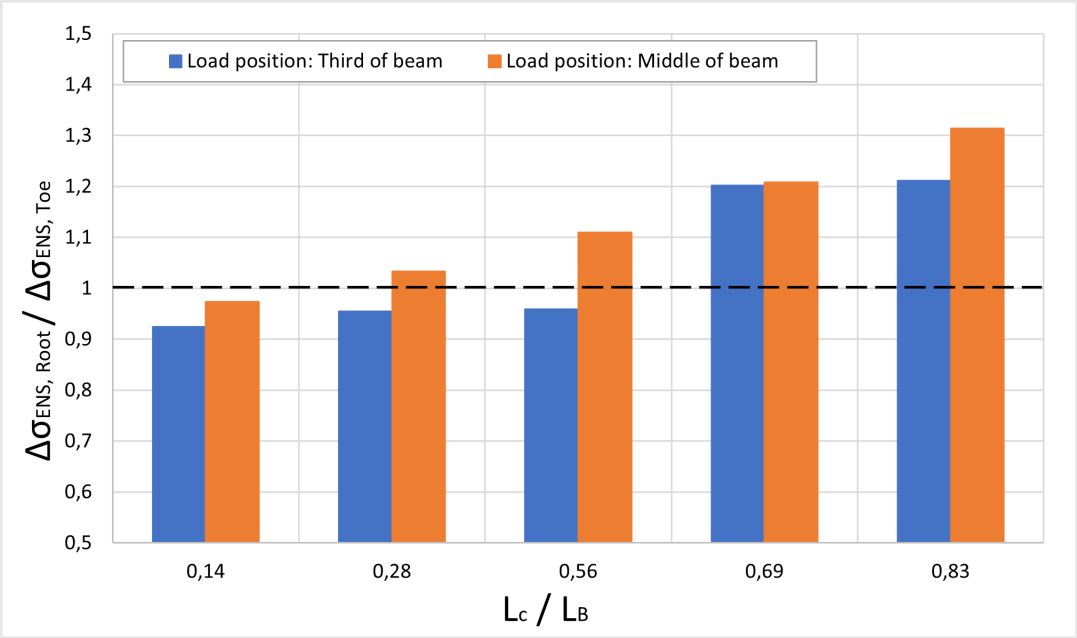

Figure 7.9: Bar graph of the ratio between root and toe stresses for different cover-plate to beam length ratio (L_C/L_B) for two loading positions.

Similarly to the previous study, the values obtained from the longest cover-plate (5,334 mm) were used as a reference to visualize the effect of changing cover-plate length. Hence, dividing the stresses obtained from each cover-plate length with the stresses of the longest cover-plate, for both loading situations. The calculated data can be seen in Table 7.7 and is visualized Figure 7.10.

Table 7.7: The ratio between maximum principal stresses (at weld toe and root) for cover-plates of different lengths and the maximum principal stresses for the cover-plate of the maximum thickness ($L_c = 5,334$ mm). The stresses can be found in Table 7.6.

L_c [mm]	$\frac{L_c}{L_{c,max}}$	**Load position: Third of beam**		**Load position: Middle of beam**	
		$\frac{\Delta\sigma_{ENS_{Toe}}}{\Delta\sigma_{ENS_{Toe,max}}}$	$\frac{\Delta\sigma_{ENS_{Root}}}{\Delta\sigma_{ENS_{Root,max}}}$	$\frac{\Delta\sigma_{ENS_{Toe}}}{\Delta\sigma_{ENS_{Toe,max}}}$	$\frac{\Delta\sigma_{ENS_{Root}}}{\Delta\sigma_{ENS_{Root,max}}}$
889	0.17	0.61	0.46	0.74	0.55
1778	0.33	0.63	0.50	0.75	0.59
3556	0.67	0.72	0.57	0.76	0.65
4445	0.83	0.78	0.77	0.85	0.78
5334	1	1	1	1	1

It is observed in the table and figure that when reducing the cover-plate length from the longest (5,334 mm) to the original length of 3,556 mm, the weld toe and root stresses decreased with 28% and 43% respectively, for when the load is positioned at a third of the beam. In contrast, when the load was placed at the middle of the beam, the stresses

decreased by 24% and 35% respectively. In addition, both loading situations showed that the largest decreases occur at weld root. Since the results demonstrate a decrease of 54% and 45% in root stresses when the length is reduced by 6 times (5,334 mm to 889 mm).

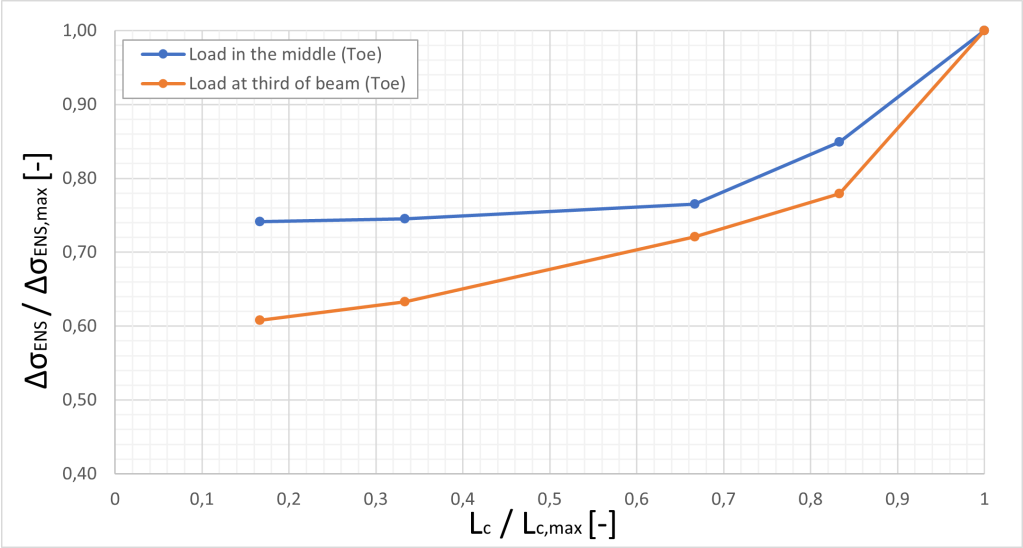

(a) Toe

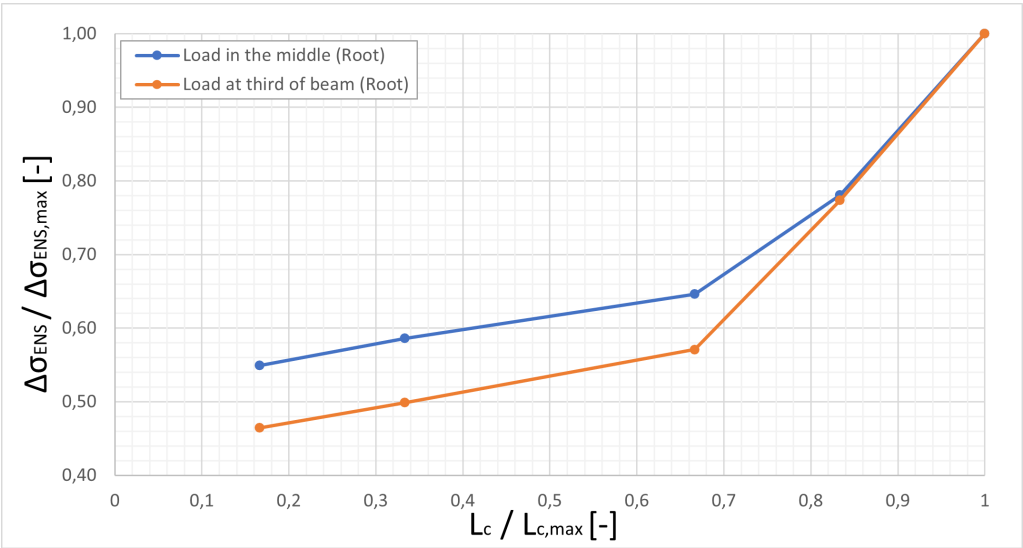

(b) Root

Figure 7.10: Graphs show the effect cover-plate length has on the effective notch stresses at weld toe and root for the two loading positions.

With the FE analysis results shown in Table 7.6, the effective notch stresses at the weld toe and root were derived for each cover-plate length for nominal stresses of 40, 50, 60, 70 and 80 MPa. With the effective notch stresses, the characteristic load cycles for the weld toe and root were calculated for HFMI-treated cover-plates. The resulting effective notch stresses at the weld toe and root, as well as the determined load cycles are shown in Table 7.8 for when the load is applied at a third of the beam and in Table 7.9 for when the load is placed at the middle of the beam. The same calculations were performed for the respective stress ranges Hui et al. used for the practical tests, and the results can be seen in Appendix D.3.2.

Table 7.8: Calculated characteristic load cycles at weld toe and root for HFMI-treated beams with different cover-plate lengths within nominal stress ranges of 40-80 MPa, as well as the ratio between load cycles of the toe and root. For when the load is placed at the third of the beam.

S_r [MPa]	ENS [MPa]		Load cycles [-]		Ratio [-]
	$\Delta\sigma_{Toe}$	$\Delta\sigma_{Root}$	$N_{Toe_{HFMI}}$	N_{Root}	$\frac{N_{Root}}{N_{Toe_{HFMI}}}$
Cover-plates length: L = 889 mm					
40	208	192	30,558,601	3,218,651	0, 11*
50	260	240	5,702,865	1,647,949	0.29*
60	311	288	2,291,853	953,674	0.42*
70	363	336	2,060,359	600,565	0.57
80	415	384	543,868	402,331	0.74
Cover-plates length: L = 1,778 mm					
40	216	206	21,296,360	2,396,544	0.12*
50	270	258	4,669,629	1,329,431	0.28*
60	324	309	1,876,619	769,346	0.41*
70	378	361	868,245	484,486	0.56
80	432	413	445,331	324,568	0.73
Cover-plates length: L = 3,556 mm					
40	246	236	7,424,932	1,733,172	0.23*
50	308	295	2,433,002	887,384	0.36*
60	369	354	977,769	513,532	0.53
70	431	413	452,379	323,391	0.71
80	492	472	232,029	216,646	0.93
Cover-plates length: L = 4,445 mm					
40	266	320	5,033,399	695,921	0, 14*
50	333	400	1,649,344	356,312	0.22*
60	399	480	662,834	206,199	0.31*
70	466	560	306,670	129,851	0.42*
80	532	640	157,924	86,990	0.55
Cover-plates length: L = 5,334 mm					
40	341	413	1,447,418	322,268	0.22*
50	427	517	474,290	165,001	0.35*
60	512	620	190,606	95,487	0.50*
70	597	724	106,844	60,132	0.56
80	683	827	71,577	40,284	0.56

* Cover-plates whose cracking mode occurs at the weld root

The red color indicates that the as-welded design curve of FAT 225 was used to calculate the design load cycles for the HFMI-treated toe.

Table 7.9: Calculated characteristic load cycles at weld toe and root for HFMI-treated beams with different cover-plate lengths within nominal stress ranges of 40-80 MPa, as well as the ratio between load cycles of the toe and root. For when the load is placed at the middle of the beam.

S_r [MPa]	ENS [MPa]		Load cycles [-]		Ratio [-]
	$\Delta\sigma_{Toe}$	$\Delta\sigma_{Root}$	$N_{Toe_{HFMI}}$	N_{Root}	$\frac{N_{Root}}{N_{Toe_{HFMI}}}$
Cover-plates length: L = 889 mm					
40	228	222	12,922,480	2,070,967	0, 16*
50	286	278	3,537,931	1,060,335	0.30*
60	343	334	1,421,815	613,620	0.43*
70	400	389	657,823	386,420	0.59
80	457	445	337,403	258,871	0.77
Cover-plates length: L = 1,778 mm					
40	230	237	12,327,182	1,707,000	0.14*
50	287	297	3,446,437	873,984	0.25*
60	344	356	1,385,046	505,778	0.37*
70	402	415	640,811	318,507	0.50*
80	459	474	328,678	213,375	0.65
Cover-plates length: L = 3,556 mm					
40	236	262	9,244,926	1,271,519	0.14*
50	295	327	3,029,377	651,530	0.22*
60	353	392	1,217,439	377,043	0.31*
70	412	458	563,266	237,438	0.42*
80	471	523	288,904	159,065	0.55
Cover-plates length: L = 4,445 mm					
40	262	316	5,477,611	721,965	0, 13*
50	327	395	1,794,904	369,646	0.21*
60	392	474	721,331	213,916	0.30*
70	458	553	333,734	134,711	0.40*
80	523	632	171,175	90,246	0.53
Cover-plates length: L = 5,334 mm					
40	308	405	2,421,176	343,444	0.14*
50	385	506	793,371	175,843	0.22*
60	462	607	318,838	101,761	0.32*
70	539	708	147,515	64,083	0.43*
80	616	810	97,462	42,931	0.44*

* Cover-plates whose cracking mode occurs at the weld root

The red color indicates that the as-welded design curve of FAT 225 was used to calculate the design load cycles for the HFMI-treated toe.

7.3.2 Stress fields

The maximum principal stress fields for three different cover-plate lengths (889 mm, 3,556 mm and 5,334 mm) were extracted from Abaqus for the two loading situations. Similarly to the thickness effect study, the FE model of the modified model in section 7.1 were used for the length effect study. Therefore, the stress fields extracted would be distributed in a similar manner to the modified model. Which the results verified. Hence, the general structural behaviour the stress fields of the modified beam describe is also accurate for different cover-plate lengths. However, the same observation as for thickness effect is also detected, that the minimum compressive stresses and maximum tensile stresses increases with the cover-plate length. Which correlate with the results previously presented in this section and can be seen in Figure 7.13 for the stress range >2 MPa.

Excluding the similarities in stress field distribution between the different cover-plate lengths and loading situations, there are some differences. To simplify the comparison between stress fields. A maximum of three different lengths were compared within the same stress ranges of 0-1 MPa, 1-2 MPa and >2 MPa for both loading situations. These stress fields can be seen in Figures 7.11, 7.12 and 7.13 respectively. The most important stress fields can be seen in Appendix D.3.3.

For the stress range of 0-1 MPa seen in sub-figures of Figure 7.11, it is observed that the same change in stress distribution occurs for longer cover-plates as for thicker cover-plates. Indicating that, the area of distribution decreases at the cover-plate and weld for longer cover-plates. This is observed to occur for both loading situations. Which means that the area and intensity of stress distribution for stress range of 1-2 MPa increases for longer cover-plates. As seen in the sub-figures of Figure 7.12.

Moreover, the maximum principal stress distribution for the stress range >2MPa does also increase for longer cover-plates. As seen in the sub-figures of Figure 7.13. It is observed that maximum principal stresses are also developed in the vicinity of weld toe and root and distributed throughout the weld. This only occurred for the two longest studied cover-plates for both loading situations. While for the shortest cover-plate only have a stress distribution at the weld notches as is seen in Figure 7.13(a) and (b).

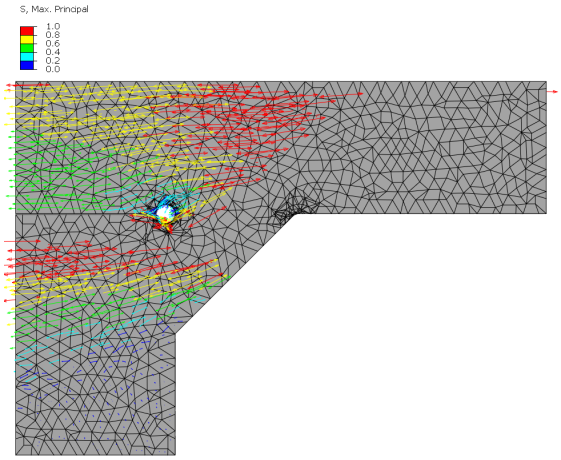

(a) Load at third of beam, $L_c = 889$ mm, stress range 0 - 1 MPa

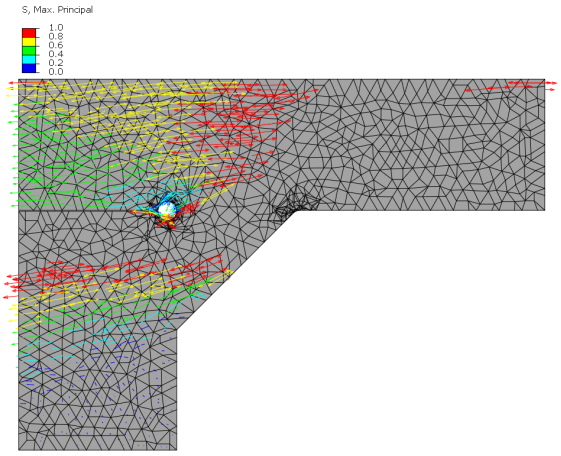

(b) Load middle of beam $L_c = 889$ mm, stress range 0 - 1 MPa

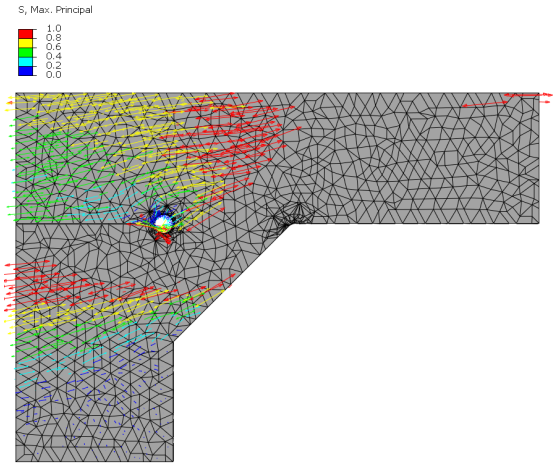

(c) Load at third of beam, $L_c = 3,556$ mm, stress range 0 - 1 MPa (from Figure 7.3(b))

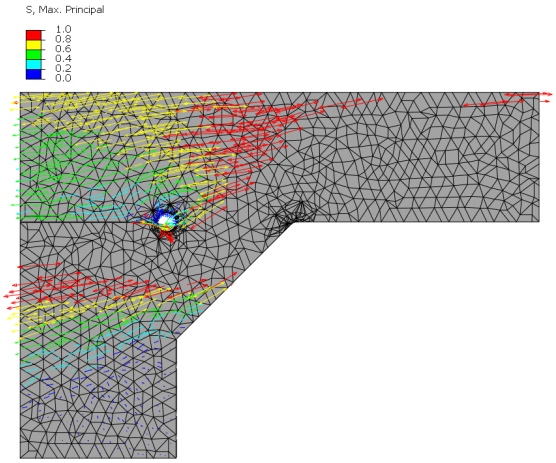

(d) Load middle of beam, $L_c = 3,556$ mm, stress range 0 - 1 MPa

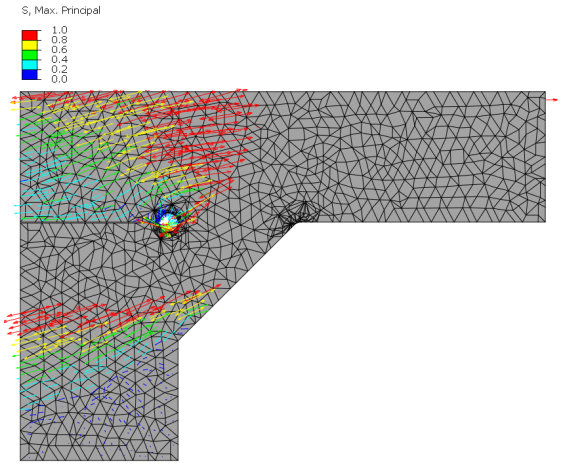

(e) Load at third of beam, $L_c = 5,334$ mm, stress range 0 - 1 MPa

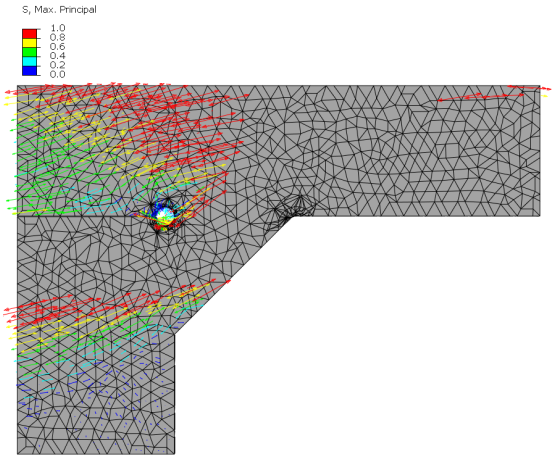

(f) Load middle of beam, $L_c = 5,334$ mm, stress range 0 - 1 MPa

Figure 7.11: Maximum principal stress fields distribution in stress range of 0 - 1 MPa for the modified beam with the two loading positions, for 3 different cover-plate lengths (889 mm, 3,556 mm and 5,334 mm), under a unit nominal stress of 1 MPa at weld toe.

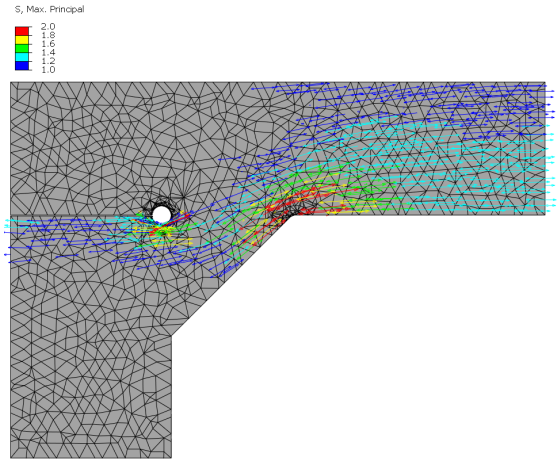

(a) Load at third of beam, $L_c = 889$ mm, stress range 1 - 2 MPa

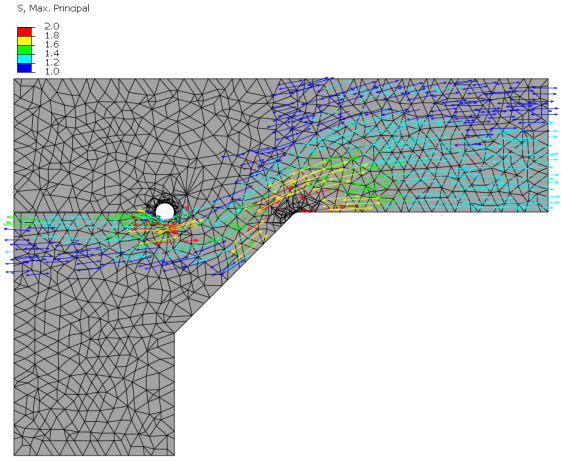

(b) Load middle of beam, $L_c = 889$ mm, stress range 1 - 2 MPa

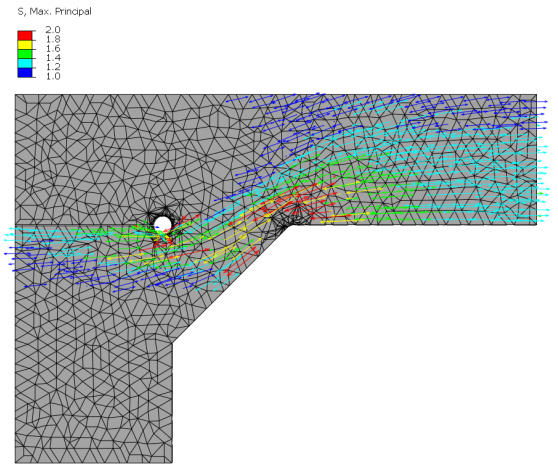

(c) Load at third of beam, $L_c = 3,556$ mm, stress range 1 - 2 MPa (from Figure 7.3(c))

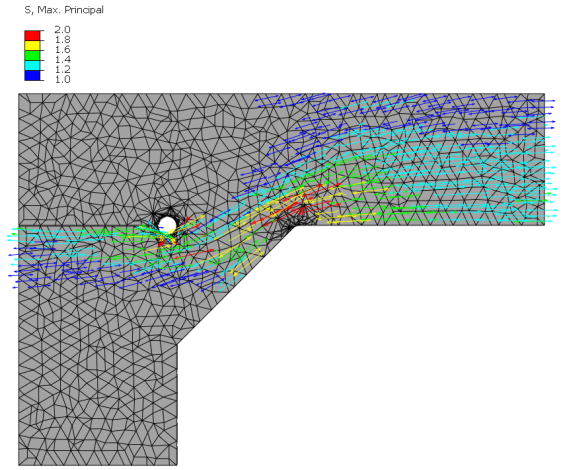

(d) Load middle of beam, $L_c = 3,556$ mm, stress range 1 - 2 MPa

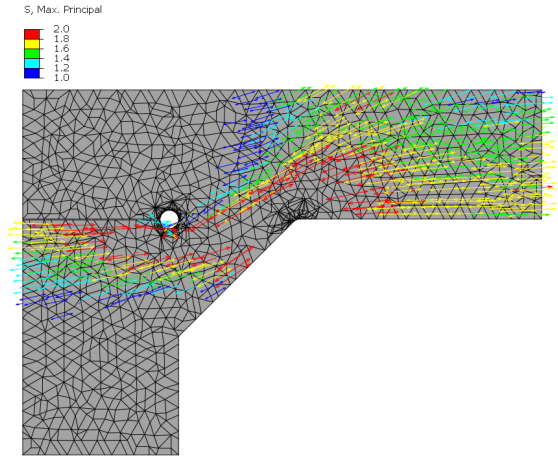

(e) Load at third of beam, $L_c = 5,334$ mm, stress range 1 - 2 MPa

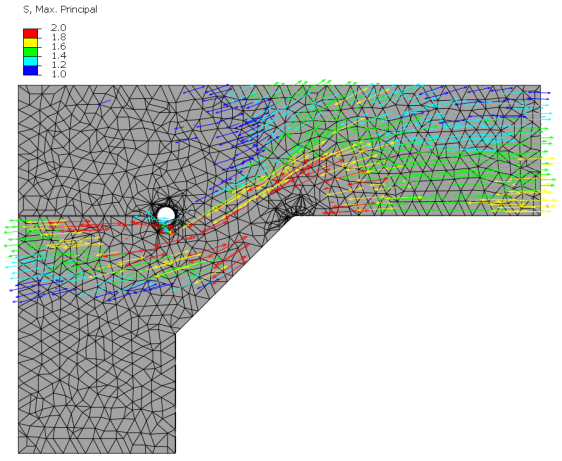

(f) Load middle of beam, $L_c = 5,334$ mm, stress range 1 - 2 MPa

Figure 7.12: Maximum principal stress fields distribution in stress range of 1 - 2 MPa for the modified beam with the two loading positions, for 3 different cover-plate lengths (889 mm, 3,556 mm and 5,334 mm), under a unit nominal stress of 1 MPa at weld toe.

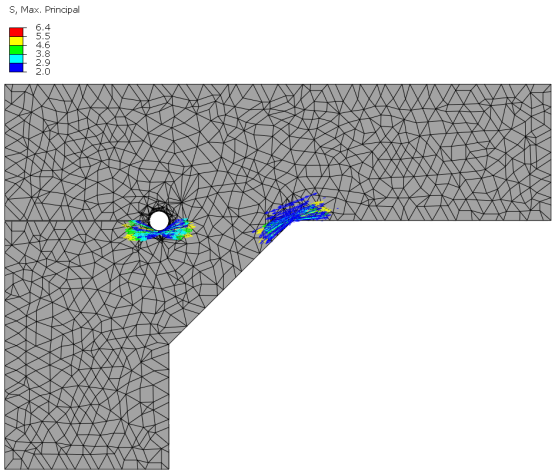

(a) Load at third of beam, $L_c = 889$ mm, stress range 2 - 6.4 MPa

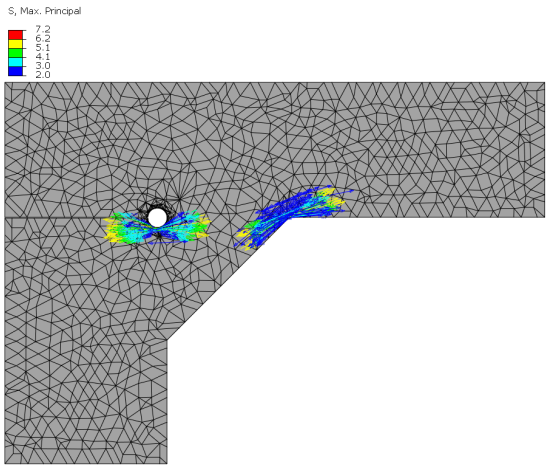

(b) Load middle of beam, $L_c = 889$ mm, stress range 2 - 7.2 MPa

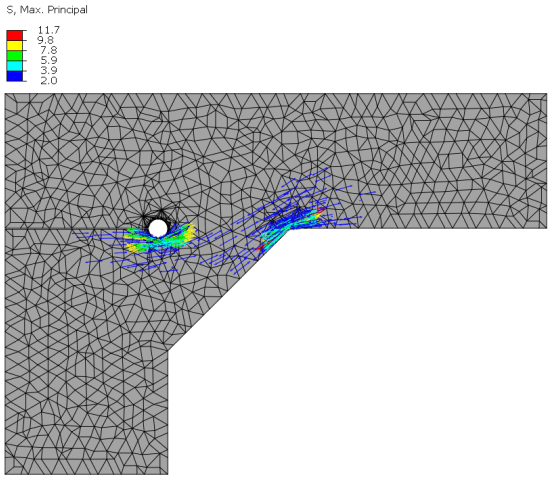

(c) Load at third of beam, $L_c = 5,334$ mm, stress range 2 - 11.7 MPa

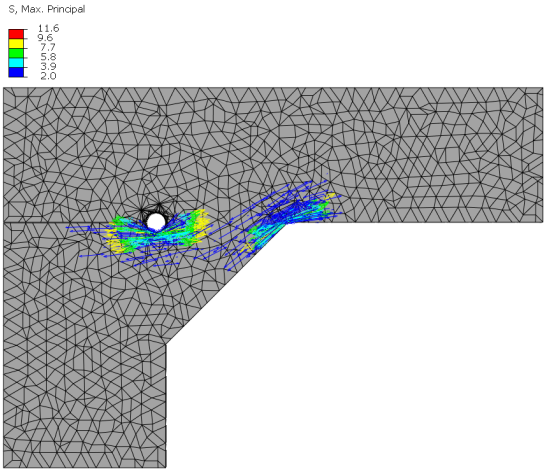

(d) Load middle of beam, $L_c = 5,334$ mm, stress range 2 - 11.6 MPa

Figure 7.13: Maximum principal stress fields distribution in stress range of >2 MPa for the modified beam with the two loading positions, for 2 different cover-plate lengths (889 mm and 5,334 mm), under a unit nominal stress of 1 MPa at weld toe.

7.4 The effect of optimizing end weld

As stated previously, HFMI treatment is only applied to the weld toe, so the weld root isn't enhanced by the treatment. Due to this, the improvement in fatigue performance is limited to the root's fatigue strength. Furthermore, the findings of the first part of this thesis show that weld root failure is the most likely failure mode for HFMI-treated cover-plated beams loaded in bending. It is therefore the purpose of this section to examine possible solutions to this problem that might be implemented. Aiming to increase the fatigue strength of the root, thereby enhancing the fatigue strength of the HFMI-treated cover plates. The suggestions are presented in the following sections.

7.4.1 Root position effect

The solution offered in this section is to incline the edge of the cover-plate so that the weld root position will be shifted, as illustrated in Figure 7.14.

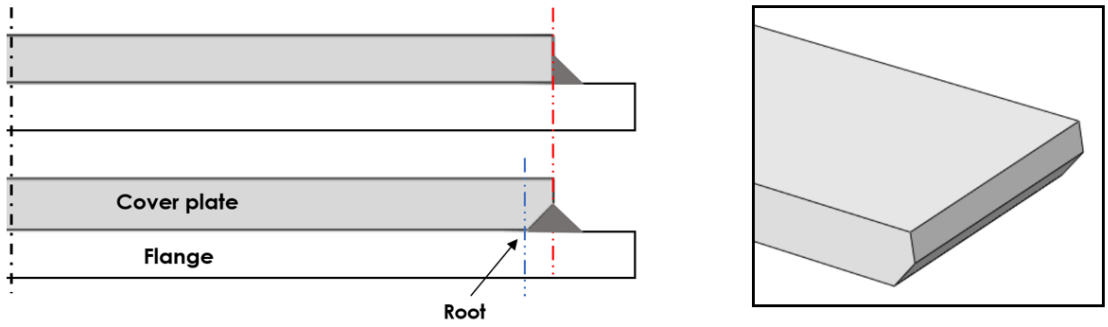

Figure 7.14: Illustration of the modification made to the edge of the cover-plate and the change in root position.

In order to examine the effect of changing weld root position has on fatigue performance of welded cover-plated beams, two additional models were created in Abaqus based on the modified model presented in section 7.1. To perform the analysis, the weld root position was altered for each model but other dimensions were kept constant. This means that the original cover-plate thickness and weld size were retained for each model, and the original dimensions are depicted in Detail A-A of Figure 4.10.

The new position of the weld root in the two models can be seen in Figure 7.15. As seen in the left figure, the cover-plate end has an inclination of 26.6° and the root has been shifted by a distance equals to the cover-plate thickness. While the cover-plate end of the second model in the right figure has an inclination of 45°, and the root has been shifted with a length equal to the weld leg-length.

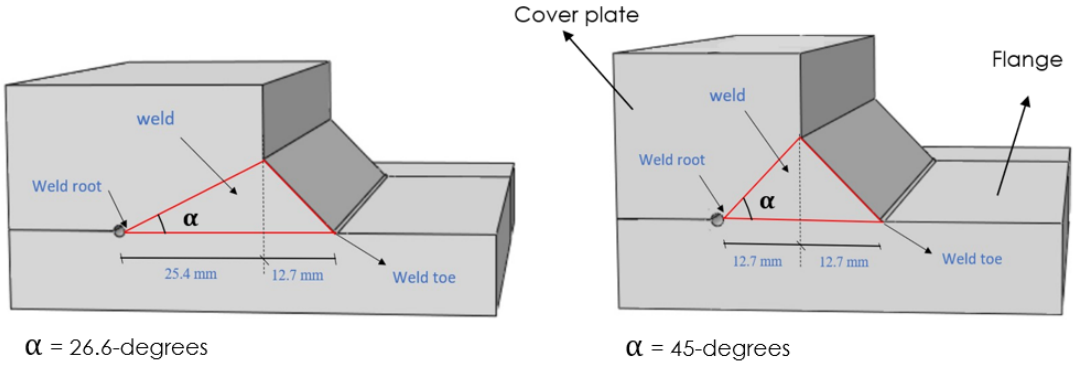

Figure 7.15: The new root positions in the studied Abaqus models.

7.4.1.1 FE results and fatigue study

The results obtained from Abaqus are the maximum principal stresses at both weld toe and root. These results can be seen in Table 7.10. As shown in the table, Changing the root position affects the stresses at both weld toe and root.

Table 7.10: Maximum principal stress results obtained from Abaqus for different root positions, assuming a unit nominal stress of 1 MPa at the weld toe. The difference between the toe and root stresses are also shown. "d" indicates the distance that the root has moved.

α [degrees]	d [mm]	$\Delta\sigma_{ENS_{Toe}}$ [MPa]	$\Delta\sigma_{ENS_{Root}}$ [MPa]	$\frac{\Delta\sigma_{ENS_{Root}}}{\Delta\sigma_{ENS_{Toe}}}$
90	0	6.15	5.9	0.96
45	12.7	5.45	4.35	0.798
26.6	25.4	5.05	3.9	0.77

In order to better visualize how root and toe stresses differ when the weld root position changes, the data acquired from the original root position (90°) was used as a reference. Therefore, the stresses obtained for each root position were divided by the stresses obtained from the original position. The calculated data can be seen in Table 7.11 and is visualized in Figure 7.16.

Table 7.11: The ratio between maximum principal stresses (at weld toe and root) for different root positions and the maximum principal stresses for the original root position. The stresses can be found in table 7.10.

α [degrees]	d [mm]	$\frac{\alpha}{\alpha_{max}}$	$\frac{\Delta\sigma_{ENS_{Toe}}}{\Delta\sigma_{ENS_{Toe,max}}}$	$\frac{\Delta\sigma_{ENS_{Root}}}{\Delta\sigma_{ENS_{Root,max}}}$
90	0	1	1	1
45	12.4	0.5	0.89	0.74
26.6	25.4	0.3	0.82	0.66

It is observed from the table and the figure that the reduction in root stresses due to the change in root position is greater than the reduction in toe stresses. When weld root was shifted by 12.7 mm (45°), weld toe and root stresses decreased by 11 % and 26 %

respectively. Furthermore, when the weld root was shifted by 25.4 mm (26.6°), the weld toe and root stresses decreased by 18 % and 34 % respectively.

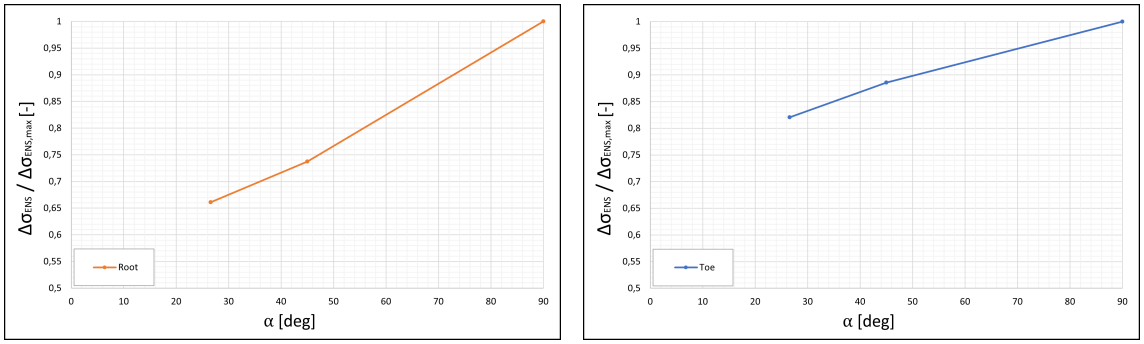

(a) Root **(b)** Toe

Figure 7.16: Graphs show the effect of changing root position has on the effective notch stresses at weld root and toe.

With the results obtained from FE analysis shown in table 7.10, the effective notch stresses at the root and toe under nominal stresses (40, 50, 60, 70 and 80) were derived for each model. With the effective notch stresses, the characteristic load cycles at weld toe and root were calculated for HFMI-treated cover-plates to perform the theoretical evaluation process. Applying the same procedure used in section 5.4.1. The results for the effective notch stresses at the toe and the root, as well as the determined load cycles, are shown in table 7.12. The same calculations were performed for the respective stress ranges Hui et al. used for the practical tests, and the results can be seen in Appendix D.4.

Table 7.12: Calculated characteristic load cycles at weld toe and root for HFMI-treated cover-plates with different root positions within the nominal stress ranges of 40-80 MPa, as well as the ratio between load cycles of the toe and root.

S_r [MPa]	ENS [MPa]		Load cycles [-]		Ratio [-]
	$\Delta\sigma_{Toe}$	$\Delta\sigma_{Root}$	$N_{Toe_{HFMI}}$	N_{Root}	$\frac{N_{Root}}{N_{Toe}}$
($\alpha = 45$ degrees)					
40	218	174	196,563,25	432,443,9	0.22*
50	272	217	446,629,4	221,411,3	0.5*
60	327	261	179,490,4	128,131,5	0.7
70	381	304	830,437	806,892	0.97
80	436	348	425,939	540,555	1.27
($\alpha = 26.6$ degrees)					
40	202	156	390,344,83	600,0725	0.15*
50	252	195	653,842,2	307,237,1	0.47*
60	303	234	262,764,5	177,799,3	0.68
70	353	273	121,572	111,966,9	0.92
80	404	312	623,552	750,091	1.2

* Cover-plates whose cracking mode occurs at the weld root.

7.4.1.2 Stress fields

The maximum principal stress fields of the two different root positions are extracted from Abaqus to be compared to the welded cover-plate of the modified beam ($\alpha = 90°$) in section 7.1. Therefore, as previously stated, the same FE model was used for the root position study by changing the root position for each analysis. As for the studied stress fields of the modified model in section 7.1.2, they were divided into 4 different stress ranges. But because the results showed that the same maximum principal stress distribution occurs for stress ranges <0 MPa and >2 MPa, these are not included in the study. Hence, only the stress ranges of 0-1 MPa and 1-2 MPa are studied. These stress ranges can be seen in the sub-figures of Figure 7.17 for the different root positions and in Appendix D.4.2.

What can be observed in Figure 7.17 is that when the root position changes, the maximum principal stresses distributed throughout the weld decrease. As can be seen in sub-figures, stresses within the stress range of 0-1 MPa are distributed throughout the weld in Figure (c) and (d), which does not occur for the 90° weld in Figure (a). This indicates that the distribution of maximum principal stresses within the range of 1-2 MPa is reduced throughout the weld. This confirms the results obtained from the FE analysis presented previously, that both root stresses and toe stresses decrease for smaller angles α.

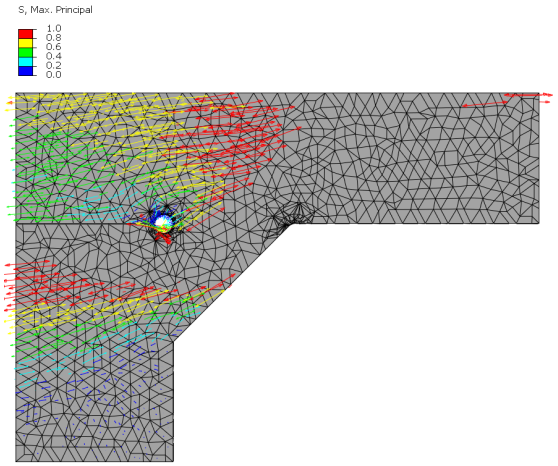

(a) Angle 90°, stress range 0 - 1 MPa

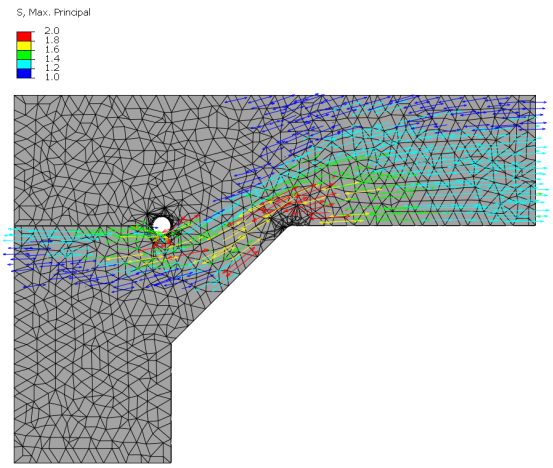

(b) Angle 90°, stress range 1 - 2 MPa

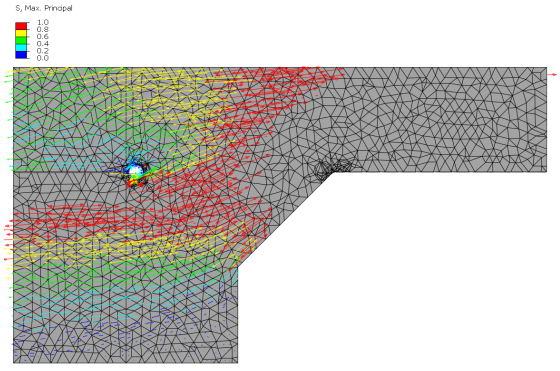

(c) Angle 45°, stress range 0 - 1 MPa

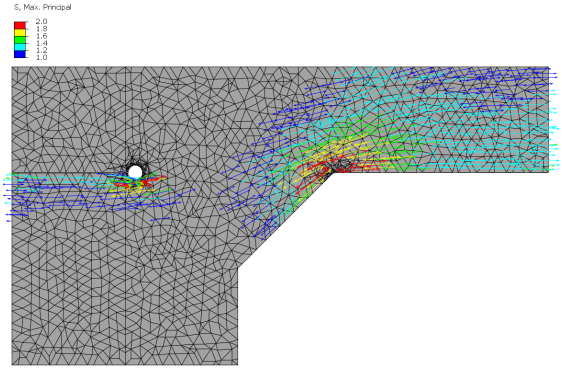

(d) Angle 45°, stress range 1 - 2 MPa

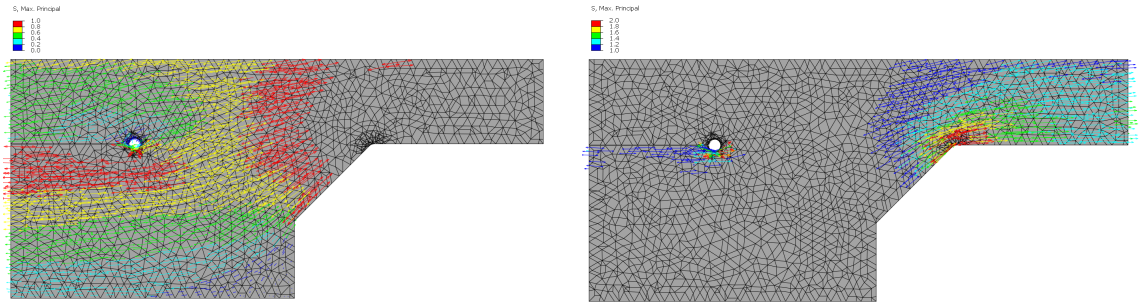

(e) Angle 26.6°, stress range 0 - 1 MPa **(f)** Angle 26.6°, stress range 1 - 2 MPa

Figure 7.17: Maximum principal stress fields distribution in stress range of 0 - 1 MPa and 1 - 2 MPa for the modified beam with the three different root positions ($\alpha = 90°$, $\alpha = 45°$ and $\alpha = 26.6°$), under a unit nominal stress of 1 MPa at weld toe.

7.4.2 Weld size effect

In order to examine the effect that changing weld size has on fatigue performance of welded cover-plated beams, one additional model was created in Abaqus based on the modified model presented in section 7.1. In this model, the weld size was altered while all other dimensions were kept constant. The original dimensions are depicted in Detail A-A of Figure 4.10 and the modified weld size can be seen in Figure 7.18. As seen in the figure, the weld size was increased so that the weld leg-length is equal to the cover-plate thickness. Utilizing this model, the maximum amount of benefit that can be obtained as a result of increasing the weld size will be estimated.

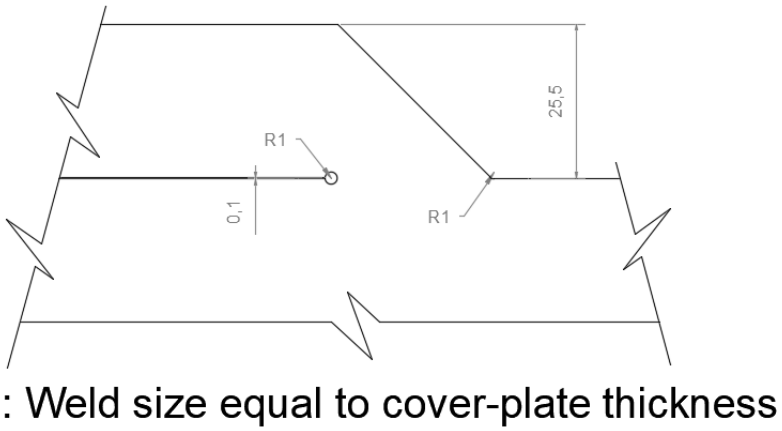

Figure 7.18: Illustration of weld details for the modified Abaqus model with larger weld, (all units are in mm).

This study was not originally planned as part of the exploratory study, but was decided at the end of the project as an additional study. The main reason for conducting this analysis was to obtain data to compare with the stresses obtained in the previous study (root position effect). This is to get a deeper understanding and estimate the effectiveness and efficiency the proposed solution presented in section 7.4.1 has on increasing root strength. But also through this study, the findings obtained by Roy and Fisher (2006) presented in section 3.3 can be verified. That a large weld increases the fatigue strength of as-welded and HFMI-treated cover-plated details.

7.4.2.1 FE results

The results obtained from Abaqus are the maximum principal stresses at both weld toe and root. These results can be seen in Table 7.13. For comparison, the results from the modified model (with weld leg-length of 12.7 mm) presented in section 7.1 are also shown in the table.

It is evident from the table that the model with larger weld size has lower stresses in both the weld toe and root. Whereas increasing the weld leg-length from 12.7 mm to 25.4 mm decreased the stresses by 9.7 % and 27 % in weld toe and root respectively.

Table 7.13: Maximum principal stress results obtained from Abaqus for both the modified model (weld leg-length equals to 12.7 mm) and the model having a weld leg-length equal to (25.4 mm) assuming 1 MPa nominal stress at the weld toe.

Weld leg-length [mm]	$\Delta\sigma_{ENS_{Toe}}$ [MPa]	$\Delta\sigma_{ENS_{Root}}$ [MPa]
12.7	6.15	5.90
25.4	5.55	4.3
Decrease	9.7 %	27 %

7.4.2.2 Stress field

The maximum principal stress fields of the modified beam with a weld leg-length equal to the cover-plate thickness (leg-length $= t_c = 25.4$) were extracted from Abaqus and can be seen in Figure 7.19 and Appendix D.5. The sub-figures in the figure illustrate the maximum principal stress distribution for 4 different stress ranges. Due to the modified beam from section 7.1 was used for the FE model, it is expected that the extracted stress fields are distributed in a similar manner to the modified beam's stress fields. This is verified when comparing the sub-figures of Figures 7.19 and 7.3. Therefore, the general description of the modified beam's stress fields can be assumed to be the same when the weld size is altered. A difference that is observed is that the minimum compressive stress in Figure(a) decreases with a larger weld. This correlates with the results previously discussed.

Leaving aside the general behaviour of the stress field distribution, there are some observations that differ from the modified beam described in section 7.1.2. For the stress field within the stress range of 0–1 MPa in Figure(b), stresses are distributed throughout the weld, which does not occur for the original modified beam. This indicates that the distribution of maximum principal stresses within the range of 1–2 MPa is reduced in the weld as indicated in Figure(c). This verifies the result obtained from the FE analysis presented previously, that root stresses are mainly reduced when the weld size is increased.

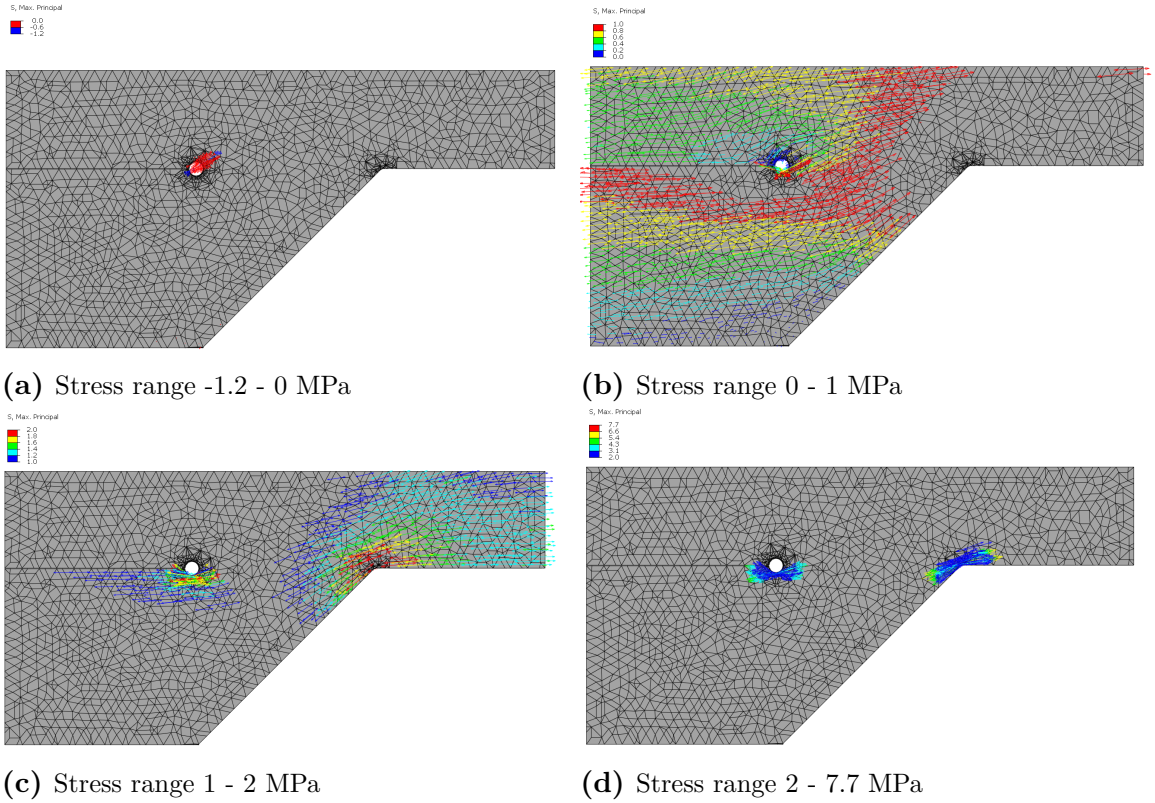

(a) Stress range -1.2 - 0 MPa

(b) Stress range 0 - 1 MPa

(c) Stress range 1 - 2 MPa

(d) Stress range 2 - 7.7 MPa

Figure 7.19: Maximum principal stress fields distribution in 4 different stress ranges for the modified beam with a weld leg-length equal to the cover-plate thickness (25.4 mm), under a unit nominal stress of 1 MPa at weld toe.

8

Discussion of exploratory studies

This chapter is going to discuss the results obtained from the exploratory study in a detailed manner. The different parts of the study will be discussed in separate sections. Additionally, some proposals to modify the existing design methods are discussed for further studies.

8.1 Effect of cover-plate position

The first exploratory study, as stated in section 7.1, was performed to analyse the effect on notch stresses when a cover-plate is attached to the middle of a beam subjected to bending, instead of at a beams edges. The results from the FE analysis determined that both the weld toe and roots maximum principal stresses increased for the modified beam, as shown in Table 7.1. When compared to Hui et al. FE analysis results.

When aligning the weld toes of the two models, the unit nominal stress of 1 MPa resulted in the same load being applied to the modified beam. Therefore, theoretically the same toe stresses should be observed in both cover-plated beams. But this is only true for the Nominal Stress method, since stress concentrations caused by change in cross-section are not accounted for, instead an overall stress estimation is calculated. Hence, when modeling according to the ENS method, the maximum principal stresses obtained from the analysis are more realistic. From the results written in section 7.1 it is evident that in reality the stresses between the two cover-plated beams are different. Which is caused by the change in cover-plate position.

Why the maximum principal stresses increased for the modified beam can be described by the stress field of the two comparable cover-plate specimens. The stress fields within the stress range of 0-1 MPa and 1-2 MPa from Hui et al. beam model in Figure 5.16 and the modified model in Figure 7.3 are assembled into Figure 8.1 to visualize the maximum principal stress differences between the two cover-plate specimens. The other stress ranges ($<$0 MPa and $>$2 MPa) were not included because, as seen in Figure 5.16 and 7.3, they have the same distribution and direction.

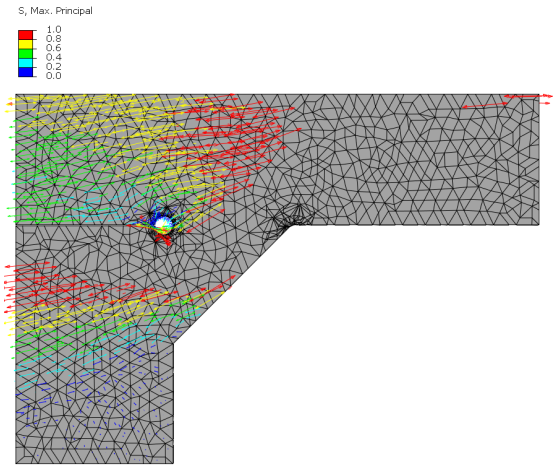

(a) Modified specimen, stress range 0 - 1 MPa

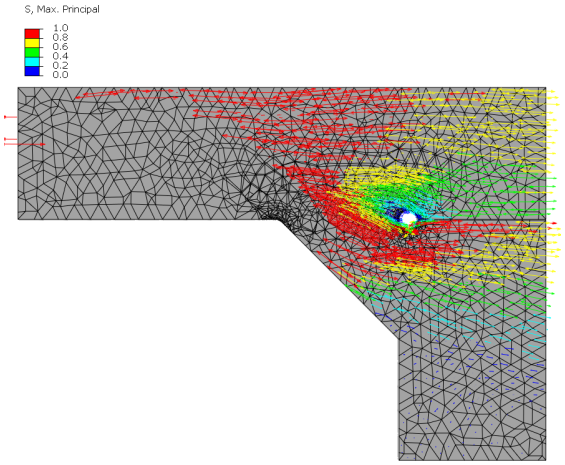

(b) Hui et al. specimen, stress range 0 - 1 MPa

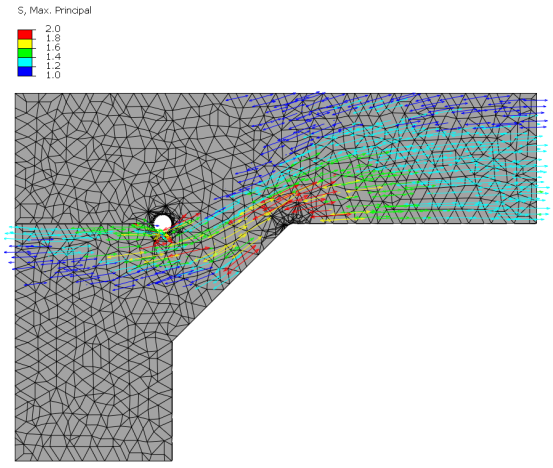

(c) Modified specimen, stress range 1 - 2 MPa

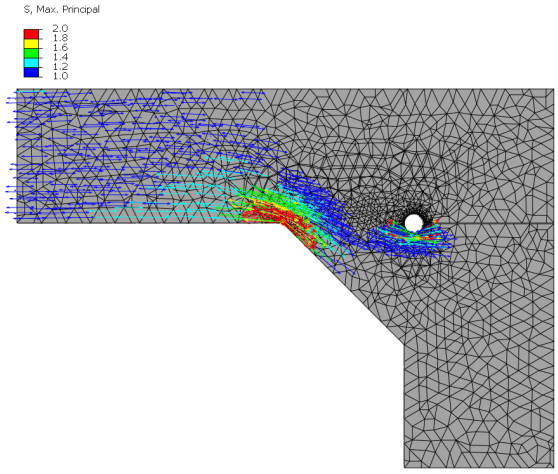

(d) Hui et al. specimen, stress range 1 - 2 MPa

Figure 8.1: Maximum principal stress field of stress ranges 0 - 1 MPa and 1 - 2 MPa, from Figure 7.3 for modified specimen and from Figure 5.16 for Hui et al. specimen, under a unit nominal stress of 1 MPa.

Figure 8.1 shows that the two cover-plate specimens have a similar stress distribution between the two stress ranges. However, as observed in Figures (c) and (d), it appears that there is a larger distribution of stresses of 1-2 MPa through the weld of the modified specimen. In addition, the stresses are also distributed further along the cover-plate's top, which does not occur with Hui et al. specimen. Because of this, higher stresses are distributed throughout the cover-plate when it is placed in the middle of a beam, compared to at a beam's edges. This instance of higher stresses at the top of the cover-plate in Figure (c), can be determined to be caused by the tensile stresses created at the beam's bottom flange due to that the maximum bending moments occurs at the middle of the beam.

This is further observed in Figures (c) and (d), since the stress distribution of the stresses within the range of 1-2 MPa for the modified specimen is transferred from the cover-plate to the beam's flange after the weld. While for Hui et al. specimen, seen in Figure (d), the distribution of stresses within the stress range of 1-2 MPa are first located in the middle of the beam's bottom flange and then divided between the cover-plate and beam's

flange after the weld. Therefore, because the stresses are divided, the maximum principal stresses concentrated at the weld toe and root are lower for Hui et al. specimen than for the modified specimen.

8.2 Cover-plate thickness effect

For the effect of cover-plate thickness, it was observed that the effective notch stresses at both the root and toe became higher with increasing cover-plate thickness. Thus, thicker cover-plates have lower fatigue strength, whereas, very thin cover-plates exhibit higher fatigue strength. This was expected because as discussed in section 2.1.1, Eurocode 3 (2008) specifies different fatigue categories depending on cover-plate thickness and its relationship to flange thickness, as shown in Figure 2.7. IIW also has the same consideration, that a reduction in fatigue strength is required when designing cover-plates with a thickness greater than 25 mm. The reduction factor can be calculated with Equation 2.4. Moreover, for very thin cover-plates like the specimens studied by Leitner and Stoschka read in section 3.1, the fatigue strength can be increased by using the same Equation.

Furthermore, the results obtained from the FE analysis show that root stresses have a larger increase than toe stresses when the thickness of the cover-plate is increased to more than 20 mm, see Figure 8.2. This can be explained by the relation between cover-plate thickness and weld size. This indicates that root stresses are lower when the weld leg-length is close to the cover-plate thickness. Which is confirmed by the tests performed by Roy and Fisher (2006), where they concluded that both as-welded and HFMI-treated cover-plates have higher fatigue performance when the weld has the same size as the plate thickness. However, because the weld size was constant during the study, the proportion between weld size and cover-plate thickness did not follow design recommendations. Which means that the stress results for the thicker cover-plates will be lower in reality than those reported in this study, since a larger weld size will be used.

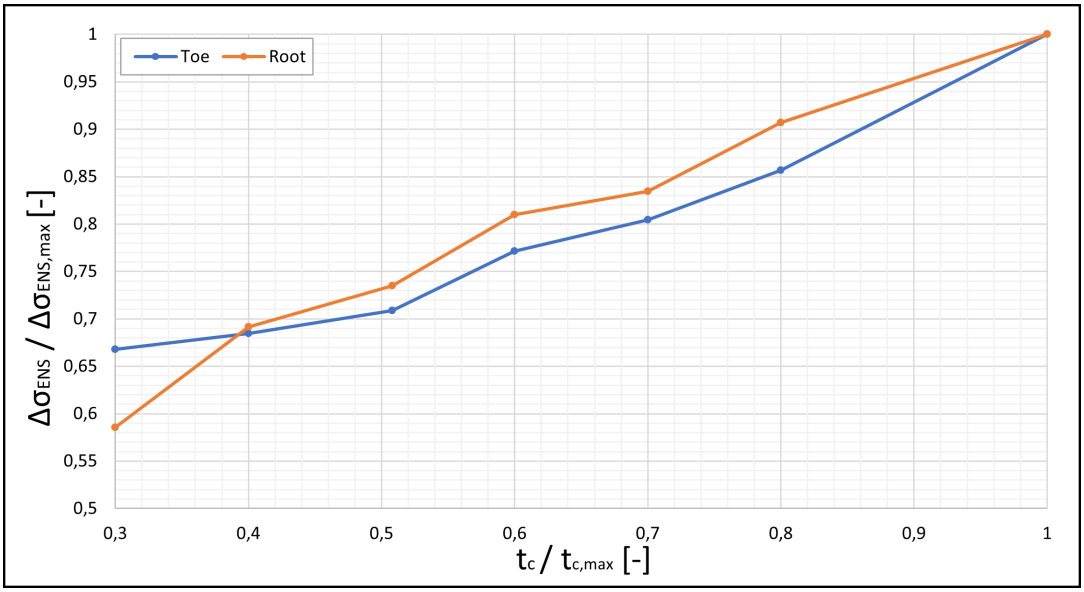

Figure 8.2: Graph shows the effect of cover-plate thickness has on the effective notch stresses at both the weld root and toe.

The low fatigue strength of thicker cover-plates is attributed to the fact that increasing the thickness will increase the cover-plate's stiffness. Thus, strengthening its resistance to bending and deformation, as well as its capability to withstand external forces. Which in turn will lead to higher stresses in the weld resulting in lower fatigue strength.

8.3 Cover-plate length effect

For the effect of cover-plate length, it was observed that the effective notch stresses at both the weld root and weld toe increase for longer cover-plates. Additionally, after a specific cover-plate length, root stresses become larger than toe stresses. Thus, indicating that fatigue strength decreases with a higher cover-plate to beam length ratio (L_C/L_B). This could explain the findings obtained by Fisher et al. (1979) described in section 2.1.1. Where Fisher et al. recommended a lower detail category for large welded cover-plated structures.

However, in Eurocode 3 only the thickness effect is regarded when designing cover-plated details with the Nominal Stress method. But according to the FE analysis results obtained in this study, it has been demonstrated that very long cover-plates have a more significant effect on notch stresses than plate thickness. For example, the effective notch stresses at weld toe and root for the longest tested cover-plate (which have a plate thickness of $t_c = 25.4mm$) are 8.534 MPa and 10.337 MPa when the load is positioned at a third of the beam. While the stresses for the thickest tested cover-plate ($t_c = 50mm$) are 8.685 MPa and 8.028 MPa, which can be seen in Tables 7.6 and 7.3.

Why design guidelines do not include length effect could be explained by that the initial tests were conducted on small specimens or on specimens loaded axially, where the cover-plate length does not affect fatigue performance. Although it seems that the length of cover-plates affects the fatigue performance of large structures', there is a lack of research on full-size beams. The reason for this might be because welded cover-plates are no longer used for large structures. However, to use HFMI treatment on larger cover-plated structures loaded in bending, the length effect could be a requirement to consider when designing. Because it is determined by the test results of previous studies discussed in chapter 6, that HFMI-treated cover-plated beams subjected to bending will highly crack and fail at weld root. Thereby, there may be a possible risk of sudden root failure for extensive long cover-plates since root stresses become higher than toe stresses.

With the exploratory studies, it is observed that longer cover-plates have lower fatigue performance. This behavior can be explained by the deflection δ cased by bending, seen in Figure 8.3. The cover-plate is a separate structural component that wants to remain in its original state (straight). Therefore, when the beam bends due to the applied load, the stiffness of the cover-plate will impose vertical stresses upon the weld. Creating additional tensile stresses that increase weld toe and root stresses. This is verified with the maximum principal stress field shown in Figures 7.12 and 7.13. Where it is observed that for the longest cover-plates, stresses above >2 MPa are accumulated throughout the weld and not only at weld toe and root. Even though, the stiffness of longer cover-plates is lower than for shorter cover-plates. The FE analysis results show that for equally thick cover-plates, a greater increase in weld toe and root stresses occurs for longer cover-plates than for shorter. Hence, indicating that beam's deflection has more impact on notch stresses.

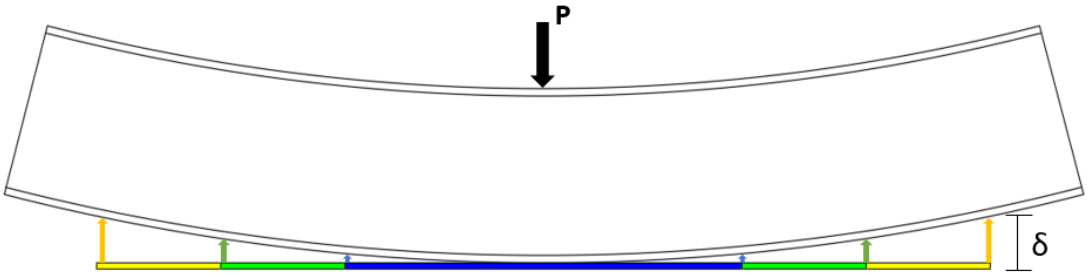

Figure 8.3: Illustration of the tensile stresses inflicted on the cover-plate for different lengths, caused by the beam's deflection.

More research is needed to determine the effect of the cover-plate length, and if it is a factor to be considered. Then the acceptable cover-plate lengths and cover-plate to beam ratios L_C/L_B need to be determined. For the modelled beams in this study. The ratio where root stresses become higher than the toe stresses is estimated to be $L_C/L_B = 0.6$ for the modeled beam with the load positioned at the third of the beam, and $L_C/L_B = 0.2$ for the modeled beam with the load positioned at the middle of the beam. The ratios (L_C/L_B) differ between the two models because of the different loading conditions.

However, it is observed that if the section with a constant moment is not to be considered. The cover-plate with a length of 1,778 mm (the modified beam), seen in Figure 7.8, has an extended cover-plate length of 558.8 mm from the loading position. If this is considered as a cover-plate for the model with the loading position at the middle of the beam, the ratio is calculated to be $L_C/L_B = 0.175$. This value is below 0.2, and would therefore explain why weld toe stress is higher than root stress for the modified beam. Consequently, from the FE analysis performed in this master's thesis, the cover-plate length to beam length ratio is determined to be about $L_C/L_B = 0.2$. Where every cover-plate longer than >20% of the beam's length will have transverse weld root stresses larger than the weld toe stresses.

Why the ratio is different for each loading situation can be explained by the difference in bending moment and shear stress distribution throughout the beams. When the load is placed at thirds of the beam, as seen in Figure 8.4(a), the maximum moment is constant over the middle of the beam, and hence there are no shear stresses. While when the load is placed at the middle of the beam, as seen in Figure 8.4(b), the maximum moment is located at the middle of the beam and the whole beam is subject to shear stresses.

From the FE analysis, the results show that there are different stress behaviours for each cover-plate length between the two loading situations. As seen in Table 7.6, the maximum principal stresses at the weld toe and root are in general larger for when the load is placed in the middle of the beam. Despite the fact that this difference might not seem particularly large (calculated to be between 1 - 15% for each notch stress). The most interesting result is that weld root stresses for the shorter cover-plates have about a 15% difference between the two loading situations. This can be related to that the cover-plates are located between the two loads and is therefore subjected to a constant moment and no shear forces, as seen in Figure 8.4(a). Thus, there is no deflection δ to be consider.

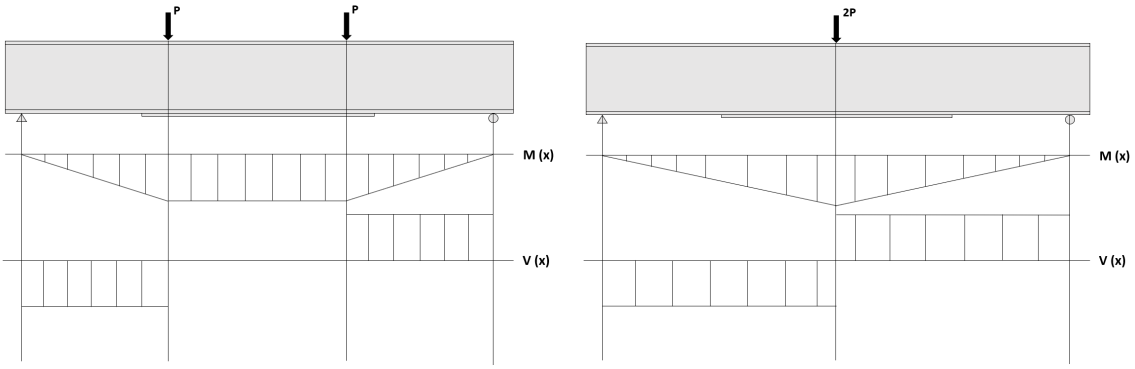

(a) The loads are positioned at a third of the beam **(b)** The load is placed at the middle of the beam

Figure 8.4: Moment and shear distribution for the tow load situations.

8.4 Effect of root position and weld size

Based on the FE analysis results, it was observed that by moving the root position, the stress in weld root was significantly reduced. A reduction of 26% and 34% were obtained when the weld root was moved by 12.7 mm ($\alpha = 45°$) and 25.4 mm ($\alpha = 26.6°$) respectively, see Figure 8.5. This indicates that applying this method to welded details will improve weld root's fatigue performance. Which makes it an effective approach to improve fatigue strength of HFMI-treated details. As mentioned previously, because the fatigue failure mode may change from toe to root in HFMI-treated cover-plates loaded in bending, failure will occur at the root before the treated toe's resistance is fully utilized. So by increasing the root's fatigue strength, the failure mode could shift back to the treated toe.

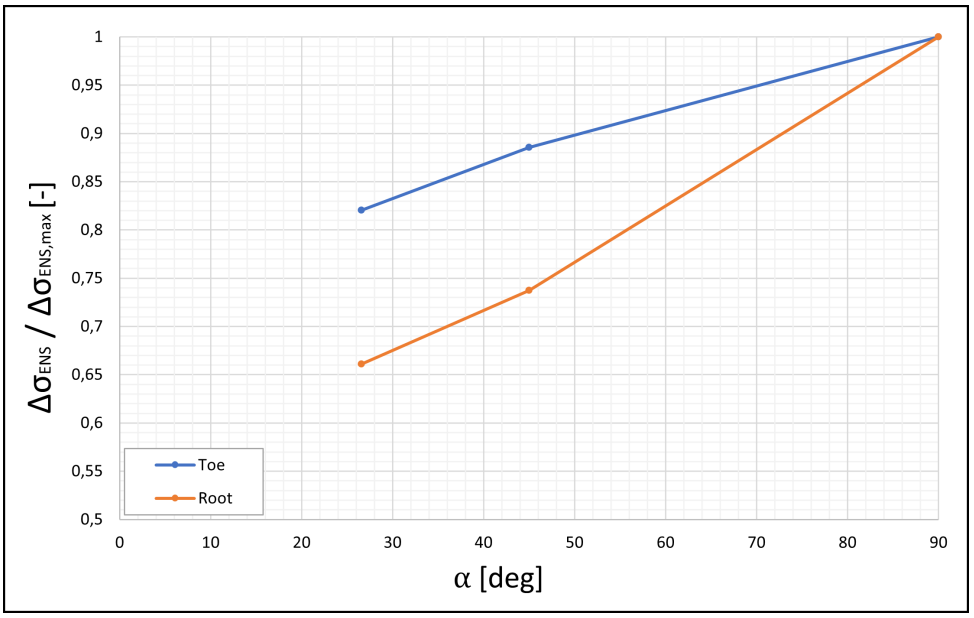

Figure 8.5: Graph show the effect of changing root position has on the effective notch stresses at both weld root and toe.

In addition, the results showed that the stresses at the toe were also decreased. A reduction of 11% and 18% were obtained when the weld root was moved by 12.7 mm ($\alpha = 45°$) and 25.4 mm ($\alpha = 26.6°$) respectively, see Figure 8.5. This is because there is larger surface area between the weld and flange, which allows the stress to be redistributed across the weld. Consequently, the toe will gain more fatigue strength as a result of the reduction of stress at the toe.

As was discussed previously in section 3.3, Roy and Fisher concluded to that a sufficient large weld size increases the fatigue strength of weld root. This was confirmed by the FE analysis in section 7.4.2. Where by increasing the weld size to the cover-plate thickness ($t_c = 25.4$ mm), a reduction in toe and root stresses of 9.7% and 27% respectively were observed. And as can be seen in Figure 8.6, the stresses obtained from this analysis are very close to the resulting stresses for the model with an $\alpha = 45°$ weld angle. Hence, by moving the root position a distance equal to the weld leg length, fatigue performance should improve to the same extent as using a large weld.

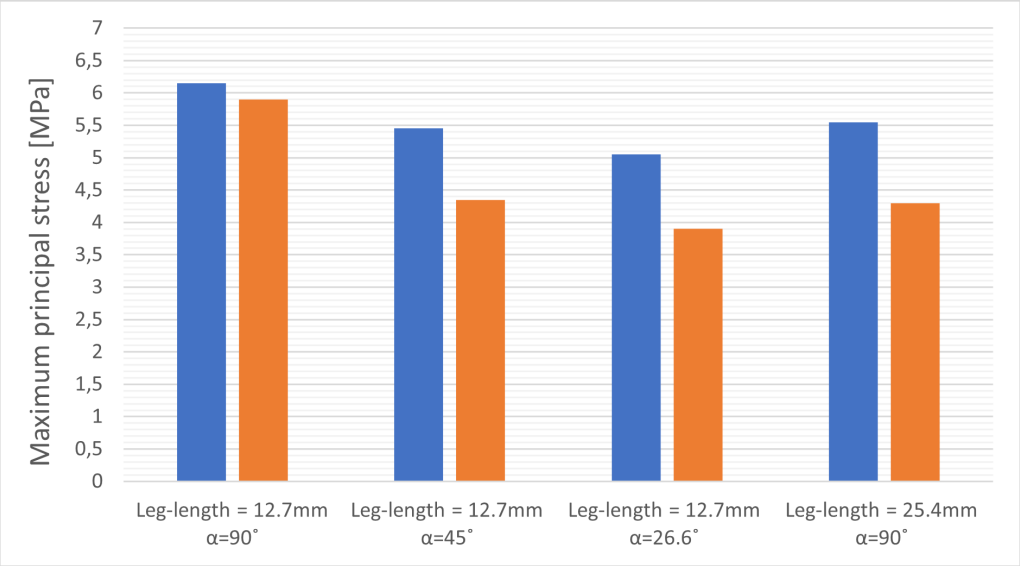

Figure 8.6: Bar graph summarising the maximum principal stress results for the FE analyses: modified beam model (Leg-length = 12.7 mm, $\alpha = 90°$), root position models (Leg-length = 12.7 mm, $\alpha = 45°$ and Leg-length = 12.7 mm, $\alpha = 26.6°$) and large weld model (Leg-length = 25.4 mm, $\alpha = 90°$).

What can be further observed in Figure 8.6 is that the most optimal root improvement method is to move the root position. Since both the weld toe and root stresses have a larger reduction for smaller angles, than for larger welds. However, very large weld size is not desired and not used in design. Moreover, the root position method utilizes less weld metal between the two alternatives, hence also provides a better weld quality for thicker cover-plates. Therefore, the use of moving the root position in HFMI-treated details is highly recommended, since it can enhance the strength of the roots without the need for large welds.

For as-welded cover-plates, cracking will occur at weld toe, so moving the weld root will not yield a significant benefit in fatigue performance. In light of the fact that only a slight increase in toe strength will occur, it may not be of significant value. This is also true for

axially loaded HFMI-treated cover-plates, because they also crack at the toe. Therefore, this solution is most appropriate for treated cover-plates loaded in bending.

8.5 Determination of load cycles using the existing design curves

For the calculation of load cycles for weld roots, the as welded FAT 225 was employed. While HFMI design curve FAT 320 was utilized for HFMI-treated toes. However, when the effective notch stresses at weld toe exceeded the corresponding stress at the interaction point between as-welded and HFMI S-N curves, see Figure 8.7, the as-welded design curve of FAT 225 was used to determine the design load cycles for the HFMI-treated toe. This is because using HFMI curve for the design yields lower load cycles than in as-welded conditions. In this case, the fatigue performance of the detail will be significantly underestimated. Nevertheless, the use of the as-welded S-N curve still leads to conservative results, because it ignores the improvements achieved from the treatment.

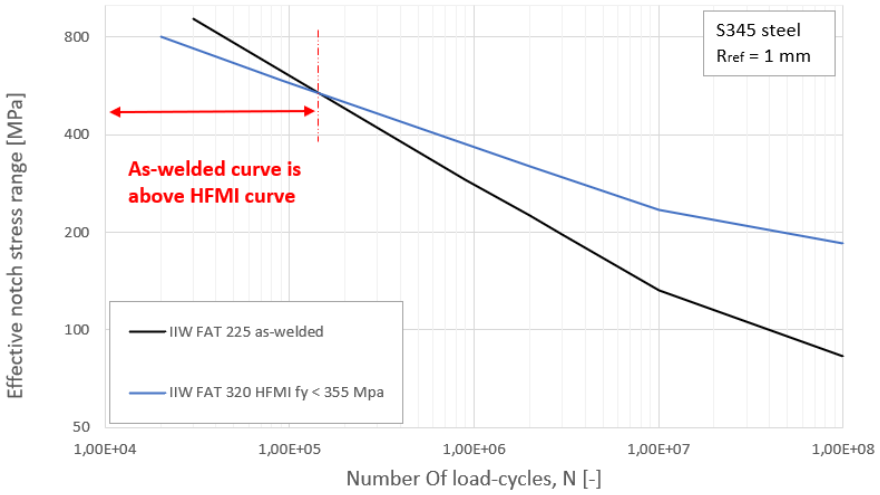

Figure 8.7: The relationship between S-N design curve FAT 225 and HFMI S-N curve FAT 320.

8.6 Proposed modifications to design methods

8.6.1 Effective Notch Stress method

For designing according to ENS method, see section 2.3.2, the characteristic load cycles at the root are calculated using the as-welded fatigue curve FAT 225. Which will give very conservative results, since all specimens that failed at the root in Hui et al. test were lying above the recommended S-N curves for HFMI-treated details FAT 320 and even FAT 360, see Figure 8.8. Accordingly, the HFMI curve FAT 320 can be applied to weld root and still produce a safe design. It should be mentioned that although this curve is for HFMI-treated details with a steel yield strength $f_y < 355$ MPa, it is regarded as being applicable to all types of steel due to the fact that the root strength is not affected by steel quality.

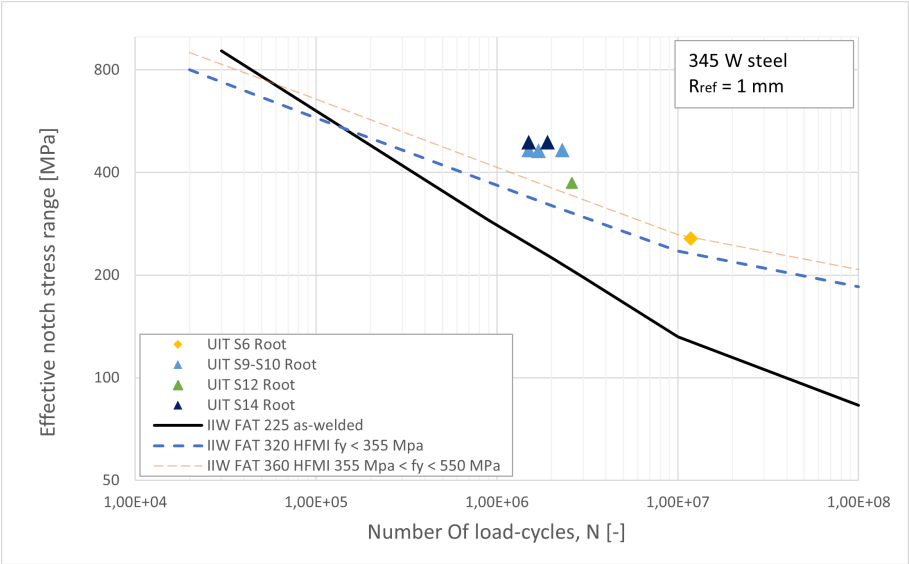

Figure 8.8: S-N graph from FE analysis results for specimens that failed at weld root in Hui et al. test, from Figure 5.14 in section 5.4.1.

Example of how to design fatigue life of HFMI-treated cover-plate loaded in bending:

- To estimate the fatigue life of cover-plated detail of steel with yield strength $f_y < 355$ MPa, the effective notch stresses at both weld toe and root have to be computed. Thereafter, the characteristic load cycles for both root and toe are calculated using the same curve FAT 320. The lowest number of load cycles should be used in the design.
- On the other hand, when estimating the fatigue life of cover-plated detail of steel with yield strength $f_y \geq 355$ MPa, the characteristic load cycles for the weld root are calculated using fatigue curve FAT 320, while the load cycles for the toe are calculated using the corresponding IIW recommended fatigue curve for each steel strength.

8.6.2 Nominal Stress method

The results of the study showed that the existing design method (using the IIW recommended curves) ,presented in section 2.3.1.2, is not applicable for HFMI-treated cover-plated beams loaded in bending, because of the failure mode shifting. So, the curves can be used only for axially loaded cover-plates, where toe failure is expected.

According to the provided data from Roy and Fisher (2006) and Hui et al. (2018) test's results, it was concluded that fatigue strength for treated specimens is of category C (FAT 90). Thus, it can be established that FAT 90(56) HFMI fatigue curve shown in Figure 8.9 is possible to be used for design. Because the steel strength of the tested beams was $f_y < 355$ MPa, this fatigue curve was chosen. The curve is also regarded as being applicable to all types of steel due to the fact that the root strength is not affected by steel quality.

However, the test results of the exploratory study showed that the stress conditions are different for when the cover-plate is located at the edge vs the middle of the beams bottom flange. Hence, due to higher stresses and a smaller margin between toe and root stresses,

it could be predicted that the FAT-class need to be reduced. Following with this assumption, the fatigue strength can be estimated to be around 80 MPa, according to Figure 8.9. However, there is not any provided practical tests to confirm this assumption.

Furthermore, when designing using the nominal stress method the effect of cover-plate thickness is considered, but not the length. However, the exploratory study showed that the cover-plate's length could be a factor to consider during design. On the other side, using root improving techniques (e.g changing root position) could allow a higher fatigue S-N curve to be used.

In conclusion, this curve was chosen based on fatigue strength of the weld root. Thus, it is expected to be applicable for all HFMI-treated cover-plated beams loaded in bending, regardless of the failure mode.

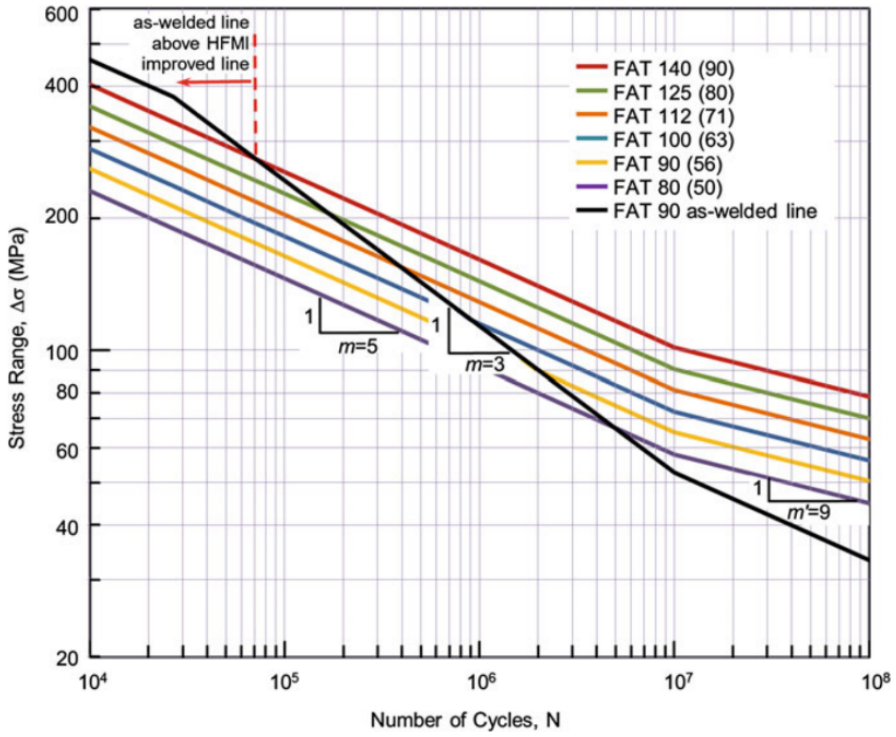

Figure 8.9: characteristic nominal stress S-N curves for HFMI-treated welded joints of steel strength $f_y < 355$ MPa, under stress ratio $R \leq 0.15$. The value within the "()" represents the FAT-class of the corresponding joint in as-welded state. [Source: Marquis and Barsoum (2016. From Figure 2.13(a) in section 2.3.1.2]

9
Conclusion

In light of the extensive study conducted in this project, it has been concluded that HFMI-treatment is an effective approach that significantly increases the fatigue performance of welded cover-plated beams subjected to bending. By comparing the fatigue strength of HFMI-treated cover-plates to their bolted counterparts, it was confirmed that HFMI-treated cover-plates possess the potential to replace bolted cover-plates currently employed in practice. Where the treated cover-plates can not only match bolted connections' fatigue strength, but potentially surpass it, which makes them an appealing and viable alternative for strengthening steel bridges.

From all reviewed previous research it is evident that the weld root is the most likely failure location for HFMI-treated cover-plates subjected to bending. Consequently, it can be assumed that the fatigue strength of these cover-plates is limited by the weld root's fatigue strength. Based on this study, there are two practical recommendations in this regard to maximize the fatigue performance of HFMI-treated cover-plates:

1. Optimal weld size: The weld size has a direct effect on the root's fatigue strength, so it is imperative to select an appropriate weld size.

2. Change of root position: It is highly recommended to implement the technique presented in this study for HFMI-treated details loaded in bending. Which involves moving the root position by inclining the edge of the cover-plate. This approach can effectively enhance the root strength without the need for large welds.

Moreover, it was concluded from the exploratory study that the length of the cover-plate is a factor that exerts a notable impact on stresses at weld toe and root in cover-plated structures loaded in bending. This finding highlights that the length effect can be a requirement for consideration when designing for fatigue life.

Furthermore, looking at the existing fatigue assessment methods, it can be concluded that ENS method is an applicable approach to determine fatigue life. However, without any modifications to S-N curves, the result will be conservative for HFMI-treated cover-plated beams.

For the Nominal Stress method, there are no applicable design S-N curves for HFMI-treted cover-plates loaded in bending. Therefore, a suggestion based on this study can be made that could serve as a starting point for developing a design method. With further studies and analyses, S-N curves for cover-plated structures can be created. Which can be applied in two different ways: Either by creating S-N curves that consider both weld toe and root failure and only toe stress is considered when designing. The other method would be to create separate S-N curves for toe and root failure. And which curve to use is decided by determining what failure mode would occur based on different parameters.

9.1 Further studies

Further studies in this filed can be to perform practical tests and FE analyses on full-scale HFMI-treated cover-plated beams in bending when the cover-plate is in the middle of the beam. As well as finalizing what variables that can influence the detail category. This can include:

- Conducting in-depth analyses to establish if the length of cover-plates has an impact on the detail category of HFMI-treated cover-plated beams.
- Further investigate the possibilities of improving weld roots' fatigue strength. This could include conducting further in-depth analyses to determine the effect the change of root position has on the detail category for HFMI-treated cover-plates.

Lastly, these studies are to establish a working design approach and S-N curves that can be used to design HFMI cover-plated beams in bending with the Nominal Stress method.

Bibliography

6th Framework Programme of EU. (2007). *Sustainable Bridges - Assessment for Future Traffic Demands and Longer Lives* (J. Bién, L. Elfgren, & J. Olofsson, Eds.). Dolnośląskie Wydawnictwo Edukacyjne.

Albrecht, P., Asce, M., & Lenwari, A. (2007). Fatigue-Proofing Cover Plates. *Journal of Bridge Engineering*, *12*(3), 275–283. https://doi.org/10.1061/ASCE1084-0702200712:3275

Al-Emrani, M., & Åkesson, B. (2020). *STEEL STRUCTURES Course Literature-VSM 191*. Chalmers University of Technology.

Al-Emrani, M., & Aygül, M. (2014). *Fatigue design of steel and composite bridges* (tech. rep.). Chalmers university of technology. Göteborg, Sweden.

Bowman, M. D., Fu, G., Zhou, Y. E., Connor, R. J., & Godbole, A. A. (2012). *Fatigue Evaluation of Steel Bridges*. Transportation Research Board. https://doi.org/10.17226/22774

Department of Transportation. (2017). *Structure Inspection Manual Part 2-Bridges Chapter 1-General* (tech. rep.). Department of Transportation. Wisconsin, USA.

European Standard. (2022). Eurocode 3 - Design of steel structures - Part 1.9:Fatigue.

European standard. (2008). Eurocod 3: Design of steel structures - Part 1-9: Fatigue. www.sis.se

Fisher, J. W. (1977). *Bridge fatigue guide design and details* (tech. rep.). American Institute Of Steel Construction. Chicago, IL, USA.

Fisher, J. W. (1997). Evolution of Fatigue-Resistant Steel Bridges. *Transportation Research Record*, *1594*(1), 5–17. https://doi.org/10.3141/1594-01

Fisher, J. W., Albrecht, P. A., Yen, B. T., Klingerman, D. J., & McNamee, B. M. (1974). *Fatigue strength of steel beams with welded stiffeners and attachments* (tech. rep.). Transportation Research Board, National Academy of Sciences. Washington, D.C, Transportation Research Board, National Research Council.

Fisher, J. W., Basler, K., Muller, J. A., Ozell, A. M., & Zuurbier, G. W. (1967). Commentary On Welded Cover-plated Beams. *Journal of the Structural Division*, *93*(4), 95–122.

Fisher, J. W., Frank, K. H., Hirt, M. A., & Mcnamee, B. M. (1969). *Effect of weldments on the fatigue strength of steel beams, Final Report, September 1969 (70-25) Recommended Citation* (tech. rep.). Fritz Laboratory Reports, Paper 323. Bethlehem, PN, USA. http://preserve.lehigh.edu/engr-civil-environmental-fritz-lab-reports/323

Fisher, J. W., Hausammann, H., & Pense, A. W. (1979). *Retrofitting procedures for fatigue damage full scale welded bridge beams, Final Report* (tech. rep.). Lehigh Preserve Institutional Repository. Bethlehem, PA, USA. https://preserve.lib.lehigh.edu/

Fricke, W. (2011). *Fracture and Fatigue of Welded Joints and Structures* (K. A. Macdonald, Ed.). Woodhead Publishing Limited.

Fricke, W. (2010). *Guideline for the Fatigue Assessment by Notch Stress Analysis for Welded Structures* (tech. rep.). International Institute of Welding. Hamburg, Germany.

Fricke, W. (2013). IIW guideline for the assessment of weld root fatigue. *Welding in the World*, *57*(6), 753–791. https://doi.org/10.1007/s40194-013-0066-y

Fuštar, B., Lukačević, I., & Dujmović, D. (2020). High-Frequency mechanical impact treatment of welded joints. *Gradjevinar*, *72*(5), 421–436. https://doi.org/10.14256/JCE.2822.2019

Gurney, T. R. (1979). *Fatigue of Welded Structures* (2nd Edition). Cambridge University Press.

Haghani, R., Al-Emrani, M., & Heshmati, M. (2012). Fatigue-prone details in steel bridges. *Buildings*, *2*(4), 456–476. https://doi.org/10.3390/buildings2040456

Heshmati, M., Al-Emrani, M., & Edlund, B. (2012). *Fatigue Assessment of Weld Terminations in Welded Cover-Plate Details; a Comparison of Local Approaches* (tech. rep.). Nordic Steel Construction Conference. Oslo, Norway.

Hobbacher, A. F. (n.d.). *THE NEW IIW RECOMMENDATIONS FOR FATIGUE ASSESSMENT OF WELDED JOINTS AND COMPONENTS-A COMPREHENSIVE CODE RECENTLY UPDATED* (tech. rep.). Jade University of Applied Sciences. Wilhelmshaven, Germany.

Hobbacher, A. F. (2016). *IIW Collection Recommendations for Fatigue Design of Welded Joints and Components* (C. Mayer, Ed.; Second). Springer Nature Switzerland AG. https://doi.org/10.1007/978-3-319-23757-2

Hu, J. (2011). A study on cover plate design and monopole strengthening application. *Thin-Walled Structures*, *49*(9), 1098–1107. https://doi.org/10.1016/j.tws.2011.04.002

Hui, J. F., Lloyd, J. B., & Connor, R. J. (2018). *Fatigue life improvement of welded girders with ultrasonic impact treatment* (tech. rep.). Purdue Univercity. West Lafayette, IN, USA.

Kaffenberger, M., Malikoutsakis, M., Savaidis, G., & Vormwald, M. (2012). Fatigue resistance of weld ends. *Computational Materials Science*, *52*(1), 287–292. https://doi.org/10.1016/j.commatsci.2011.01.022

Kühn, B., Lukić, M., Nussbaumer, A., Günther, H.-P., Helmerich, R., Herion, S., Kolstein, M. H., Walbridge, S., Androic, B., Dijkstra, O., Bucak, Ö., Sedlacek, G., Bijlaard, F., Géradin, M., Pinto, A., & Dimova, S. (2008). *Assessment of Existing Steel Structures: Recommendations for Estimation of Remaining Fatigue LifeFirst Edition, February 2008EUR 23252 EN - 2008* (tech. rep.). European Commission, Joint Research Centre. Luxembourg.

Leitner, M., & Stoschka, M. (2020). Effect of load stress ratio on nominal and effective notch fatigue strength assessment of HFMI-treated high-strength

steel cover plates. *International Journal of Fatigue*, *139*. https://doi.org/10.1016/j.ijfatigue.2020.105784

Marquis, G. B., & Barsoum, Z. (2016). *IIW Collection IIW Recommendations for the HFMI Treatment For Improving the Fatigue Strength of Welded Joints* (IIW International Institute of Welding, Ed.). Springer Nature. https://doi.org/10.1007/978-981-10-2504-4

Marquis, G. B., Mikkola, E., Yildirim, H. C., & Barsoum, Z. (2013). Fatigue strength improvement of steel structures by high-frequency mechanical impact: Proposed fatigue assessment guidelines. *Welding in the World*, *57*(6), 803–822. https://doi.org/10.1007/s40194-013-0075-x

Mohammadzadeh, M., & Bhowmick, A. (2022). Behavior of steel I-beams reinforced while under load. *Engineering Structures*, *257*. https://doi.org/10.1016/j.engstruct.2022.114080

Radaj, D., Sonsino, C. M., & Fricke, W. (2006). *Fatigue Assessment of Welded-Joints by Local Approaches* (Second edition). Woodhead Publishing Limited.

Roy, S., & Fisher, J. W. (2006). Modified AASHTO design S-N curves for post-weld treated welded details. *Bridge Structures*, *2*(4), 207–222. https://doi.org/10.1080/15732480601103630

Roy, S., Fisher, J. W., & Yen, B. T. (2003). Fatigue resistance of welded details enhanced by ultrasonic impact treatment (UIT). *International Journal of Fatigue*, *25*(9-11), 1239–1247. https://doi.org/10.1016/S0142-1123(03)00151-8

Roy, S., & Fisher, J. W. (2005). Enhancing Fatigue Strength by Ultrasonic Impact Treatment. *Steel Structures*, 241–251.

Shams-Hakimi, P. (2017). *Performance of high-frequency mechanical impact treatment for bridge application* (Doctoral dissertation). Chalmers university of technology. Göteborg, Sweden, Chalmers University of Technology.

Takamori, H. (1999). *Improving fatigue strength of welded joints* (Doctoral dissertation). Lehigh University. Bethlehem, PN, USA.

Vilhauer, B., Bennett, C. R., Matamoros, A. B., & Rolfe, S. T. (2012). Fatigue behavior of welded coverplates treated with Ultrasonic Impact Treatment and bolting. *Engineering Structures*, *34*, 163–172. https://doi.org/10.1016/j.engstruct.2011.09.009

Wang, Y. Q., Zong, L., Zhu, R. X., Liu, X. Y., & Shi, Y. J. (2015). Behavior of I-section steel beam welding reinforced while under load. *Journal of Constructional Steel Research*, *106*, 278–288. https://doi.org/10.1016/j.jcsr.2014.12.020

A

Appendix A: Leitner and Stoschka, 2020

A.1 Stress fields

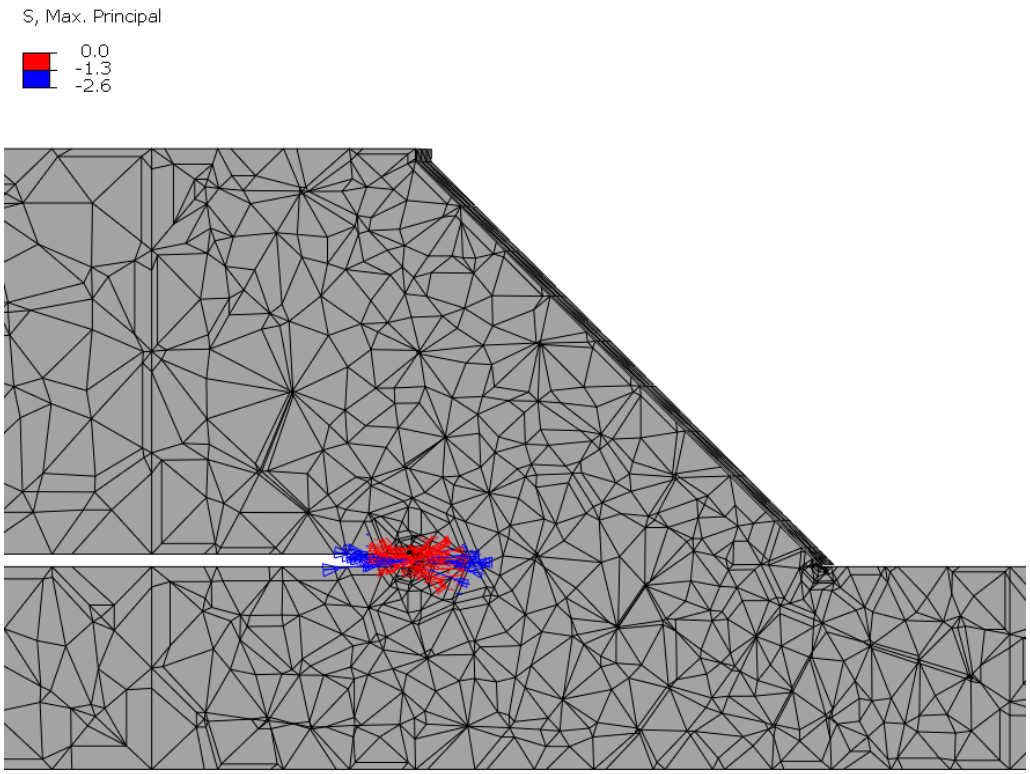

Figure A.1: Maximum principal stress field distribution in stress range -2.6 - 0 MPa for Leitner and Stoschka test model loaded axially, under a unit nominal stress of 1 MPa.

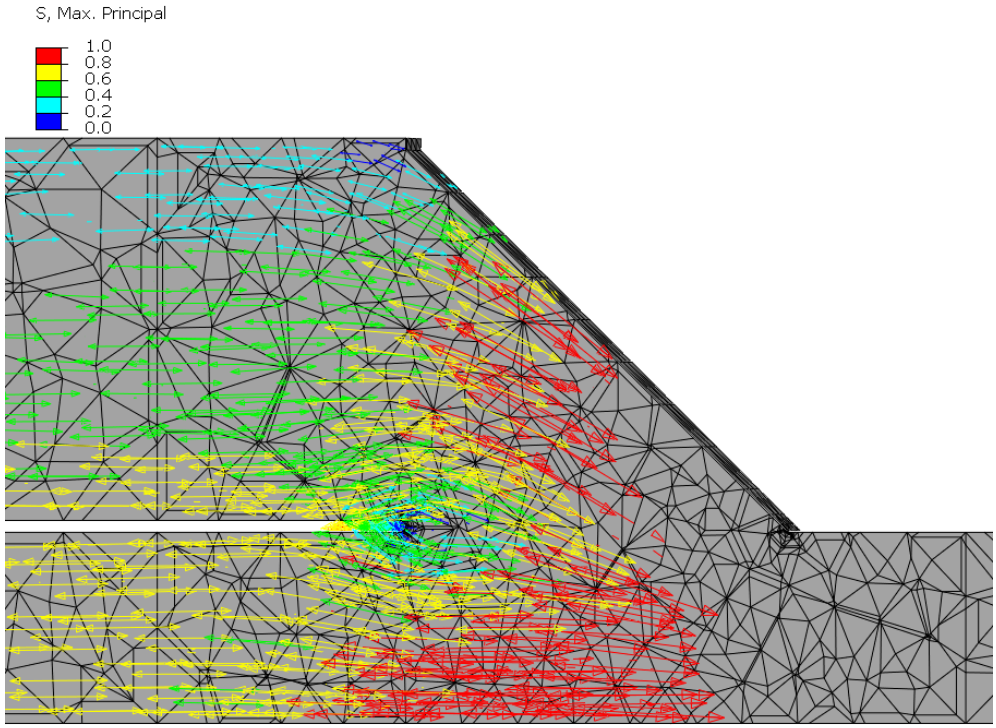

Figure A.2: Maximum principal stress field distribution in stress range 0 - 1 MPa for Leitner and Stoschka test model loaded axially, under a unit nominal stress of 1 MPa.

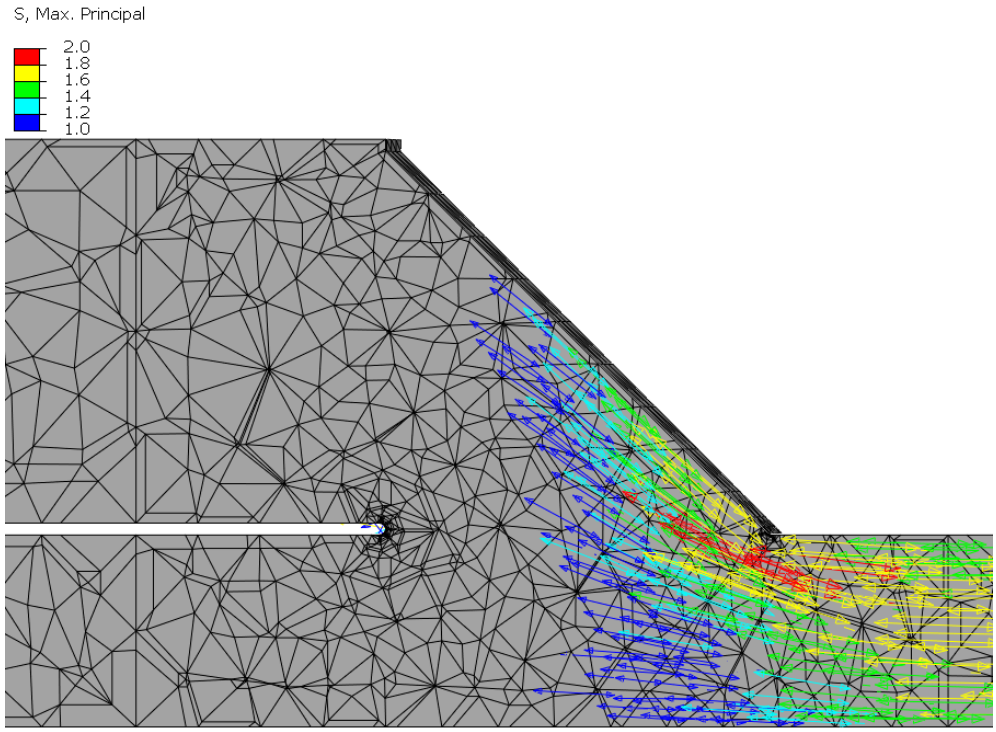

Figure A.3: Maximum principal stress field distribution in stress range 1 - 2 MPa for Leitner and Stoschka test model loaded axially, under a unit nominal stress of 1 MPa.

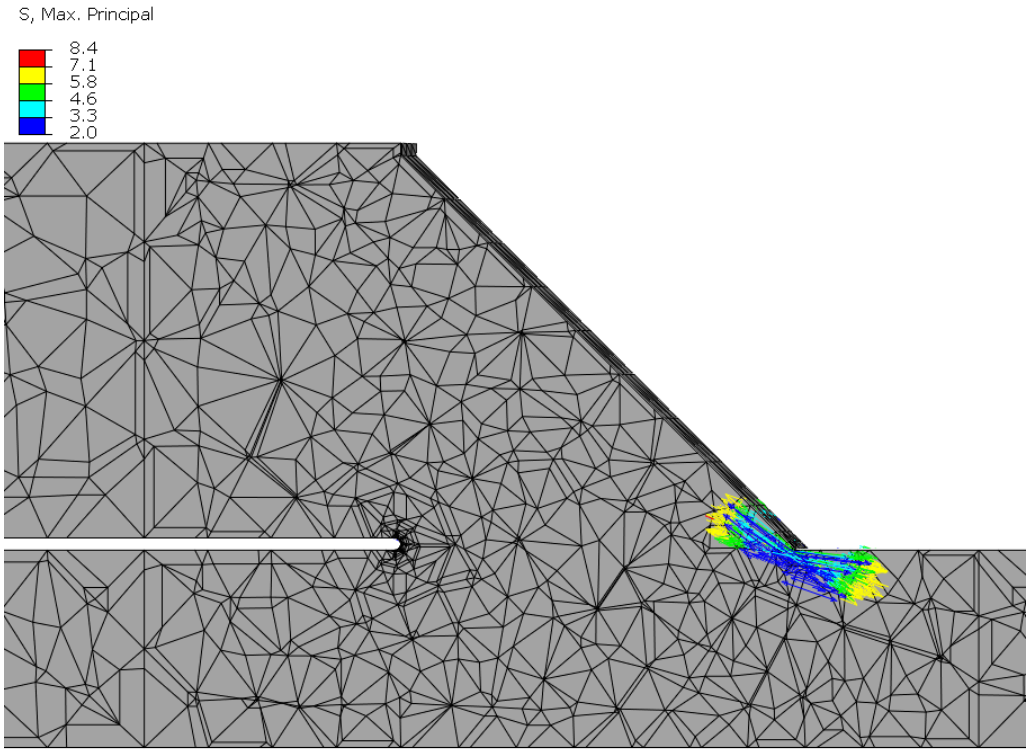

Figure A.4: Maximum principal stress field distribution in stress range -2 - 8.4 MPa for Leitner and Stoschka test model loaded axially, under a unit nominal stress of 1 MPa.

A.2 Stress through weld

The stresses through the weld is assembled by the nodal values interacting with the "paths" added in Abaqus. The paths for Leitner and Stoschka test model can be seen in Figure A.5 and the numerical stress curves for each path in Figure A.6.

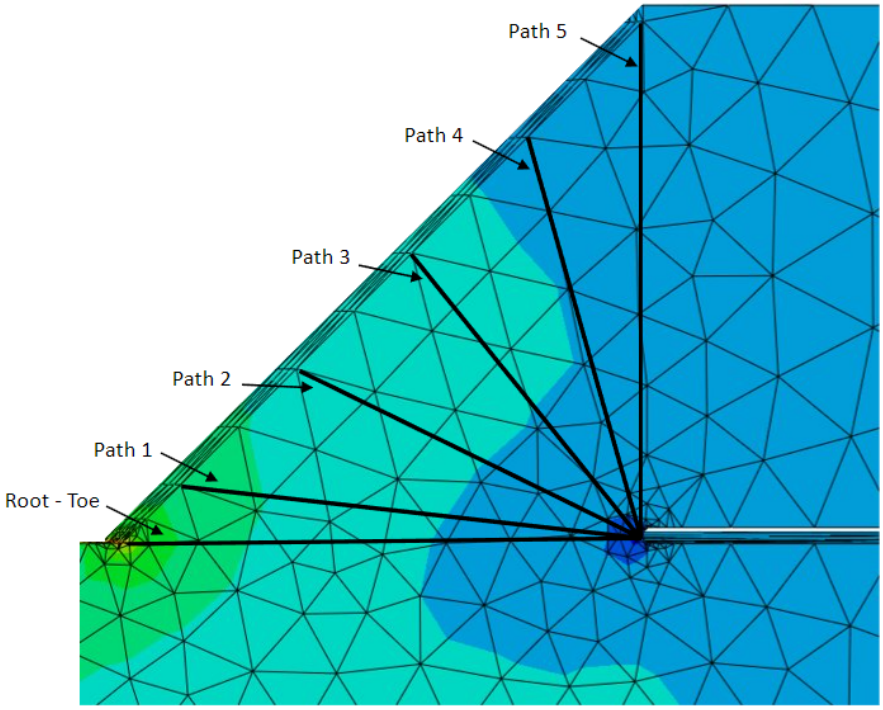

Figure A.5: The "paths" applied to Leitner and Stoschka test model in Abaqus to obtain the nodal stresses through the weld

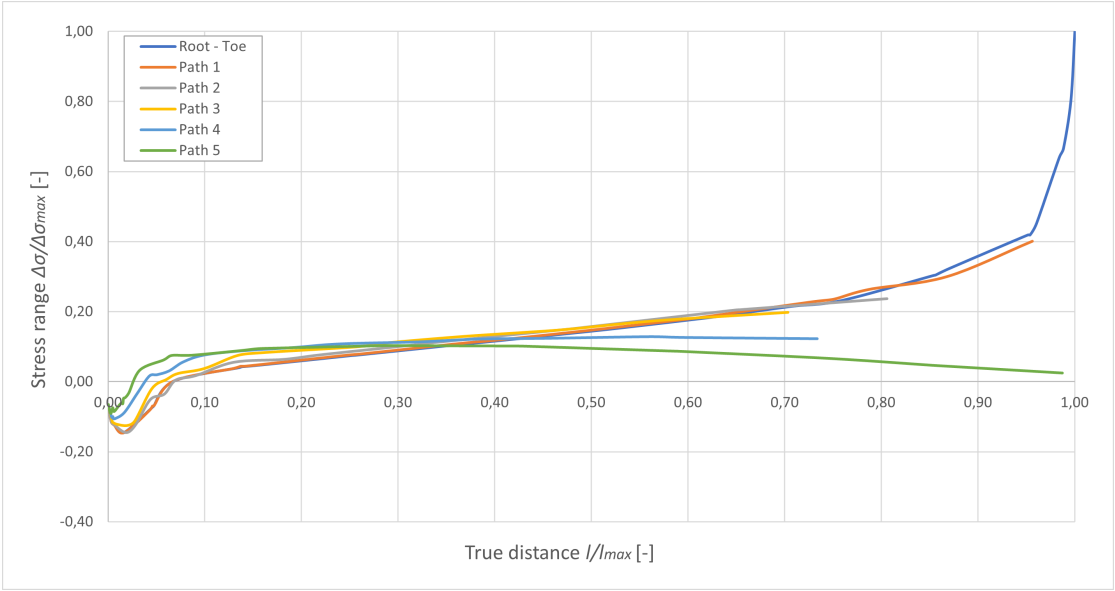

Figure A.6: Maximum principal stress distribution through weld leg-length between root (x=0) and toe (x=1) for all "paths" of Leitner and Stoschka test specimen seen in Figure A.5

B

Appendix B: Vilhauer et al, 2011

B.1 Calculation of applied load

Dimensions

Flange-girder	Cover-plate	Fillet weld
$L_{fg} = 1270\ mm$	$L_{cp} = 660\ mm$	$a = 7.94\ mm$
$b_{fg} = 114\ mm$	$b_{cp} = 76.2\ mm$	$Leg_{Length} = 11.23\ mm$
$t_{fg} = 25.4\ mm$	$t_{cp} = 25.4\ mm$	$HFMI_{longtud} = 152\ mm$

Known values

$c = 12.7\ mm$ (Distance to the neutral axis to weld toe)

$L_{toe} = 305mm - Leg_{Length} = 294\ mm$ (Distance from support to weld toe)

$I_{fg} = \frac{b_{fg} \cdot t_{fg}^3}{12} = 1.557 \cdot 10^5\ mm^4$ (Inertia of the girder-flange)

1. Calculation of the applied load for each given nominal stress

The stress at the weld toe is known, and is used to calculate the moment at the weld toe and thereafter the applied load, P_V.

· Calculate the bending moment at the end weld toe, derived from Equation 3.1:
Where: $\sigma_{NS} = \frac{M_{toe} \cdot c}{I_{fg}} \rightarrow M_{toe} = \frac{\sigma_{NS} \cdot I_{fg}}{c}$

The bending moment for each nominal stress is calculated:

σ_{NS}	58.6 MPa	96.5 MPa	138 MPa	193 MPa
M_{toe}	$7.183 \cdot 10^5\ Nmm$	$1.183 \cdot 10^6\ Nmm$	$1.692 \cdot 10^6\ Nmm$	$2.366 \cdot 10^6\ Nmm$

· The load P_V is calculated with the moment equation derived from basic mechanic equation from the structural model seen in following figure:

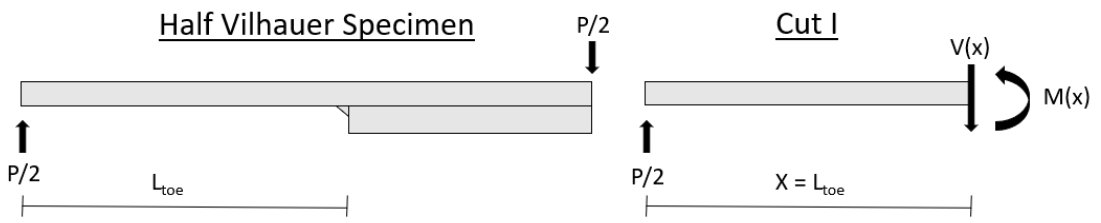

Moment equation: $M_{toe}(x) = \frac{P_V \cdot L_{toe}}{2} \rightarrow P_V = \frac{M_{toe}(x) \cdot 2}{L_{toe}}$

With the moment equation derived from basic mechanics the applied load, P_V, is calculated for each nominal stress:

σ_{NS}	58.6 MPa	96.5 MPa	138 MPa	193 MPa
P_V	4,890 N	8,053 N	11,520 N	16,110 N

· The load that would be used for the Abaqus model is a quarter of the total load ($P_{V,a} = \frac{P}{4}$):

σ_{NS}	58.6 MPa	96.5 MPa	138 MPa	193 MPa
$P_{V,a}$	1,223 N	2,013 N	2,879 N	4,027 N

2. Calculation of the applied load for Abaqus analysis

The unit load $P_{V,u}$ is calculated following the same steps as the previous calculation of the applied load for each nominal stress. Instead the nominal stress is defined as 1 MPa.

$\sigma_{u.NS} = 1\ MPa$

· Calculate the bending moment at the end weld toe, derived from Equation 3.1:
Where: $M_{u.toe} = \frac{\sigma_{u.NS} \cdot I_{fg}}{c} = 1.226 \cdot 10^4\ Nmm$

· The unit load $P_{V,u}$ is calculated with the moment equation derived from basic mechanic equation:
Moment equation: $P_{V,u} = \frac{M_{u.toe}(x) \cdot 2}{L_{toe}} = 83.453\ N$

· The unit load applied in the Abaqus model is calculated as a quarter of the total unit load
Hence: $P_{V,u.a} = \frac{P_{V,u}}{4} = 20.863\ N$

· The calculated load $P_{V,u.a}$ is confirmed by multiplying the load with the given nominal stress, to determine that the applied load is the same as previously calculated. Which is verified below:

$P_{58,6} = P_{V,u.a} \cdot 58.6 = 1,223\ N$ OK!
$P_{96.5} = P_{V,u.a} \cdot 96.5 = 2,013\ N$ OK!
$P_{138} = P_{V,u.a} \cdot 138 = 2,879\ N$ OK!
$P_{193} = P_{V,u.a} \cdot 193 = 4,027\ N$ OK!

B.2 Classification of mesh element size of specimen model

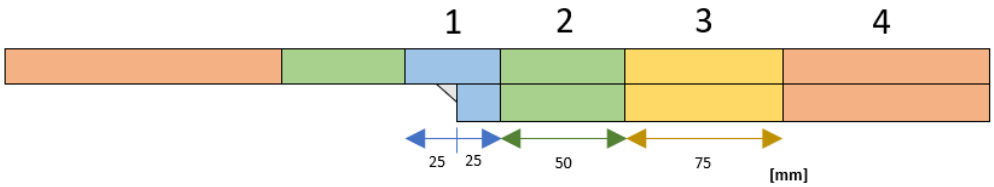

Figure B.1: Classification of the six main partition regions, where each region has the following mesh element size: 2.5 mm, 5 mm, 7.5 mm and 12.7 mm [Writers own figure basted on the Vilhauer et al. (2012) specimen]

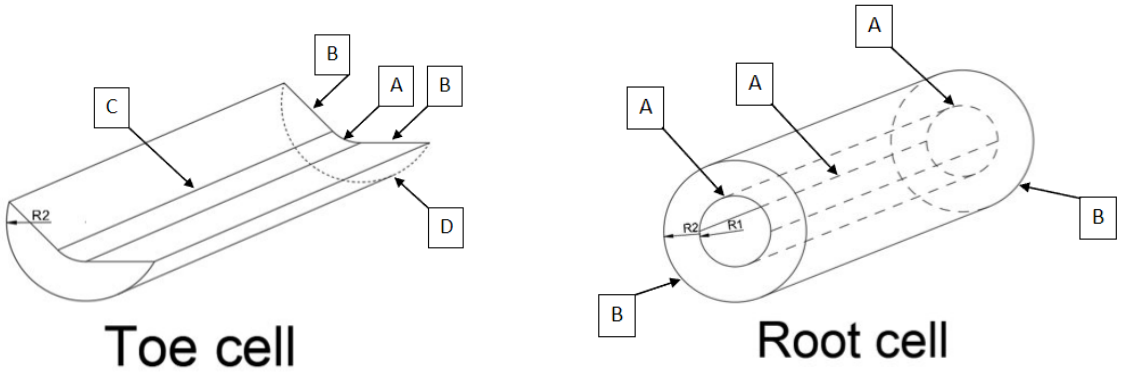

(a) Toe cell idealised

(b) Root cell idealised

Figure B.2: The idealised version of toe and root notch cells used in Abaqus [Writers own figure]

The mesh element size that was applied to the edges seen in Figure B.2 can be seen in the Tables on the next page

Toe cell mesh element size as seen in Figure B.2(a) [mm]

	Element size for 0.3 mm				Element size for 0.25 mm				Element size for 0.2 mm				Element size for 0.15 mm				Element size for 0.1 mm			
	A	B	C	D	A	B	C	D	A	B	C	D	A	B	C	D	A	B	C	D
1	0.3	0.35	0.4	0.5	0.25	0.3	0.35	0.5	0.2	0.25	0.3	0.5	0.15	0.2	0.25	0.5	0.1	0.15	0.2	0.5
2	0.35	0.4	0.45	0.5	0.3	0.35	0.4	0.5	0.25	0.3	0.35	0.5	0.2	0.25	0.3	0.5	0.15	0.2	0.25	0.5
3	0.4	0. 45	0.5	0.5	0.35	0.4	0.45	0.5	0.3	0.35	0.4	0.5	0.25	0.3	0.35	0.5	0.2	0.25	0.3	0.5
4	0.45	0.5	0.55	0.5	0.4	0.45	0.5	0.5	0.35	0.4	0.45	0.5	0.3	0.35	0.4	0.5	0.25	0.3	0.35	0.5

Root cell mesh element size as seen in Figure B.2(b) [mm]

Element size for 0.3 mm		Element size for 0.25 mm		Element size for 0.2 mm		Element size for 0.15 mm		Element size for 0.1 mm	
A	B	A	B	A	B	A	B	A	B
0.3	0.5	0.25	0.5	0.2	0.5	0.15	0.5	0.1	0.5

B.3 Convergence study of test results, detailed

Table B.1: Collection of 5 maximum principal stresses and their average at weld toe and root for all notch sizes (r_{ref} =0.3, 0.25, 0.2, 0.15 and 0.1) of Vilhauer et al. Abaqus model loaded under a unit nominal stress of 1 MPa at the weld toe.

Nominal stress of 1 MPa		
Mesh	Stress Toe [MPa]	Stress Root [MPa]
0.3	3.631	1.94
	3.618	1.933
	3.633	1.87
	3.593	1.864
	3.589	1.863
Average:	3.613	1.894
0.25	3.838	1.923
	3.686	1.883
	3.659	1.909
	3.645	1.869
	3.639	1.878
Average:	3.693	1.892
0.2	3.728	1.911
	3.743	1.915
	3.704	1.926
	3.681	1.91
	3.679	1.909
Average:	3.707	1.914
0.15	3.747	1.92
	3.695	1.919
	3.694	1.916
	3.693	1.915
	3.697	1.902
Average:	3.705	1.914
0.1	3.724	1.91
	3.76	1.903
	3.737	1.902
	3.711	1.9
	3.709	1.901
Average:	3.728	1.903

B.4 Calculation of characteristic load cycles

For the calculation of load cycles the following equations are applied, Equation 5.3 and 5.4:

(1) $N = 2 \cdot 10^6 (\frac{\Delta\sigma_C}{\Delta\sigma_{i,Ed}})^{m_1}$ for $\Delta\sigma_{i,Ed} \geq \Delta\sigma_D$

(2) $N = N_D (\frac{\Delta\sigma_D}{\Delta\sigma_{i,Ed}})^{m_2}$ for $\Delta\sigma_L \leq \Delta\sigma_{i,Ed} \leq \Delta\sigma_D$ and $N_D = 10^7$

Design values for Vilhauer et al. test

All values are for Effective Notch Method (ENS) taken from Figure 2.18 and 2.4 in section 2.3.2

As-welded FAT 225		HFMI-treated FAT 320	
$\Delta\sigma_{C.A} = 225\ MPa$	$m_{1.A} = 3$	$\Delta\sigma_{C.HFMI} = 320\ MPa$	$m_{1.HFMI} = 5$
$\Delta\sigma_{D.A} = 132\ MPa$	$m_{2.A} = 5$	$\Delta\sigma_{D.HFMI} = 235\ MPa$	$m_{2.HFMI} = 9$
$\Delta\sigma_{L.A} = 83\ MPa$			

Load cycles at weld toe and root for as-welded (CONTROL) specimen and at weld root for UIT-treated specimen (UIT and UIT/BOLT) are calculated using the values for S-N curve FAT 225. Load cycles at weld toe for UIT-treated specimen are calculated using the values for S-N curve FAT 320. Hence, for the corresponding effective not stresses the load cycles equals to:

$\Delta\sigma_{NS}$:	58.6 MPa	96.5 MPa	138 MPa	193 MPa
$\Delta\sigma_{ENS_{Toe}}$:	210 MPa	358 MPa	511 MPa	715 MPa
$\Delta\sigma_{ENS_{Root}}$:	109 MPa	185 MPa	264 MPa	369 MPa

Load cycles at Toe (As-welded)

· $\Delta\sigma_{NS} = 58.6$ MPa $\rightarrow$ Equation (1) $\Rightarrow N = 2 \cdot 10^6 (\frac{\Delta\sigma_{C.A}}{210})^{m_{1.A}} = 2,459,913$

· $\Delta\sigma_{NS} = 96.5$ MPa $\rightarrow$ Equation (1) $\Rightarrow N = 2 \cdot 10^6 (\frac{\Delta\sigma_{C.A}}{358})^{m_{1.A}} = 496,511$

· $\Delta\sigma_{NS} = 138$ MPa $\rightarrow$ Equation (1) $\Rightarrow N = 2 \cdot 10^6 (\frac{\Delta\sigma_{C.A}}{511})^{m_{1.A}} = 170,732$

· $\Delta\sigma_{NS} = 193$ MPa $\rightarrow$ Equation (1) $\Rightarrow N = 2 \cdot 10^6 (\frac{\Delta\sigma_{C.A}}{715})^{m_{1.A}} = 62,325$

Load cycles at Root (As-welded and UIT-treated)

· $\Delta\sigma_{NS} = 58.6$ MPa $\rightarrow$ Equation (2) $\Rightarrow N = 10^7 (\frac{\Delta\sigma_{D.A}}{109})^{m_{2.A}} = 25,677,896$

· $\Delta\sigma_{NS} = 96.5$ MPa $\rightarrow$ Equation (1) $\Rightarrow N = 2 \cdot 10^6 (\frac{\Delta\sigma_{C.A}}{185})^{m_{1.A}} = 3,598,010$

· $\Delta\sigma_{NS} = 138$ MPa $\rightarrow$ Equation (1) $\Rightarrow N = 2 \cdot 10^6 (\frac{\Delta\sigma_{C.A}}{264})^{m_{1.A}} = 1,238,129$

· $\Delta\sigma_{NS} = 193$ MPa $\rightarrow$ Equation (1) $\Rightarrow N = 2 \cdot 10^6 (\frac{\Delta\sigma_{C.A}}{369})^{m_{1.A}} = 453,418$

Load cycles at Toe (UIT-treated)

· $\Delta\sigma_{NS} = 58.6$ MPa $\rightarrow$ Equation (2) $\Rightarrow N = 10^7 (\frac{\Delta\sigma_{D.HFMI}}{210})^{m_{2.HFMI}} = 27,519,283$

· $\Delta\sigma_{NS} = 96.5$ MPa $\rightarrow$ Equation (1) $\Rightarrow N = 2 \cdot 10^6 (\frac{\Delta\sigma_{C.HFMI}}{358})^{m_{1.HFMI}} = 1,141,208$

· $\Delta\sigma_{NS} = 138$ MPa $\rightarrow$ Equation (1) $\Rightarrow N = 2 \cdot 10^6 (\frac{\Delta\sigma_{C.HFMI}}{511})^{m_{1.HFMI}} = 192,608$

· $\Delta\sigma_{NS} = 193$ MPa $\rightarrow$ Equation (1) $\Rightarrow N = 2 \cdot 10^6 (\frac{\Delta\sigma_{C.A}}{715})^{m_{1.A}} = 62,325$

(Stress is above where the curves cuts each other, therefore, the equation for as-welded joints is used)

B.5 Stress fields

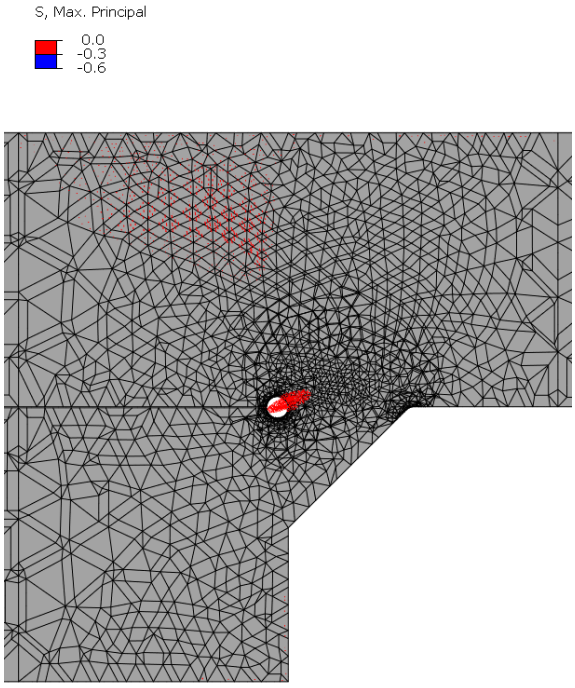

Figure B.3: Maximum principal stress field distribution in stress range -0.6 - 0 MPa for Vilhauer et al. test model loaded in bending, under a unit nominal stress of 1 MPa at weld toe.

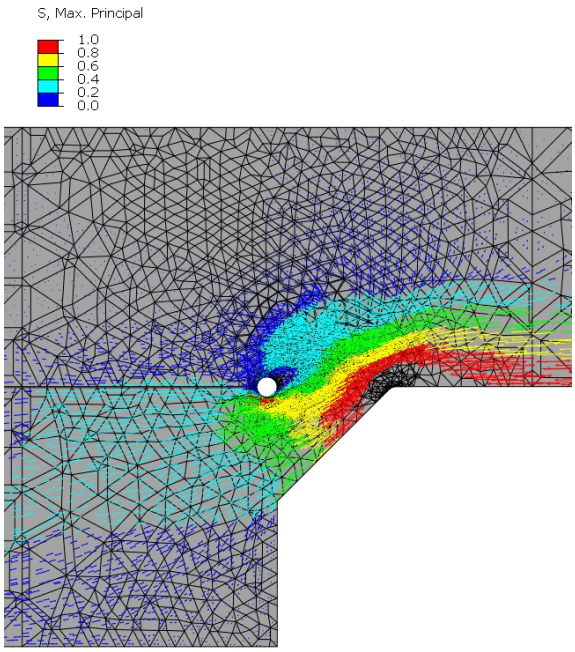

Figure B.4: Maximum principal stress field distribution in stress range 0 - 1 MPa for Vilhauer et al. test model loaded in bending, under a unit nominal stress of 1 MPa at weld toe.

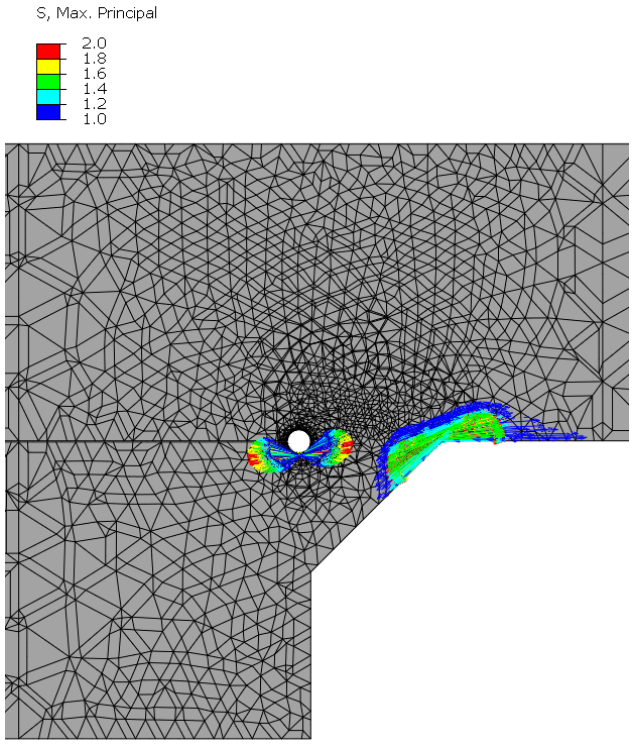

Figure B.5: Maximum principal stress field distribution in stress range 1 - 2 MPa for Vilhauer et al. test model loaded in bending, under a unit nominal stress of 1 MPa at weld toe.

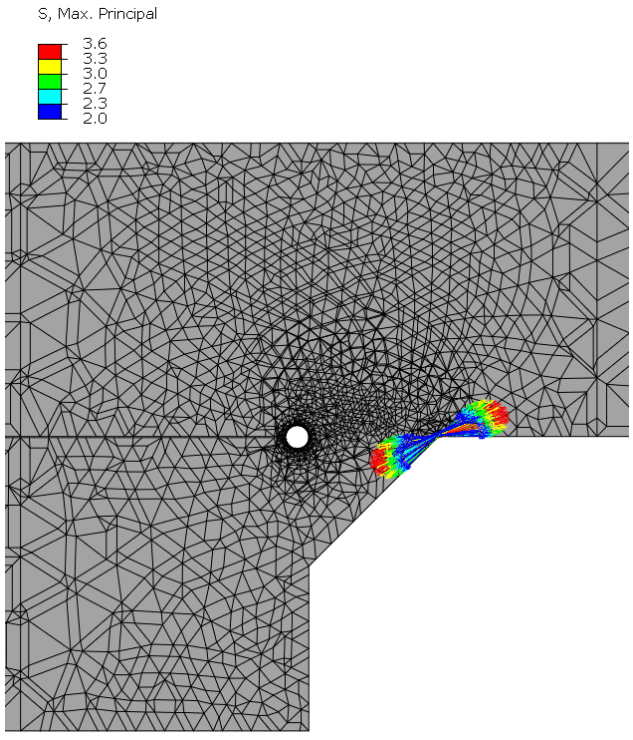

Figure B.6: Maximum principal stress field distribution in stress range 2 - 3.6 MPa for Vilhauer et al. test model loaded in bending, under a unit nominal stress of 1 MPa at weld toe.

B.6 Stress through weld

The stresses through the weld is assembled by the nodal values interacting with the "paths" added in Abaqus. The paths for Vilhauer et al. test model can be seen in Figure B.7 and the numerical stress curves for each path in Figure B.8.

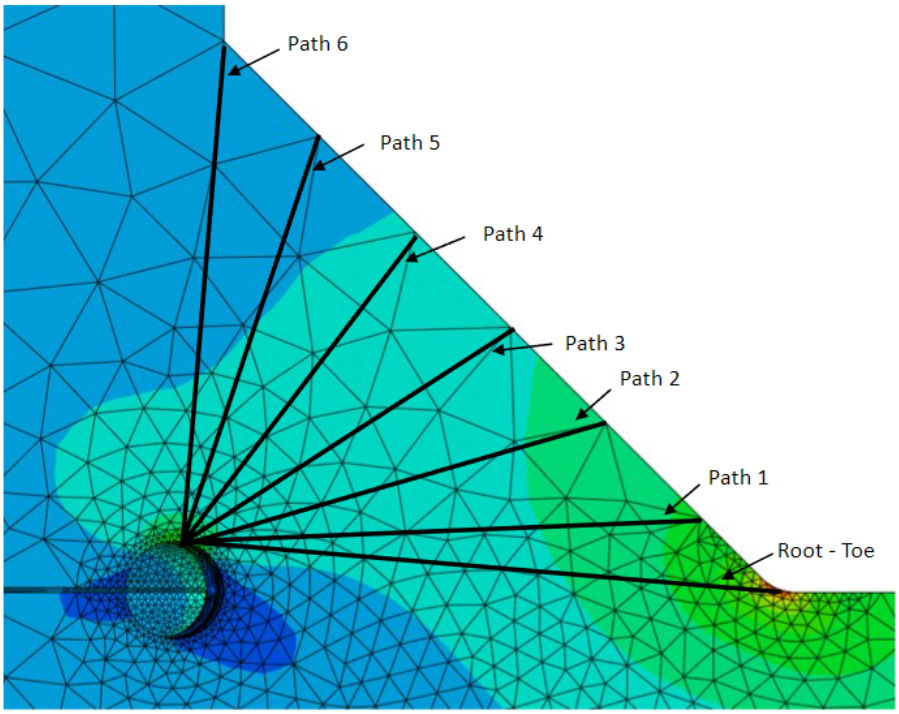

Figure B.7: The "paths" applied to Vilhauer et al. test model in Abaqus to obtain the nodal stresses through the weld

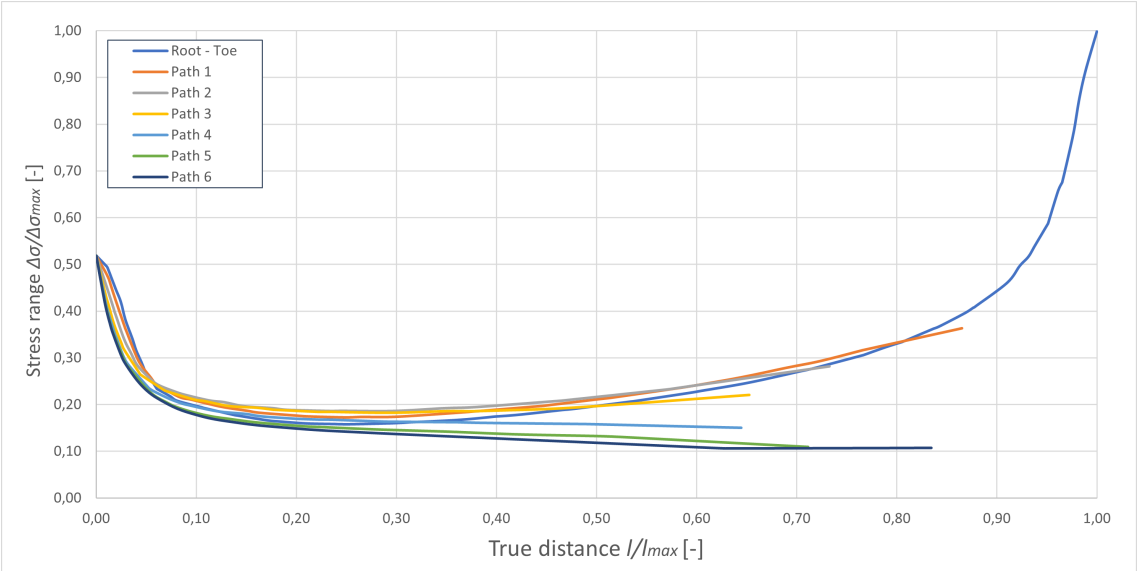

Figure B.8: Maximum principal stress distribution through weld leg-length between root (x=0) and toe (x=1) for all "paths" of Vilhauer et al. test specimen seen in Figure B.7

C

Appendix C: Hui et al, 2018

C.1 Test matrix

Table C.1: Vilhauer et al. planned test matrix for the piratical analysis of the cover-plated beam loaded in bending. [Source: Table 3.2 from Hui et al. (2018), *p.34*]

S_{min} [KSI]	S_r [KSI]		
	10.5	**14**	**18**
1.5	S5	S1, S2, S3, S4, S7, S8	S9, S10
9	S6	S11, S12	S13, S14

Table C.2: Vilhauer et al. applied test matrix for the piratical analysis of the cover-plated beam loaded in bending. [Source: Table 4.1 from Hui et al. (2018), *p.35*]

ID	Load		Nominal Flexural Stress											
			S = M c / I						S = ε E					
			Intermediate Stiffeners			Cover Plate			Intermediate Stiffeners			Cover Plate		
	P_{min}	P_{max}	S_{min}	S_{max}	S_r	S_{min}	S_{max}	S_r	S_{min}	S_{max}	S_r	S_{min}	S_{max}	S_r
#	kip	kip	ksi	ksi	ksi	ksi	ksi	ksi	ksi	ksi	ksi	ksi	ksi	ksi
1	10.4	108.7	2.0	20.9	**19**	1.5	15.6	**14**	2.0	21.0	**19**	1.6	16.6	**15**
2	10.1	104.2	1.9	20.0	**18**	1.5	15.0	**14**	2.0	19.6	**18**	1.5	15.5	**14**
3	10.0	102.7	1.9	19.7	**18**	1.4	14.8	**13**	2.0	19.8	**18**	1.6	15.8	**14**
4	10.0	104.2	1.9	20.0	**18**	1.4	15.0	**14**	2.0	19.3	**17**	1.5	15.3	**14**
5	10.0	83.0	1.9	15.9	**14**	1.4	11.9	**10**	1.9	15.4	**14**	1.4	12.2	**11**
6	61.6	135.2	11.8	25.9	**14**	8.8	19.4	**11**	11.5	25.2	**14**	9.2	20.0	**11**
7	10.0	104.0	1.9	20.0	**18**	1.4	14.9	**14**	1.8	19.8	**18**	1.6	17.7	**16**
8	10.0	104.0	1.9	20.0	**18**	1.4	14.9	**14**	1.8	20.1	**18**	1.6	17.7	**16**
9	10.5	135.0	2.0	25.9	**24**	1.5	19.4	**18**	2.0	25.2	**23**	1.6	20.8	**19**
10	10.5	135.5	2.0	26.0	**24**	1.5	19.5	**18**	2.2	25.8	**24**	1.6	21.2	**20**
11	62.4	160.0	12.0	30.7	**19**	9.0	23.0	**14**	12.2	31.0	**19**	9.9	24.8	**15**
12	62.0	162.0	11.9	31.1	**19**	8.9	23.3	**14**	11.7	30.1	**18**	9.8	25.0	**15**
13	62.7	187.7	12.0	36.0	**24**	9.0	27.0	**18**	11.3	34.4	**23**	9.0	28.5	**20**
14	62.6	187.7	12.0	36.0	**24**	9.0	27.0	**18**	11.3	34.8	**24**	9.2	29.2	**20**

C.2 Calculation of applied load

Dimensions

I-beam	Cover-plate	Fillet weld
$L = 6400.8\ mm$	$L_{cp1} = 1358.9\ mm$	$Leg_{Length} = 12.4\ mm$
$h = 702\ mm$	$L_{cp2} = 1397\ mm$	
$b_f = 254\ mm$	$b_{cp} = 190.5\ mm$	
$t_f = 28\ mm$	$t_{cp} = 25.4\ mm$	
$h_w = 646\ mm$		
$t_w = 15.5\ mm$		

Known values

$c = 351\ mm$ (Distance to the neutral axis to weld toe)

$L_{support} = 152.4\ mm$ (Distance from beam edge to support)

$L_{toe1} = L_{cp1} - L_{support} + Leg_{Length} = 1219\ mm$ (Distance from support to weld toe for S1-S6 beams)

$L_{toe2} = L_{cp2} - L_{support} + Leg_{Length} = 1257\ mm$ (Distance from support to weld toe for S7-S14 beams)

$I = 1.979 \cdot 10^9\ mm^4$ (Inertia of the I-beam)

Calculation of the applied load for Abaqus analysis

The unit load $P_{H,u}$ is calculated following the same steps as performed in Appendix B.1(2). Where the load is determined based on a unit nominal stress of 1 MPa.

$\sigma_{u.toe} = 1\ MPa$

· Calculate the bending moment at the end weld toe, derived from Equation 3.1:

Where: $M_{u.toe} = \frac{\sigma_{u.toe} \cdot I}{c} = 5.638 \cdot 10^6\ Nmm$

· The unit load $P_{H,u}$ is calculated with the moment equation derived from basic mechanic equation from the structural model seen in following figure:

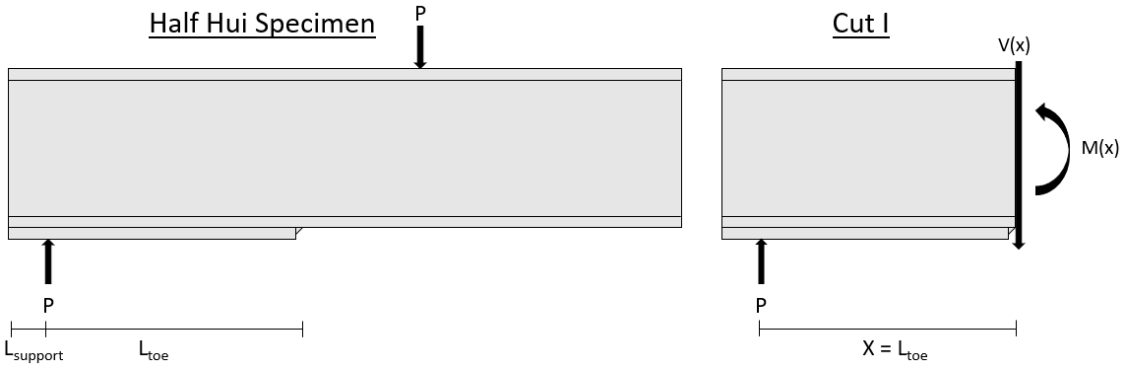

Moment equation: $M_{u.toe}(x) = P \cdot L_{toe} \rightarrow P = \frac{M_{u.toe}(x)}{L_{toe}}$

Where: $P_{H,u1} = \frac{M_{u.toe}(x)}{L_{toe1}} = 4,624\ N$

Where: $P_{H,u2} = \frac{M_{u.toe}(x)}{L_{toe2}} = 4,484\ N$

· The unit load applied in the Abaqus model is calculated as half of the total load
Hence: $P_{H,u.a1} = \frac{P_{H,u1}}{2} = 2,312\ N$
Hence: $P_{H,u.a2} = \frac{P_{H,u2}}{2} = 2,242\ N$

For the load calculation of Vilhauer et al. test in Appendix B.1, a verification was performed for the calculated load derived from the unit nominal stress of 1 MPa, which was proven to be accurate. Hence, because this verification was performed for the previous analysis applied load, it is not performed for this analysis.

C.3 Test results

Table C.3: Hui et al. fatigue test results of piratically tested cover-plate specimens, includes load cycles for termination details. The stars represent the beams with shorter cover-plate specimens (S1-S6), the read colour represents the cover-plate specimens that cracked at weld root and the blue collor represents the cover-plate specimens that cracked at weld toe. [Source: Table 4.2b from Hui et al. (2018), *p.37*]

Untreated Cover Plates

	Specimen	Type	Detail	Position	S_r	$N_{, Failure}$	$N_{, End\ of\ Test}$
★	S1	CONTROL	CP	SOUTH	13.7		2.5E+6
	S1	CONTROL	CP	NORTH	13.7		2.5E+6
★	S2	CONTROL	CP	SOUTH	13.1	817.8E+3	
	S2	CONTROL	CP	NORTH	13.1	1.1E+6	
	S7	CONTROL	CP	SOUTH	13.5	235E+3	
	S7	CONTROL	CP	NORTH	13.5	414E+3	
	S8	CONTROL	CP	SOUTH	13.5	627E+3	
	S8	CONTROL	CP	NORTH	13.5	627E+3	

Treated Cover Plates

	Specimen	Type	Detail	Position	S_r	$N_{, Failure}$	$N_{, End\ of\ Test}$
★	S3	UIT	CP	SOUTH	12.9		6.6E+6
	S3	UIT	CP	NORTH	12.9		6.6E+6
★	S4	UIT	CP	SOUTH	13.1		6.2E+6
	S4	UIT	CP	NORTH	13.1		6.2E+6
★	S5	UIT	CP	SOUTH	10.2		13.1E+6
	S5	UIT	CP	NORTH	10.2		13.1E+6
★	S6	UIT	CP	SOUTH	10.2		13.0E+6
	S6	UIT	CP	NORTH	10.2	11.8E+6	
	S9	UIT	CP	SOUTH	17.9	1.7E+6	
	S9	UIT	CP	NORTH	17.9	1.7E+6	
	S10	UIT	CP	SOUTH	18.0	2.3E+6	
	S10	UIT	CP	NORTH	18.0	1.5E+6	
	S11	UIT	CP	SOUTH	14.0		5.7E+6
	S11	UIT	CP	NORTH	14.0		5.7E+6
	S12	UIT	CP	SOUTH	14.4	1.3E+6	
	S12	UIT	CP	NORTH	14.4	2.6E+6	
	S13	UIT	CP	SOUTH	18.0	1.4E+6	
	S13	UIT	CP	NORTH	18.0	1.3E+6	
	S14	UIT	CP	SOUTH	19.0	1.5E+6	
	S14	UIT	CP	NORTH	19.0	1.9E+6	

C.4 Effective notch stress calculation

Table C.4: Effective notch stress at toe and root for each nominal stress of Hui et al. test model for both the short (above table) and long cover-plate (below table) specimens. Identifies also the beam and type och specimen.

Beams with shorter cover-plates				
Specimen	Type	S_r [MPa]	$\Delta\sigma_{ENS,Ed.Toe}$ [MPa]	$\Delta\sigma_{ENS_{Root}}$ [MPa]
-	-	1	4.32	3.64
S1	CONTROL	94.458	408	344
S2	CONTROL	90.32	390	329
S3	UIT	88.94	384	324
S4	UIT	90.32	390	329
S5	UIT	70.326	304	256
S6	UIT	70.326	304	256

Beams with longer cover-plates				
Specimen	Type	S_r [MPa]	$\Delta\sigma_{ENS,Ed.Toe}$ [MPa]	$\Delta\sigma_{ENS_{Root}}$ [MPa]
-	-	1	4.372	3.75
S7	CONTROL	93	407	349
S8	CONTROL	93	407	349
S9	UIT	123.4	540	463
S10	UIT	124.1	543	465
S11	UIT	96.5	422	362
S12	UIT	99.28	434	372
S13	UIT	124.1	543	465
S14	UIT	131	573	492

C.5 Calculation of characteristic load cycles

For the calculation of load cycles the following equations are applied, Equation 5.3 and 5.4:

(1) $N = 2 \cdot 10^6 (\frac{\Delta\sigma_C}{\Delta\sigma_{i,Ed}})^{m_1}$ for $\Delta\sigma_{i,Ed} \geq \Delta\sigma_D$

(2) $N = N_D (\frac{\Delta\sigma_D}{\Delta\sigma_{i,Ed}})^{m_2}$ for $\Delta\sigma_L \leq \Delta\sigma_{i,Ed} \leq \Delta\sigma_D$ and $N_D = 10^7$

Design values for Hui et al. test

All values are for Effective Notch Method (ENS) taken from Figure 2.18 and 2.4 in section 2.3.2

As-welded FAT 225		HFMI-treated FAT 320	
$\Delta\sigma_{C.A} = 225\ MPa$	$m_{1.A} = 3$	$\Delta\sigma_{C.HFMI} = 320\ MPa$	$m_{1.HFMI} = 5$
$\Delta\sigma_{D.A} = 132\ MPa$	$m_{2.A} = 5$	$\Delta\sigma_{D.HFMI} = 235\ MPa$	$m_{2.HFMI} = 9$
$\Delta\sigma_{L.A} = 83\ MPa$			

Load cycles at weld toe and root for as-welded (CONTROL) specimen and at weld root for UIT-treated specimen (UIT) are calculated using the values for S-N curve FAT 225. Load cycles at weld toe for UIT-treated specimen are calculated using the values for S-N curve FAT 320. Hence, for the corresponding effective notch stresses in Table C.4 the load cycles equals to:

∘ All effective notch stresses in Table C.4 are larger than $\Delta\sigma_{i,Ed} \geq \Delta\sigma_D$, hence only equation (1) is applied for the load cycle calculation.

Example calculating load cycles for S1 and S3:

$\cdot S1 : \Delta\sigma_{NS} = 94.458$
$\rightarrow N_{Toe} = 2 \cdot 10^6 (\frac{\Delta\sigma_{C.A}}{408})^{m_{1.A}} = 335,282$
$\rightarrow N_{Root} = 2 \cdot 10^6 (\frac{\Delta\sigma_{C.A}}{344})^{m_{1.A}} = 560,476$

$\cdot S3 : \Delta\sigma_{NS} = 88.94$
$\rightarrow N_{Toe_{HFMI}} = 2 \cdot 10^6 (\frac{\Delta\sigma_{C.HFMI}}{384})^{m_{1.HFMI}} = 801,448$
$\rightarrow N_{Root} = 2 \cdot 10^6 (\frac{\Delta\sigma_{C.A}}{324})^{m_{1.A}} = 671,401$

Table C.5: Calculated characteristic load cycles for Hui et al. as-welded specimens (CONTROL) at weld toe and root, as well as the ratio between load cycles of toe and root.

CONTROL					
Specimen (S_r [MPa])	ENS [MPa]		Load cycles [-]		Ratio [-]
	$\Delta\sigma_{Toe}$	$\Delta\sigma_{Root}$	N_{Toe}	N_{Root}	$\frac{N_{Root}}{N_{Toe}}$
S1 (94.458)	408	344	335,282	560,476	1.67
S2 (90.32)	390	329	383,508	641,094	1.67
S7 (93)	407	349	338,913	537,075	1.58
S8 (93)	407	349	338,913	537,075	1.58

Table C.6: Calculated characteristic load cycles for Hui et al. UIT-treated specimens (UIT) at weld toe and root, as well as the ratio between load cycles of toe and root.

UIT					
Specimen (S_r [MPa])	ENS [MPa]		Load cycles [-]		Ratio [-]
	$\Delta\sigma_{Toe}$	$\Delta\sigma_{Root}$	$N_{Toe_{HFMI}}$	N_{Root}	$\frac{N_{Root}}{N_{Toe_{HFMI}}}$
S3 (88.94)	384	324	801,448	671,401	0.84
S4 (90.32)	390	329	742,064	641,094	0.86
S5 (70.326)	304	256	2,592,875	1,358,081	0.52
S6 (70.326)	304	256	2,592,875	1,358,081	0.52
S9 (123.4)	540	463	146,826	229,900	1.57
S10 (124.1)	543	465	142,732	226,031	1.58
S11 (96.5)	422	362	502,045	480,731	0.96
S12 (99.28)	434	372	435,582	441,467	1.01
S13 (124.1)	543	465	142,732	226,031	1.58
S14 (131)	573	491	121,261	192,163	1.58

The red color indicates that the as-welded S-N curve of FAT 225 was used to calculate the design load cycles for the HFMI-treated toe.

C.6 Stress fields

C.6.1 Beam with short cover-plate

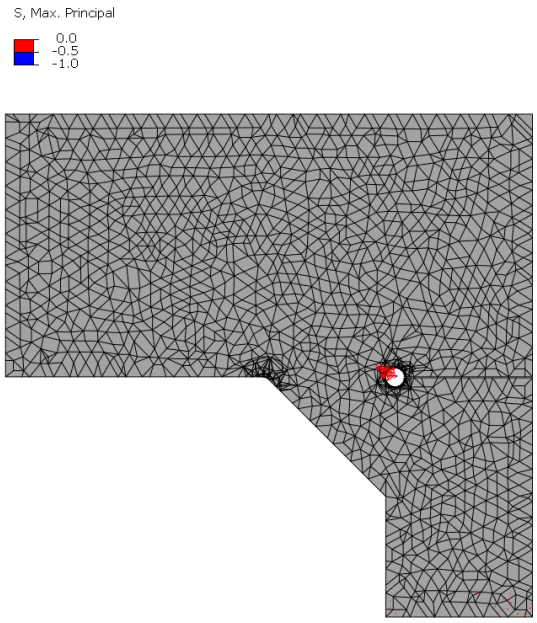

Figure C.1: Maximum principal stress field distribution in stress range -1 - 0 MPa for Hui et al. test model with the shorter cover-plate specimens (S1-S6) loaded in bending, under a unit nominal stress of 1 MPa at weld toe.

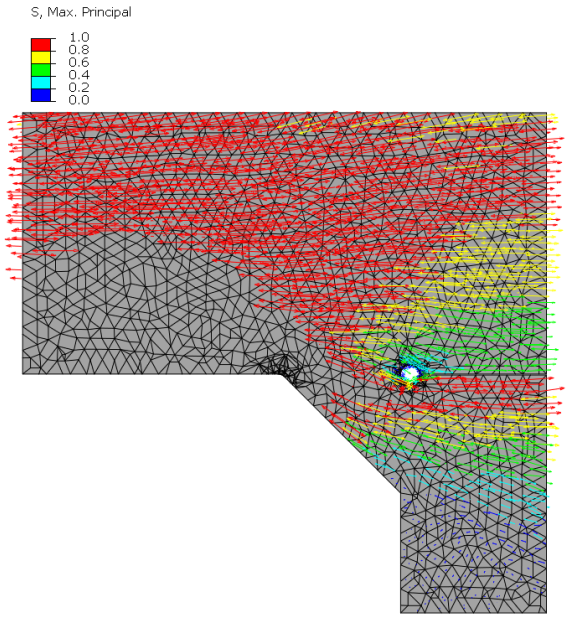

Figure C.2: Maximum principal stress field distribution in stress range 0 - 1 MPa for Hui et al. test model with the shorter cover-plate specimens (S1-S6) loaded in bendingy, under a unit nominal stress of 1 MPa at weld toe.

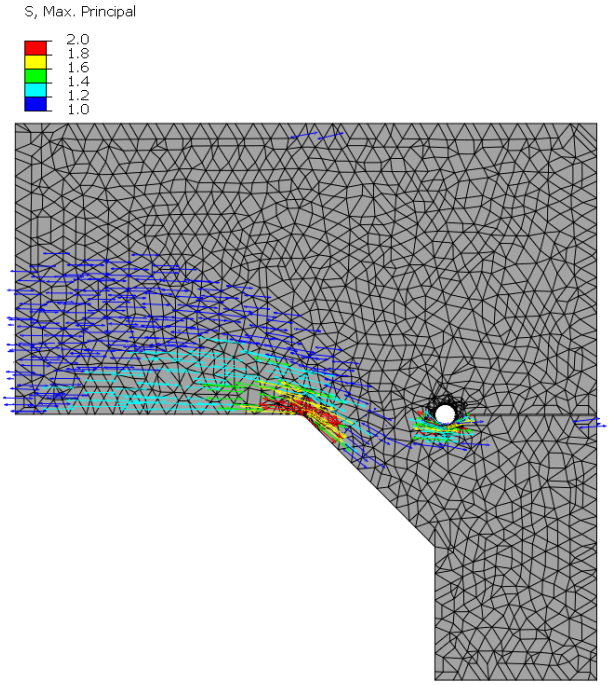

Figure C.3: Maximum principal stress field distribution in stress range 1 - 2 MPa for Hui et al. test model with the shorter cover-plate specimens (S1-S6) loaded in bending, under a unit nominal stress of 1 MPa at weld toe.

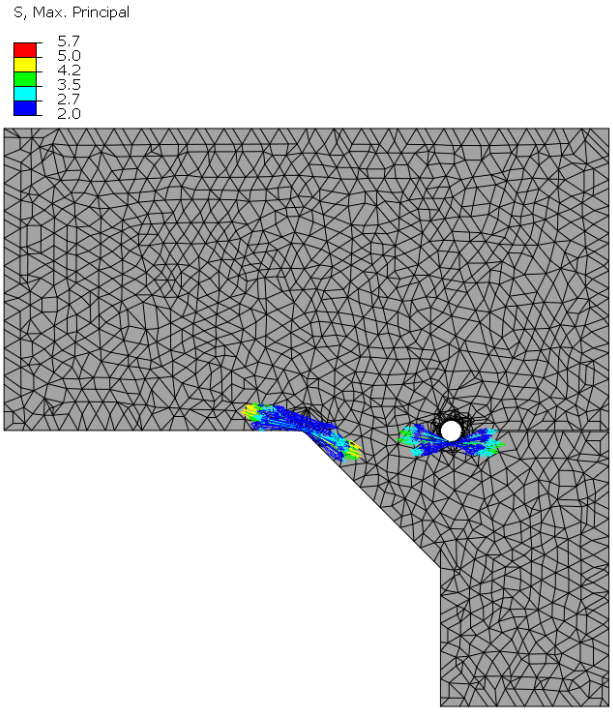

Figure C.4: Maximum principal stress field distribution in stress range 2 - 5.7 MPa for Hui et al. test model with the shorter cover-plate specimens (S1-S6) loaded in bending, under a unit nominal stress of 1 MPa at weld toe.

C.6.2 Beams with long cover-plates

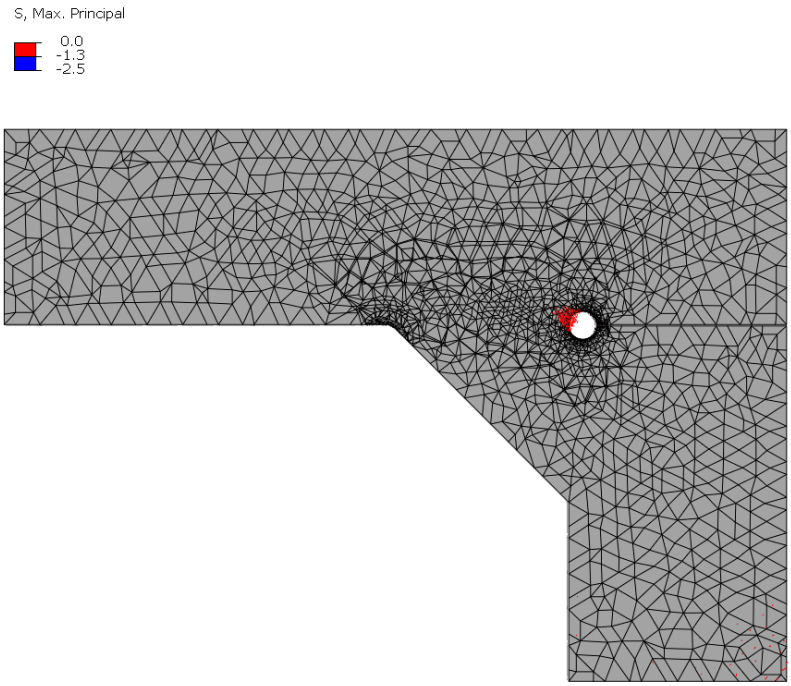

Figure C.5: Maximum principal stress field distribution in stress range -2.5 - 0 MPa for Hui et al. test model with the longer cover-plate specimens (S7-S14) loaded in bending, under a unit nominal stress of 1 MPa at weld toe.

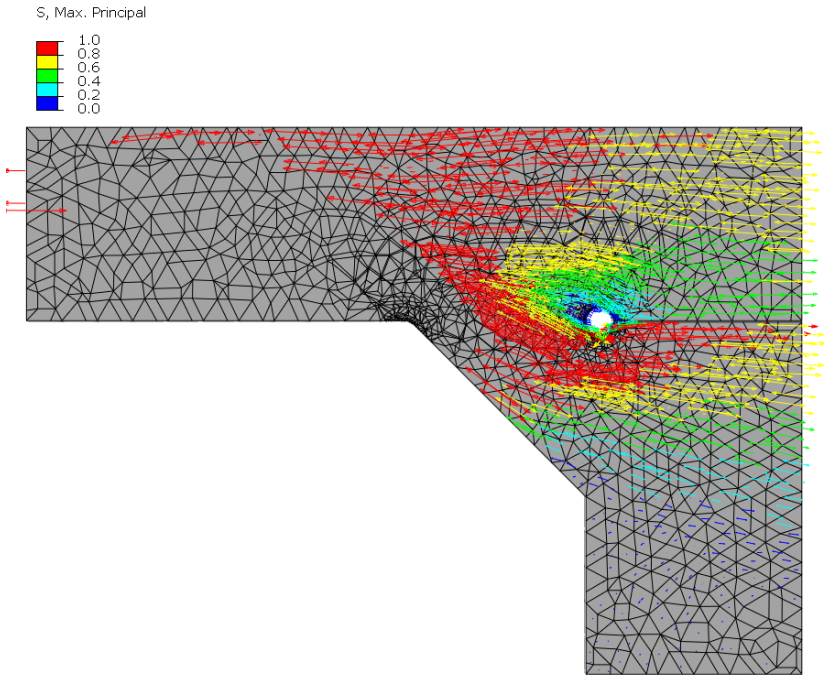

Figure C.6: Maximum principal stress field distribution in stress range 0 - 1 MPa for Hui et al. test model with the longer cover-plate specimens (S7-S14) loaded in bending, under a unit nominal stress of 1 MPa at weld toe.

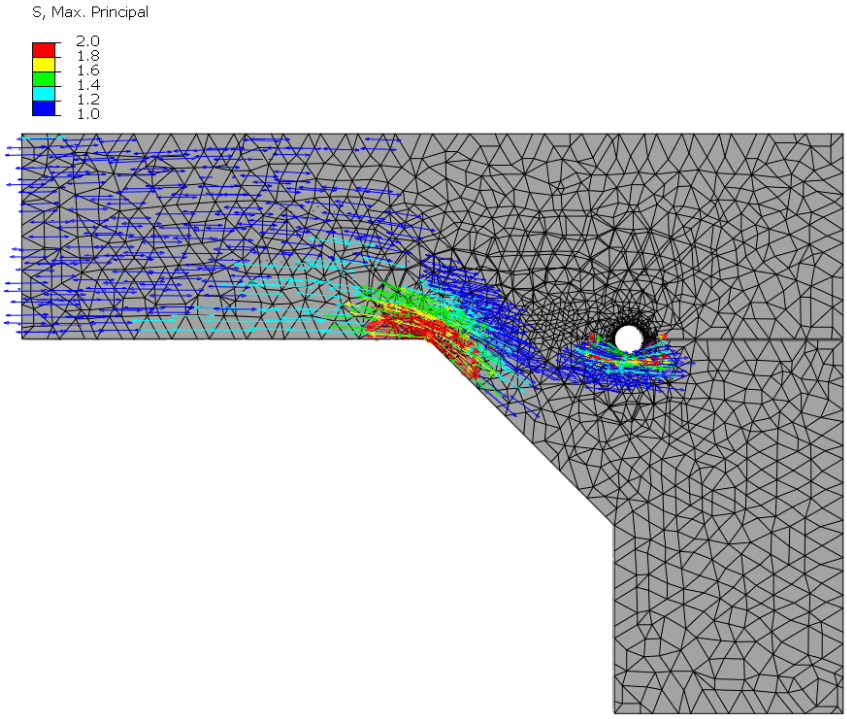

Figure C.7: Maximum principal stress field distribution in stress range 1 - 2 MPa for Hui et al. test model with the longer cover-plate specimens (S7-S14) loaded in bending, under a unit nominal stress of 1 MPa at weld toe.

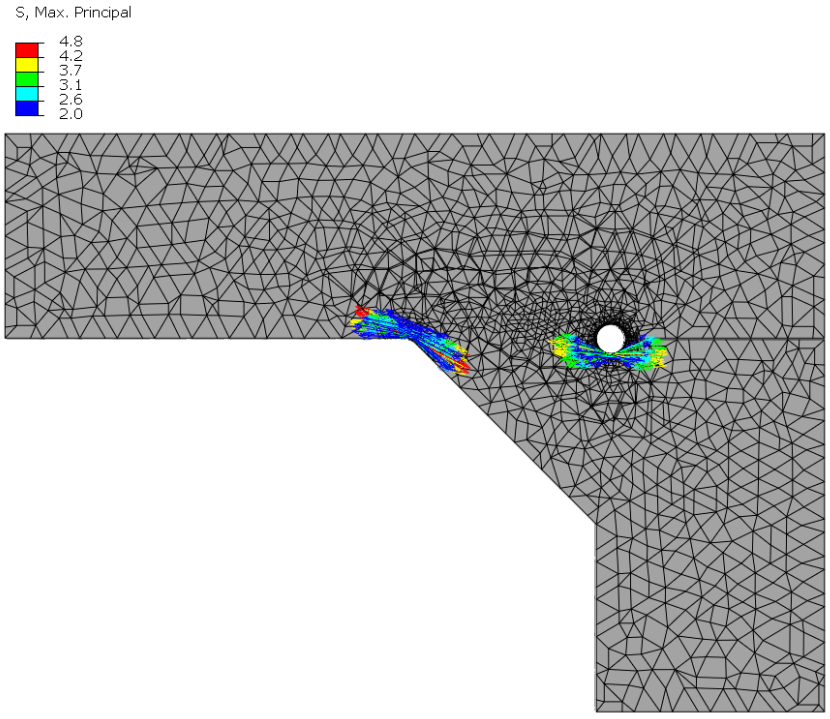

Figure C.8: Maximum principal stress field distribution in stress range 2 - 4.8 MPa for Hui et al. test model with the longer cover-plate specimens (S7-S14) loaded in bending, under a unit nominal stress of 1 MPa at weld toe.

C.7 Stress through weld

The stresses through the weld is assembled by the nodal values interacting with the "paths" added in Abaqus. The paths for Hui et al. test model can be seen in Figure C.9 and the numerical stress curves for each path in Figure C.10 for the shorter cover-plates and in Figure C.11 for the longer cover-plates.

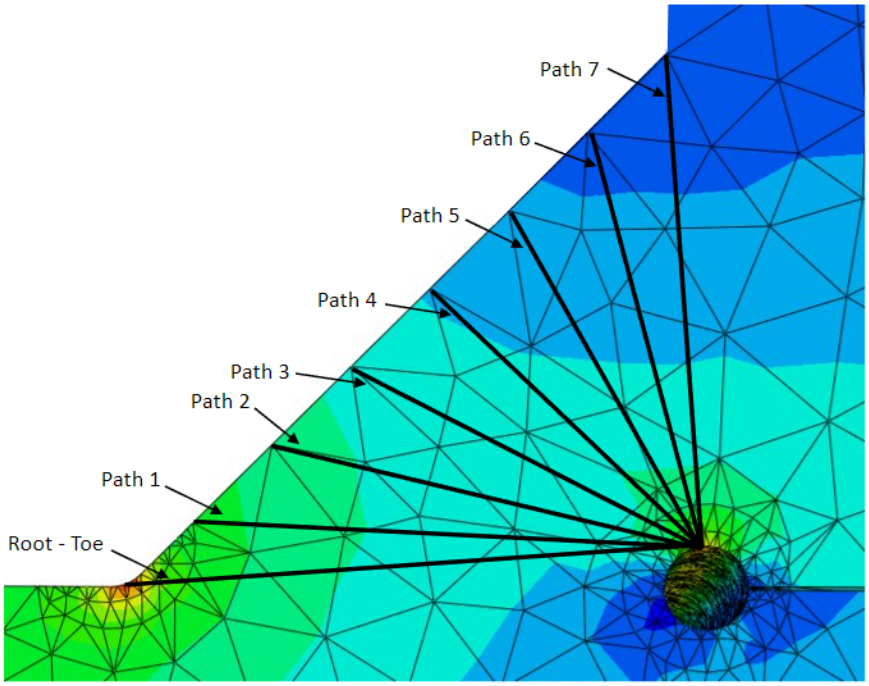

Figure C.9: The "paths" applied to Hui et al. test model in Abaqus to obtain the nodal stresses through the weld.

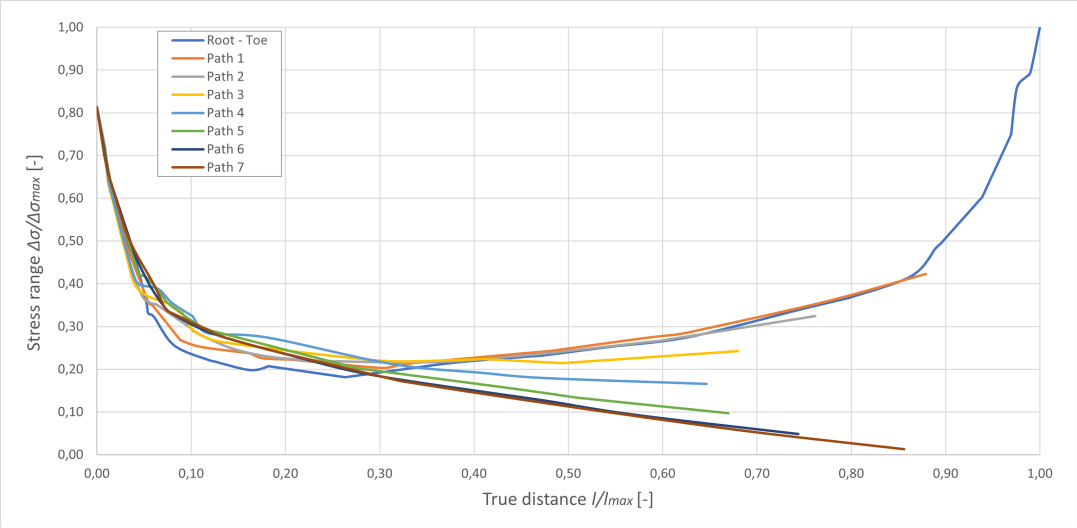

Figure C.10: Maximum principal stress distribution through weld leg-length between root (x=0) and toe (x=1) for all "paths" of Vilhauer et al. test specimen with shorter cover-plates, seen in Figure C.9.

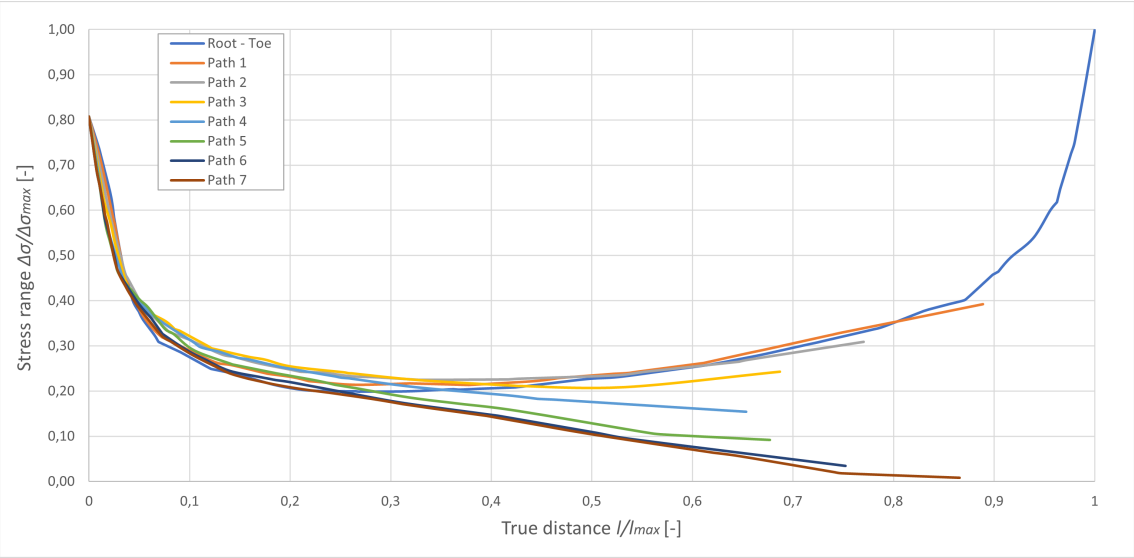

Figure C.11: Maximum principal stress distribution through weld leg-length between root (x=0) and toe (x=1) for all "paths" of Vilhauer et al. test specimen with longer cover-plates, seen in Figure C.9.

D

Appendix D: Exploratory studies

D.1 Modified beam

D.1.1 Calculation of characteristic load cycles with original nominal stresses

Table D.1: Calculated characteristic load cycles at weld toe and root for modified HFMI-treated beam within the same nominal stress ranges used in Hui et al piratical test, as well as the ratio (r) between load cycles of the toe and root.

S_r [MPa]	ENS [MPa]		Load cycles [-]		Ratio [-]
	$\Delta\sigma_{Toe}$	$\Delta\sigma_{Root}$	$N_{Toe_{HFMI}}$	N_{Root}	$\frac{N_{Root}}{N_{Toe_{HFMI}}}$
One cover-plate in the middle of the beam					
93	572	549	121,522	137,903	1.134
97	597	572	107,100	121,536	1.134
99	609	584	100,739	114,318	1.134
123	757	726	52,528	59,608	1.134
124	764	732	51,143	58,037	1.134

Only as-welded S-N curve of FAT 225 was used to calculate the characteristic load cycles for the HFMI-treated toe.

D.1.2 Stress fields

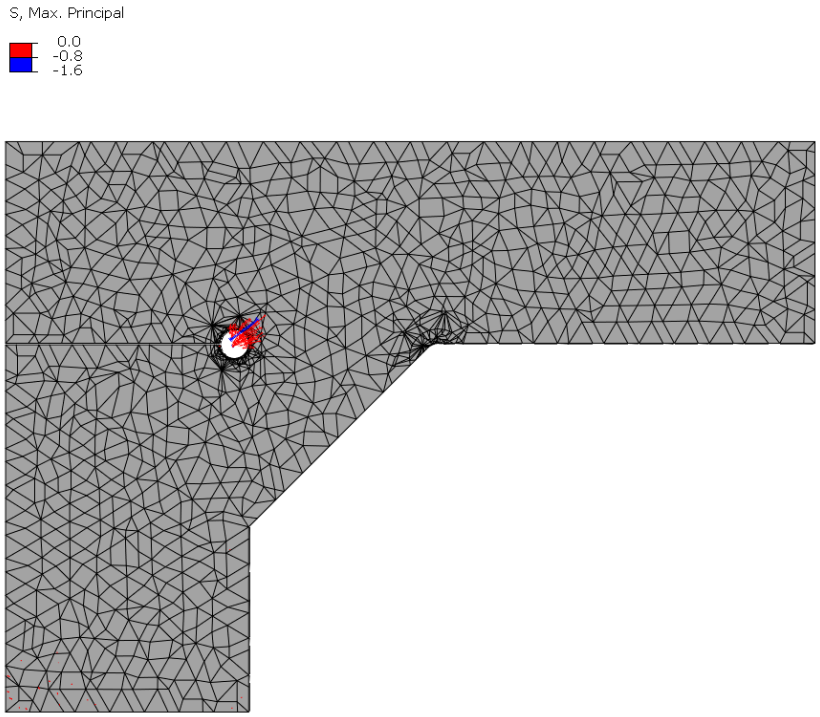

Figure D.1: Maximum principal stress field distribution in stress range -1.6 - 0 MPa for modified beam model loaded in bending, under a unit nominal stress of 1 MPa at weld toe.

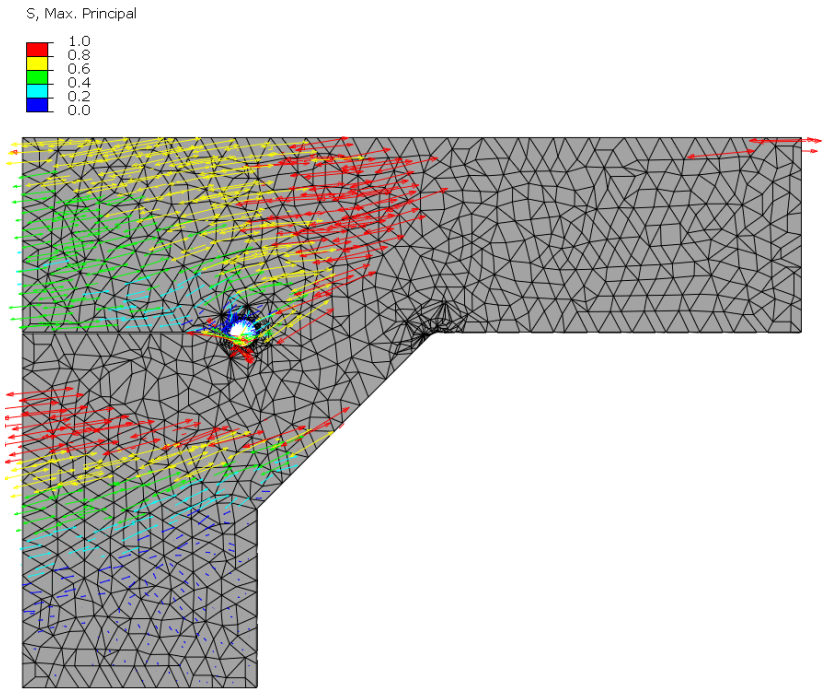

Figure D.2: Maximum principal stress field distribution in stress range 0 - 1 MPa for modified beam model loaded in bending, under a unit nominal stress of 1 MPa at weld toe.

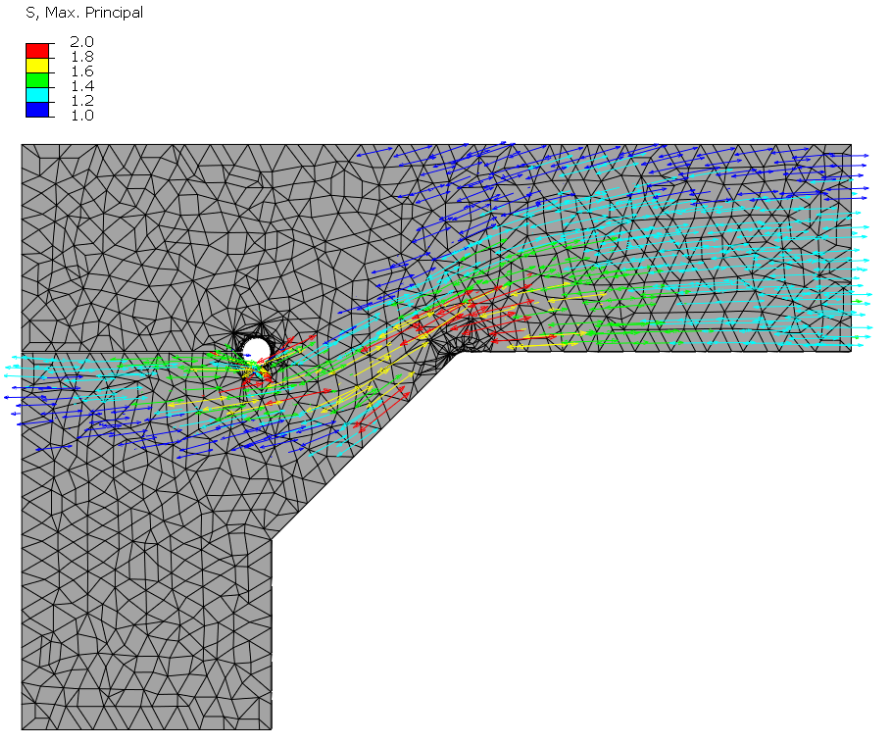

Figure D.3: Maximum principal stress field distribution in stress range 1 - 2 MPa for modified beam model loaded in bending, under a unit nominal stress of 1 MPa at weld toe.

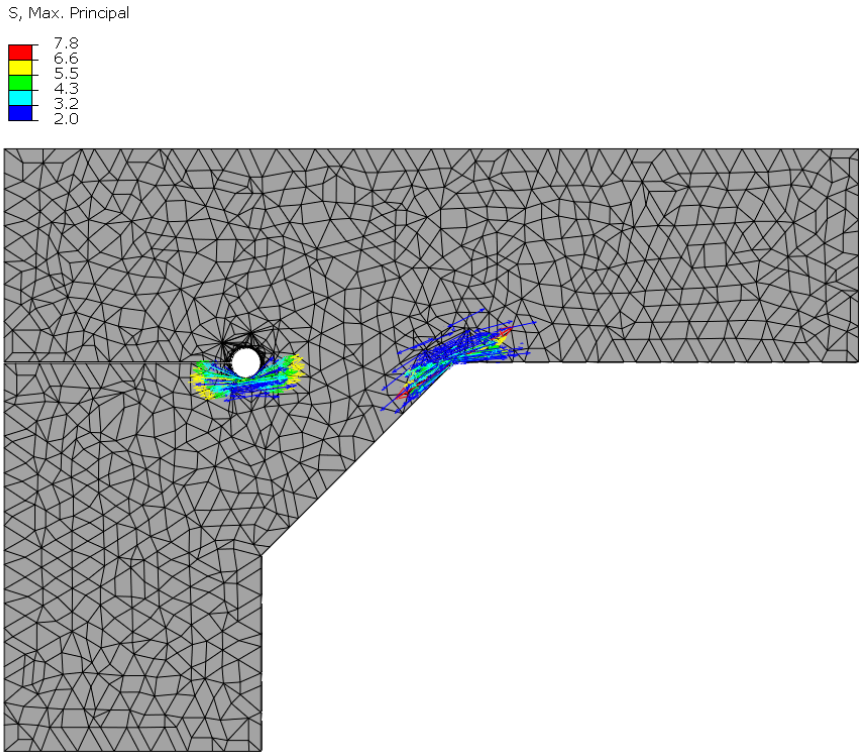

Figure D.4: Maximum principal stress field distribution in stress range 2 - 7.8 MPa for modified beam model loaded in bending, under a unit nominal stress of 1 MPa at weld toe.

D.2 Thickness effect

D.2.1 Details of studied cover-plate thicknesses

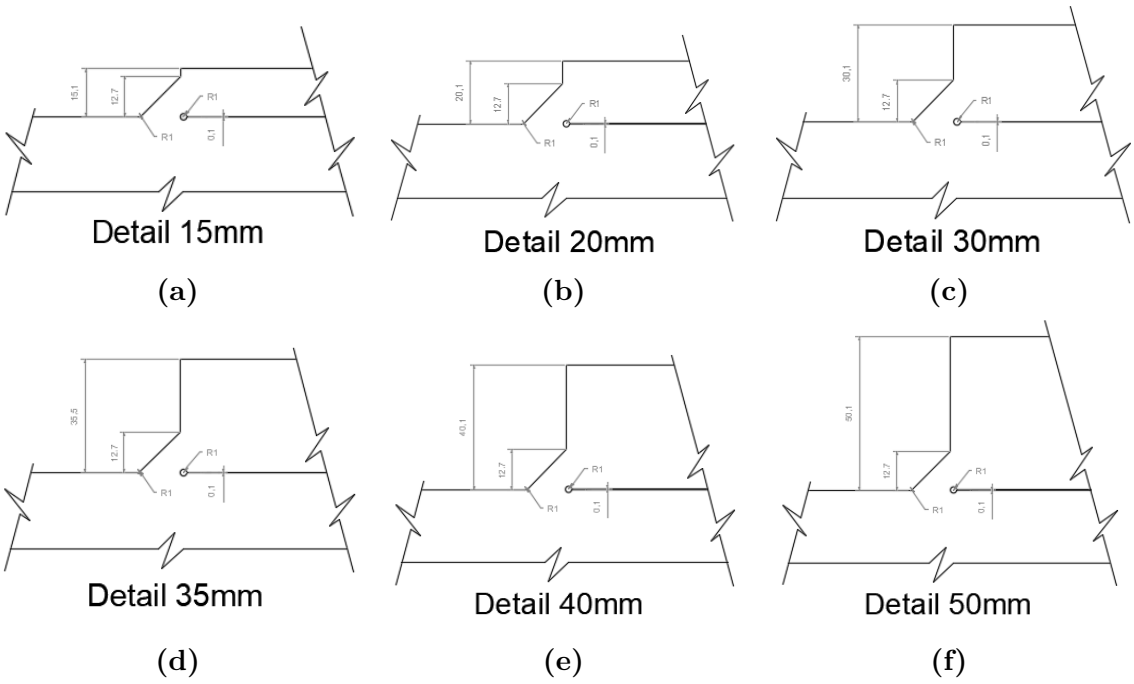

Figure D.5: The notch detailing of the 6 additional studied cover-plate thicknesses that was modeled in Abaqus. The originals detailing can be seen in Detail A-A in Figure 4.10.

D.2.2 Calculation of characteristic load cycles with original nominal stresses

Table D.2: Calculated characteristic load cycles at weld toe and root for HFMI-treated beams with different cover-plate thicknesses subjected to the same nominal stress ranges used in Hui et al test, as well as the ratio (r) between load cycles of the toe and root.

S_r [MPa]	ENS [MPa]		Load cycles [-]		Ratio [-]
	$\Delta\sigma_{Toe}$	$\Delta\sigma_{Root}$	$N_{Toe_{HFMI}}$	N_{Root}	$\frac{N_{Root}}{N_{Toe_{HFMI}}}$
Cover-plate thickness: 15 mm					
93	539	437	146,969	272,279	1.86
97	563	456	127,932	240,419	1.88
99	574	465	120,334	226,140	1.88
123	713	578	62,745	117,915	1.88
124	719	583	61,239	115,085	1.88
Cover-plate thickness: 20 mm					
93	553	516	134,863	165,672	1.23
97	577	538	118,857	240,419	1.23
99	588	549	111,798	226,140	1.23
123	731	683	58,294	117,915	1.23
124	737	688	56,895	115,085	1.23
Cover-plate thickness: 25.4 mm					
93	573	549	121,522	137,903	1.134
97	597	572	107,100	121,536	1.134
99	609	584	100,739	114,318	1.134
123	757	726	52,528	59,608	1.134
124	764	732	51,143	58,037	1.134
Cover-plate thickness: 30 mm					
93	635	616	89,088	97,624	1.09
97	662	642	78,515	86,038	1.09
99	676	655	73,852	80,928	1.09
123	839	814	38,508	42,198	1.09
124	847	822	37,493	41,086	1.09
Cover-plate thickness: 35 mm					
93	650	623	83,070	94,168	1.13
97	678	650	73,211	82,992	1.13
99	692	663	68,863	78,063	1.13
123	859	824	35,907	40,704	1.13
124	867	831	34,960	39,631	1.13
Cover-plate thickness: 40 mm					
93	692	677	68,772	73,407	1.07

97	722	706	60,610	64,695	1.07
99	737	721	57,010	60,852	1.07
123	915	895	29,726	31,730	1.07
124	923	903	28,943	30,894	1.07
Cover-plate thickness: 50 mm					
93	808	747	43,233	54,740	1.27
97	842	779	38,102	48,244	1.27
99	860	795	35,840	45,379	1.27
123	1068	987	18,688	23,661	1.27
124	1078	996	18,195	23,038	1.27

The blue color indicates that the HFMI-treated S-N curve of FAT 320 was used to calculate the design load cycles for the HFMI-treated toe. (The as-welded S-N curve FAT 225 was used for the others)

D.2.3 Stress fields

Plate thickness $t_c = 15$ mm

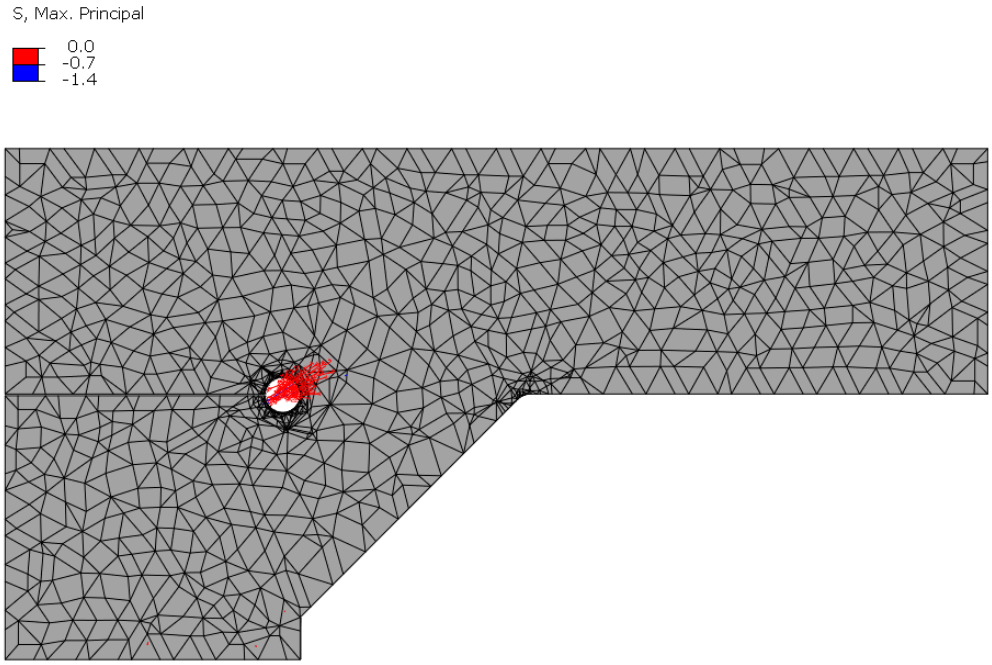

Figure D.6: Maximum principal stress field distribution in stress range -1.4 - 0 MPa for modified beam model with cover-plate thickness $t_c = 15$ mm loaded in bending, under a unit nominal stress of 1 MPa at weld toe.

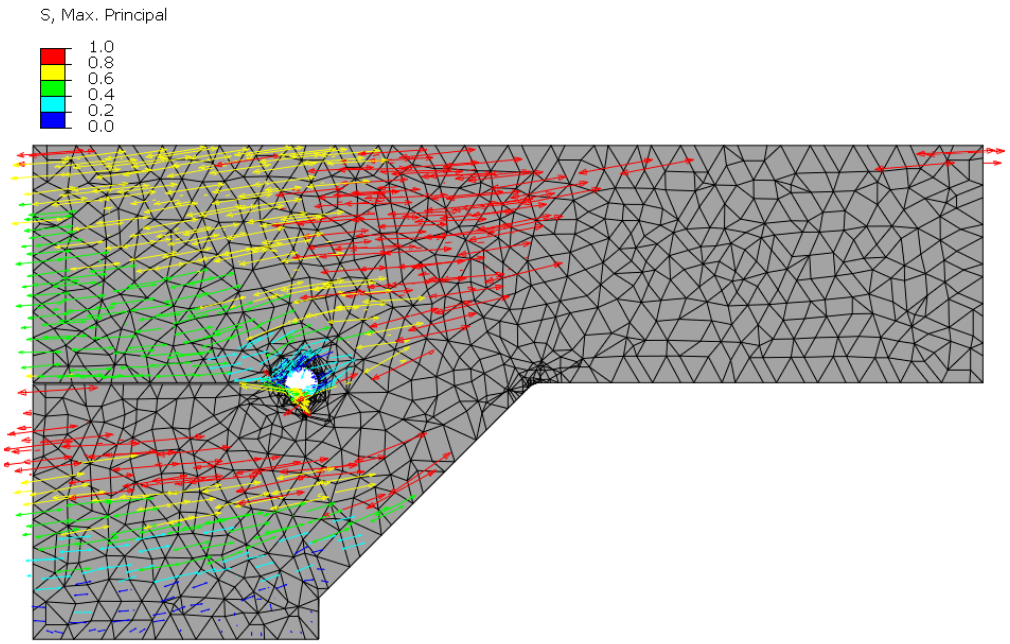

Figure D.7: Maximum principal stress field distribution in stress range 0 - 1 MPa for modified beam model with cover-plate thickness $t_c = 15$ mm loaded in bending, under a unit nominal stress of 1 MPa at weld toe.

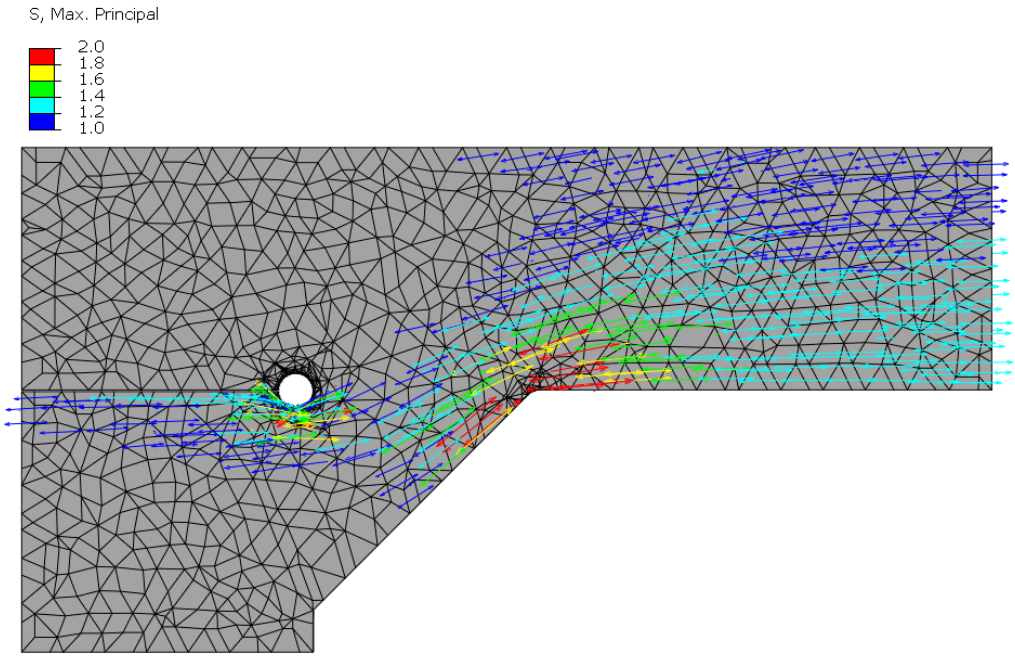

Figure D.8: Maximum principal stress field distribution in stress range 1 - 2 MPa for modified beam model with cover-plate thickness $t_c = 15$ mm loaded in bending, under a unit nominal stress of 1 MPa at weld toe.

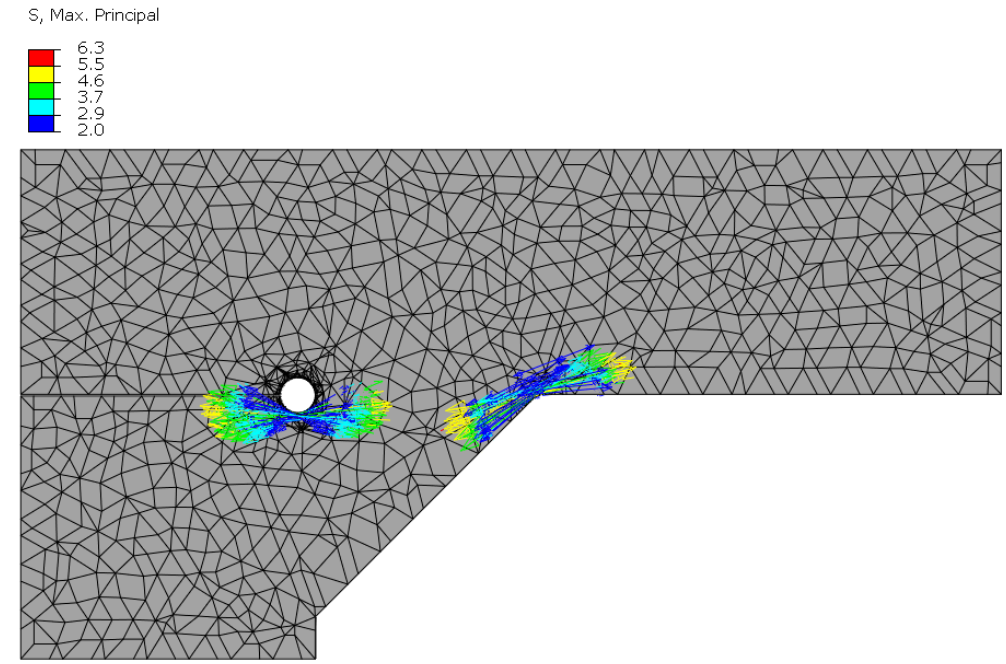

Figure D.9: Maximum principal stress field distribution in stress range 2 - 6.3 MPa for modified beam model with cover-plate thickness $t_c = 15$ mm loaded in bending, under a unit nominal stress of 1 MPa at weld toe.

Plate thickness $t_c = 50$ mm

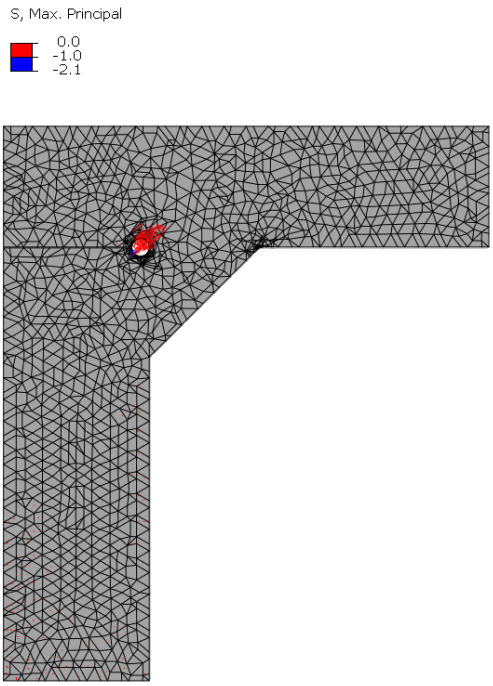

Figure D.10: Maximum principal stress field distribution in stress range -2.1 - 0 MPa for modified beam model with cover-plate thickness $t_c = 50$ mm loaded in bending, under a unit nominal stress of 1 MPa at weld toe.

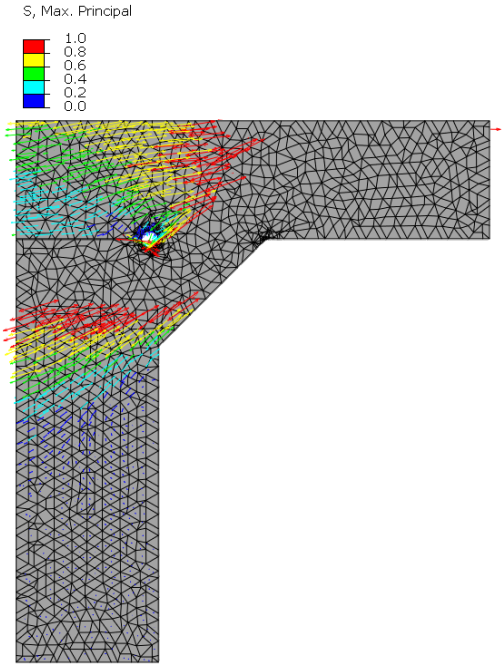

Figure D.11: Maximum principal stress field distribution in stress range 0 - 1 MPa for modified beam model with cover-plate thickness $t_c = 50$ mm loaded in bending, under a unit nominal stress of 1 MPa at weld toe.

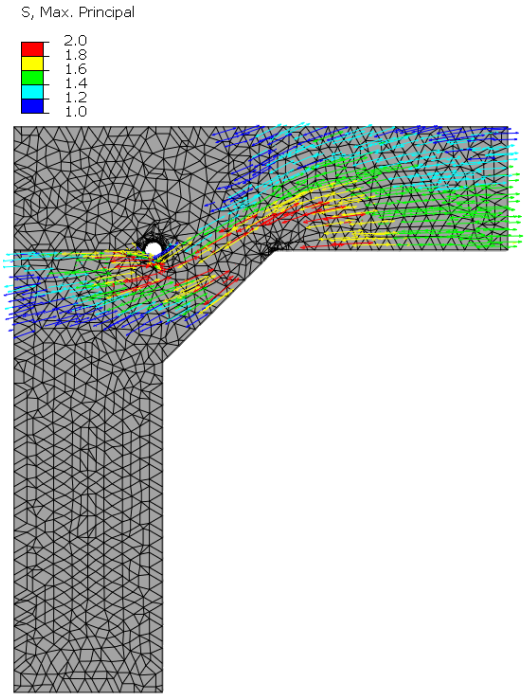

Figure D.12: Maximum principal stress field distribution in stress range 1 - 2 MPa for modified beam model with cover-plate thickness $t_c = 50$ mm loaded in bending, under a unit nominal stress of 1 MPa at weld toe.

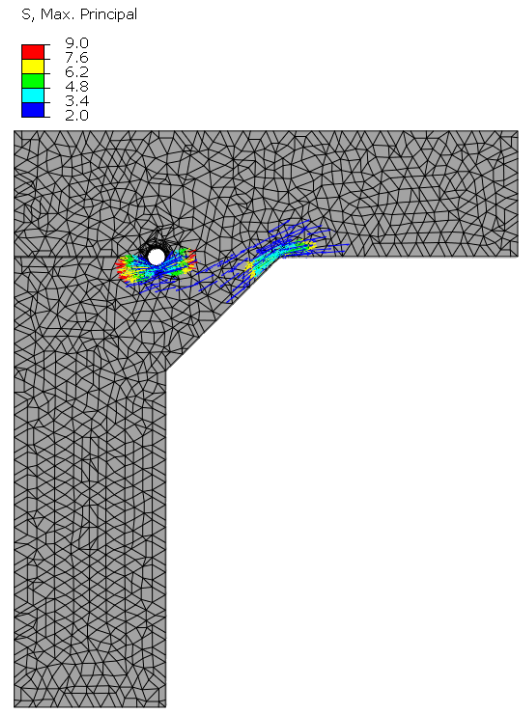

Figure D.13: Maximum principal stress field distribution in stress range 2 - 9.0 MPa for modified beam model with cover-plate thickness $t_c = 50$ mm loaded in bending, under a unit nominal stress of 1 MPa at weld toe.

D.3 Length effect

D.3.1 Calculation of applied load for each cover-plate length and loading situation

Dimensions

I-beam	Cover-plate	Fillet weld
$L = 6,400.8\ mm$	$L_{cp1} = 889\ mm$	Leg-Length=11.23 mm
$h = 702\ mm$	$L_{cp2} = 1,778\ mm$	
$b_f = 254\ mm$	$L_{cp3} = 3,556\ mm$	
$t_f = 28\ mm$	$L_{cp4} = 4,445\ mm$	
$h_w = 646\ mm$	$L_{cp5} = 5,334\ mm$	
$t_w = 15.5\ mm$	$b_{cp} = 190.5\ mm$	
	$t_{cp} = 25.4\ mm$	

Known values

$c = 351\ mm$ (Distance to the neutral axis to weld toe)

$L_{support} = 152.4\ mm$ (Distance from beam edge to support)

$L_{toe1} = L_{cp1} - L_{support} + Leg - Length = 2,590.8\ mm$ (Distance from support to weld toe for cover-plate 889 mm)

$L_{toe2} = L_{cp2} - L_{support} + Leg - Length = 2,146.3\ mm$ (Distance from support to weld toe for cover-plate 1,778 mm)

$L_{toe3} = L_{cp3} - L_{support} + Leg - Length = 1,257.3\ mm$ (Distance from support to weld toe for cover-plate 3,556 mm)

$L_{toe4} = L_{cp4} - L_{support} + Leg - Length = 812.8\ mm$ (Distance from support to weld toe for cover-plate 4,445 mm)

$L_{toe5} = L_{cp5} - L_{support} + Leg - Length = 368.3\ mm$ (Distance from support to weld toe for cover-plate 5,334 mm)

$L_{load.D1} = 1,828.8\ mm$ (Distance from support to load positioned about a third of beam)

$I = 1.979 \cdot 10^9\ mm^4$ (Inertia of the I-beam)

Calculation of the applied load for Abaqus analysis

The unit load $P_{i,u}$ is calculated following the same steps as performed in Appendix B.1(2). Where the load is determined based on a unit nominal stress of 1 MPa.

$\sigma_{u.toe} = 1\ MPa$

· Calculate the bending moment at the end weld toe, derived from Equation 3.1:

Where: $M_{u.toe} = \frac{\sigma_{u.toe} \cdot I}{c} = 5.638 \cdot 10^6\ Nmm$

Loading position: Third of beam (D1)

· The unit load $P_{i,u.D1}$ is calculated for all cover-plate lengths with the moment equation derived from basic mechanic equation from the structural model seen in following figure:

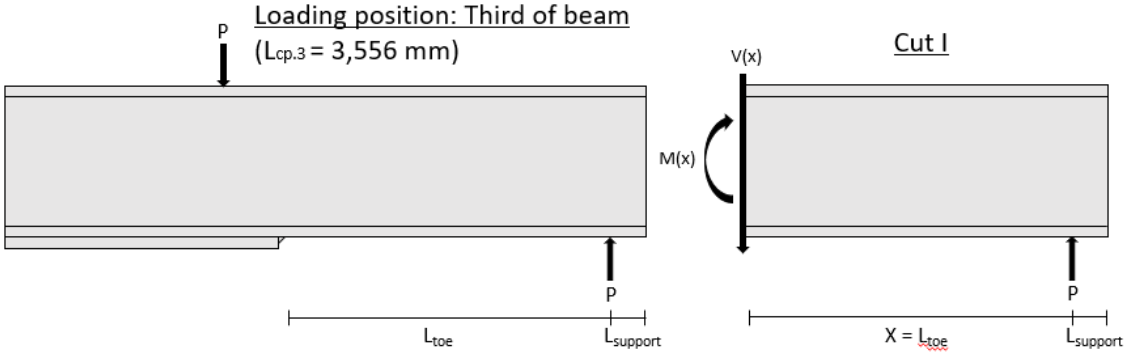

Moment equation: $M_{u.toe}(x) = P \cdot L_{toe.i} \rightarrow P = \frac{M_{u.toe}(x)}{L_{toe}}$

Where: $P_{1,u.D1} = \frac{M_{u.toe}(x)}{L_{load.D1}} = 3,083\ N$
Where: $P_{2,u.D1} = \frac{M_{u.toe}(x)}{L_{load.D1}} = 3,083\ N$
Where: $P_{3,u.D1} = \frac{M_{u.toe}(x)}{L_{toe3}} = 4,484\ N$
Where: $P_{4,u.D1} = \frac{M_{u.toe}(x)}{L_{toe4}} = 6,937\ N$
Where: $P_{5,u.D1} = \frac{M_{u.toe}(x)}{L_{toe5}} = 15,309\ N$

· The unit load applied in the Abaqus model is calculated as half of the total load
Hence: $P_{1,u.aD1} = \frac{P_{1,u.D1}}{2} = 1,541\ N$
Hence: $P_{2,u.aD1} = \frac{P_{2,u.D1}}{2} = 1,541\ N$
Hence: $P_{3,u.aD1} = \frac{P_{3,u.D1}}{2} = 2,242\ N$
Hence: $P_{4,u.aD1} = \frac{P_{4,u.D1}}{2} = 3,468\ N$
Hence: $P_{5,u.aD1} = \frac{P_{5,u.D1}}{2} = 7,654\ N$

Loading position: Middle of beam (D2)

· The unit load $P_{i,u.D2}$ is calculated for all cover-plate lengths with the moment equation derived from basic mechanic equation from the structural model seen in following figure:

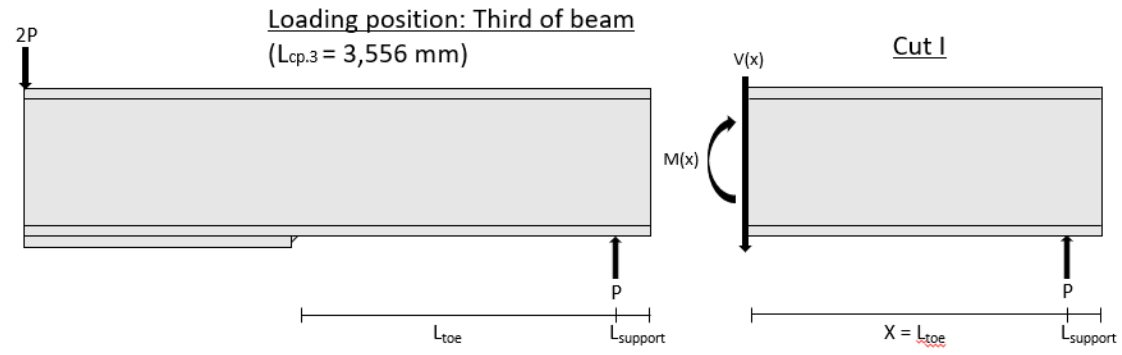

Moment equation: $M_{u.toe}(x) = 2P \cdot L_{toe.i} \rightarrow P = \frac{M_{u.toe}(x)}{2 \cdot L_{toe}}$

Where: $P_{1,u.D2} = \frac{M_{u.toe}(x)}{2 \cdot L_{toe1}} = 2,176\ N$
Where: $P_{2,u.D2} = \frac{M_{u.toe}(x)}{2 \cdot L_{toe2}} = 2,627\ N$
Where: $P_{3,u.D2} = \frac{M_{u.toe}(x)}{2 \cdot L_{toe3}} = 4,484\ N$
Where: $P_{4,u.D2} = \frac{M_{u.toe}(x)}{2 \cdot L_{toe4}} = 6,937\ N$
Where: $P_{5,u.D2} = \frac{M_{u.toe}(x)}{2 \cdot L_{toe5}} = 15,309\ N$

· The unit load applied in the Abaqus model is calculated as half of the total load
Hence: $P_{1,u.aD2} = \frac{P_{1,u.D2}}{2} = 1,088\ N$
Hence: $P_{2,u.aD2} = \frac{P_{2,u.D2}}{2} = 1,313\ N$
Hence: $P_{3,u.aD2} = \frac{P_{3,u.D2}}{2} = 2,242\ N$
Hence: $P_{4,u.aD2} = \frac{P_{4,u.D2}}{2} = 3,468\ N$
Hence: $P_{5,u.aD2} = \frac{P_{5,u.D2}}{2} = 7,654\ N$

For the load calculation of Vilhauer et al. test in Appendix B.1, a verification was performed for the calculated load derived from the unit nominal stress of 1 MPa, which was proven to be accurate. Hence, because this verification was performed for the previous analysis applied load, it is not performed for this analysis.

D.3.2 Characteristic load cycles with original nominal stress

Table D.3: Calculated characteristic load cycles at weld toe and root for HFMI-treated beams with different cover-plate lengths subjected to the same nominal stress ranges used in Hui et al test, as well as the ratio (r) between load cycles of the toe and root.

S_r [MPa]	ENS [MPa]		Load cycles [-]		Ratio [-]
	$\Delta\sigma_{Toe}$	$\Delta\sigma_{Root}$	$N_{Toe_{HFMI}}$	N_{Root}	$\frac{N_{Root}}{N_{Toe_{HFMI}}}$
Cover-plates length: L = 889 mm					
93	483	446	256,170	256,097	1.00
97	503	466	207,532	225,704	1.09
99	514	475	187,399	212,299	1.13
123	638	590	87,571	110,698	1.26
124	644	595	85,469	108,041	1.26
Cover-plates length: L = 1778 mm					
93	502	480	209,758	206,598	0.98
97	424	500	169,931	182,079	1.07
99	535	510	153,446	171,266	1.12
123	664	634	77,675	89,302	1.15
124	667	639	75,810	87,159	1.15
Cover-plates length: L = 4445 mm					
93	617	744	96,240	55,372	0.58
97	645	776	84,819	48,801	0.58
99	659	792	79,781	45,902	0.58
123	818	984	41,600	23,935	0.58
124	825	992	40,601	23,360	0.58
Cover-plates length: L = 5334 mm					
93	794	961	45,561	25,642	0.56
97	828	1,003	40,154	22,599	0.56
99	845	1,023	37,769	21,257	0.56
123	1,050	1 271	19,694	11,084	0.56
124	1,058	1,282	19,221	10,818	0.56

The blue color indicates that the HFMI-treated S-N curve of FAT 320 was used to calculate the design load cycles for the HFMI-treated toe. (The as-welded S-N curve FAT 225 was used for the others)

D.3.3 Stress fields

Stress range 0 - 1 MPa

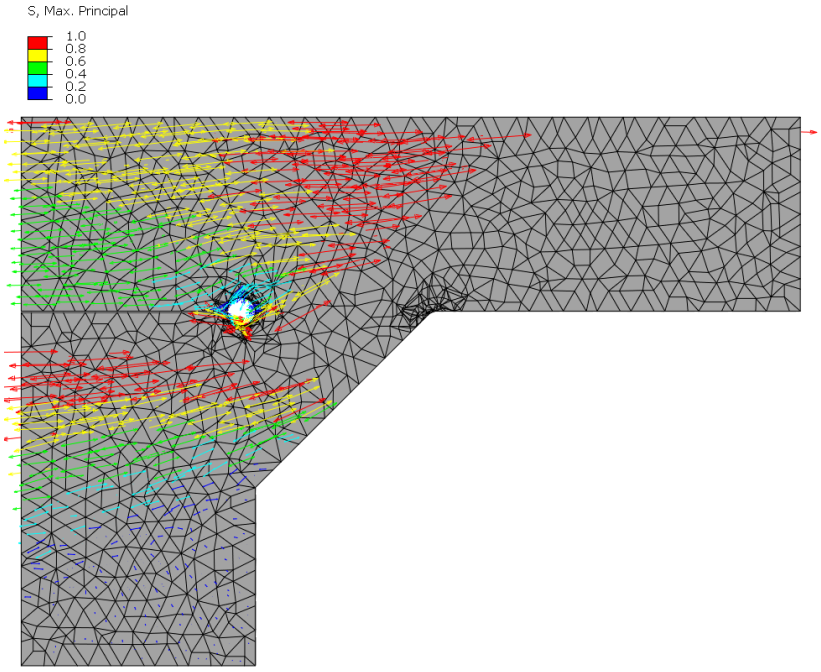

Figure D.14: Maximum principal stress field distribution in stress range 0 - 1 MPa for modified beam model loaded at third of beam with cover-plate length $L_c = 889$ mm loaded in bending, under a unit nominal stress of 1 MPa at weld toe.

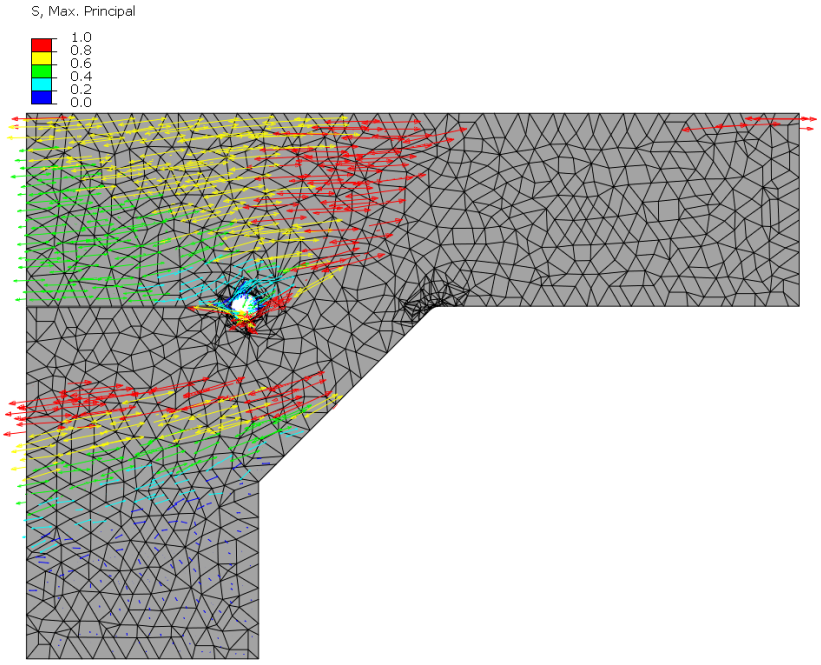

Figure D.15: Maximum principal stress field distribution in stress range 0 - 1 MPa for modified beam model loaded in middle of beam with cover-plate length $L_c = 5,334$ mm loaded in bending, under a unit nominal stress of 1 MPa at weld toe.

Stress range 1 - 2 MPa

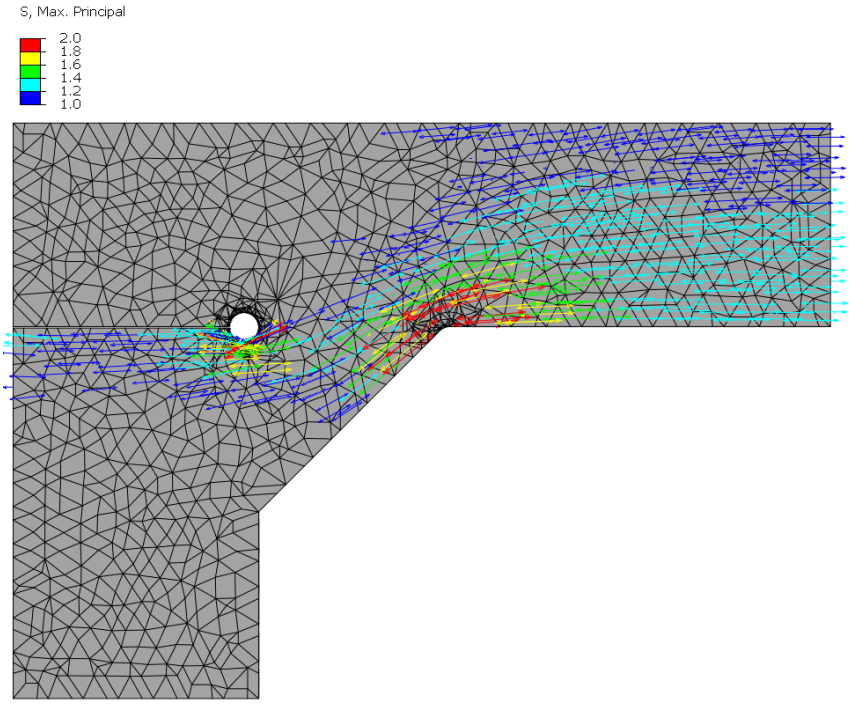

Figure D.16: Maximum principal stress field distribution in stress range 1 - 2 MPa for modified beam model loaded at third of beam with cover-plate length $L_c = 889$ mm loaded in bending, under a unit nominal stress of 1 MPa at weld toe.

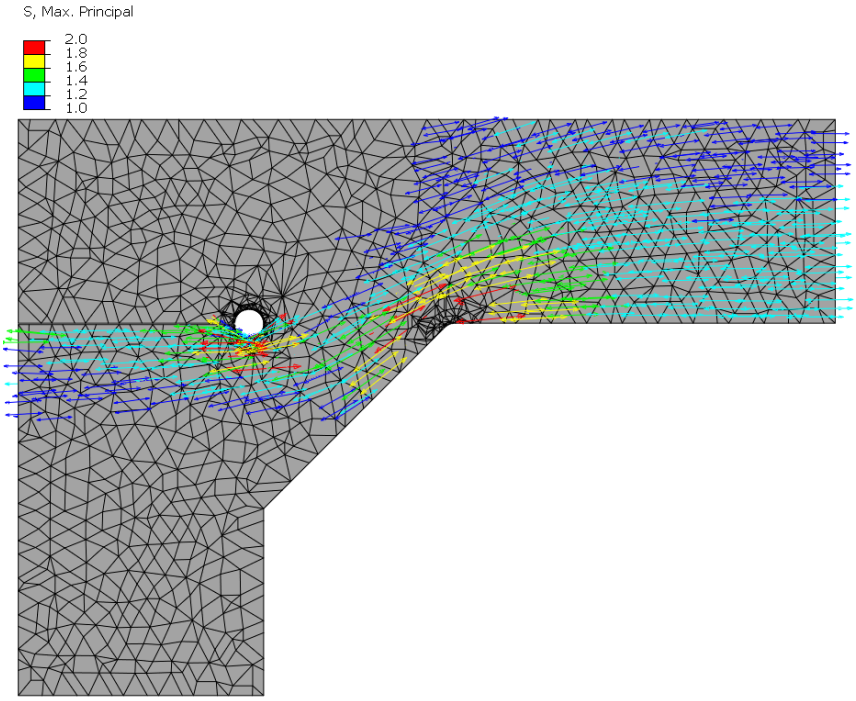

Figure D.17: Maximum principal stress field distribution in stress range 1 - 2 MPa for modified beam model loaded in middle of beam with cover-plate length $L_c = 5,334$ mm loaded in bending, under a unit nominal stress of 1 MPa at weld toe.

Stress range 2 - Max MPa

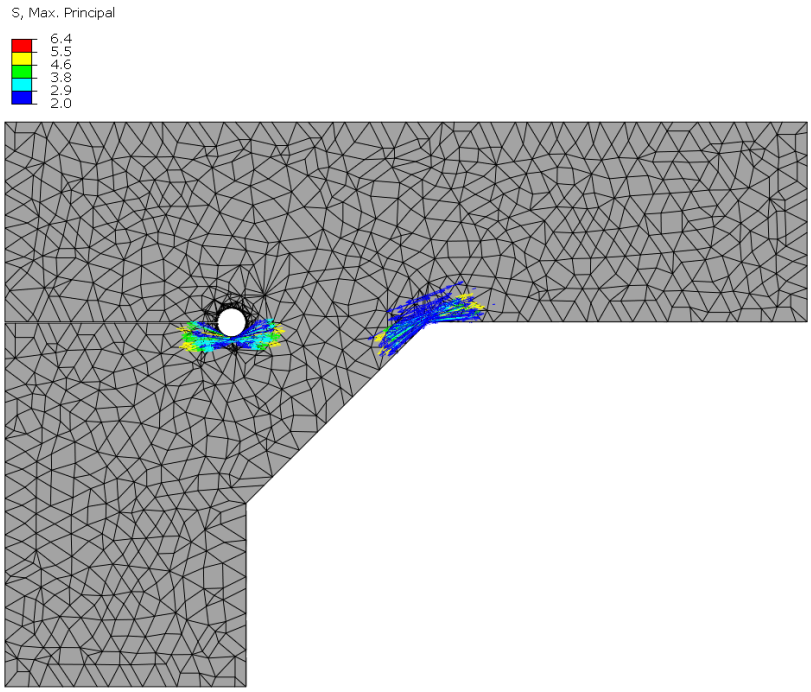

Figure D.18: Maximum principal stress field distribution in stress range 2 - 6.4 MPa for modified beam model loaded at third of beam with cover-plate length $L_c = 889$ mm loaded in bending, under a unit nominal stress of 1 MPa at weld toe.

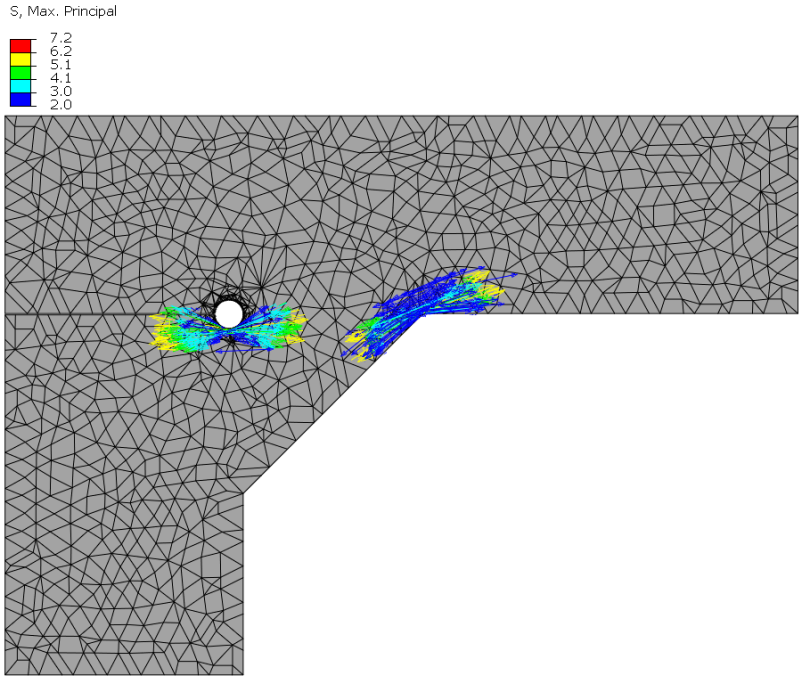

Figure D.19: Maximum principal stress field distribution in stress range 2 - 7.2 MPa for modified beam model loaded in middle of beam with cover-plate length $L_c = 5,334$ mm loaded in bending, under a unit nominal stress of 1 MPa at weld toe.

D.4 Root position effect

D.4.1 Characteristic load cycles with original nominal stress

Table D.4: Calculated characteristic load cycles at weld toe and root for HFMI-treated beams with Cover-plates having different root positions subjected to the same nominal stress ranges used in Hui et al test, as well as the ratio (r) between load cycles of the toe and root.

S_r [MPa]	ENS [MPa]		Load cycles [-]		Ratio [-]
	$\Delta\sigma_{Toe}$	$\Delta\sigma_{Root}$	$N_{Toe_{HFMI}}$	N_{Root}	$\frac{N_{Root}}{N_{Toe_{HFMI}}}$
Root distance from the toe: d = 12.7 mm					
93	507	405	200,624	344,081	1.72
97	529	422	162,532	303,246	1.87
99	540	431	146,765	285,236	1.94
123	670	535	75,626	148,729	1.97
124	976	539	73,811	145,159	1.97
Root distance from the toe: d = 25.4 mm					
93	470	363	293,703	477,458	1.63
97	490	378	237,938	420,793	1.77
99	500	386	214,856	395,802	1.84
123	621	480	95,058	206380	2.17**
124	626	484	69,697	201,427	2.17**

** Cover-plates whose cracking mode is at the weld toe

The red color indicates that the as-welded S-N curve of FAT 225 was used to calculate the characteristic load cycles for the HFMI-treated toe.

D.4.2 Stress fields

Root position, $\alpha = 45°$

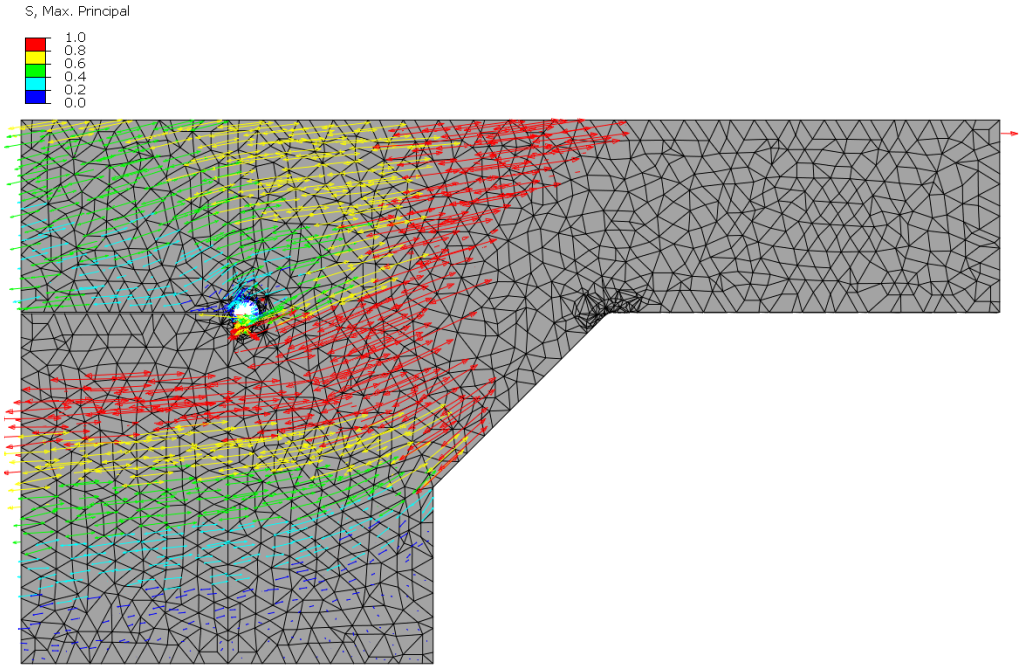

Figure D.20: Maximum principal stress field distribution in stress range 0 - 1 MPa for modified beam model with a changed root position of $\alpha = 45°$ loaded in bending, under a unit nominal stress of 1 MPa at weld toe.

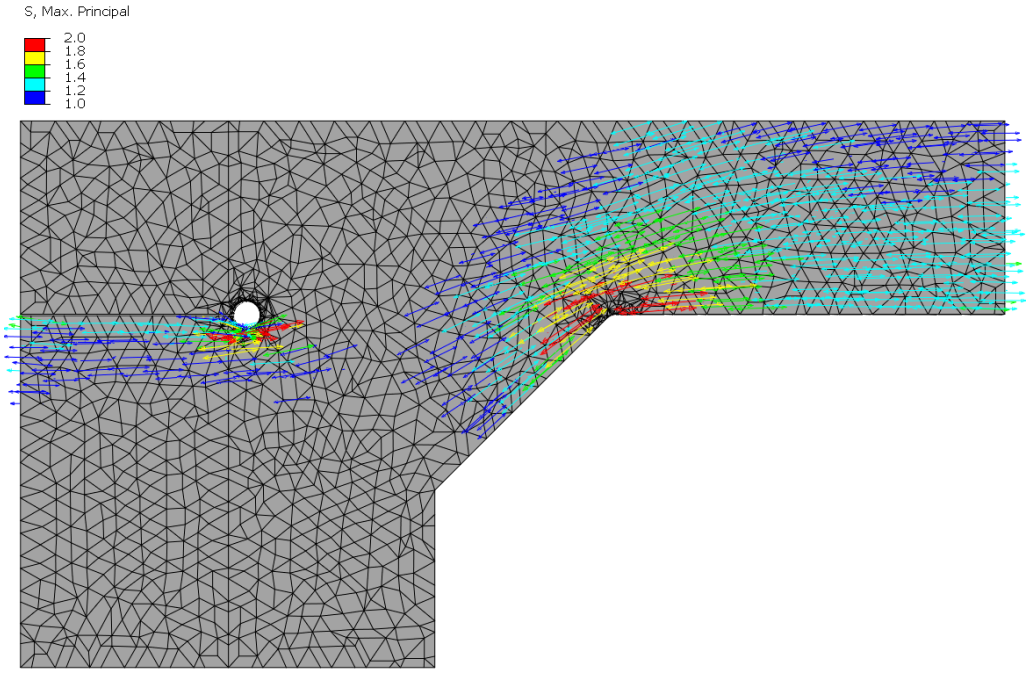

Figure D.21: Maximum principal stress field distribution in stress range 1 - 2 MPa for modified beam model with a changed root position of $\alpha = 45°$ loaded in bending, under a unit nominal stress of 1 MPa at weld toe.

Root position, $\alpha = 26.6°$

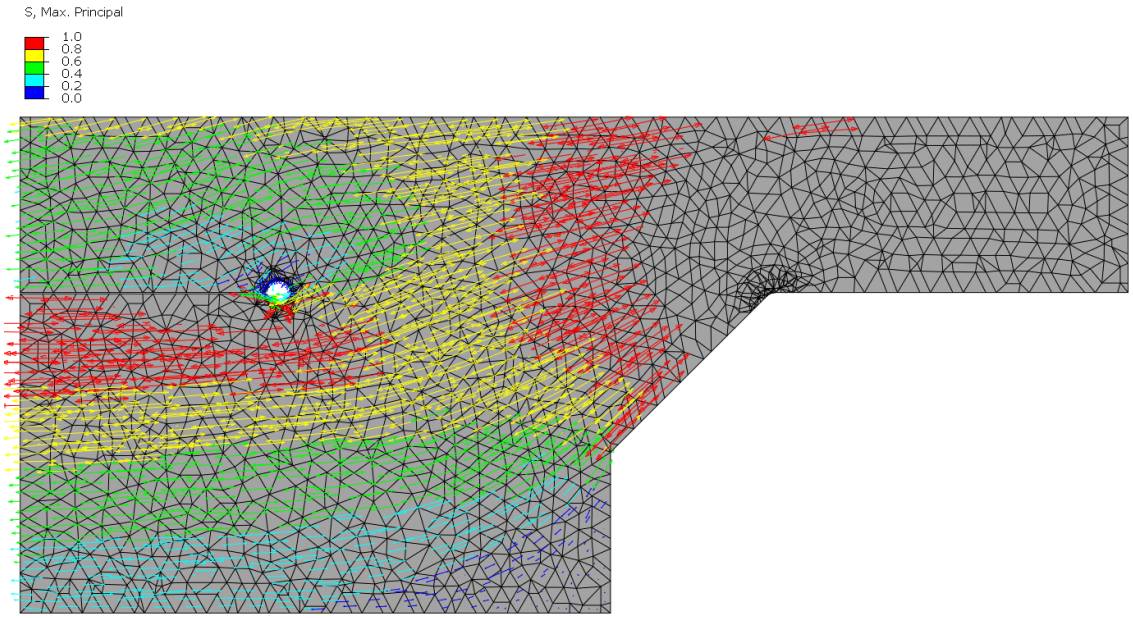

Figure D.22: Maximum principal stress field distribution in stress range 0 - 1 MPa for modified beam model with a changed root position of $\alpha = 26.6°$ loaded in bending, under a unit nominal stress of 1 MPa at weld toe.

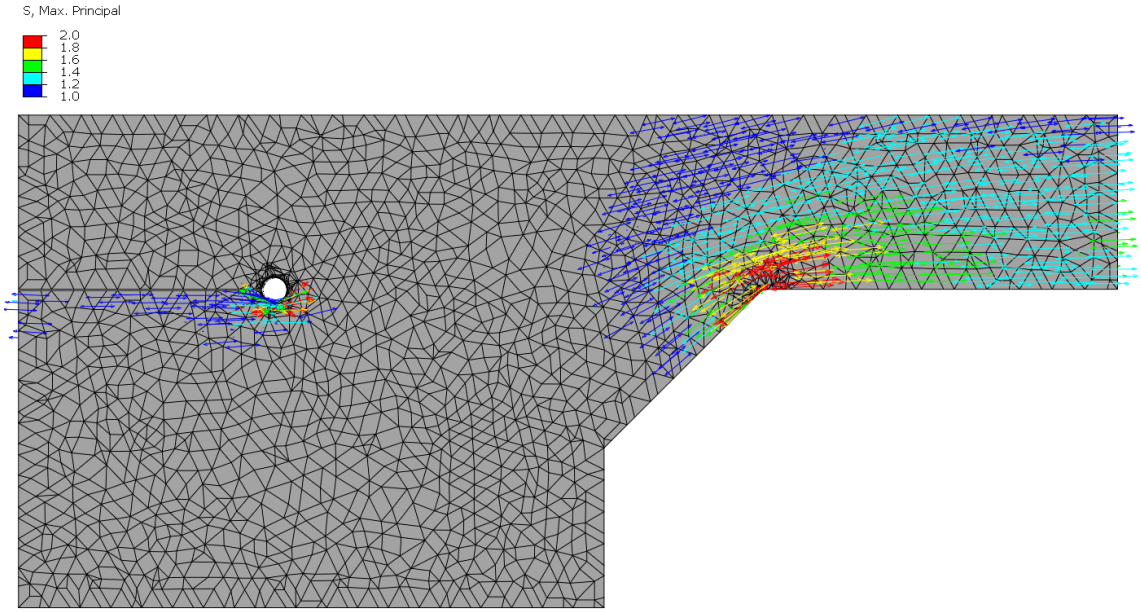

Figure D.23: Maximum principal stress field distribution in stress range 1 - 2 MPa for modified beam model with a changed root position of $\alpha = 26.6°$ loaded in bending, under a unit nominal stress of 1 MPa at weld toe.

D.5 Weld size effect

Stress fields

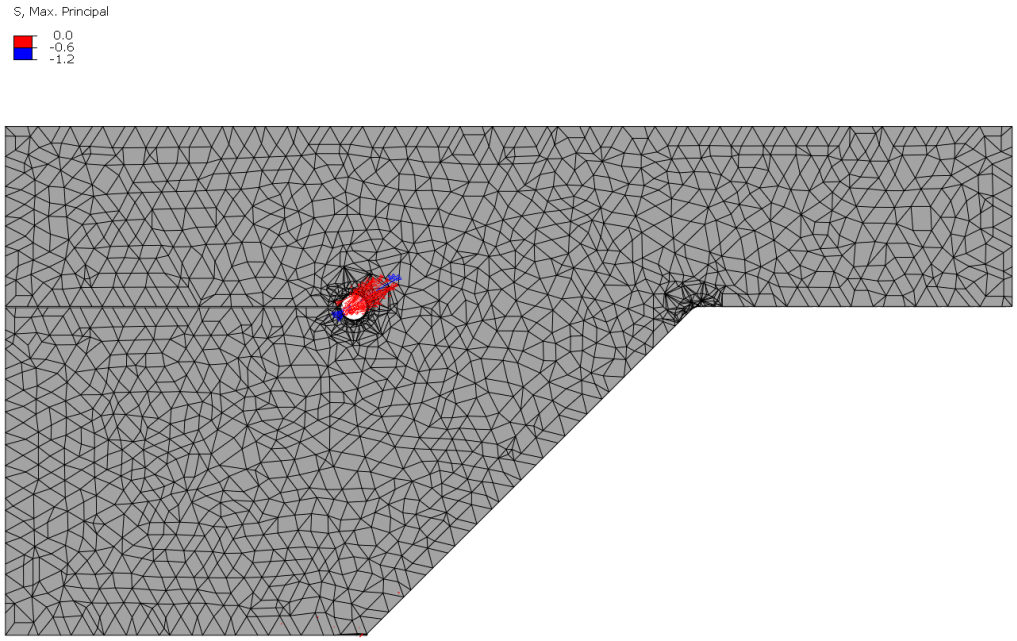

Figure D.24: Maximum principal stress field distribution in stress range -1.2 - 0 MPa for modified beam model with a weld leg-length of 25.4 mm loaded in bending, under a unit nominal stress of 1 MPa at weld toe.

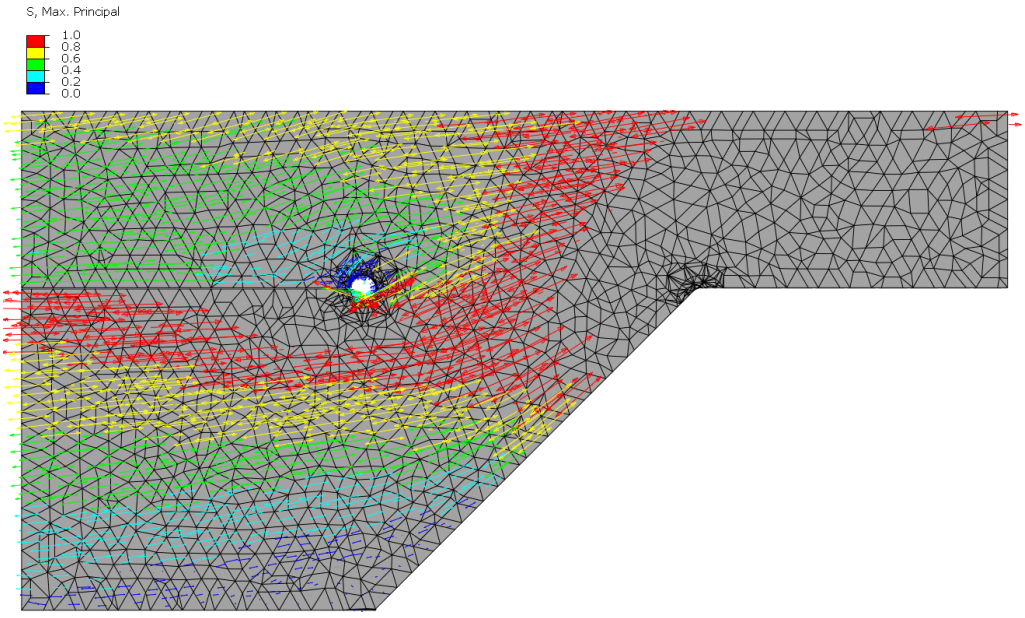

Figure D.25: Maximum principal stress field distribution in stress range 0 - 1 MPa for modified beam model with a weld leg-length of 25.4 mm loaded in bending, under a unit nominal stress of 1 MPa at weld toe.

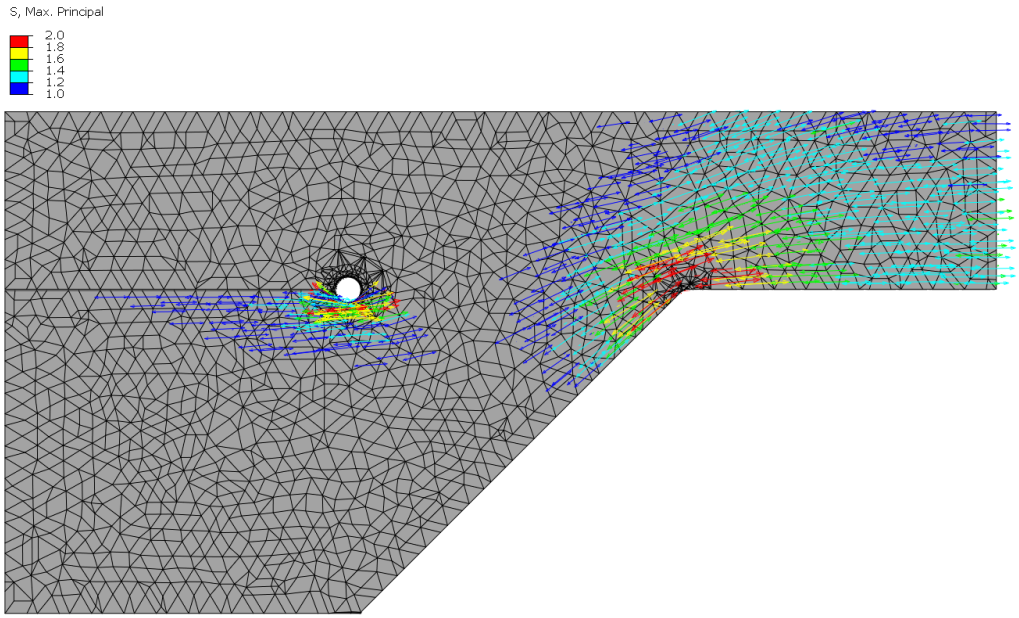

Figure D.26: Maximum principal stress field distribution in stress range 1 - 2 MPa for modified beam model with a weld leg-length of 25.4 mm loaded in bending, under a unit nominal stress of 1 MPa at weld toe.

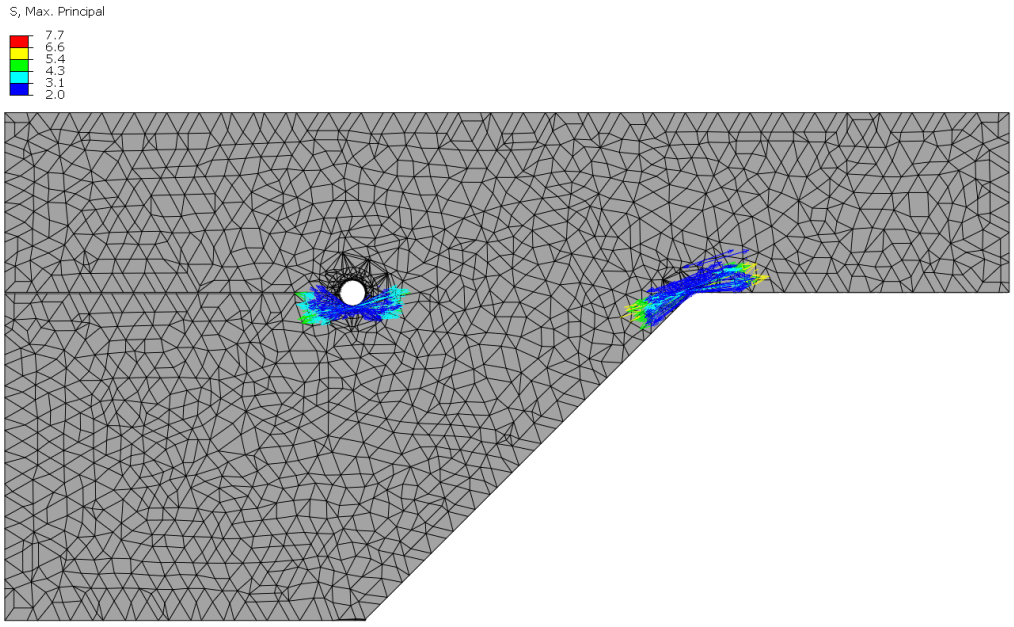

Figure D.27: Maximum principal stress field distribution in stress range 2 - 7.7 MPa for modified beam model with a weld leg-length of 25.4 mm loaded in bending, under a unit nominal stress of 1 MPa at weld toe.